Leachate Transport Modeling for Gazipur landfill site for suggesting ameliorative measures

Submitted by

ANJALI,

Scientist C, Groundwater Hydrology Disivion

National Institute of Hydrology,Roorkee

Section – 1 (About Organizations Involved&Study Team)

1.1 Project Title: Leachate Transport Modeling for Gazipur landfill site for suggesting ameliorative measures

1.2 Lead Research Organization

Name of the organization: National Institute of Hydrology, Roorkee
Head of the organization: Dr. M.K.Goel, Director
Address: Jal Vigyan Bhawan, NIH, Roorkee-247667, UK
Telephone 01332 249 201, Fax: 01332 273976

1.3 Principal Investigator (PI) from Lead Organization

Name & Designation: Anjali, Scientist C,GWHD
Date of birth: March 05, 1991
Address: Environmental Hydrology Division, NIH, Roorkee-247667, UK
Telephone- 01332-249232, Mobile: 9435273568
Email: **anjali.nihr@gov.in**, **anjali.civil.iit@gmail.com**

1.4 Co-PIs from Lead Organization

Name & Designation: Dr. Sudhir Kumar, Scientist G & Former Director, NIH
Date of birth: November 05, 1963
Address: Hydrological Investigation Division, NIH, Roorkee-247667, UK
Telephone: 01332-249212, Fax: 01332-275969, Mobile: 9897024025
Email**: skumar.nihr@gov.in**

Name & Designation: Dr. J. V. Tyagi, Scientist G & Former Director, NIH
Date of birth: August 15, 1962
Address:Environmental Hydrology Division, NIH, Roorkee-247667, UK
Telephone: 01332-249203, Fax: 01332-272123, Mobile: 9897736025
Email**: tyagi.nihr@gov.in**

Name & Designation: Dr. M. K. Sharma, Scientist F, EHD
Date of birth: May 20, 1967
Address: Environmental Hydrology Division, NIH, Roorkee-247667, UK
Telephone- 01332-249235, Fax: 01332-272123, Mobile: 9927221049
Email:**sharmamk.1967@gmail.com**

1.5 Partner Institutions (if any)

Name of the organization: Central Ground Water Board (Delhi unit)

1.6 Principal Investigator (PI) from Partner Organization

Dr. G.Vijy Kumar, Senior Hydrogeologist, CGWB

Section – 2 (Summary of the Proposal)

2.1 Project Title: Leachate Transport Modeling for Gazipur landfill site for suggesting ameliorative measures

2.2 End-user Department/Organization/Agency: Delhi Jal Board, New Delhi.
New Delhi Municipal Corporation

2.3 Duration of the project: 4 Years

2.4 Lead Organization: National Institute of Hydrology, Roorkee

2.5 Partner Organization (if any): Central Groundwater Board (Delhi unit)

2.6 PI and Co-PI from Lead Organization:

PI: Ms. Anjali, Scientist C GWHD

Co-PI: Dr.Sudhir Kumar, Scientist G & Head, HID
Dr. J. V. Tyagi, Scientist G & Head, EHD
Dr. M.K. Sharma, Scientist D, EHD

2.7 Total Cost of Project (Rs.)

a) Lead Organization - Rs. 76,10,800
b) Partner Organization - NIL

2.8 Project Summary (Max. 200 words)

Historically, landfills have been the most common method of organized waste disposal and remain so in many places around the world. On one hand, the properly managed landfill can become a source of energy generation and on the other, a poorly managed landfill can become a source of air and water pollution. Solid waste landfills comprise a variety of solid, semi-solid, and small quantities of liquid wastes. These landfills generally remain open for decades before undergoing closure and post closure phases. During this period, contamination of air by the obnoxious gasses produced in the landfill and contamination of groundwater by the percolation of leachate occurs.

Groundwater quality assessment can reflect the extent and effect of leachate percolation at various locations in NCR and their associated health risk. While Isotopic study of Leachate characteristics will help in separating the groundwater pollution caused by leachate percolation from other source of pollution affect the groundwater of the region under consideration. In the present study, an attempt shall be made to characterize the Leachate and to study its transport through groundwater by carrying out groundwater quality assessment and isotopic study in NCR region.

CHAPTER 1
INTRODUCTION

Historically, landfills have been the most common method of organized waste disposal and remain so in many places around the world. On one hand, the properly managed landfill can become a source of energy generation and on the other a poorly managed landfill can become a source of air and water pollution. Solid waste landfills comprise a variety of solid, semi-solid, and small quantities of liquid wastes. These landfills generally remain open for decades before undergoing closure and post closure phases. During this period, contamination of air by the obnoxious gasses produced in the landfill and contamination of groundwater by the percolation of leachate occurs.

1.1 Background & Motivation for the Study

The growth in population, urbanization and industrialization has led to the increase in the generation of solid waste all over the world. It is believed that the rate of waste generation is an index of socio-economic development and an economic prosperity of a country. This is evident from the fact that the rate of waste generation is more prominent in the developing countries where there is an increased rate of unplanned urbanization of the cities.

In India, the total Indian urban population amounts to approximately 285 million. The cities which have more than 100,000 populations contribute to more than 72 per cent of the total municipal solid waste. The growth rate of population in urban India is much higher than that in rural India. If the growth in population continues with the existing trend, then the projected population in percentage of the total population living in urban areas would reach 41.4 percent. Since waste generated by the city depends on its population and per capita income, it is estimated that the quantity of Municipal Solid Waste (MSW) would reach 17,000 – 25,000 MT per day by 2021. (Talyan et al 2007).

For solid waste management in Delhi, twenty landfill sites were identified and developed since 1975, and of which 15 have already been closed and two were suspended. At present only three landfill sites are in operation. They are namely, Bhalaswa catering the needs of northern part of Delhi, Okhala in the southern part and Gazipur in the eastern part of Delhi.

The improper management and operation of landfill is creating sever environmental impact on surface and subsurface water because of leachate production by the waste disposed. This resulted in degradation in river, groundwater and land quality in the city of Delhi.

In order to design and implement appropriate treatment and disposal actions in the landfill, it is necessary to know the quantitative and qualitative characteristics of the leachate produced as accurately as possible. The factors affecting the chemical composition and the production rate of leachate include the characteristics of the waste (initial composition, particle size, density and so on), the interaction between the percolating landfill moisture and the waste, the hydrology and climate of the site, the landfill design and the operational variables, microbial processes taking place during the stabilization of the waste, and the stage of the landfill stabilization. Most of these factors change during the operational period of the landfill as the landfill is developed causing significant changes in leachate quality and quantity.

This study aims to develop a numerical model for a landfill which is in its operational phase. The study takes two factors into consideration namely the effect of time-development of landfill on the hydraulic properties and composition of the waste. The model also simulates the change in temperature along the depth of the waste layer taking into account the biochemical degradation and convectional heat transferred through moisture flow. Finally, the leachate produced from the waste heap is obtained and it is being partitioned into various components. An assessment of movement of these leachate components through groundwater has also been carried out. The model has been applied to the Gazipur Landfill site, which is shown in Fig 1.1.

Fig 1.1.Gazipur landfill site, New Delhi, India

1.2 Scope and Objectives

The developed model considers the time development of the landfill, effect of overburden pressure and multiphase nature the contaminate taking seasonal variation into account. The research is thus an attempt to model the landfill holistically and give the best possible results for designing the landfill and chalking out operational and management plans of landfill to controlling the water pollution.

The specific objectives of the study are:

I. Understanding of hydrodynamics of groundwater flow in the study area.
II. Chemical characterization of Leachate.
III. Isotopic characterization of leachate and its variation due to recharge and extraction of groundwater.
IV. Assessment of Micro-plastic and metals (Hg, Ni, Co) in landfill leachate.
V. Modelling of leachate migration pattern in groundwater in space and time.
VI. Suggesting ameliorative measures for contaminant plume migration.
VII. Dissemination of knowledge and findings to stakeholders through manuals, leaflets, booklets and workshops/training programs.

3.2.1 Brief Description of the Objectives

The population in the National Capital Region (NCR) has increased significantly during the past few decades and is still growing. Therefore, assessment of groundwater quality and quantity is essential for sustainable management of groundwater resources. Increasing demand of water due to growing population and infrastructure development in the region has led to overexploitation of groundwater. The depleting groundwater levels in the region has increased the vulnerability of groundwater to contaminant pollution. The disposal of waste in non-engineered landfill sites increases the risk of groundwater pollution through percolation of liquids which have high concentration of hazardous chemicals. But the extent to which waste dumping is responsible for groundwater deterioration is very difficult to quantify and predict. Thus, most of the studies focus on groundwater quality assessment in and around the landfill area. Modeling the leachate transport through groundwater entirely on these studies lacks reliability. The present PDS attempts to bridge this gap by prepare a holistic model of leachate transport in ground water.

CHAPTER 2
LITERATURE REVIEW

This Chapter includes the review of the literatures studied to aims at the methodology required to achieve the identified objectives. This Chapter is divided into different sections as per the themes required for the development of the groundwater model. Each section gives the literature details or the identified themes.

2.1 Characterization of Landfill Leachate

(Sharma & Jain, 2019) this study investigates the current state of municipal solid waste (MSW) generation, composition, and management in Indian cities. According to data from 2015, urban India produced approximately 62 million metric tons of solid waste, equivalent to 450 grams per person per day. Of this, about 82 percent of municipal solid waste was collected, leaving 18 percent unattended. A mere one-fourth of the collected waste underwent processing, while the remainder was openly disposed of. Efficiency in waste collection ranged from 70 to 95 percent in large cities, but in smaller cities, it fell below 50 percent due to financial constraints and inadequate infrastructure. Key challenges include source segregation of waste, door-to-door collection, recycling and reuse alternatives, treatment technologies, land availability, and disposal expertise. In response, the study assesses government solid waste management regulations, financial support, incentives, and their limitations, offering recommendations. Additionally, the study explores international comparisons of MSW management and waste processing technologies employed in specific regions of India.

(Naveen et al., 2014) conducted a study on the characteristics of landfill leachate, particularly focusing on the salts present in the leachate generated from the Mavallipura landfill site. The analysis revealed that alkalinity levels followed a trend of leachate (sample 1) > Pond leachate > Well leachate. The study also found a high concentration of iron among the metals detected. The elevated electrical conductivity (EC) value (4210µS/cm) suggested organic matter degradation. Various cations and anions were observed in the leachate. Notably, chloride content was high among the anions, indicating the presence of soluble salts from municipal solid waste (MSW). Among the cations, higher concentrations of Na+ and K+ were noted. These ions are significant for plant growth and are derived from vegetable residues and household waste. Elevated K+ concentration in groundwater serves as an important indicator of landfill leachate pollution. The

study found that the BOD/COD ratio of the leachate was less than 0.63, making it suitable for chemical waste treatment. This research underscores the importance of understanding leachate quality for planning and implementing effective measures to protect the groundwater and surface water quality in the vicinity."

(Mor, Ravindra, Dahiya, et al., 2006) The study conducted at the Gazipur landfill site in Delhi, India, a thorough assessment was undertaken to evaluate the environmental impact on the area. This investigation involved the collection of samples from both leachate and groundwater for analysis. The samples were meticulously tested for various parameters, including the presence of heavy metals such as Cd, Cr, Cu, Fe, Ni, Pb, and Zn, as well as microbiological factors like total coliform and faecal coliform in both groundwater and leachate. The findings revealed a notable and adverse influence on groundwater quality due to the infiltration of leachate, as demonstrated by moderately elevated concentrations of various substances including chloride, nitrate, sulfate, ammonium, phenol, iron, zinc, and chemical oxygen demand. These substances collectively act as reliable indicators of groundwater contamination. Furthermore, the study factored in the depth and proximity of wells to the pollution source. An especially concerning aspect was the presence of total coliform and fecal coliform in groundwater, raising significant concerns about its suitability for uses like domestic water supply due to potential health risks. This study thus highlights the critical need for addressing and mitigating the environmental and health-related challenges associated with the Gazipur landfill site.

(Singh et al., 2017) assess the characteristics of leachate and its impact on soil and the growth of Triticum aestivum (wheat) plants. The growth parameters of the wheat plants exhibited a positive response when the soil was treated with diluted leachate and fertilizers compared to the control soil. The application of a 450 ml leachate dose to the wheat plants resulted in the highest harvest index (HI), indicating that leachate can serve as an effective fertilizer. Additionally, the study evaluated the non-carcinogenic risks associated with trace elements present in the leachate.

Hazard quotient (HQ) values for the trace elements (Cu, Ni, Mn, Zn, and Cr) were calculated, and it was determined that the risk was generally not significant, except in cases where 600 ml of leachate was used for soil irrigation. At the 600 ml leachate dose, the harvest index was found to decrease, possibly due to an increase in soil salinity. This research suggests an optimal leachate

dose for irrigation purposes, which can be instrumental in reducing the environmental burden of waste in the surrounding area.

(Mor, Ravindra, De Visscher, et al., 2006) The analysis revealed a notable presence of degradable organic components at the Gazipur landfill site in Delhi, India. These organic materials decompose, producing methane, a significant contributor to global warming. Using a first-order decay model based on waste composition, waste age, and the total waste volume, the study estimated the methane generation potential at the Gazipur landfill, resulting in a figure of 15.3 Gg/year. This accounts for approximately 1-3% of India's existing estimates for landfill methane emissions. By extrapolating from the Gazipur investigation, the study estimated Indian landfill methane emissions at 1.25 Tg/year or a methane generation potential of 1.68 Tg/year, aligning with existing estimates. The study also compared the FOD model with a triangular model, finding both suitable for methane generation estimation. However, the FOD model indicated a more gradual decrease in emissions post-closure, leading to higher gas production predictions beyond a decade of closure. Additionally, the research delved into the regional and global consequences of national landfill methane emissions.

(Tripathi et al., 2021) The environmental impact of the Gazipur landfill on air, water, and land in its vicinity was rigorously assessed. The research uncovered substantial methane emissions, approximately 300 mg/m²/h, and corresponding N2O emissions ranging from 826 to 1,730 g/m²/h in summer and 230 to 973 g/m²/h in winter, establishing the Gazipur Landfill as a prominent regional air pollution source. Leachate analysis unveiled a pH of 6.8, an electrical conductivity of 23,500 μS/cm, and total dissolved solids at 26,826 mg/L, indicating the presence of inorganic constituents. High BOD and COD values, 18,200 mg/L and 25,400 mg/L, respectively, signified substantial organic content, alongside elevated NO3- and Si levels of about 370 mg/L and 336 mg/L. Groundwater analysis featured parameters including total hardness (412 to 560 ppm), alkalinity (98 to 164 ppm as CaCO3), total suspended solids (630 to 810 ppm), TDS (615 to 760 ppm), BOD (20 to 30 ppm), and pH (7 to 7.6), while soil analysis indicated slightly basic, stratified soil. These findings underscore the environmental challenges posed by the Gazipur landfill, with far-reaching implications for regional air and water quality, emphasizing the urgency of effective remediation and responsible waste management practices.

(Babbar et al., 2017) examined the impact of leachate from the Ghazipur landfill on groundwater. Groundwater samples around the landfill indicated clear contamination due to leachate percolation. The levels of various contaminants like TDS, Cl-, SO2+, NO3-, NH4+, and Fe were significantly elevated, making the water unsuitable for drinking and domestic use. The samples had a pH between 7.5 and 8.5 and contained high levels of ammonia nitrogen and nitrate. Iron and steel waste was also found in the groundwater. Bacteriological analysis revealed that the samples were unsafe. However, the quality of groundwater improved with greater well depth and distance from the contamination source as leachate percolation decreased.

(Ramaiah et al., 2017) Investigates the properties of municipal solid waste (MSW) from the Ghazipur and Okhla dumps in Delhi, India, using a direct shear test. It reveals that the MSW has a relatively low compression ratio (Cc0) ranging from 0.11 to 0.17, primarily due to a higher presence of inert materials like soil-like fractions and less compressible elements such as textiles and plastics. The shear strength of the MSW is displacement-dependent, with apparent cohesion (c0) and friction angle (/0) values falling within the range reported in literature. The study also proposes a simplified shear strength envelope (c0 = 17 kPa and /0 = 32 degrees) for MSW, based on a global database, which can serve as a preliminary reference for evaluating landfill stability under drained conditions in the absence of site-specific data.

(Ahmed et al., 2020) study delves into the impact of seasonal variations on leachate from three active landfill sites in Delhi, India, revealing the release of contaminants that surpass regulated disposal limits. The contaminants, including conductivity, TDS, BOD, COD, TKN, NH3-N, org-N, heavy metals, chlorides, and sulfates, exceed permissible levels. The study also highlights the substantial disposal of industrial and hazardous waste materials in these landfills. Furthermore, inland surface waters show elevated concentrations of substances like TDS, COD, BOD, Cl-, CN-, and As, breaching established limits that govern waste disposal quantities. Notably, these landfills are already operating at or beyond their capacity, indicating that adding more waste would prolong the leaching of a higher volume of toxic substances.

(Bhalla et al., 2013) examines how the age of a municipal solid waste (MSW) landfill site in Ludhiana, India, and seasonal variations impact leachate characteristics. The landfill lacks essential engineering features like a bottom liner or leachate collection system, causing leachate to seep into the environment. Leachate samples were collected from the base of waste piles,

revealing high concentrations of organic and inorganic substances that exceed acceptable limits. Heavy metals are found in small amounts, likely due to the domestic waste nature of the landfill. As time passes and during rainy seasons, various parameters in the leachate increase because solid waste degrades and combines with rainwater. This emphasizes the significant influence of landfill age and seasonal changes on leachate composition and underscores the necessity to halt unregulated MSW dumping.

2.2 Physico-Chemical Methods Adopted For Leachate Treatment

Various leachate treatment options are suggested based on waste composition. Customizing treatments offers benefits such as safe disposal but comes with cost implications and sludge generation.

(Aziz et al., 2007) examined the effectiveness of the coagulation-flocculation process in treating color in semi-aerobic landfill leachate from Malaysia. They investigated different coagulants, including Alum, FeSO4, and Fe2(SO4)3, at various dosages to reduce color in the leachate. The study also assessed the impact of pH on color removal and found that the best results occurred at pH 4 and 12. Among the coagulants, FeCl3 proved most effective, removing 94% of the color at pH 4 with a dose of 0.8 g/L. The study revealed that lower pH levels were more effective in color removal due to humic acid precipitation, and color was primarily associated with organic matter, turbidity, and suspended solids.

(Mohajeri et al., 2010) explored Fenton oxidation impact on color and organic matter removal from MSW landfill leachate. They investigated factors like pH, molar ratio, reaction time, agitation rate, and Fenton reagent concentration. The best results, with 78.3% color and 58.1% COD removal, were achieved at pH 3, a Fe2+/H2O2 ratio of 1:3, 400 rpm agitation, and a 120-minute reaction time. Higher temperatures (>50°C) were found to have a negative effect on COD removal due to floc destabilization. The study recommended adding the Fenton reagent incrementally for better effectiveness.

(Kashitarash et al., 2012) investigate the use of iron nanoparticles for leachate treatment, capitalizing on their small size and high surface area for effective pollutant removal. This method achieved removal rates of 47.94% for COD, 35% for BOD5, 55.6% for total solids, and 76.7% for color. The optimal iron nanoparticle dosage was 2.5g/L, and the best removal rates were achieved

in a quick 10-minute reaction. Iron nanoparticles attracted the highest amount of humic acid within the pH range of 3-9, with removal efficiency declining as pH increased. This is because iron nanoparticles carry a positive charge at lower pH levels and a negative charge at higher pH levels, making them effective at adsorbing negatively charged humic acid. Additionally, the BOD5/COD ratio increased from 0.34 to 0.73, indicating enhanced potential for subsequent biological leachate treatment.

2.3 Assessment of Micro Plastic, Phthalate, Pesticides And Metals In Landfill Leachate

(Singh et al., 2023) examined the issue of microplastics (MP) pollution originating from landfills used for waste management. Plastics in landfills degrade into MPs, posing environmental and health risks. The review covers the process of plastic degradation, types of MPs in landfill leachate (LL), and potential toxicity. It evaluates various MP removal methods, including chemical and biological treatments. Younger landfills have higher MP concentrations, with specific polymers like polypropylene, polystyrene, nylon, and polycarbonate contributing. Primary treatments like chemical precipitation and electrocoagulation remove 60-99% of MPs, while tertiary treatments achieve rates of up to 90-99%. Advanced techniques like MBR + UF + NF offer even higher removal capabilities.

(Wowkonowicz & Kijeńska, 2017) study focuses on phthalate diesters (PAEs) in landfill leachate, with a specific emphasis on the region of Poland. They conducted a year-long study in 2015/16, collecting and analyzing leachate samples from five municipal landfills, the first large-scale investigation of its kind in Poland. The study revealed the widespread presence of PAEs in all landfill leachate samples, with Di (2-ethylhexyl) phthalate (DEHP) being the most prominent. DEHP levels often exceeded the EU surface water limit in 75% of the samples, raising concerns for water quality. Notably, DEHP levels remained consistent even at a closed landfill site, emphasizing the environmental significance of PAEs in leachate.

(Haarstad & Maehlum, 2008) investigated the presence of pesticides in Norwegian MSW landfills. They examined untreated and treated leachate samples and leachate sediments, identifying 12 pesticide compounds. The most frequently detected and concentrated group was phenoxy acids, particularly mecoprop. Significantly, all samples, whether treated or untreated, exceeded the maximum limit for pesticide concentration in drinking water, with six compounds surpassing environmental toxicity limits. These findings underscore concerns about the presence of pesticides,

especially phenoxy acids, in landfill leachate, highlighting potential environmental and public health risks.

2.4 Using Hydrus to Simulate the Flow

(Aljaradin et al., 2011) used the HYDUS-2D, a numerical model for analyzing water flow and solute transport, to investigate the impact of landfill cover thickness and initial soil moisture content on the movement of chloride through the soil beneath the landfill. Various simulation scenarios were run over a 30-year period, accounting for changing cover thickness and soil moisture levels based on seasonal climate data. The result revealed that the maximum chloride concentration in the soil profile remained lower than that in municipal solid waste (MSW) leachate for all scenarios and locations throughout the simulation period. With increasing landfill cover thickness, the concentration of chloride at specific locations decreased, along with an extended time needed to reach those levels. Additionally, the findings indicated that the influence of initial soil moisture content on chloride reduction became more significant with thicker covers. Based on these results, it was recommended to use a landfill cover to reduce chloride levels, with a 50 cm cover thickness being suitable for lower initial soil moisture content.

(Anwar & Thien, 2015) This article investigates the potential leaching of heavy metals from the Rottnest Island landfill in Western Australia, with a specific focus on Copper and Zinc due to their elevated levels in the local groundwater. The researchers employed the HYDRUS-1D model to simulate how heavy metal leachate moves through the soil profile. This modeling was tailored to the site-specific conditions of the Rottnest Island landfill from 1996 to 2010, considering various factors related to soil-water-chemical interactions. The result shows that the heavy metal migration in the soil is strongly influenced by the adsorption coefficient (kd), and initial concentration significantly affects leachate contamination. Longitudinal dispersion has a moderate impact on solute transport, while the diffusion coefficient does not affect contaminant migration in the soil. Initial soil moisture and saturated hydraulic conductivity have minimal effects on leachate transport in the landfill site.

(Waisczik & De Lima, 2020) The disposal of municipal solid waste (MSW) is a significant challenge due to the potential environmental threats posed by leachate and gases generated during decomposition. Landfills are commonly used for MSW disposal due to their protective systems that reduce the risk of contamination. This study, conducted at the Timbó landfill in Santa Catarina,

Brazil, aims to estimate leachate generation and assess the impact of profile composition. The researchers used HYDRUS-1D to simulate unsaturated fluid flow through multiple layers. Soil matrix data and hydraulic properties were gathered from previous studies and pedotransfer functions. Data related to MSW properties were obtained from literature. Thirteen layers were simulated with boundary conditions, mimicking atmospheric variability on the top cover and free drainage at the profile's bottom for two hydrologic years (2017-2019).

The study found that HYDRUS-1D overestimated leachate volume by approximately 33.67% when compared to field measurements. The layer distribution exhibited an attenuation effect on leachate production, consistent with the landfill's design.

(Pontedeiro et al., 1987) compiles findings from three distinct studies conducted in Brazil utilizing HYDRUS-1D to evaluate different waste disposal sites. The first study focuses on predicting the long-term transport of radionuclides vertically through a landfill and the underlying unsaturated zone, followed by lateral transport in groundwater. This application pertains to a conventional mining installation containing naturally occurring radioactive materials (NORMs). The second study investigates water fluxes into and through a municipal solid waste (MSW) landfill in Rio de Janeiro, with a focus on two cover systems aimed at reducing percolation. One employs a capillary barrier made from MSW compost, while the other uses a vegetation cover with grass or native plants. The third application revolves around a near-surface repository holding 137Cs waste originating from the 1987 CsCl tele therapy source accident in Goiania. Long-term simulations were conducted to analyze the transport of 137Cs from the repository through the concrete liner beneath the waste and into the underlying vadose zone, affecting groundwater. These studies highlight HYDRUS-1D adaptability in addressing diverse waste-related challenges across different contexts and settings.

(Botros et al., 2012) conducted a study in-depth analysis of a deep vadose zone in an agricultural site. This involved extensive data collection and modeling to understand the storage of nitrate in the vadose zone. Surprisingly, despite differences in unsaturated flow patterns, all models produced similar estimates of nitrate storage for repeated water and fertilizer applications. However, these estimates were significantly higher than field measurements. The research suggests that the physical variability of deep vadose zones may not greatly affect the transport of pollutants applied to the surface. It also challenges our understanding of nitrate behavior in the

vadose zone and indicates the presence of an immobile moisture domain not explained by traditional models. This immobile domain must be considered in simulating nitrate transport in situations involving cyclical infiltration with gravitational flux.

2.5 Source Apportionment

(Machiwal & Jha, 2015) conducted a study in the Udaipur district to identify the sources of groundwater contamination in a hard-rock aquifer system, employing multivariate statistical analyses and GIS-based geostatistical modeling techniques. Their research utilized box-whisker plots to unveil associations between rainfall and groundwater quality, which were subsequently validated through the Groundwater Quality Index (GQI), ranging from 69 to 76 in Cluster I and 73 to 78 in Cluster II. Cluster analysis delineated two distinct site clusters based on groundwater contamination, primarily driven by geological factors. The study also revealed significant increasing trends ($p < 0.05$) in fluoride, sodium, electrical conductivity (EC), and total dissolved solids (TDS) at most sites, while a notable decrease in silica levels at 40% of the sites suggested the possibility of recent rainfall recharge replacing older groundwater. The spatial distribution of increasing trends was influenced by anthropogenic processes. The results of Principal Component Analysis (PCA) indicated that groundwater contamination in Cluster I was predominantly attributed to anthropogenic sources, whereas Cluster II exhibited a stronger presence of natural and geogenic processes. Key principal components, particularly those related to major ions and soil leaching pollution factors, played a pivotal role in shaping the overall geochemical processes.

In the study conducted in the Peenya industrial area of Bangalore, (Gulgundi & Shetty, 2016) set out to evaluate and compare three distinct models, namely APCS-MLR, Unmix, and PMF with the aim of apportioning the sources contributing to variations in groundwater quality. The research sought to provide insights into the appropriateness and efficacy of these models for this specific environmental context. To gauge the characteristics of these models, a regression analysis was performed, which involved comparing the parameters modeled by each approach against quantified values obtained from the study area. The outcomes were notably encouraging, with all three models demonstrating a substantial capacity to replicate the observed concentrations, particularly in cases with highly similar sources contributing to groundwater quality variations. Nevertheless, the APCS-MLR model emerged as the frontrunner, showcasing the strongest correlation and the closest alignment with unity. This highlighted the APCS-MLR model's

exceptional capability in accurately depicting and understanding the sources of groundwater quality variations in the challenging Peenya industrial area of Bangalore.

(Jiang et al., 2019) used a holistic approach to address nonpoint source pollution in Huaihe River, China. Their methodology combined various analytical tools to pinpoint the sources of NPS pollution in this critical region. Over a span of two years (2011-2012), they diligently monitored key water quality parameters, including NH3-N, COD, DO, and pH on a weekly basis at 27 monitoring stations. The study area was subject to a wide range of influences, both from human activities and natural factors. Their approach, guided by multiple correspondence analyses, highlighted that certain monitoring stations, such as 3, 9 and 21, exhibited distinct characteristics that set them apart from the rest. Hierarchical cluster analysis (HCA) further grouped all the monitoring stations into four distinct categories, providing valuable insights into the diversity of water quality issues in the Huaihe River. Utilizing positive matrix factorization (PMF) analysis, the research identified four distinct factors for each group across different seasons. These factors were closely linked to the primary causes of water quality deterioration, particularly associated with discharges from urban, agricultural, and industrial land uses. Notably, the study uncovered seasonal variations in NPS pollution, potentially influenced by natural processes such as changes in the hydrological regime. In summary, this research underscores the applicability of the PMF model in identifying nonpoint source pollution in surface waters and emphasizes the importance of addressing pollution from urban, agricultural, and industrial activities to enhance water quality within the Huaihe River basin.

References

Ahmed, S., Joshi, R., & Kumar, S. (2020). Seasonal variation of leachate quality at active landfill sites in Delhi, India. *Proceedings of the Institution of Civil Engineers: Municipal Engineer*, *173*(3), 157–170. https://doi.org/10.1680/jmuen.17.00039

Aljaradin, M., Persson, K. M., & Aboulila, T. S. (2011). Evaluation of the Cover Effect in Mafraq Landfill –Jordan Using Hydrus-2d Simulation. *Iwwg*, *13*(March), 581–582.

Anwar & Thien, 2015. (2015). Investigating Leachate Transport at Landfill Site Using HYDRUS-1D. *International Journal of Environmental Science and Development*, *6*(10), 741–745. https://doi.org/10.7763/ijesd.2015.v6.691

Aziz, H. A., Alias, S., Adlan, M. N., Faridah, Asaari, A. H., & Zahari, M. S. (2007). Colour removal from landfill leachate by coagulation and flocculation processes. *Bioresource Technology*, *98*(1), 218–220. https://doi.org/10.1016/j.biortech.2005.11.013

Babbar, P., Verma, S., & Mehmood, G. (2017). Groundwater Contamination From Non-Sanitary Landfill Sites – A Case Study on The Ghazipur Landfill Site, Delhi (India). *International Journal of Applied Environmental Sciences*, *12*(11), 1969–1991. https://doi.org/10.37622/ijaes/12.11.2017.1969-1991

Bhalla et al., 2013. (2013). Effect of Age and Seasonal Variations on Leachate Characteristics of Municipal Solid Waste Landfill. *International Journal of Research in Engineering and Technology*, *02*(08), 223–232. https://doi.org/10.15623/ijret.2013.0208037

Botros, F. E., Onsoy, Y. S., Ginn, T. R., & Harter, T. (2012). Richards Equation–Based Modeling to Estimate Flow and Nitrate Transport in a Deep Alluvial Vadose Zone. *Vadose Zone Journal*, *11*(4). https://doi.org/10.2136/vzj2011.0145

Gulgundi, M. S., & Shetty, A. (2016). Identification and Apportionment of Pollution Sources to Groundwater Quality. *Environmental Processes*, *3*(2), 451–461. https://doi.org/10.1007/s40710-016-0160-4

Haarstad, K., & Maehlum, T. (2008). Pesticides in Norwegian Landfill Leachates. *The Open Environmental & Biological Monitoring Journal*, *1*(1), 8–15. https://doi.org/10.2174/1875040000801010008

Jiang, J., Khan, A. U., Shi, B., Tang, S., & Khan, J. (2019). Application of positive matrix factorization to identify potential sources of water quality deterioration of Huaihe River, China. *Applied Water Science*, *9*(3), 1–14. https://doi.org/10.1007/s13201-019-0938-4

Kashitarash, Z. E., Taghi, S. M., Kazem, N., Abbass, A., & Alireza, R. (2012). Application of iron nanaoparticles in landfill leachate treatment-case study: Hamadan landfill leachate. *Journal of Environmental Health Science and Engineering*, *9*(1), 1–5.

Machiwal, D., & Jha, M. K. (2015). Identifying sources of groundwater contamination in a hard-rock aquifer system using multivariate statistical analyses and GIS-based geostatistical modeling techniques. *Journal of Hydrology: Regional Studies*, *4*, 80–110. https://doi.org/10.1016/j.ejrh.2014.11.005

Mohajeri, S., Aziz, H. A., Isa, M. H., Bashir, M. J. K., Mohajeri, L., & Adlan, M. N. (2010). Influence of Fenton reagent oxidation on mineralization and decolorization of municipal landfill leachate. *Journal of Environmental Science and Health - Part A Toxic/Hazardous Substances and Environmental Engineering*, *45*(6), 692–698. https://doi.org/10.1080/10934521003648883

Mor, S., Ravindra, K., Dahiya, R. P., & Chandra, A. (2006). Leachate characterization and assessment of groundwater pollution near municipal solid waste landfill site. *Environmental Monitoring and Assessment*, *118*(1-3), 435–456. https://doi.org/10.1007/s10661-006-1505-7

Mor, S., Ravindra, K., De Visscher, A., Dahiya, R. P., & Chandra, A. (2006). Municipal solid waste characterization and its assessment for potential methane generation: A case study. *Science of the Total Environment*, *371*(1-3), 1–10. https://doi.org/10.1016/j.scitotenv.2006.04.014

Naveen, B. P., Sivapullaiah, P. V, Sitharam, T. G., & Ramachandra, T. V. (2014). *LAKE 2014 : Conference on Conservation and Sustainable Management of Wetland Ecosystems in CHARACTERIZATION OF LEACHATE FROM MUNCIPAL LANDFILL AND ITS EFFECT*

ON SURROUNDING WATER BODIES. *November*, 1–9.

Pontedeiro, E. M., Ottoni, V., & Genuchten, M. T. Van. (1987). *HYDRUS-1D modeling applications to waste disposal problems in Brazil*. 1–12.

Ramaiah, B. J., Ramana, G. V., & Datta, M. (2017). Mechanical characterization of municipal solid waste from two waste dumps at Delhi, India. *Waste Management*, *68*, 275–291. https://doi.org/10.1016/j.wasman.2017.05.055

Sharma, K. D., & Jain, S. (2019). Overview of Municipal Solid Waste Generation, Composition, and Management in India. *Journal of Environmental Engineering*, *145*(3). https://doi.org/10.1061/(asce)ee.1943-7870.0001490

Singh, S., Janardhana Raju, N., & RamaKrishna, C. (2017). Assessment of the effect of landfill leachate irrigation of different doses on wheat plant growth and harvest index: A laboratory simulation study. *Environmental Nanotechnology, Monitoring and Management*, *8*, 150–156. https://doi.org/10.1016/j.enmm.2017.07.005

Singh, S., Malyan, S. K., Maithani, C., Kashyap, S., Tyagi, V. K., Singh, R., Malhotra, S., Sharma, M., Kumar, A., Panday, B. K., & Pandey, R. P. (2023). Microplastics in landfill leachate: Occurrence, health concerns, and removal strategies. *Journal of Environmental Management*, *342*(February), 118220. https://doi.org/10.1016/j.jenvman.2023.118220

Tripathi, A., Singh, A., & Minhas, C. M. (2021). Environmental Impacts of Ghazipur Landfill on its Surroundings. *International Research Journal of Engineering and Technology*, *8*(2). www.irjet.net

Waisczik, D. H. D. R., & De Lima, J. T. (2020). Leachate production estimation for a landfill in south of Brazil using Hydrus-1D. *E3S Web of Conferences*, *195*, 1–6. https://doi.org/10.1051/e3sconf/202019501016

Wowkonowicz, P., & Kijeńska, M. (2017). Phthalate release in leachate from municipal landfills of central Poland. *PLoS ONE*, *12*(3), 1–11. https://doi.org/10.1371/journal.pone.0174986

CHAPTER 3

Study Area and Data Used

3.1 Description of study area

The Gazipur Landfill site is one of the major Landfill sites located in East Delhi and is managed and operated by East Delhi Municipal Corporation (EDMC). The Location map showing the study area is given in

Figure & 3.2 below. The EDMC having a population of about 50 Lakh and about 10.5 lakhs households have a per capita waste generation rate ranging from 150 to 600 grams generate about 2700 tons of MSW per day, out of which about 2000 TPD (74%) is disposed in Gazipur Landfill (Delhi Economic Survey Report, 2020-2021). The Gazipur Landfill site is spread across 28 hectares having approximate dimensions of 680 m long and 360 m wide (Ramaiah et al., 2017). The site, situated approximately at coordinates 28°37'28.45"N and 77°19'39.05"E, was established in 1984 and spans an elevation range from 72 to 247 meters above mean sea level (Fig. 3.3 a). Its surroundings are characterized by the presence of Fish, Eggs, and Poultry markets to the north, the Hindon Canal to the east, residential areas to the south, and the Ghazipur Dairy Farm to the west. Additionally, numerous other buildings encircle the site (Tripathi et al., 2021). This geographic description offers a comprehensive view of the site's location and its immediate surroundings, providing context for its placement within the broader landscape (Tripathi et al., 2021). Many water bodies like Yamuna River, Hindon River, Hindon cut canal, Gazipur drain and Sanjay Lake are situated near to the site. The Dumpsite reached an approximate height of about 65 meters in 2019 and was having 14 million Tons of legacy waste(DPCC, 2021). During the physical survey of the Gazipur landfill site, it was discovered that the non-degradable fraction contained ferrous and non-ferrous metals, earthenware, construction and demolition waste, plastic, glass and ceramics. The biodegradable part contained paper, cardboard, poultry waste, slaughterhouse waste, fish market waste, leather, rubber etc. (Mor et al., 2006). In contrast to engineered sanitary landfills, the Ghazipur landfill does not have a liner system to prevent leachate from seeping

beneath the surface or a system for removing leachate from the waste mass and the site is necessarily categorized as an open dump. Due to lack of proper compacting equipment and improper site management the waste is simply unloaded at site without proper compaction and soil cover which leads to slope failures and tension cracks. Moreover, the site also contains hot loads like fuels, tires, chemicals, leaves, smolders etc. and due to sufficient air circulation, they lead to frequent surface and subsurface fires(*GHAZIPUR LANDFILL REHABILITATION REPORT*, 2017). As per district reports from the CGWB, the primary soil types in the study area include sandy, loamy, sand, sandy loam, and silty loam. However, this study reveals the prevalence of two distinct soil types: loam and clayey loam, classified under two hydrologic soil groups, as depicted in Figure 3.3b. The findings indicate that Lo5-2a, characterized by loamy soil, encompasses a

significant portion of the area, particularly in the eastern, northern, and southern sectors of the study area.

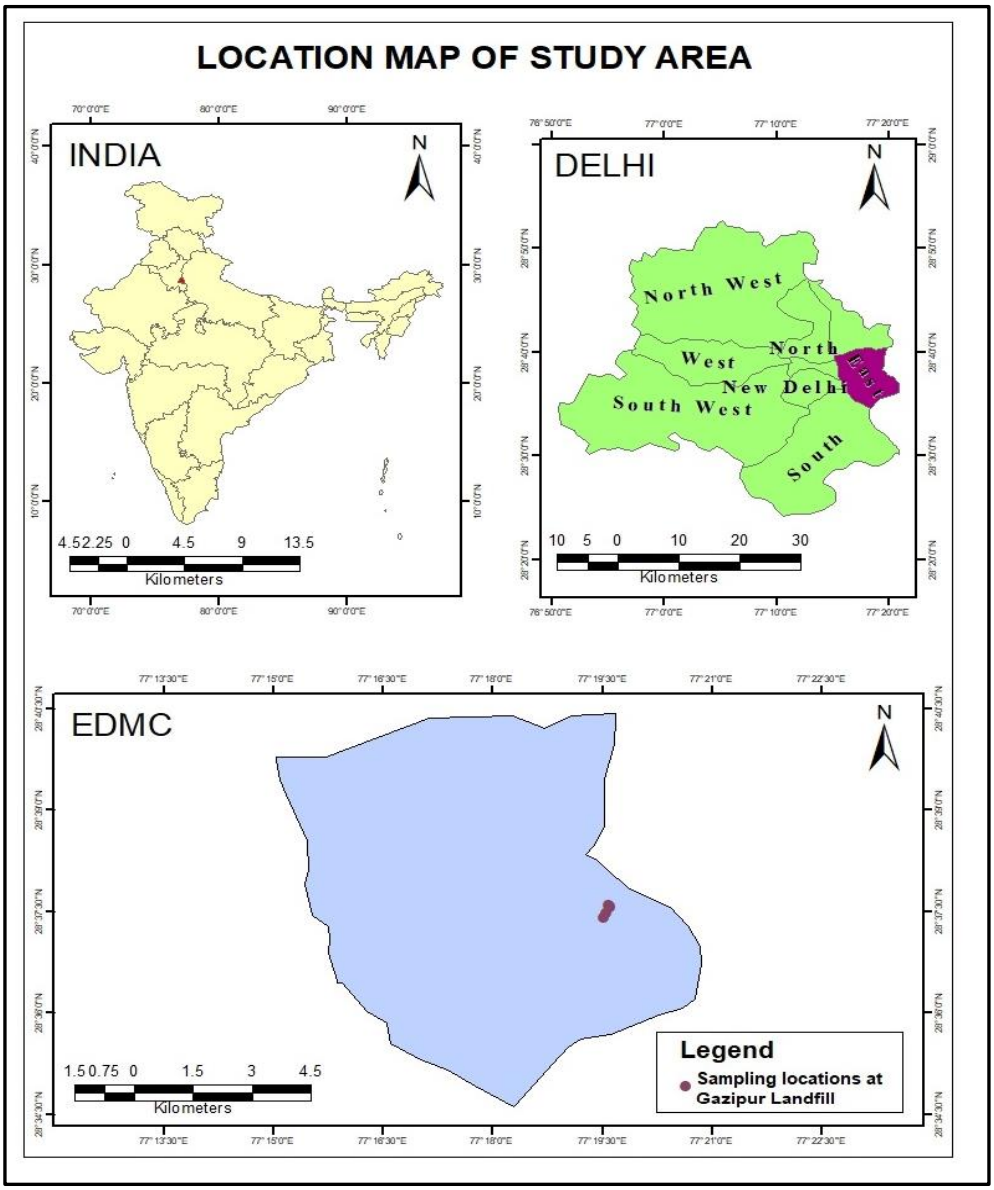

Figure 3.1: Description of study area

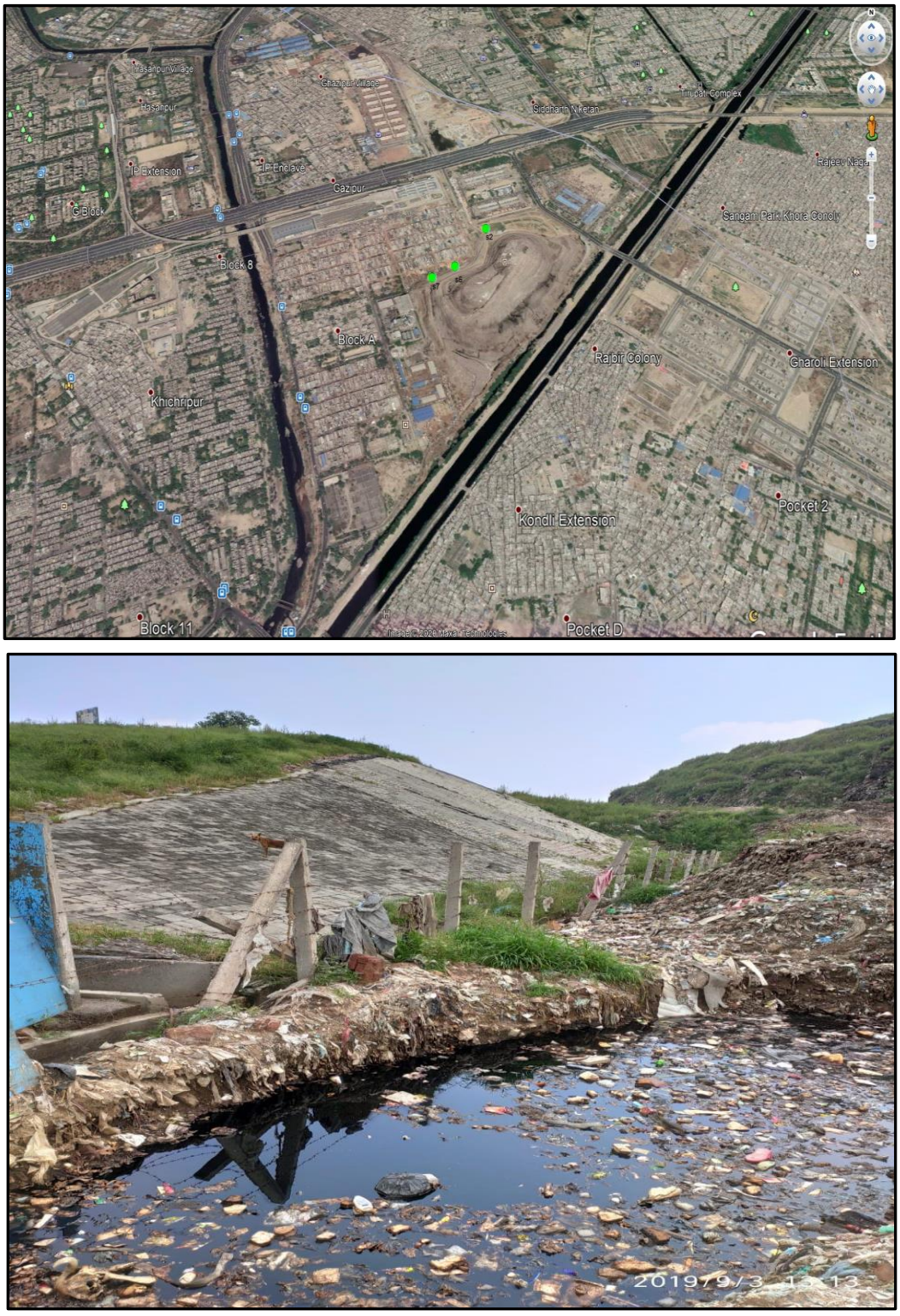

Figure 3.2: Location of Ghazipur landfill site, East Delhi & Leachate emerging from Ghazipur landfill

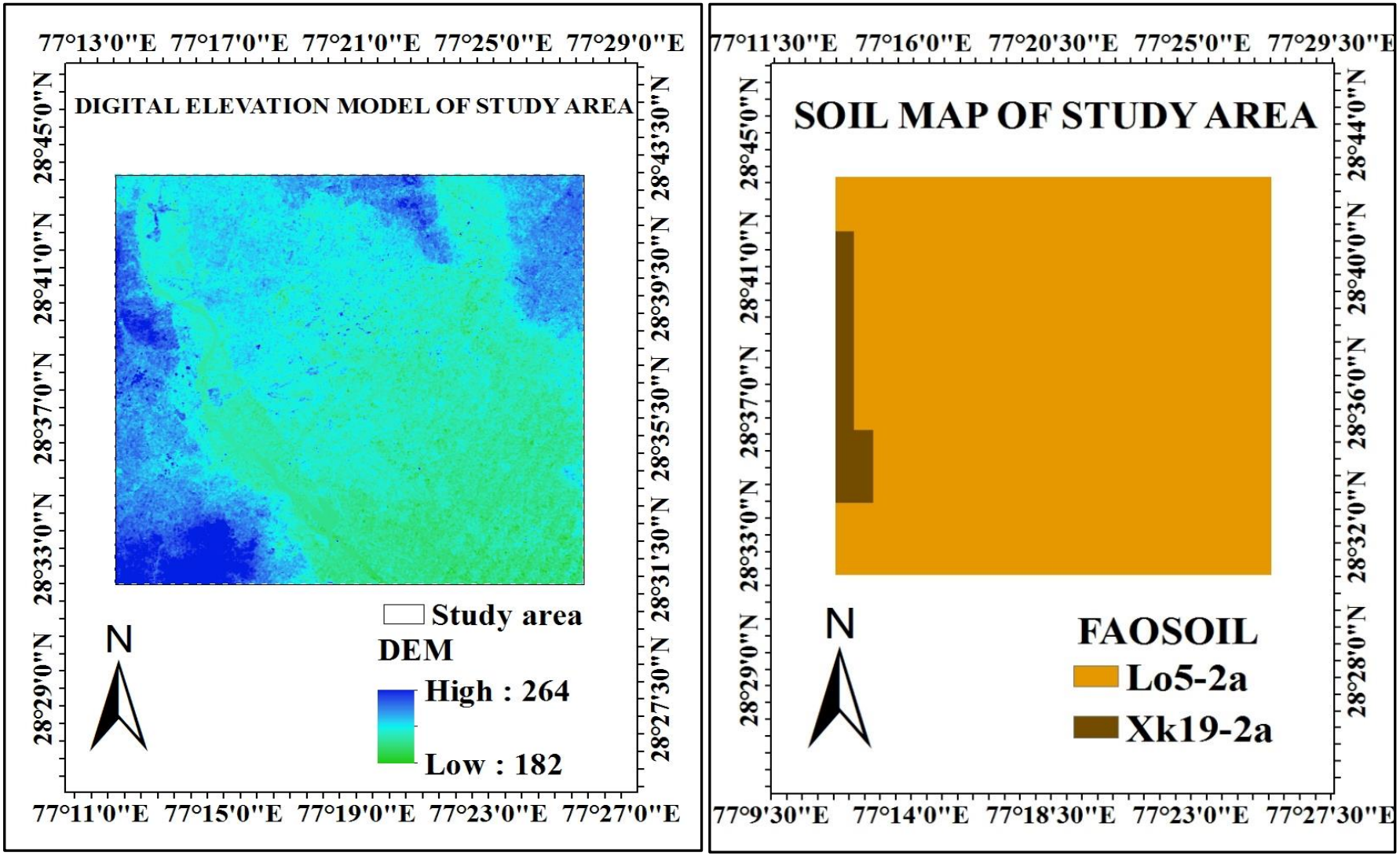

Figure 3.3 a) Digital Elevation Model & b) Soil Map of study area

3.1.1 Landuse Landcover

The results derived from the analysis of the land use/land cover (LULC) map of Ghazipur, Delhi, utilizing Landsat-8 data, reveal compelling insights into the region landscape dynamics. A significant area measuring 500.63 square kilometers denotes the urban expanse, constituting approximately 85.6% of the total land area. The significant urban expansion spans across all compass directions— eastern, western, northern and southern—indicating a widespread development and urbanization trend throughout the Ghazipur area (Fig 3.4).

In contrast, agricultural land usage has diminished, now occupying a mere 9.02% of the study area (Fig.3.4). This decline signifies a persistent trend of transitioning agricultural spaces toward alternative land uses, indicating a departure from conventional cultivation practices. These alterations may stem from diverse factors, including urban encroachment, evolving land-use policies, or economic diversification.

Water bodies, encompassing a modest 2.48% of the total area, assume crucial ecological significance and play pivotal roles in the region hydrology and environmental balance. Simultaneously, the categorization of barren land, covering 2.9% of the area, suggests areas with limited or no vegetation cover, potentially influenced by various land-use transformations or environmental variables (Fig 3.4).

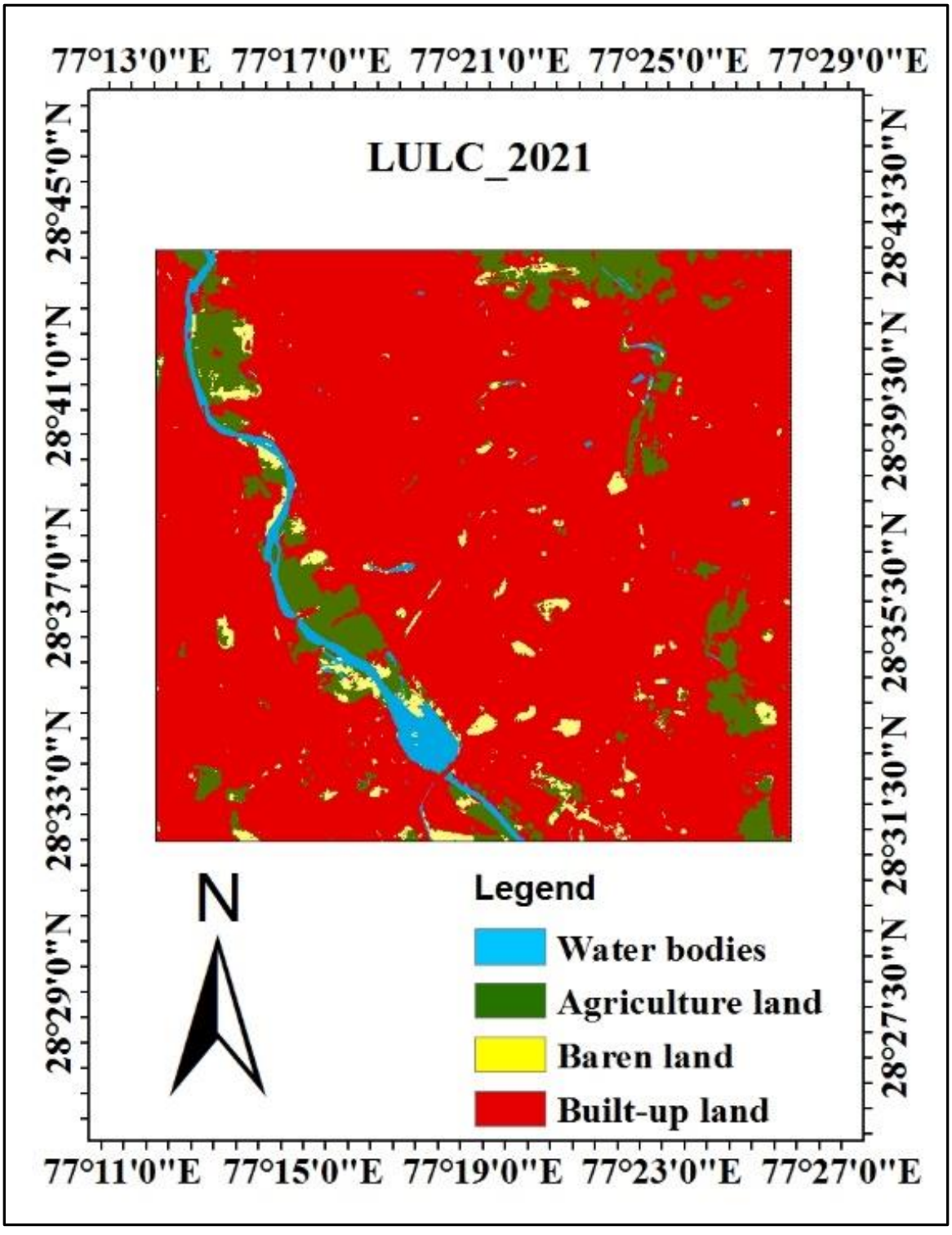

Figure. 3.4 Land use Land cover of the study area

3.1.2 Hydrogeological Frame-Work of Ghazipur Landfill Site

The study site displays a geological composition comprising alluvial formations at the surface and underlying quartzite hard rock situated around 100 meters below ground level (bgl). The movement and distribution of groundwater are primarily dictated by the hydrogeological characteristics of the site. Therefore, an intricate analysis of the landfill site's hydrogeology is imperative to comprehend the dynamics of leachate migration into the groundwater and its subsequent contamination. Over an extended period, leachate has been penetrating the subsurface strata at the Ghazipur landfill site. There is potential for uncontaminated aquifers in the vicinity, possibly attributed to the presence of a substantial clay layer or the existence of confined sources. The strata beneath the landfill site primarily comprise approximately 134 meters of quaternary alluvium, followed by weathered and fractured quartzite layers. To investigate the properties and nature of the aquifer material, the Central Ground Water Board (CGWB) has established numerous shallow and deep piezometers and exploratory tube wells within the Ghazipur SLF region. A comprehensive summary of the lithological details obtained from these CGWB-constructed piezometers, spanning both shallow depths (15 meters) and deeper levels (134 meters), has been compiled in Tables 3.1 and 3.2 for detailed analysis.
The analysis drawn from the lithological data is visually illustrated in the sub-surface geological cross-section (Figure 2). This cross-section provides a detailed depiction of the underground layers and their composition within the studied area.

It highlights a diverse mixture of fine and medium sand, alongside coarse hard kankar, extending to a depth of 50 meters below ground level (bgl). This composition suggests the possibility of a single aquifer system extending to this depth. However, within this sand composition, occasional thin layers of clay silt were identified at specific locations. Moreover, the presence of clay was predominantly noted below the 50-meter depth mark.

The delineation of three distinct aquifers becomes evident within specific depth ranges. These aquifers are demarcated by the presence of clay silt horizons. Separating these aquifers are layers characterized by a blend of silt with minor clay and kankar, contributing to the differentiation between the aquifer systems

Table 3.1: Detail of Aquifer Material (15m shallow piezometer of SLF)

SI.No	Location	Granual zones encountered (m bgl)	Lithology
1	SLF Office- 50m north of SLF site office	7-12	Sand
	North of SLF site office	12-15	Sand with Kankar
2	Poultry Farm-50 m	4-15	Silty clay with Kankars
3	Bio-gas plant-50 m	4.5-12	Sand with silt
	West to landfill border	12-15	Clay and Kankars

Table 3.2: Lithological Data of Fish Market, Ghazipur (134 m depth)

Depth range in m bgl	Thickness (m)	Lithological detail
0.00-14.45	14.45	Light yellow clay with minor coarse to gravel size kankar
14.45-21.35	6.9	Sand with clay silt admixed with fine sand and kankars
21.35-24.13	2.78	Gravel and kankar with minor silt and fine Sand
24.13-34.10	9.97	Silty clay with traces of kankar
34.10-41.89	7.79	Gravel with minor silt and fine sand
41.89-51.46	9.57	Sand fine-grained along with tracers of gravel
51.46-65.10	13.64	Clay with silt
65.10-131.55	66.45	Sticky clay
131.55-134.55	3	Gravel with fine sand

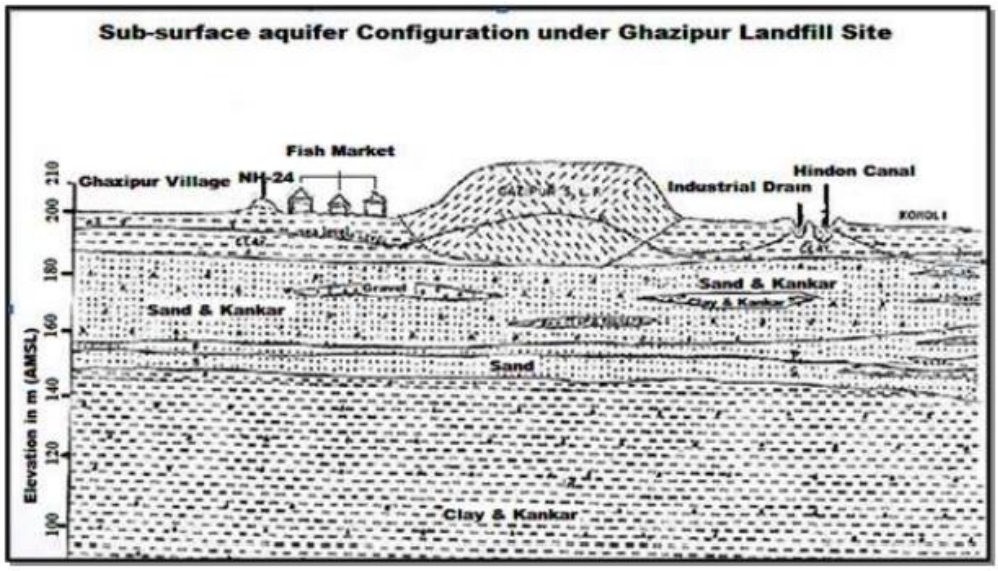

Figure 3.5: Sub-surface geological cross section of Ghazipur landfill (Source: (Babbar et al., 2017)

3.2 Drainage

The study area is encompassed within the drainage basins of several significant rivers, including the Yamuna, Hindon Cut Canal, and Hindon, along with their respective tributaries (Fig.3.6a) Additionally, Gazipur drains contribute to the drainage network within this region. The geomorphic map depicted below in Figure 3.6

3.2.1 Yamuna River

The Yamuna River courses through the eastern part of the Delhi area, exhibiting lateral movement along a north-south axis. Initially, its direction shifted steadily eastward and later westward, eventually being contained due to a depression caused by a north-south trending fault (Thussu, 2001). The right paleobank of the Yamuna is situated north of Delhi around Narela, curving almost perpendicular at Wazirabad and then tracing the ridge boundary further south (Thussu, 2001). In the northern region of Delhi, numerous paleochannels and abandoned river courses of the Yamuna contribute to the extensive alluvial floodplain flanking both sides of the river (Fig.3.6 b).

The Yamuna River serves as a critical water source for various industries in the region, encompassing textiles, paper, and chemical manufacturing. Here are key aspects highlighting the river significance in meeting the industrial demands of these districts:

Water Supply: The Yamuna river provides a significant amount of water for industrial activities in Gazipur Delhi. The river water is used for various purposes such as cooling, processing, and washing. Industries that are located near the river have easy access to this critical resource.

Wastewater Disposal: Industries generate a significant amount of wastewater, which needs to be treated and disposed of appropriately. The Yamuna river provides an outlet for industrial wastewater, which is treated to meet the environmental standards before being discharged back into the river.

Transportation: The Yamuna river is an important transportation route for industries located in the study area. Industries can transport raw materials and finished goods using the river, reducing transportation costs and improving supply chain efficiency.

Power Generation: The Yamuna river is also used for generating hydroelectric power, which is a clean and renewable source of energy. Industries located near the river can benefit from this power source, reducing their reliance on traditional sources of energy.

However, it is essential to ensure that the industrial use of the Yamuna river is sustainable and does not have a detrimental impact on the environment or the local communities. Industries must comply with the environmental regulations and take steps to minimize their impact on the river's ecological health. The Yamuna river is a vital resource for meeting the industrial demand of the region, and it is crucial to protect and conserve this resource for future generations.

3.2.2 Hindon River

The river Hindon enters southeast of the village of Tavelagarhi in the Binauli block and forms the eastern boundary between the districts of Baghpat and Meerut. Its flood plains are highly developed. The banks are steep and have ravines in its lower reaches it almost flows through the flood plains of river Yamuna (Fig.3.6 b).

The Hindon River is a significant river in the industrial districts of western U.P region, flowing through the districts of Ghaziabad and Meerut. The river originates in the Saharanpur district and flows into the Yamuna river near Noida. The Hindon river has ecological, social, and economic importance in the area. Here are some of the key reasons why the Hindon river is important in this region:

Ecological Importance: The Hindon river is a vital ecosystem in the region and supports a diverse range of flora and fauna. The river provides a habitat for various aquatic and bird species, including some rare and endangered species. The river's catchment area also supports a range of vegetation that is essential for maintaining the ecological balance of the region.

Water Supply: The Hindon river is a crucial source of water for various activities in the region, including irrigation, drinking, and industrial uses. The river's water is used for agriculture, fisheries, and other industries, which contribute significantly to the economy of the region.

Groundwater Recharge: The Hindon river also helps in recharging the groundwater in the region. The river's water percolates into the ground, replenishing the groundwater resources that are essential for agriculture and other activities.

Flood Control: The Hindon river helps in mitigating the risk of floods in the region. The river's catchment area acts as a natural sponge, absorbing excess rainfall and reducing the risk of flooding in downstream areas.

Cultural Importance: The Hindon river also has cultural and historical significance in the region. The river flows through several historical sites, including the Ghaziabad Fort and the Dargah of Hazrat Shah Alam. The river is also considered sacred by the local communities, who hold various religious ceremonies and rituals on its banks.

The Hindon River also plays an essential role in meeting the industrial demand of the Ghaziabad and Gautam Buddha Nagar districts. Industries located in these areas use the river's water for various purposes, such as cooling, processing, and washing. Here are some of the ways in which the Hindon River is important in meeting the industrial demand of these districts. Despite its importance, the Hindon river is facing significant challenges, including pollution and encroachment. Industries located near the river often discharge untreated wastewater into the river, which can harm the river's ecosystem and affect the water quality. The encroachment of the river banks and the destruction of the river's catchment area is also leading to the degradation of the river's ecosystem. It is essential to protect and conserve the Hindon river, ensuring that it can continue to provide ecological, social, and economic benefits to the region.

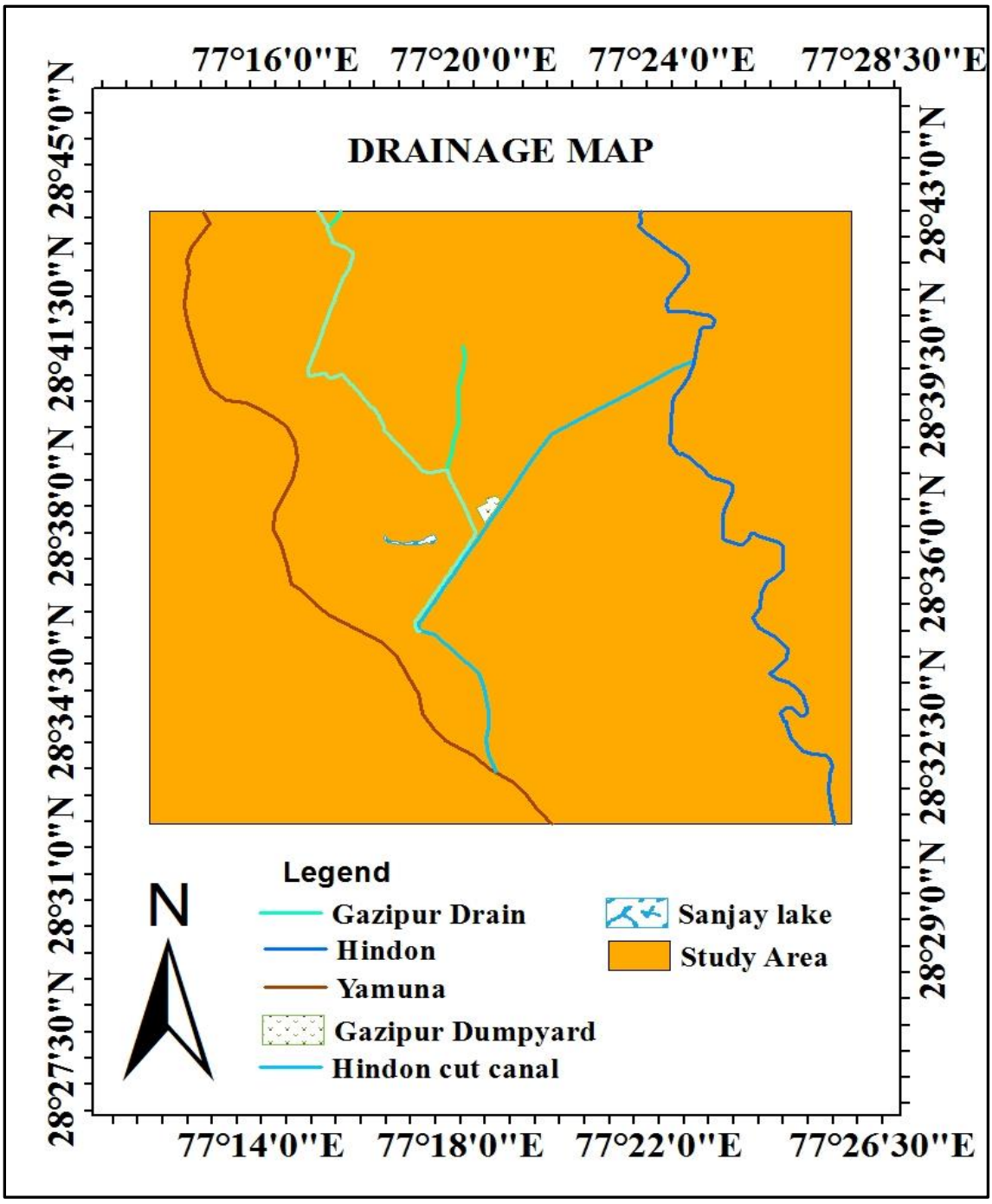

Figure. 3.6 a) Drainage Map of the study area

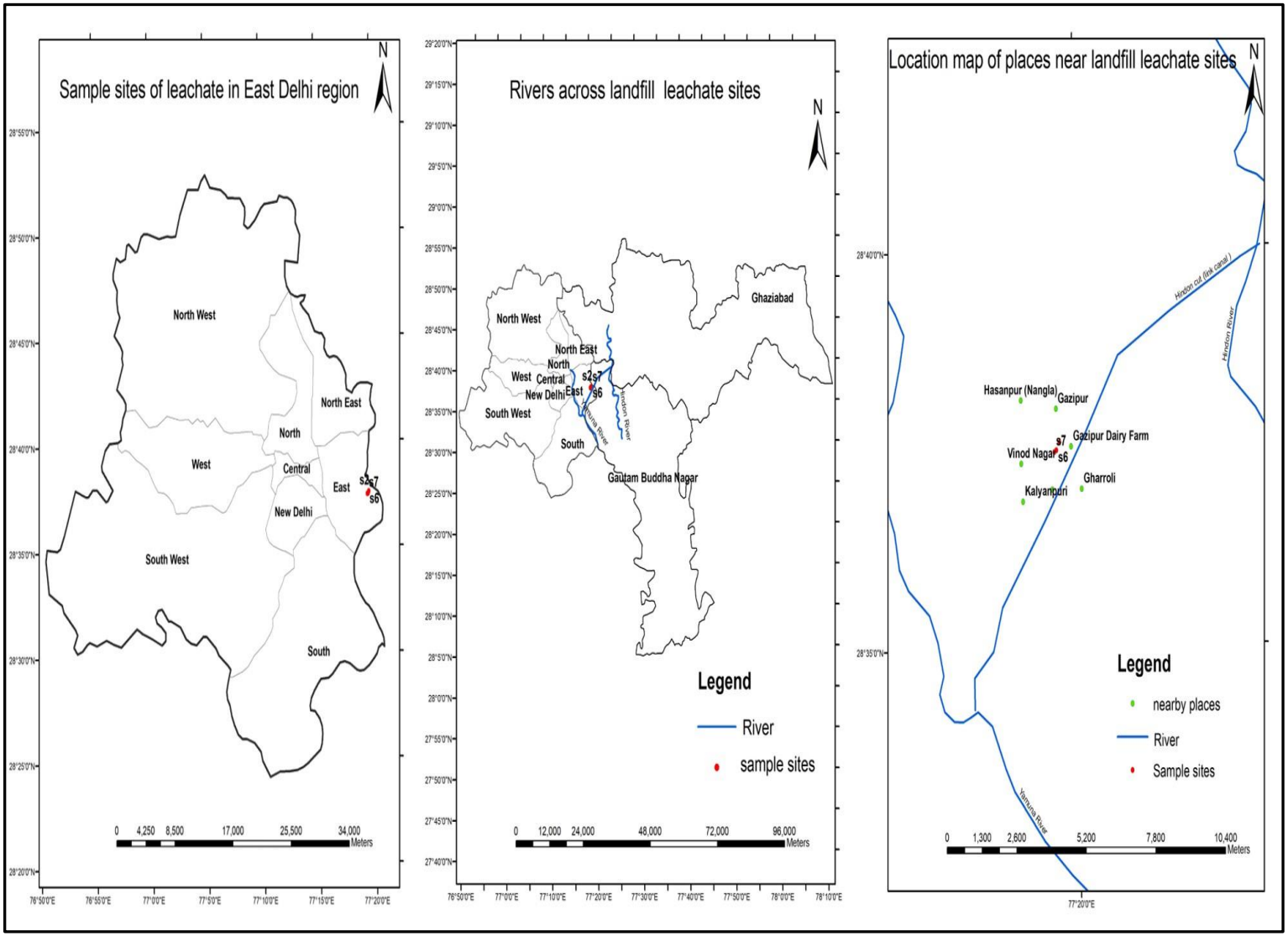

Figure 3.6 b) Location maps of nearby places and rivers in proximity of landfill site

3.3 Lakes and Pond

Ghazipur in East Delhi are home to several lakes and ponds that are important surface water resources in the region. Here are some of the major ones:

Sanjay Lake: This lake is located in the Sanjay Nagar area and is home to several species of birds and fish. It is also a popular spot for picnics and boating (Fig 3.7).

Boating lake: The Gazipur Boating Lake, situated in Delhi, represents an ecosystem supporting various avifauna and aquatic species (Fig 3.8).

Khora Pond: The Khora pond is situated in the Khora Colony area of Gazipur, Delhi. It is an important water body within this locality, serving various purposes such as supporting local ecology, providing a water source, and potentially serving as a recreational area for nearby residents (Fig 3.10).

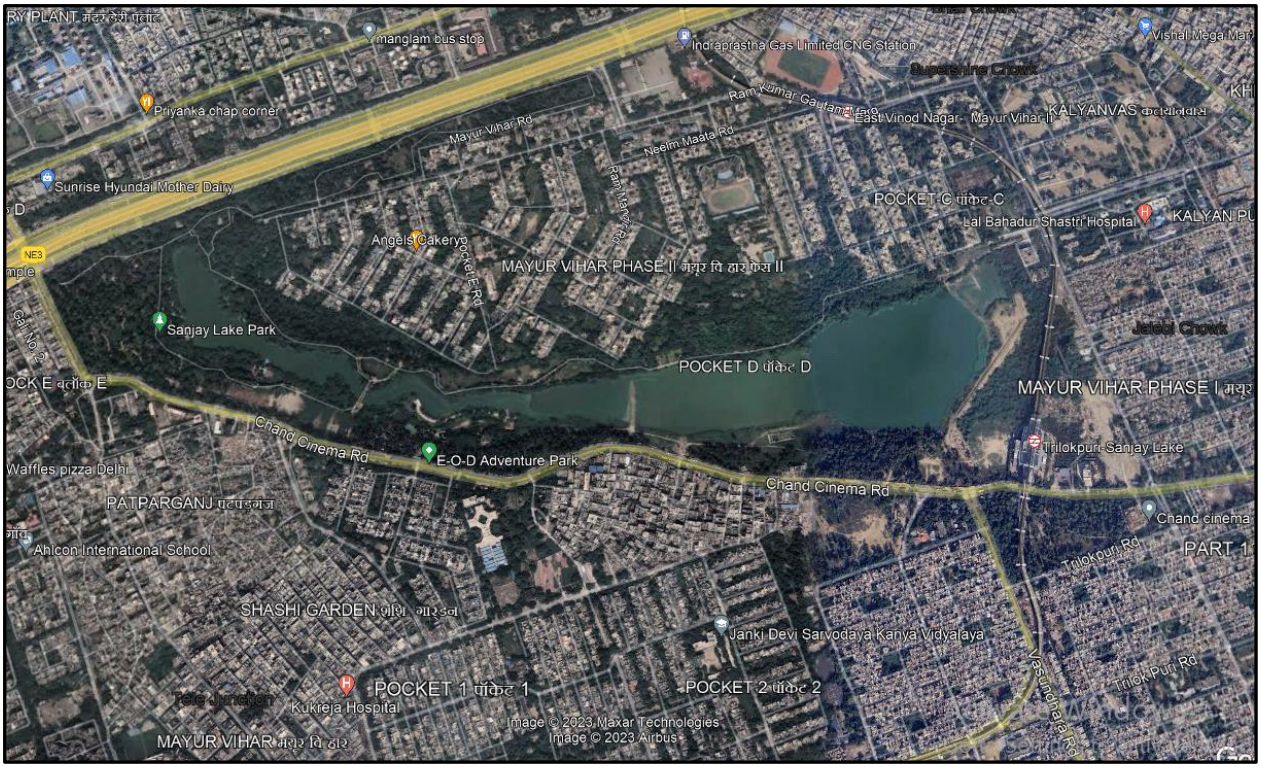

Figure 1.7 Sanjay lake in Gazipur, Delhi

Figure 3.8 Boating Lake in Gazipur, Delhi

3.4 Wetland:

- The wetland in Sector 77 Noida, Uttar Pradesh Gazipur, Delhi, offer vital ecosystems supporting diverse flora and fauna. These areas, characterized by their waterlogged conditions, are critical for maintaining ecological balance, serving as habitats for various migratory birds and indigenous species. Wetlands also play a crucial role in water purification, flood regulation, and groundwater recharge, contributing significantly to the region's environmental health and sustainability.
- The Wetland in Nyay Khand I, Indirapuram, Ghaziabad, Uttar Pradesh, This wetland acts as a natural sponge, absorbing excess rainwater, aiding in flood control, and enhancing groundwater recharge (Fig. 3.9).

Figure 3.9 Wetland in Nyay Khand I, Indirapuram, Ghaziabad, Uttar Pradesh

Figure 3.10 : Khora Pond located in the study area

Chapter 4: Chemical characterization of Landfill leachate and groundwater surrounding Ghazipur

4.1 Methodology approach

The overall approach followed to achieve the objectives is shown in figure 4.1. Primarily, literature review was done specifically on landfill leachate characteristics. The leachate data was collected from EDMC (East Delhi Municipal Corporation) report, and various research articles of journals such as International journal of advanced research and innovation, Environmental claims journal, Bioresource technology reports, SAGE journal etc. The data was then compiled and assessed further. Also, the leachate characterization was done from the landfill sampling sites 1, 2,3,4,5, 6 and 7. The assessment was based on how each parameter in leachate is exceeding the permissible discharge limits. The major parameters that were focused included organic constituents, inorganic constituents and metal constituents. An experiment was performed in order to determine the color, chemical oxygen demand, and total organic carbon present in leachate sample. Secondly, a decolorization experiment was conducted in order to remove the color from the leachate. Further, after decolorization the efficacy of color removal, COD and TOC removal were estimated. The parameters such as COD and TOC represents the organic matter present in leachate. Therefore, decolorization can be referred as one of the treatment techniques for organic matter removal. The treatment method adopted for this study was coagulation- flocculation method using $FeCl_3$ as a coagulant and advanced oxidation technique using Fenton reagent. Both the techniques were compared in terms of efficiency towards color and above parameters removal. The experiment was conducted at pH range 3-7 for both the processes. The experiment conducted to achieve decolorization of landfill leachate is expressed in figure 4.3. Then correlation analysis was done to check the strength of relationship between pH and percentage of color, COD and TOC removal. This was done to analyze the effect of pH on constituent's removal rates. Therefore, spearman correlation coefficient was calculated by using Minitab 18.0. Thirdly, human health risk assessment was carried out in order to analyze the impact of groundwater contaminated with leachate. Leachate percolation is a major environmental issue in case of landfill that are devoid of any type of single/ double liner system. If this leachate enters the surface or groundwater body, then it can constitute an adverse impact on human health as well as ecology of a particular area. Therefore, a temporal analysis of HHRA (Human health risk assessment) was done to assess the variation in risk to human health

which is caused by Ghazipur landfill leachate. The risk was calculated for both the age groups i.e. child and adult. The risk estimation approach followed for Ghazipur leachate is shown in figure 4.2. Firstly, the leachate data comprising heavy metal constituents such as lead, cadmium, chromium and nickel was collected from the year 2003 to 2019. Then in order to estimate the impact of leachate on groundwater, a hypothetical assumption of leachate spillage in 1:100 dilution was done. The dilution factor of 1:100 tend to be a good estimate as when the toxic leachate mixes with groundwater, then its constituents will also be applied to dilution (Christensen et al., 2001). Similar assumptions with 1:100 dilution factor was made for the same landfill by Ghosh et al, 2015. Secondly, chronic daily intake (CDI) was calculated in a year wise manner. This value determines the daily consumption of contaminated water. Further risk due to consumption of groundwater from the wells situated nearby landfill area is calculated by slope factor value. This value estimates the risk of having cancer due to exposure to a toxic contaminant. Therefore, cancer risk was evaluated by using chronic daily intake and slope factor values. The carcinogenic risk was compared for both the age groups i.e. child and adult. The comparison was made in order to determine the vulnerability of either of the age groups. The purpose of this study includes the variation of risk in a year wise manner and how it changes. Also, it was also analyzed that which metal is more accountable for posing risk to human health in the following years.

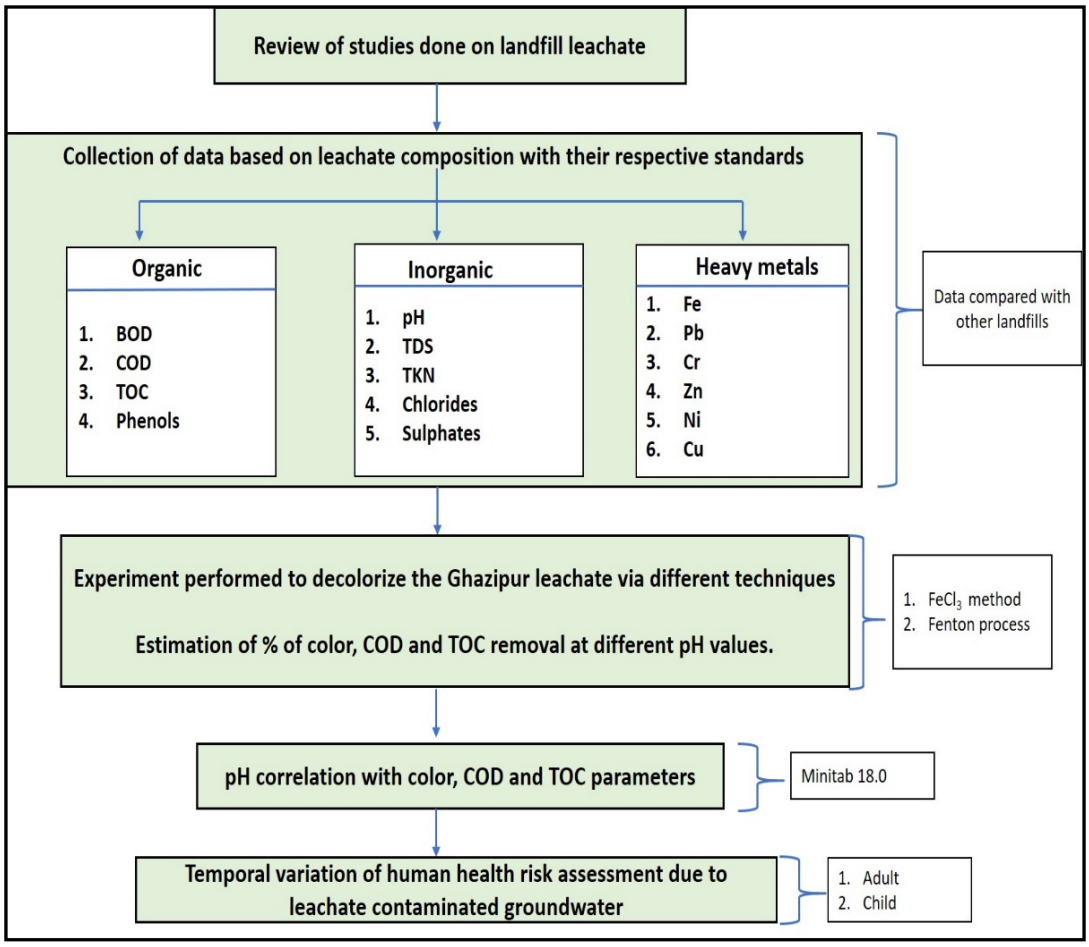

Figure 4.1: Outline of methodology

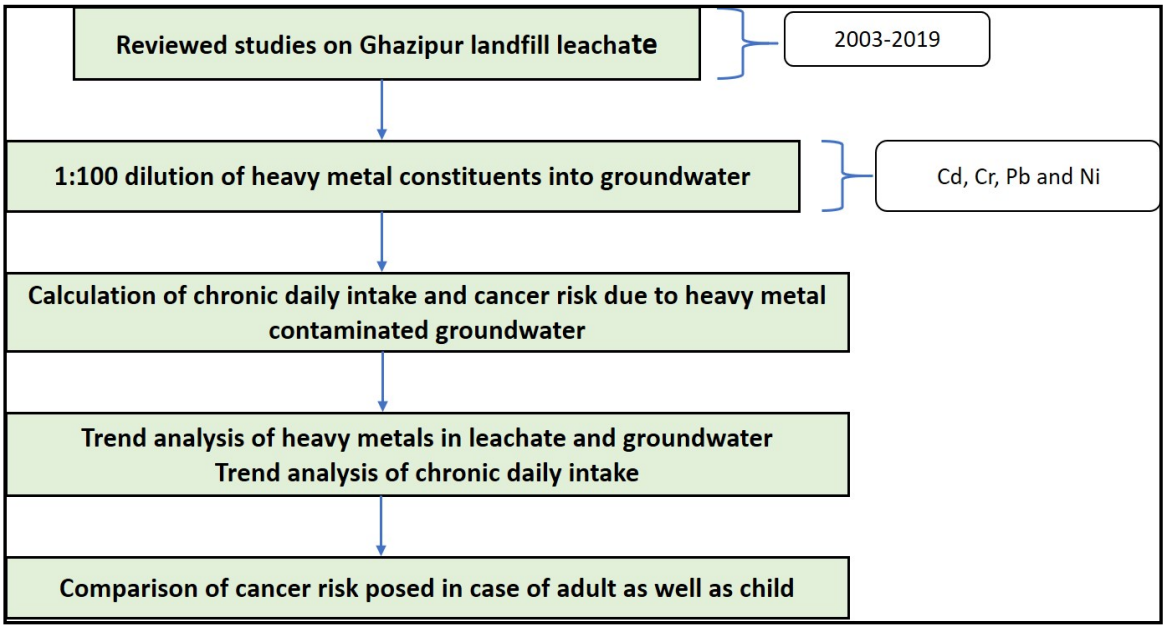

Figure 4.2: Outline of risk methodology

Figure 4.3: Brief representation of decolorization experiment

4.1.1 Leachate characterization

4.1.1.1 Sample Collection and preservation

Sampling objective is to collect a part of material that is small enough to be conveniently carried yet big enough for analytical purposes, while still properly reflecting the sampled material. This aim indicates that the relative proportions or concentrations of all key components will be the same in the samples as they are in the substance being sampled, and that there will be no major compositional changes prior to testing. Before sending a sample to a laboratory for examination, it is the responsibility of the sampler to gather a valid and representative sample. Because it's becoming more important to make sure that data is accurate and representative, more attention is being paid to the right ways to collect, track, and store samples.

Procedure

Discrete grab samples were obtained from the stream of leachate running down the depth of the landfill to provide a spatial and temporal picture of the sampling area. The collected samples are shown in Fig 4.4 below. A record was kept for each sample collected by affixing a label with the relevant information to the sample containers and noting the sample identification number, date, precise location of sample collection, sample type, and collector's name. The summary of sampling is listed in Table 4.1 below(“APHA,” 2012).

Table 4.1: Sampling Summary

Sl. No.	Determination	Container	Minimum Sample Size mL	Sample Type	Preservation	Maximum Storage Recommended	Regulatory
1	BOD	Glass	1000	Grab	Cool, 6^0C	6 h	48 h
2	COD	Polyethylene Plastic	100	Grab	Add H_2SO_4 to pH<2; Cool, 6^0C	7 d	28 d
3	Chloride	Polyethylene Plastic	50	Grab	Not required	-	28 d
4	Nitrate	Polyethylene Plastic	100	Grab	Analyze as soon as possible; Cool, 6^0C	48 h	48 h
5	pH	Polyethylene Plastic	50	Grab	Analyze immediately	0.25 h	0.25 h
6	EC	Polyethylene Plastic	50	Grab	Analyze immediately	-	-

Figure 4.4: Collected leachate samples

4.1.1.2 pH analysis

pH is an indicator of hydrogen ion activity in a solution, which is expressed as $-\log_{10}a(H^+)$, where $a(H^+)$ is the activity of the hydrogen ions(*HACH HQ11d Portable Meter User Manual*, 2020). Basically, it represents the intensity of acidity("APHA," 2012). pH is a test that is commonly used in water chemistry and is considered one of the most important tests. In landfill leachates also many processes depend on pH.

Method used

In this study the measurement of pH is done by United States Environmental Protection Agency (US EPA) Electrode method which is based on standard method 4500-H^+B("APHA," 2012) using Hach HQ11d portable meter(*HACH HQ11d Portable Meter User Manual*, 2020) as shown in fig. 4.5 below. In this method an electric potential is developed at the glass/liquid interface at a

constant temperature and the pH of the solution follows a linear relationship with this potential which is ultimately used to measure the pH of the solution.

Apparatus required

Hach HQ11d portable meter, glass beakers, wash bottle with deionized water and pH buffer solutions having pH values 4, 7 and 10.

Procedure

First of all, calibrate the instrument by using pH buffer solutions and store the results. After calibration rinse the probe with deionized water and dry it using lint free cloth. Take the sample in beaker and put the probe in it, remove the air bubbles and push read button on the instrument. Result for pH of the leachate sample is obtained on instrument screen once the reading becomes stable.

Figure 4.5: Portable pH and EC meter

4.1.1.3 Electrical conductivity analysis

The conductivity of a solution determines how well it can carry an electric current. Ions determine this ability through their mobility, valence, and total concentration. The temperature of measurement also affects it. Conducting ions are derived from inorganic dissolved solids, so most inorganic compounds in aqueous solutions act as good conductors. Alternatively, organic chemical solutions have very low conductivity due to their inability to dissociate into ions in aqueous solutions("APHA," 2012; *HACH HQ11d Portable Meter User Manual*, 2020).

Method used

In this study the measurement of pH is done by United States Environmental Protection Agency (US EPA) direct measurement method which is based on standard method 2500-B("APHA," 2012) using Hach HQ11d portable meter with conductivity probe(*HACH HQ11d Portable Meter User Manual*, 2020). The physical design of the conductivity probe is defined in such a way that in this method an electric potential difference is applied between the electrodes and due to the electrical resistance of the solution a decrease in voltage occurs which is measured by the instrument to give us the conductivity of solution for each centimeter.

Apparatus required

Hach HQ11d portable meter with conductivity probe, 100 mL polypropylene beaker, wash bottle with deionized water and standard KCl conductivity solution having conductivity 1413 S/cm at 25 ^{o}C.

Procedure

First of all, calibrate the instrument by using standard conductivity solution and store the results. After calibration rinse the probe with deionized water and dry it using lint free cloth. Take the sample in beaker and put the probe in it, remove the air bubbles and push read button on the instrument. Result for conductivity of leachate sample is obtained on instrument screen once the reading becomes stable.

4.1.1.4 Biochemical oxygen demand (BOD) analysis

Biochemical oxygen demand (BOD) analysis is performed to determine the relative oxygen requirements of polluted wastewaters and industrial effluents. BOD analysis measures the oxygen demand to biochemically degrade the organic matter, to oxidize inorganic materials and

to meet the nitrogenous oxygen demand by incubating the test sample for a specified period. The ultimate BOD measures the oxygen required to completely degrade the organic matter and the ultimate nitrogenous demand. To measure the carbonaceous BOD separately to interference of nitrogenous BOD is removed by addition of inhibitor chemical during analysis. The measurement of BOD is generally done for 5 days and for it the sample is incubated at a temperature of 20^0C for 5 days and measuring the change in dissolved oxygen before and after incubation("APHA," 2012). Samples collected for BOD analysis must be analyzed with 2 hours of collection but if distance between laboratory and sampling site is more than we can preserve the samples at less than 6^0C and should begin the analysis within 6 hours of sampling.

Method used

In this study the BOD measurement is done by respirometry method using Oxitop measuring system which gives us BOD values by pressure measurement via piezoresistive electronic pressure sensors. The temperature of the sample should be between 15^0C to 20^0C to measure the BOD by this method.

Apparatus required

The apparatus required are Oxitop measuring system, inductive stirring system, Incubator (temperature 20^0C1K), brown sample bottles (nominal volume 510ml), stirring rods, stirring rod remover, suitable overflow measuring beakers, rubber quivers, nitrification inhibitor (allylthiourea) and sodium hydroxide.

Procedure

First of all, estimate the range in which BOD of the sample is expected to fall, then according take the sample volume for analysis according to the Table 4.2 given below:

Table 4.2: Sample volume and multiplication factor for BOD analysis

Sample Volume(ml)	Measuring range (mg/l)	Factor
432	0-40	1
365	0-80	2
250	0-200	5
164	0-400	10
97	0-800	20
43.5	0-2000	50

After deciding the sample volume, wash and rinse the brown BOD bottle in which samples are to taken. Now exactly measure the sample volume using overflow measuring beakers and put them in BOD bottles. After taking the sample, add nitrification inhibitor, put the magnetic stirrer in the bottle, place the rubber quiver in the neck of bottle and put 2 NaOH tablets into the rubber quiver with the help of tweezers. Now tightly screw Oxitop directly on the sample bottle and place the bottle in the incubator at 20^0C for 5 days. During 5 days of incubation the sample is continuously stirred and the Oxitop automatically stores the daily BOD every 24 hours. After 5 days take out the bottles and note down the BOD value displayed on the Oxitop display. The final result of BOD is obtained by multiplying the displayed value by the multiplication factor as shown in table above(*Oxitop Manual*, 2008).

4.1.1.5 Chemical oxygen demand (COD) analysis

Chemical Oxygen Demand (COD) analysis is performed to analyze the strength of polluted wastewaters and leachates. COD measures how efficiently water consumes oxygen during the chemical decomposition of organic matter and the oxidation of inorganic substances such as ammonia and nitrate. By definition COD refers to the amount of an oxidant reacting with the leachate sample under controlled conditions then this amount of oxidant consumed is expressed in terms of its oxygen equivalent(“APHA,” 2012). The COD value is always greater than BOD value because of the fact that more oxygen equivalents can always be decomposed by chemical action as compared to microbial action(Abdul Syukor et al., 2021). The factors affecting COD test are digestion time, reagent strength and extent of pollution of sample(“APHA,” 2012).

Method used

In this study open reflux method("APHA," 2012) is used for determining COD of Leachate samples. This method is based on the principle of refluxing a highly acidic solution having excess potassium dichromate($K_2Cr_2O_7$) concentration and measuring the remaining unreduced $K_2Cr_2O_7$ by titrating the solution with ferrous ammonium sulfate which ultimately gives us the consumed amount of $K_2Cr_2O_7$ and hence the COD is calculated in terms of oxygen equivalents.

Apparatus and chemicals required

Reflux apparatus consisting of COD tubes, heating block and air condensers, pipets, volumetric flasks, Erlenmeyer flasks, burette with burette stand, funnel, stirring rods, measuring cylinder, analytical balance, desiccator, Ferroin indicator solution, Mercuric sulphate ($HgSO_4$) powder, technical grade Ag_2SO_4 powder, conc H_2SO_4, primary standard grade dried $K_2Cr_2O_7$, Ferrous ammonium sulfate.

Reagents preparation

The standard methods followed for preparing the reagents were adopted from APHA, 2012.

Standard potassium dichromate solution (0.04167M):

Add 12.259 g $K_2Cr_2O_7$ to distilled water and make the solution volume 1000 ml.

Sulfuric acid reagent:

Add 5.5 g Ag_2SO_4 powder per kilogram of conc H_2SO_4 and keep it for 2 days to dissolve.

Standard Ferrous ammonium sulfate (FAS) titrant (0.25M):

Add 98 g $Fe(NH_4)_2(SO_4)_2 \cdot 6H_2O$ and 20 mL conc H_2SO_4 to distilled water and allow it to cool. Now dilute the solution to 1000 mL.

Standardization of Ferrous ammonium sulfate (FAS) titrant:

Add earlier prepared standard potassium dichromate solution to distilled water and make up the solution to 100 mL then add 30 mL conc H_2SO_4 and allow to solution to cool. Titrate this solution against FAS to be standardized using 2 to 3 drops of ferroin indicator. Now find the molarity of FAS solution using the relation("APHA," 2012):

Molarity of FAS Volume of FAS used, mL = Volume of 0.04167M $K_2Cr_2O_7$ solution titrated, mL 0.2500

Procedure

Pipet out 50 mL of each sample in different COD tubes and same amount of distilled water in another COD tube. Add 1 g $HgSO_4$ powder to each tube. Slowly add 5 mL sulfuric acid reagent to each tube with continuous mixing so that $HgSO_4$ gets dissolved. Add 25 mL standard $K_2Cr_2O_7$ solution to all tubes and mix. Place all the tubes on heating block of refluxing unit and add 70 mL sulfuric acid reagent to each tube. Attach air condensers to all tubes and allow the solutions to reflux for 2 hours at 150^0C as shown in fig 4.6 below. After refluxing let the solutions cool to room temperature. Now titrate excess $K_2Cr_2O_7$ against FAS using 2 to 3 drops of ferroin indicator. During titration when color of solution sharply changes from blue-green to reddish brown for the first time, end point of titration is reached. Finally calculate the COD of samples using the following relation:

In this relation, is mL of FAS used during titration of sample, is mL of FAS used during titration of blank and is the molarity of FAS as found during standardization.

Figure 4.6: COD samples digestion in laboratory

4.1.1.6 Chloride analysis

Anions such as chloride (Cl^-) having high mobility make up the majority of inorganic anions in wastewater("APHA," 2012; Kohn et al., 2016). In Municipal solid waste, chloride constitutes 0.1 to 0.7% of the mass of which about 40% can leach out. Chemically, chloride does not undergo any biological changes or bind to medium material. It infiltrates similar to groundwater. Hence chloride is used as a tracer to predict hydrological pathways, trace contaminant plume movement and many other similar applications(Haarstad & Mæhlum, 2007; Kohn et al., 2016). In landfill leachate, chloride is the most significant component of total dissolved solids, if its concentration is high than the process of converting waste to energy in waste to energy plants is hampered significantly. In many cases, chloride percolates through the soil near the landfill and can cause surface salt formation and a rise in soil alkalinity, which in turn causes soil loss(Chen et al., 2017).

Method used

In this study Argentometric method("APHA," 2012) is used for the determination of chloride concentration in leachate samples. This method is based on the principle that when a sample containing chloride is titrated against standard silver nitrate solution using potassium chromate as indicator, quantitative precipitation of silver chloride precedes the formation of red silver chromate and the end point of titration is indicated by a sharp change in color.

Apparatus and chemicals required

250 mL Erlenmeyer flasks, 50 mL burette along with stand, pipet, measuring cylinder, funnel analytical balance, potassium chromate indicator, $AgNO_3$ powder, NaCl.

Reagent preparation

The standard methods followed for preparing the reagents were adopted from APHA,2012.

Standard silver nitrate titrant solution (0.0141M):

Add 2.395 g $AgNO_3$ to distilled water and dilute the solution to 1000 mL while dissolving. Standardize this solution against NaCl before using it for titration.

Standard sodium chloride (0.0141M or 0.0141N):

Add 824.0 mg NaCl to distilled water and dilute the solution to 1000 mL while dissolving.

Procedure

Take 100 mL leachate sample in an Erlenmeyer flask and add 1 mL potassium chromate indicator to it. Now titrate it against standard silver nitrate solution till a consistent color change to a pinkish yellow end point occurs. Standardize the $AgNO_3$ titrant solution and evaluate reagent blank value. Now calculate the chloride concentration of the leachate sample by using the relation("APHA," 2012)

In this relation, is the volume(mL) of titrant used for sample, is the volume(mL) of titrant used for blank and is the normality of standard silver nitrate solution.

4.1.1.7 Nitrate analysis

Nitrate is a highly mobile anionic species and out of various forms of nitrogen present in wastewaters and leachates it is of greatest interest("APHA," 2012; Kohn et al., 2016). Nitrates can easily penetrate though the medium because of its high solubility which can contaminate drinking water supplies and lead to various health problems like methemoglobinemia in infants. If nitrate reaches surrounding water bodies, then it can cause problems like eutrophication. Nitrate determination can be a difficult process due to the fact that several constituents can interfere.

Method used

In this study nitrate measurement is done by cadmium reduction method using powder pillows with Hach DR 2800 portable spectrophotometer. This instrument has an integrated system for analysis of the prepared sample placed in ready to use bar coded reagent vial also known as cuvettes in wavelength range of 340 to 900 nm(Dimitrova et al., 2013b; *HACH DR 2800 Spectrophotometer Procedures Manual*, 2007).

Apparatus required

Hach DR 2800 portable spectrophotometer, volumetric flask 100 mL, two glass sample cells having optical path length 1 inch square along with stoppers, NitraVer® 5 Nitrate Reagent Powder Pillow, 10mL.

Procedure

Switch on the spectrophotometer and start program 355 N, Nitrate HR PP on it. Fill one of the sample cells with 10 mL of sample, add NitraVer® 5 Nitrate Reagent Powder Pillow to it and close it with stopper. Start 1 minute reaction timer on the instrument and shake the cell vigorously until the timer expires. Start 5 minutes reaction timer on the instrument and let the sample rest till this timer expire to allow the reaction to take place. During reaction cadmium reduces nitrate in sample to nitrite, this nitrite reacts with sulfanilic acid to form diazonium salt as an intermediate and this salt forms an amber colored solution upon coupling with gentisic acid. The amber color development in the sample shows the presence of nitrate in it. If amber color is not developed then dilute the sample and repeat the procedure thus far. After the second timer expires, fill the second sample cell with 10 mL of diluted sample, clean the cell and insert it into the cell holder in the instrument. Push ZERO and the display shows 0.0 mg/L NO_3^- N.

Now clean the prepared sample and within 1 minute after the 5 minutes timer expires insert this sample into the cell holder. Push READ and results showing NO_3^- N concentration in mg/L for the diluted sample appear on screen. Finally multiply this result with the dilution factor of sample to obtain the NO_3^- N concentration for the original sample (*HACH DR 2800 Spectrophotometer Procedures Manual*, 2007).

The data based on organic, inorganic and metal constituents of the leachate was collected and analyzed further. Ghazipur leachate components were compared with other landfills components. Also, the concentration of the elements found in leachate were compared with standard discharge values. The organic components that were analyzed include BOD, COD and phenols. The inorganic components include pH, EC, TDS, TKN and NH_3-N. The metal components include As, Hg, Cr, Cu, Pb, Cd, Zn, Fe, CN, Ag and Ni. The salts that were analyzed includes chlorides, sulphates, nitrate, phosphate, fluoride (anionic salts) and Na^+, K^+, Ca^{2+}, Mn^{2+} (cationic salts). All these leachate components of Ghazipur landfill were compared with other Indian landfills i.e. Mavallipura, Bhalswa, Turbhe, Okhla, Hyderabad, Kadapa, Gurgaon, Mandur, Kumbalgoud, Nyanappanhalii, Warriana, Kazzakpura, Khammam and Dhapa. The comparison was done to assess the pollution potential of Ghazipur landfill with other landfills. Additionally, some parameters were studied which impart color to leachate. These elements include turbidity, color, COD, suspended solids and TOC, through estimating these parameters, the quality of leachate can be identified before disposing it on land or into a waterbody.

4.1.2 Landfill leachate decolorization

4.1.2.1 Coagulation- flocculation technique

Coagulation-flocculation is one of the physico-chemical treatment techniques step that is used to treat waste water. Leachate is also a type of waste water and hence this technique was applied. It can be used as a primary treatment method to remove resistant non-biodegradable organic components (Renou et al., 2008). In this study, $FeCl_3$ is used as a coagulant to achieve the decolorization process. $FeCl_3$ reagent with particular doses of 0.5, 1, 1.5 g were applied to the leachate sample to test its color removal efficiency. Based on the color number obtained at each dose, an optimum dose of $FeCl_3$ was selected. The optimum dose obtained after several trials was 0.5g/50mL) because color removal efficiency was maximum at this dose. Then, finally this particular dose was selected and the experiment was proceeded following this dose. The

decolorization experiment was carried out at pH range 3 to 7. At each pH, color number was determined. This was done in order to determine the suitable pH at which efficiency of decolorization was obtained at its maximum level. Therefore, an optimum pH value was also decided through this experiment.

4.1.2.2 Advanced oxidation technique

Advanced oxidation is one of the cost-effective techniques that is used for waste water treatment purpose. In this study, Fenton reagent ($FeSO_4$.$7H_2O$ + H_2O_2) was used to treat Ghazipur landfill leachate. Fenton process is comprised of four steps: adjustment of pH, oxidation reaction, neutralization and coagulation-precipitation (Li et al., 2010). In this process, Fenton reagent (H_2O_2/Fe^{2+}) was tested in several molar ratios i.e. 10:1, 20:1 and 50:1. After trial tests, the best color removal rate was obtained at 10:1 ratio. Further this ratio H_2O_2/Fe^{2+} with molar ratios 10:1 and 0.02 moles of Fe^{2+} were applied. Therefore, according to the selected ratio,0.55 g of $FeSO_4$ and 0.618 mL H_2O_2 was used in preparation of Fenton reagent. The prepared reagent was applied to the leachate sample at each adjusted pH value i.e. from 3.0 to 7.0. After achieving decolorization, the color of the respective samples was tested via spectrophotometer. At this stage, an optimum pH range at which decolorization was achieved at its maximum level can be determined.

4.1.2.3 Chemicals and materials required

For coagulation-flocculation experiment, $FeCl_3$ (40%w/w) was used as a coagulant whereas for oxidation experiment, Fenton reagent ($FeSO_4$. $7H_2O$) and H_2O_2 (35% w/w) was used to remove the color from the raw leachate sample. Hydrochloric acid of 1N (conc.) and NaOH (1N) was used for pH adjustment. The experimental set up comprised of 250 ml beaker in which the leachate sample was placed, analytical balance, a glass stirring rod, HQ11D portable pH meter, centrifuge, microfilter paper (0.45µm), visible spectrophotometer (single beam) for color measurement.

4.1.2.4 Experimental procedure for $FeCl_3$ method

Coagulation experiments were carried out in 250 ml beaker. Each beaker was filled with 200 ml of raw leachate. Stepwise coagulation process was carried out in the following manner:

1. 200 ml raw leachate sample was taken in 250 ml beaker.
2. Pre-decided quantities of anhydrous ferric chloride (2g/200mL) were added to the flask in a single step.
3. pH was adjusted to 3.0- 7.0 in accordance with the experimental design.
4. The mixture was centrifuged for the specified time of 15 minutes at 1500 rpm velocity so that the liquid fraction is separated from solid fraction.
5. Then the mixture was allowed to settle.
6. The supernatant was then filtered through Whatman filter paper of 2.5 µm.
7. Then color of the sample was analyzed through spectrophotometer.
8. Similarly, by adjusting pH value i.e. 3.0, 3.5, 4.0, 4.5, 5.0, 5.5, 6.0, 6.5 and 7.0, the decolorization experiment was carried out to check the efficiency of the process at certain pH range.

4.1.2.5 Experimental procedure for advanced oxidation method

The experiment was performed in a 250 mL beaker in which 200 mL of raw leachate was added. Stepwise oxidation process was carried out in a following manner.

1. 100 ml of raw leachate sample was taken in a 250 mL leachate.
2. Pre - decided 10:1 molar ratio of H_2O_2/Fe^{2+} with 0.55g of Fe^{2+} and 0.618 ml of H_2O_2 was added.
3. pH of the solution was then adjusted in a range of 3.0 to 7.0.
4. The mixture was then further centrifuged at a speed of 1500 rpm for 15 minutes.
5. The supernatant was collected and then filtered through filter paper of 2.5µm.
6. Furthermore, color of the sample adjusted at different pH value was analyzed and noted via spectrophotometer.

4.1.2.6 Calculation of percentage of color removed

Primarily, the color of the raw leachate sample was determined through spectrophotometer. The calculation for color removal percentage after decolorization process was obtained using the equation:

Where, Ci is original color (Pt Co); C_f is color after treatment (Pt Co).

4.1.3 Estimation of % COD and TOC removal

After performing color removal process, the parameters such as COD (Chemical oxygen demand) and TOC (Total organic carbon) removal were estimated. Former parameter was estimated for both $FeCl_3$ and Fenton treated leachate while latter is estimated only for $FeCl_3$ treated leachate.

4.1.3.1 For COD determination

The chemical oxygen demand (COD) establishes the amount of oxygen needed for chemical oxidation of organic matter using a strong oxidant, such as $K_2Cr_2O_7$ under reflux conditions. This test determines the extent of pollution in a water body and pollution load. In this study, an open reflux method was selected for estimating COD of raw leachate and treated leachate sample. This method was suitable was wide range of wastes (APHA, 2017).

Apparatus and chemicals required: COD digester consisting of 250 mL Erlenmeyer flask, conical flask (250 mL), burette with its stand, measuring cylinder, analytical balance, desiccator, Ag_2SO_4 , $K_2Cr_2O_7$ (0.0417 M), FAS (0.25 M), ferroin indicator, $HgSO_4$ powder and sulphuric acid reagent.

Reagents preparation: The reagents prepared for conducting COD experiment is given in Table 4.3.The standard method was followed from APHA (2017).

Table 4.3: Preparation of reagents used for COD determination

S.No	Reagents used	Symbol	Preparation
1	Potassium dichromate solution (0.0417 M)	$K_2Cr_2O_7$	1. Dried potassium dichromate crystals at 103°C for 2 hours. 2. Dissolved 6.13 g of $K_2Cr_2O_7$ in distilled water and diluted to 500mL.
2	Sulphuric acid reagent	$H_2SO_4 + Ag_2SO_4$	1. Added 5.06g of Ag_2SO_4 in 500 ml conc. H_2SO_4. 2. Allowed the solution to stand for two days for complete dissolution of silver sulphate.
3	Ferrous ammonium sulphate (0.25M)	$(NH_4)_2Fe(SO_4)_2.6H_2O$	1. Dissolved 9.8g of ferrous ammonium sulphate in distilled water. 2. Added 2ml conc. H_2SO_4 and diluted to 100 ml.
4	Ferroin indicator	$C_{36}H_{24}FeN_{62}+$	1. Used purchased ferroin indicator

Experimental procedure:

1. Taken 10mL sample of blank (distilled water), raw leachate (1mL leachate and 9 mL distilled water) and 10 mL of nine decolorized leachate samples obtained from ferric chloride and Fenton process.
2. Added 0.2g of mercuric sulphate in the sample so that interference due to halides can be controlled.
3. Added 5 mL of sulphuric acid reagent to dissolve $HgSO_4$ completely in the solution.
4. Added 5 mL of potassium dichromate solution and mixed well.
5. Further, remaining 10 mL sulphuric acid reagent was added through open end of the condenser.
6. Refluxed for 2 hours.
7. Condenser was cooled and washed with distilled water.
8. Added 3 drops of ferroin indicator in the solution.
9. The solution was further titrated with 0.25 M FAS.

Calculation for COD determination of the leachate sample

The formula used to determine COD of the leachate samples was adopted from equation given by APHA (2017).

Where COD is chemical oxygen demand (mgO_2/L); A is volume (ml) of FAS for blank; B is volume (ml) of FAS for sample; M is FAS molarity and DF is dilution factor.

Also, to check the percentage of COD removal , the following equation will be used:

Where Ci is initial COD of raw leachate, C_f is final COD after leachate treatment.

4.1.3.2 For TOC determination

TOC determines the amount of organic, inorganic and total carbon present in water sample. In this study, TOC of the raw and treated leachate samples were determined through TOC analyzer instrument. The method chosen to test the total organic carbon was wet oxidation method. This analyzer is based on UV catalyzed persulphate digestion to produce carbon dioxide, which is further encountered by non-dispersive infrared sensor (EPA, 2009). The % of TOC removal is determined by using the equation:

Where Ti is initial TOC of raw leachate and T_f is final TOC of treated leachate.

4.1.4 Correlation of pH vs color, chemical oxygen demand and total organic carbon.

Correlation analysis suggests the strength of interdependency between two variables. For this study, correlation coefficient was calculated between pH of the leachate sample and the color, COD and TOC obtained at each specific pH. To check the effect of pH on color and above parameters removal, this analysis was done. It will allow to assess that if pH of the sample changes then it may have an effect (positive or negative) on color of the sample or may be any parameter that determines the organic strength of the sample.

4.1.5 Temporal assessment of Human health risk due to consumption of groundwater contaminated with leachate

Risk assessment is an evaluation tool that is not only concerned with environmental issues but also in relation to many fields such as food company, natural disasters (earthquakes), construction activities and hospitals as well (Butt et al.,2008). According to USEPA, risk is assessed in two ways i.e. human health related risk and ecological risk. However, the present study deals with human health related risk due to exposure to contaminated groundwater. For assessing carcinogenic risk, the risk assessment was carried out for four heavy metals which are lead, cadmium, chromium and nickel for the year 2003- 2019. The toxicity information of these metals is depicted in Table 4.4. These toxic heavy metals have the potential to degrade groundwater quality and it can ultimately affect the human health as people surrounding the nearby area are dependent on groundwater for drinking purposes.

Table 4.4: Toxicity characteristics of metals and their effect on human health

S.No	Heavy metals	Carcinogenic risk	Non-Cancer risk	References
1	Cadmium		Weakened bones, bone damage and pulmonary disease.	WHO, 2019
2	Chromium		Skin infections	US EPA, 2016
3	Nickel		Allergic reactions in skin and irritations in eyes.	Das et al., 2008
4	Lead		Heart disease, kidney disease and brain damage	Benefo et al., 2019

*WHO: World health organization

4.1.5.1 Calculation of chronic daily intake (CDI) and cancer risk (CR)

When highly toxic leachate enters into groundwater then its components gets diluted in ratio of 1:100 (Christensen et al., 2001). This ratio is suggested for landfill which is lined by fine to medium sand mixed with coarse hard kankar up to a depth of 50-60 m bgl (Babbar et al., 2017). Ghazipur landfill which is devoid of single/ double liner facility may result in higher infiltration and lower dilution. As leachate production varies throughout the season (Anjali, 2015) a conservative estimate of 1:100 dilutions will hold good for leachate samples collected throughout the year.

To assess cancer risk due to contaminated drinking water, (CDI) chronic daily intake (mg $Kg^{-1}day^{-1}$) is calculated for carcinogenic metals (Pb, Cd, Cr and Ni) present in leachate using equation 1 given by US EPA. Also, cancer risk (CR) associated with this intake is estimated in equation 2 given by US EPA.

(1)

Where, C_w is pollutant concentration (mg/L), IR is ingestion rate i.e. 2L per day for adult and 1L per day for child, ED is exposure duration i.e. 30 years for adult and 6 years for child, EF is exposure frequency i.e. 365 days/year, BW is body weight i.e. 70 kg for adult and 15 kg for child), AT is exposure average time i.e. 70 years.

(2)

Where, SF is slope factor (kg day mg^{-1}). Slope factor determines the potential of having cancer due to a unit dose of a chemical. SF value for Cr, Ni, Pb and Cd are 0.5, 0.91, 0.0085 and 15 respectively (Zeng et al., 2015). The acceptable risk of having carcinogenic risk should be CR< 10^{-6} (US EPA, 2004).

4.2 Results and Discussions

4.2.1 Landfill leachate analysis: its composition with discharge standards

The physico-chemical components of the raw leachate of Ghazipur sampling sites and other landfills have been compared in this study. The analysis was done on nature of leachate and hence divided into organic constituents, inorganic constituents, heavy metals and salts (cationic and anionic). Also, the elements which are responsible for imparting color to leachate are studied. These elements are turbidity, COD, suspended solids and TOC. Further the color (Pt Co), was also analyzed for such landfill leachate. Most of the leachate color-based studies were done for Malaysia, Morocco, Mexico and Iran landfills. This was done for the purpose of treatment of landfill leachate before discharge.

4.2.1.1 Analysis of inorganic constituents present in leachate

The inorganic constituents characterized in Ghazipur leachate were pH, electrical conductivity (EC), TDS (total dissolved solids), TKN (total Kjeldhal nitrogen) and NH_3-N (ammonical nitrogen) and these constituents were compared with other Indian landfills with respect to their discharge standard limits. The concentration of these components of Ghazipur leachate with other landfills leachate were shown in figure 4.7. The mean pH value of Ghazipur leachate was 8.35. This alkaline pH value specified that the landfill has already entered in methanogenic phase. The pH noted in this study is similar to previous studies done earlier on Indian landfills (Kumar and Singh., 2019; Souza and Somashekhar., 2013; Kaushik et al., 2016 and De et al., 2016).The Ghazipur landfill site is in operational stage since more than 30 years and as the site reaches older stage, the leachate pH also tend to change from acidic to alkaline range (Hussein et al., 2019). The EC values of the Ghazipur leachate was 36366.67 µS/cm. These EC values when compared with other landfill sites were much higher in comparison to other landfill sites of India. However, the conductivity values for all the landfills were above the standard limit of 1400µS/cm except Turbhe landfill of Mumbai. Electrical conductivity indicates the presence of ions in the leachate sample. These ions include calcium, magnesium, sodium and potassium (Johanson and Carlson, 1976). Parameter such as EC and TDS have a strong correlation (Fan et al., 2006). In this study, reported TDS values of Ghazipur leachate was 23274.67 mg/L which is above the permissible limit of 2100 mg/L. However, this value is highest among all the other landfills leachate values except for Okhla landfill. High concentration of EC and TDS denoted the presence of dissolved inorganic and organic components in the leachate sample. The mean concentration of TKN of Ghazipur leachate was 680 mg/L which was found to be much lower than landfill leachate of Kazzakpura and Dhapa but above the permissible limit of 100 mg/L. The higher concentration of TKN observed in Ghazipur leachate site indicated that it can be due to household wastes. The presence of this component shows the presence of reducing environment (Bag et al., 2016). The mean concentration of ammonical nitrogen in Ghazipur leachate was 265.7 mg/L. This may be due to occurrence of deamination reactions during leachate stabilization (Crawford and Smith, 1985). Although the NH_3-N concentration of Ghazipur site was lower as compared to Bangalore and Kolkata landfill sites but it is still above the disposal standards of 50 mg/L.

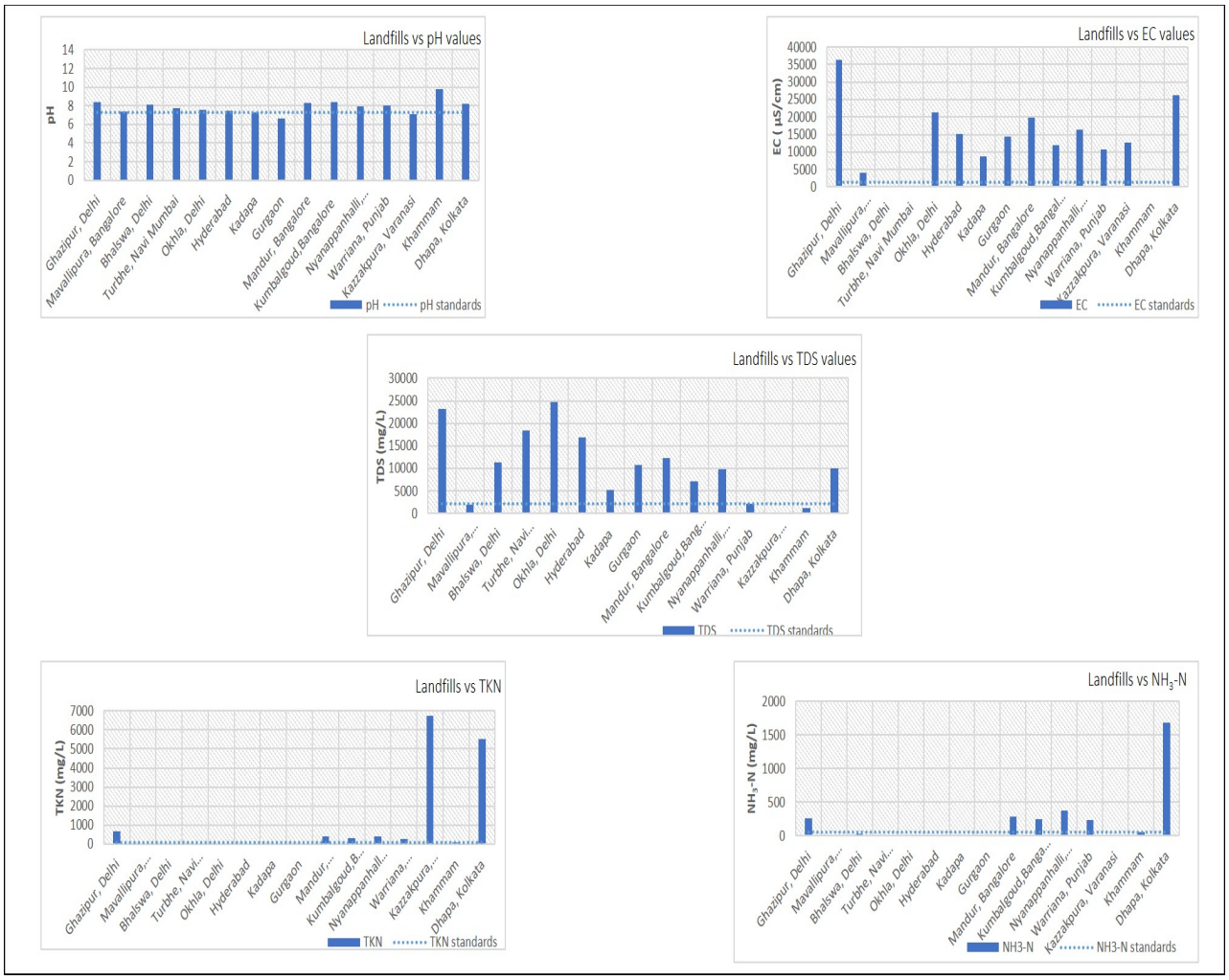

Figure 4.7: Graphs showing comparison of inorganic constituents of GL vs other landfills

4.2.1.2 Analysis of organic constituents present in leachate

The organic constituents characterized in Ghazipur leachate were BOD, COD and Phenols. The concentration of these constituents was further compared with other landfills with respect to their discharge limits. The constituent concentration is shown in figure 4.8. The mean BOD concentration of Ghazipur leachate was 12100 mg/L and found to be much higher than the leachate discharge standards of 30 mg/L, which is rather higher than all the other landfills considered in this study. This suggests the wastes in these landfills has high organic content which has not yet been stabilized. The mean concentration of COD was found to be 50,000 mg/L which is far above the permissible limit of 250 mg/L. The COD indicates the organic strength and microbial activity for leachate decomposition. It is also useful to determine the treatment

technique and extent of waste degradation (Kumari et al., 2018). The COD of Ghazipur leachate was found to be highest among all the Indian landfills stated in this study. This determines that mostly biodegradable type of waste is received by this landfill. The mean concentration of phenol was found to be 5 mg/L which is beyond the permissible limit of 1 mg/L and also highest as compared to landfills of Bangalore and Kolkata. This indicates that the landfill may receive agricultural waste also.

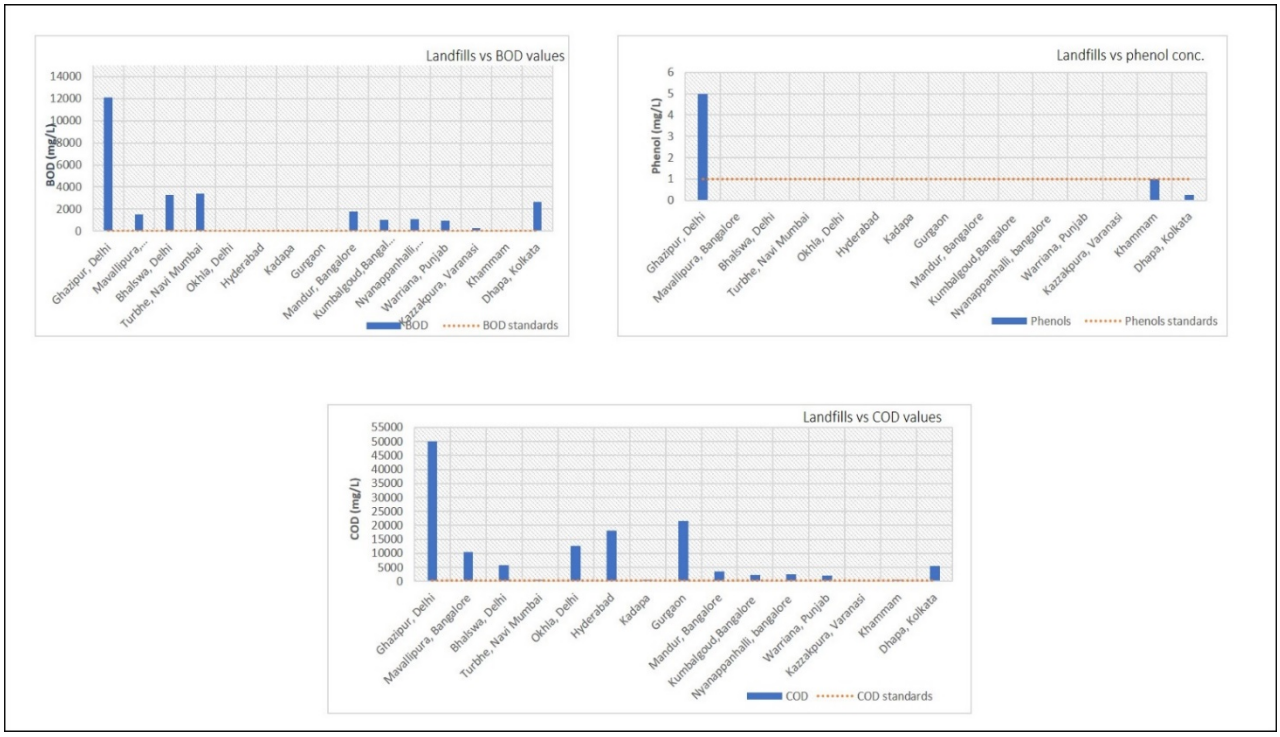

Figure 4.8: Graphs showing comparison of organic constituents of GL vs other landfills

4.2.1.3 Analysis of metal constituents present in leachate

The metal constituents characterized in Ghazipur leachate were chromium, copper, lead, cadmium, zinc, iron and nickel. The value of these constituents was further compared with other Indian landfills with respect to their discharge standards. The concentration of these elements is shown in figure 4.9. The mean concentration of chromium in Ghazipur leachate was 0.125 mg/L which is almost similar to the studies reported by Souza and Soma Shekhar., 2013. The chromium values were within the discharge limits of 2 mg/L. The mean concentration of copper was 3.01 mg/L, which is line with the standards. However, Turbhe, Nyanappanhalli and Warriana landfills have high concentration of copper. This may be due to the disposal of

unsegregated municipal waste in the landfill site (Bag et al., 2016). The mean concentration of lead was found to be 0.58 mg/L which is almost similar to the other Indian landfills cited in this study except Gurgaon, Bangalore, Punjab and Varanasi landfills. The lead values for Ghazipur leachate have exceeded the discharge limit of 0.1 mg/L. The occurrence of lead in leachate may be due to the disposal of lead-based pipes and paints (Mor et al., 2006). The mean concentration of cadmium was found to be 0.05 mg/L which is within the standard limit of 0.1 mg/L. Cd level shows that landfill may have also received industrial type of waste. The mean concentration of Zn in Ghazipur leachate was found to be 11.6 mg/L which is beyond the acceptable discharge limit of 5 mg/L. The major sources of zinc can be fertilizers and pesticides used as agrochemicals (Bag et al., 2016). However, among all the landfills, Warriana dumping site accounts for the maximum levels of zinc. This may be due to the excessive use of chemical fertilizers in agricultural field of Punjab. The mean concentration of iron for Ghazipur leachate was 0.13 mg/L which is below the standard discharge limit of 3mg/L. However, it was observed that other Indian landfills have high levels of iron present in leachate (Naveen et al., 2014; Kumar and Singh., 2019; Mishra et al., 2016; Somani et al., 2019; Kaushik et al., 2016 and Pandey et al., 2014). The mean concentration of nickel in Ghazipur leachate was found to be 1.78 mg/L and was almost similar to other Indian landfill values, which is below the permissible discharge limit of 3 mg/L.

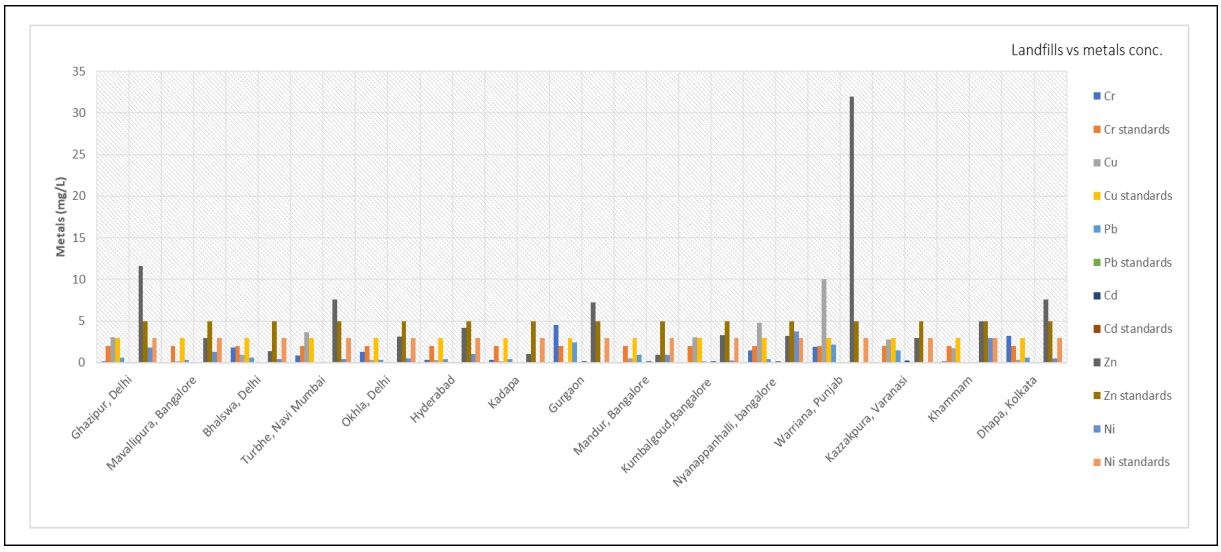

Figure 4.9: Graphs showing comparison of heavy metal constituents of GL vs other landfills

4.2.1.4 Analysis of salts present in leachate

The type of salts analyzed were cationic (Na^+ & K^+)and anionic (Cl^-, SO_4^{2-}, NO_3^-, PO_4^{3-} and F^-). The concentration of these salts present in Ghazipur leachate is compared with other Indian landfills in figure 4.10. Among the cations, the highest concentration for sodium, potassium, calcium and manganese was observed in Mavallipura, Dhapa and Warriana landfill respectively. Ions such as sodium and potassium are mostly obtained from vegetable residues and domestic wastes and increased concentration of these ions can cause leachate pollution (Naveen et al., 2014). The concentration of all these cations is specific to the waste volume and the ongoing stability age in the landfill (Mohanty et al., 2019). Among anions, the highest concentration for chloride, sulphate, nitrate, phosphate and fluoride was observed in Okhla, Gurgaon, Nyanappanhalli, Turbhe and Ghazipur landfill respectively. For chloride, the sorption, complexation and precipitation reactions are negligible, therefore it is one of the conservative pollutants (Bag et al., 2016). The presence of sulphate can be due to organic waste decomposition or may be inert waste. The presence of nitrates in leachate can be due to the oxidation of ammonium to nitrite and then nitrate (Naveen et al., 2014). The presence of phosphate in leachate can be a result of decomposition of phosphoproteins in organic matter.

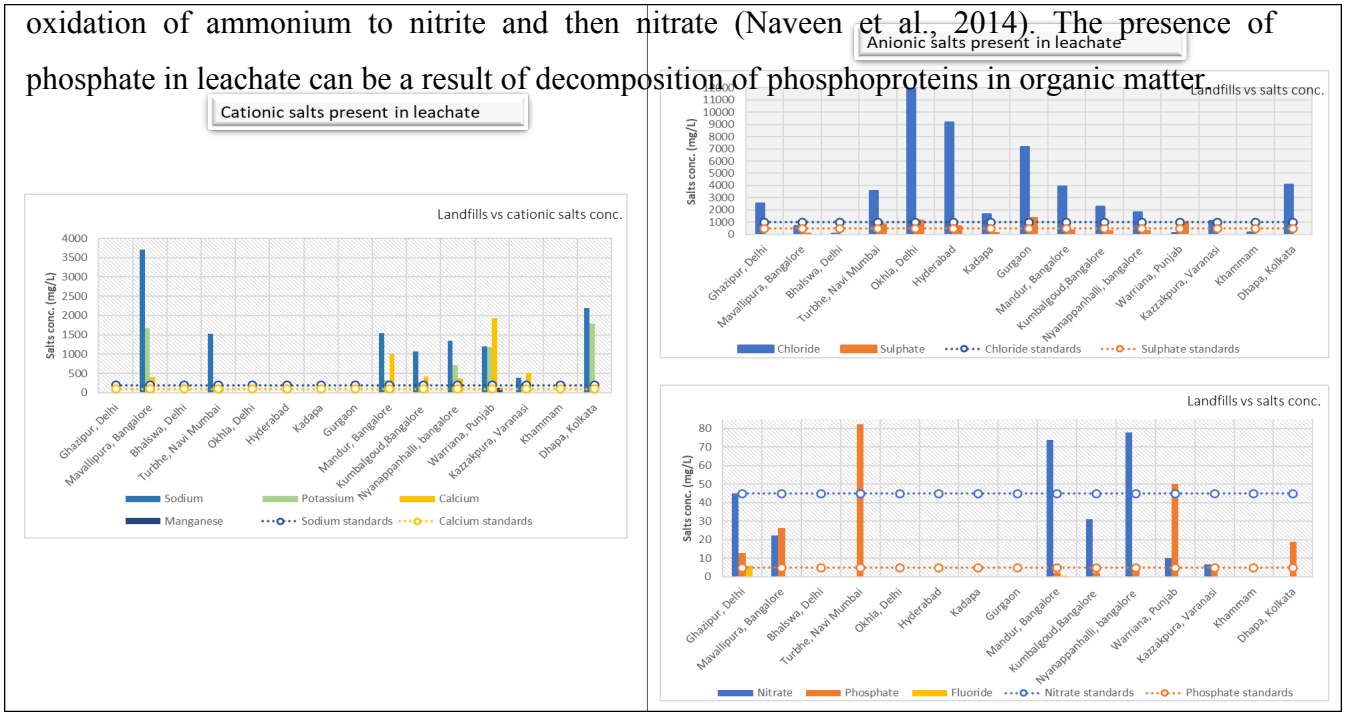

Figure 4.10: Graphs showing comparison of salt constituents of GL vs other landfills

4.2.1.5 Elements of concern imparting color to landfill leachate

According to several studies done earlier, the occurrence of color in leachate is due to the presence of organic matter with some insoluble elements that represent turbidity and total suspended solids. The organic matter present in leachate is estimated by chemical oxygen

demand and total organic carbon measures. The elements measured such as turbidity (NTU), COD (mg/L), suspended solids (mg/L), TOC (mg/L) and color (Pt Co) for different landfills is presented in Table 4.5.

Table 4.5: Elements of concern estimating color in landfill leachate

Elements	Reference	Colour	Turbidity	COD	Suspended solids	TOC
Landfills						
Pulau Burung, Malaysia	Aziz et al., 2007	2430–8180	50–450	1533–3600	159–1120	NA
Pulau Burung, Malaysia	Mohajeri et al., 2014	4200	280	2360	151	NA
Mérida, Mexico	Maruffo et al., 2017	10900	160.41	4180.44	156.66	2808
Pulau Burung, Malaysia	Amr and Aziz 2012	4100	NA	2180	197	NA
Hamadan, Iran	Kashitarash et al., 2012	15000	NA	85000	200000	NA
Kermanshah, Iran	Ahmadian et al., 2013	3045	NA	3895	1460	1438
Pulau Burung, Malaysia	Kamaruddin et al., 2015	3334	1546	935	1437	NA
Kulim, Malaysia	Ramirez-Sosa et al., 2012	1936	8.55	1892	6336	NA
Mediouna, Morocco	Chaouki et al., 2016	4.87	106	7680	5.7	NA
Sahom, Malaysia	Azmi ei al., 2014	8960	280	2740	510	NA

4.2.2 Landfill leachate decolorization via coagulation-flocculation technique

The decolorization experiment was conducted by using a coagulant such as ferric chloride. The actual color, COD and TOC of the raw and treated leachate sample at difference pH (3.0, 3.5, 4.0, 4.5, 5.0, 5.5, 6.0, 6.5 and 7.0) values is shown in Table 4.6. The variation observed in leachate color at each adjusted pH is shown in figure 4.11. Percentage of color removal efficiencies as per fixed $FeCl_3$ dosage of 2 g/ 200 mL for each pH is shown in figure 4.12. The percentage of COD and TOC removal efficiencies obtained from decolorized samples are presented in Fig 4.13 and figure 4.14 respectively. Results showed that the removal of color, COD and TOC increases with decrease in pH values and decreases with increase in pH at fixed coagulant dose of 2g/200 mL. 99.7% and 99.6% removal of color in raw leachate was obtained at pH 3.5 and 4.0 respectively. Therefore, the best pH range at which the color removal was maximum was 3.5- 4.0. Also, the decolorized samples showed highest COD removal of 98.64%, 98.5% at pH 3.5 and 4.0 respectively whereas the highest TOC removal was 99.9% and 99.7%

obtained at pH 3.5 and 4.0 respectively. It can be observed that lower pH has a great significance on these parameters removal rates. At lower pH, the Fe^{3+} reacts with hydroxyl ions of the leachate. This will result in the formation of ferric hydroxide [$Fe(OH)_3$]. Also, various studies reported that $FeCl_3$ act as a good coagulant used for physico-chemical treatment of leachate. When $FeCl_3$ is added in raw leachate then Fe^{3+} ions tend to react with negative colloids in order to neutralize their charge and this will result in destabilization of colloids (Rui at al., 2012). However, an optimum dose of the coagulant should be determined because if the dose of the coagulant will increase then it will lead to re stabilization of colloids. Thus, ferric chloride can be used as a coagulant for leachate pretreatment to remove non-biodegradable organic matter (Renou et al., 2008).

Table 4.6: Raw and treated leachate parameter values through Ferric chloride

	Ghazipur leachate parameters		
pH	**Color (PtCo)**	**COD (mg/L)**	**TOC (ppm)**
8.27 (Raw leachate)	13360	50000	1278
3.0	84	680	137.73
3.5	45	760	0.72
4.0	52	760	3.47
4.5	87	800	102.19
5.0	78	840	102.01
5.5	303	28000	320.9
6.0	882	36000	395.78
6.5	2190	44000	483
7.0	4392	48000	480

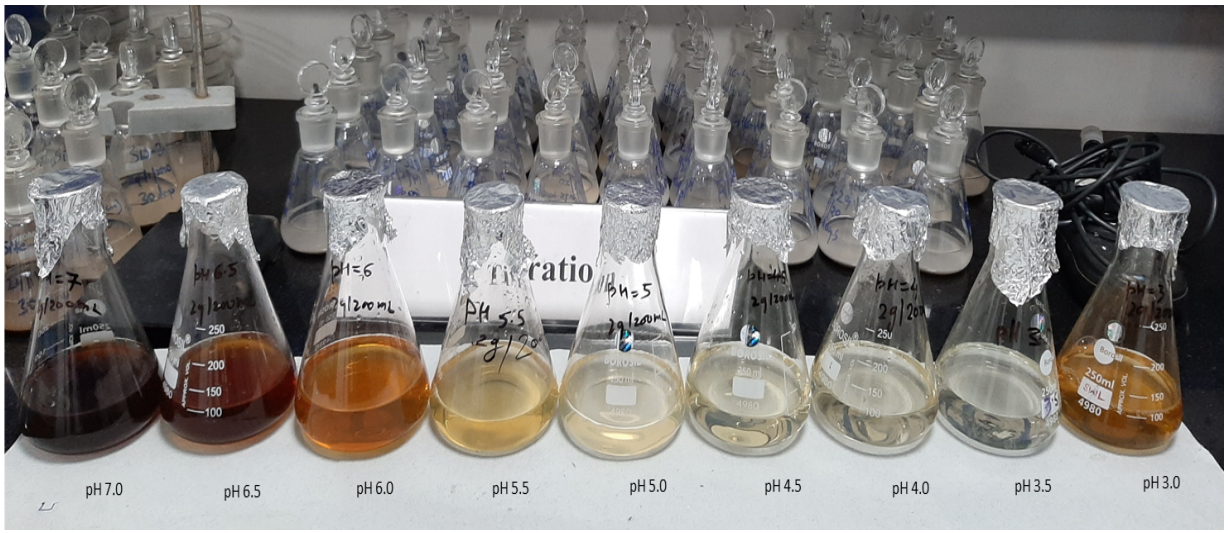

Figure 4.11 : Variations in leachate color at each pH adjustment with optimum $FeCl_3$ dosage

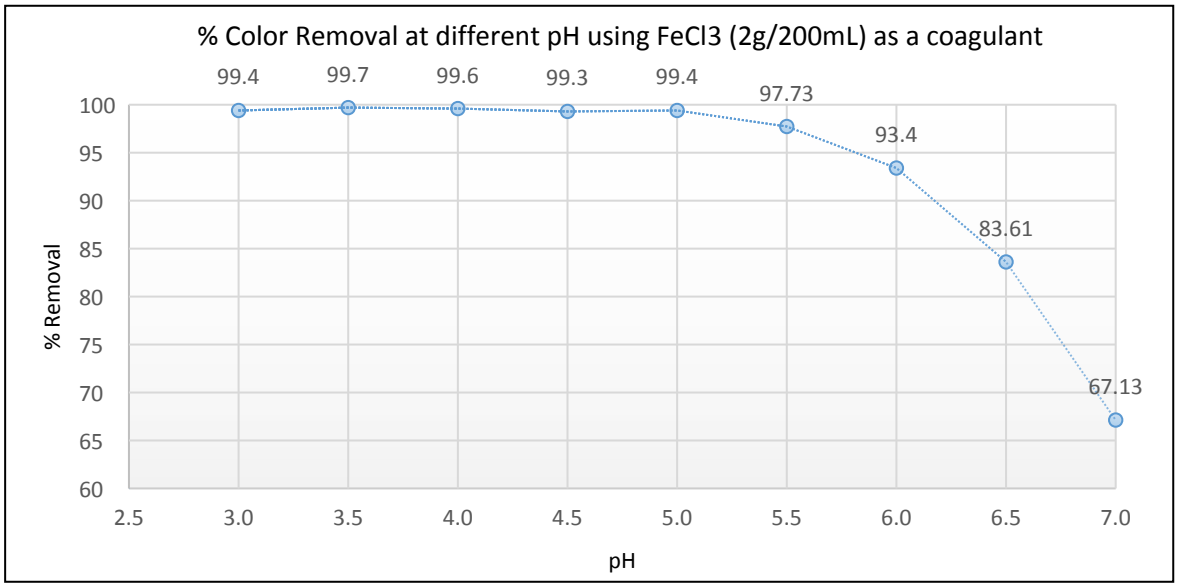

Figure 4.12 : Effect of Ferric chloride treatment on color removal efficiency.

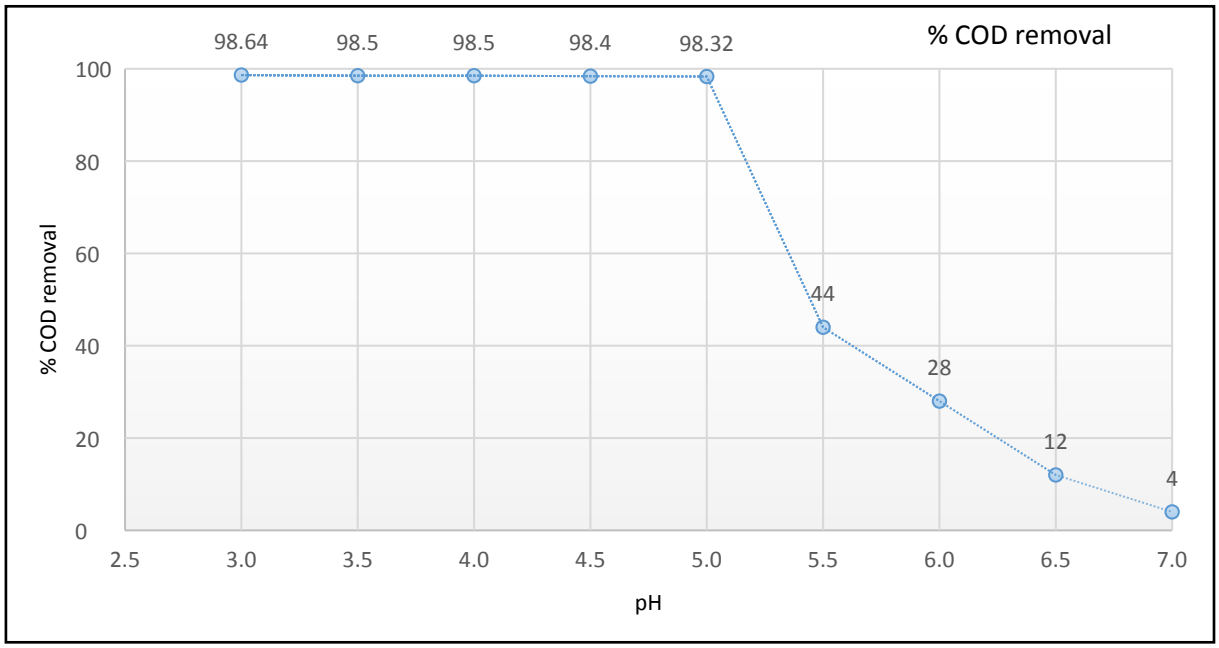

Figure 4.13 : Effect of leachate decolorization on COD removal efficiency

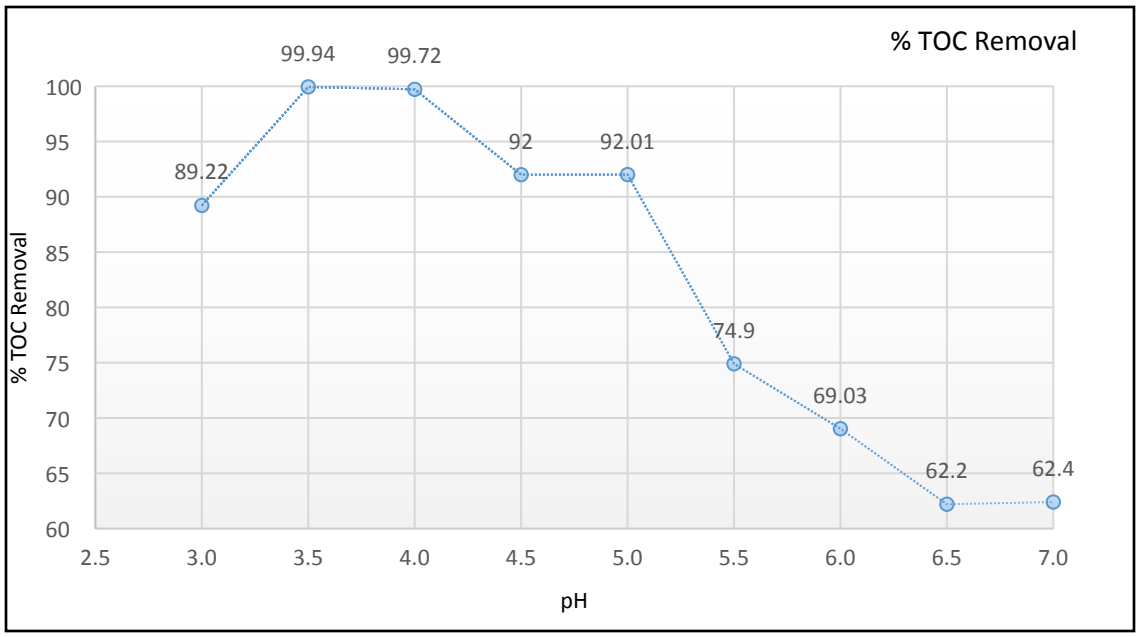

Figure 4.14: Effect of leachate decolorization on TOC removal efficiency

4.2.3 Landfill leachate decolorization via advanced oxidation process

The decolorization experiment was done by using another reagent i.e. ($FeSO_4$+H_2O_2). The values estimated for color and chemical oxygen demand for raw and treated leachate are shown in Table 4.7. Also, the variation in color achieved at each adjusted pH and coagulant dose of 10:1 molar ratio is shown in figure 4.15. The percentage of color and COD removal efficiencies as per fixed $FeSO_4$ (0.55 g) and H_2O_2 (0.618 ml) is presented in figure 16 and figure 17 respectively. The result analysis showed that the color and COD removal rates increased with reduction in pH values. The best removal in color is obtained at pH 3.0, 3.5 and 4.0. The results obtained are in line with studies done previously by Kang and Hwang., 2000; Tengrui et al., 2007 and Ahmadian et al., 2013. Whereas at higher pH, the color removal efficiency was minimum i.e. 17.5% and 12.2 % at pH 6.5 and 7.0 respectively. This is because of the fact that at high pH, the Fe^{2+} ions precipitates as Fe $(OH)_3$ and H_2O_2 gets decomposed into oxygen. This decomposition process will reduce the concentration of H_2O_2 in the solution, due to which oxidation of resistant organic material will not occur. In addition to this, the Fenton molar ratio of 10:1 chosen in this study after conducting several trials, is regarded as best for landfill leachate treatment perspective. In Fenton reaction, H_2O_2 having high oxidation potential reacts with ferrous ion, this will lead to production of hydroxyl radical that will help in the degradation of non- biodegradable organic fraction. However, the presence of chloride and bicarbonate ions in the leachate can interfere in

the oxidation reactions (Bagastyo et al., 2018). Therefore, the removal rate cannot be achieved upto 100%. After decolorization, the maximum percentage of COD removal was obtained at pH range 3.5-4.0. After increment in pH, the percentage of COD removal also declined. This is due to the precipitation if iron as Fe $(OH)_3$, due to which H_2O_2 could not react with Fe^{2+} ions and unable to generate hydroxyl radicals for the purpose of organic matter oxidation.

Table 4.7: Raw and treated leachate parameter values through Fenton process

	Ghazipur leachate parameters	
pH	**Colour (PtCo)**	**COD (mg/L)**
8.27 (Raw leachate)	13360	50000
3.0	350	6000
3.5	332	7500
4.0	269	7500
4.5	442	12500
5.0	648	13500
5.5	657	16000
6.0	8650	40000
6.5	11025	48000
7.0	11730	48000

Figure 4.15: Variation in leachate color at each adjusted pH with optimum Fenton dose

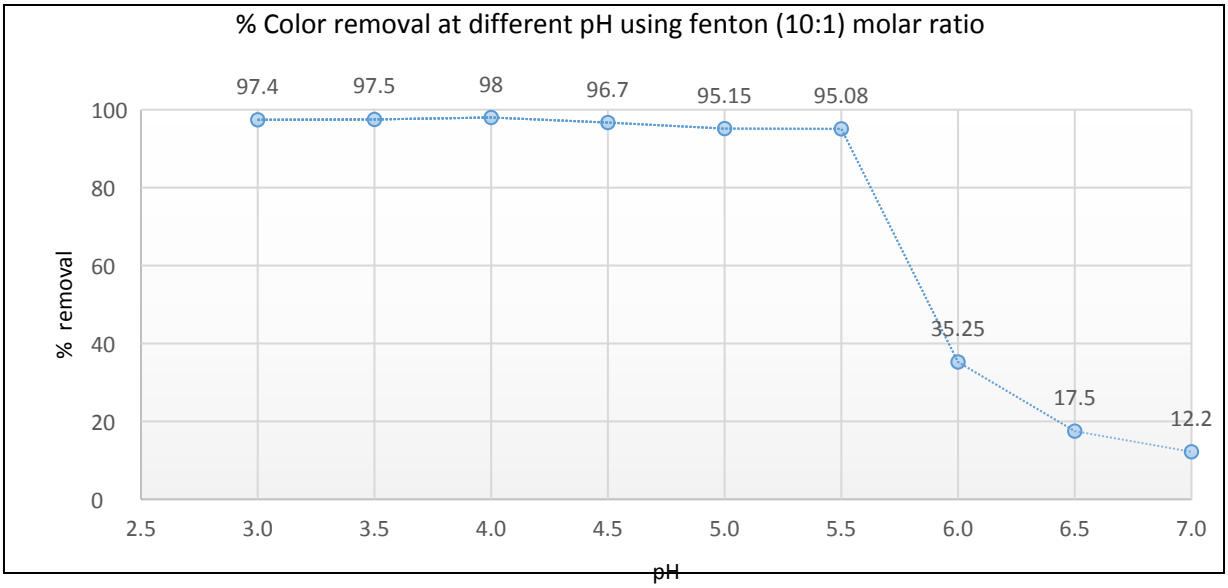

Figure 4.16: Effect of Fenton treatment on color removal efficiency

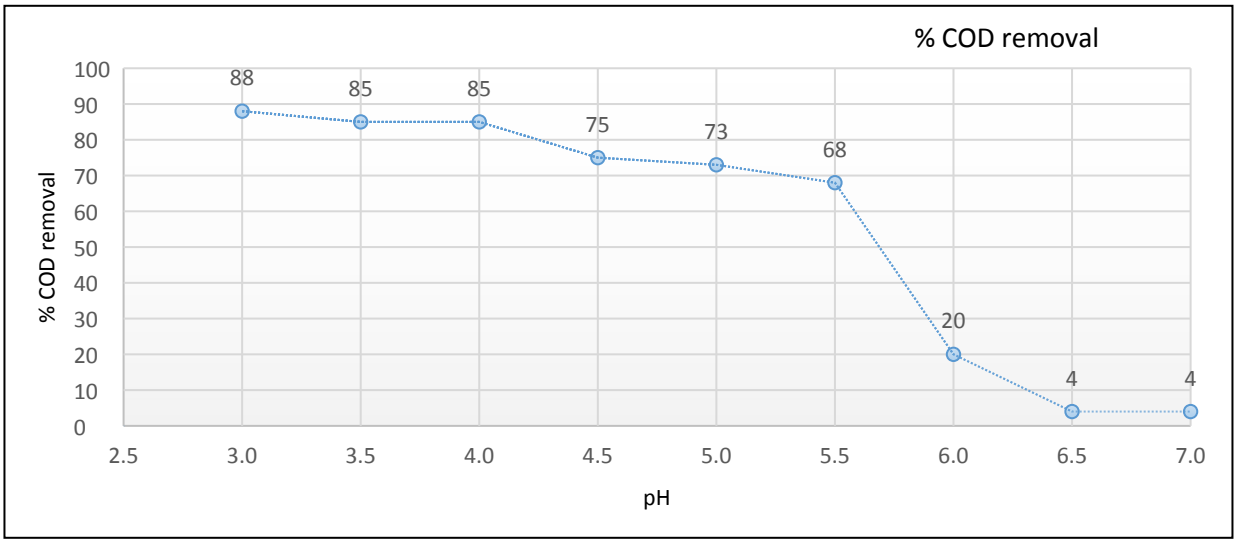

Figure 4.17: Effect of Fenton decolorization on COD removal efficiency

4.2.4 Correlation analysis of pH vs leachate parameters

The spearman correlation coefficient was calculated for pH vs color, COD and TOC and pH vs % color removal, % COD removal and % TOC removal for both the processes i.e. Fenton and $FeCl_3$. The comparison of coefficient values is presented in figure 4.18. The correlation coefficient between pH and color is 0.867 and 0.933 for $FeCl_3$ and Fenton treatment respectively. This indicated that with increase in pH the color also gets increased. At high pH, the oxidation reaction becomes very slow. Whereas, the correlation coefficient between pH and % color removal is -0.904 and -0.933 for both $FeCl_3$ and Fenton processes. This indicated that the color

removal efficiency decreased with increase in pH values. The correlation coefficient between pH and COD is 0.996 and 0.992 and between pH and % COD removal is -0.996 and -0.992 for $FeCl_3$ and Fenton treatment processes respectively. The correlation coefficient between pH and TOC is 0.8 and between pH and % TOC removal is -0.8 for $FeCl_3$ treatment. These results suggest that pH have a significant strong positive correlation with color, COD and TOC and a strong negative correlation with pH, COD and TOC values.

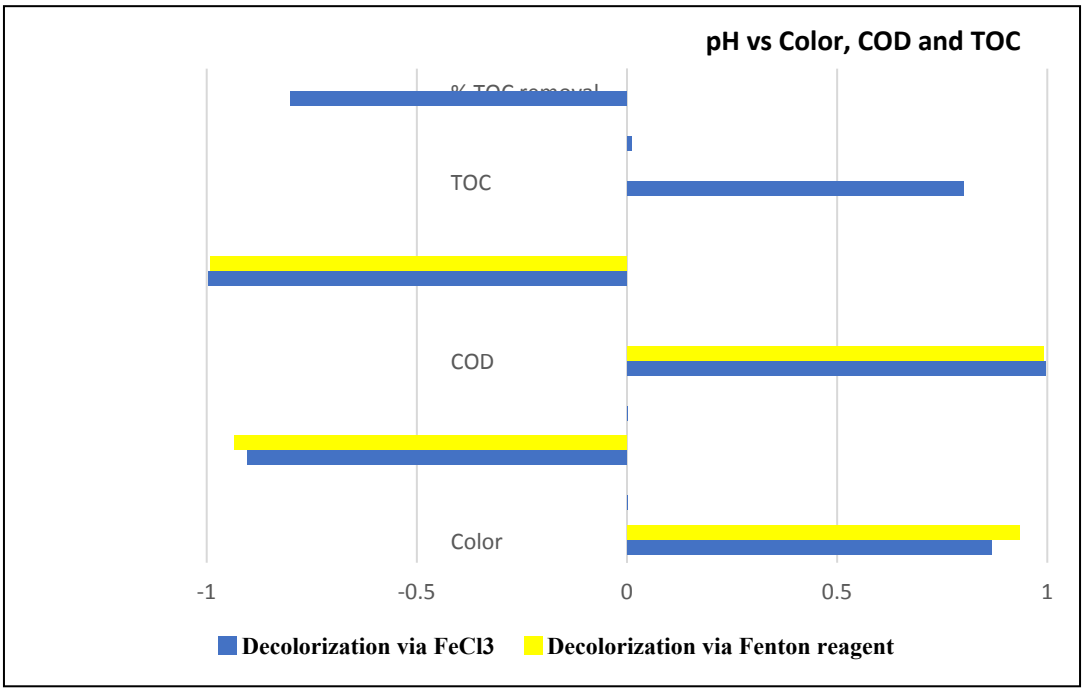

Figure 4.18: Correlation between pH and treated leachate parameters

4.2.5 Estimation of heavy metal concentration in groundwater

The heavy metals concentration of Cd, Cr, Ni and Pb in groundwater is estimated by applying a dilution factor of 1:100. Each metal concentration in the Ghazipur landfill leachate for each sampling year is multiplied by 0.01 for the purpose of estimating its concentration in unconfined aquifers. The calculated values of heavy metals in groundwater is presented in Table 4.8. The variation of these metals with time and their comparison with Indian standards is shown in figure 4.19.

Table 4.8: Calculated year wise data of heavy metals (mg/L) present in groundwater table

Year	Cd	Cr	Ni	Pb
2003	0.0006	0.0029	0.0041	0.0154
2012	0.0002	0.0092	0.004	0.0011
2014	NA	0.004	0.0025	0.068
2015	NA	0.0119	0.0051	0.007
2016	0.00475	0.0245	0.00354	0.0525
2017	NA	0.0097	0.0236	0.0156
2019	0.00058	0.00125	0.0178	0.0058

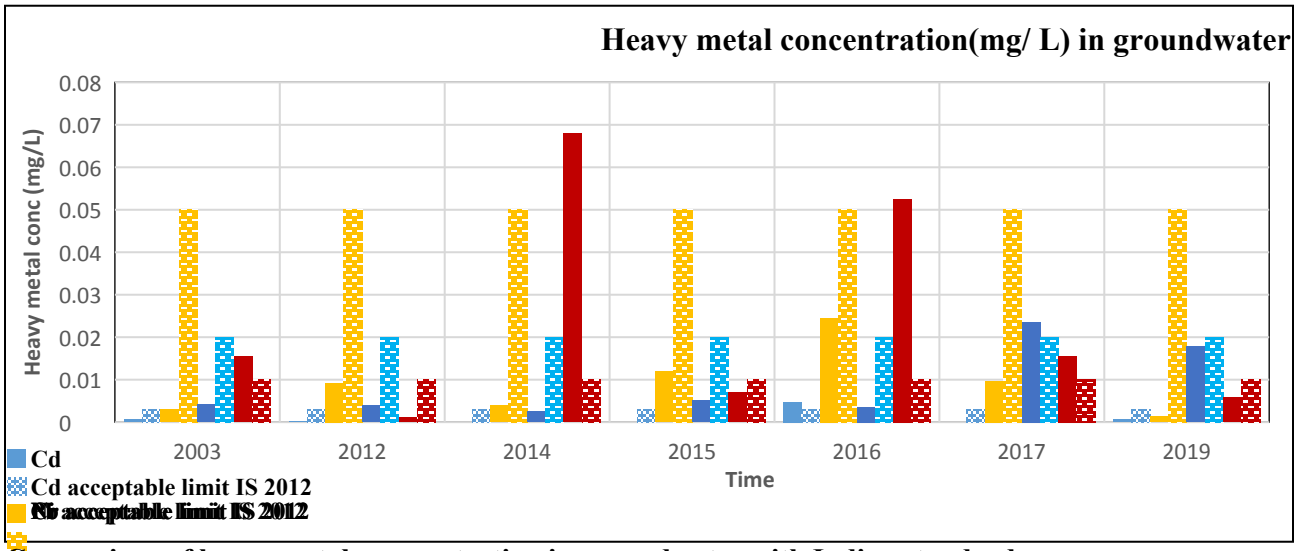

Figure 4.19: Comparison of heavy metals concentration in groundwater with Indian standards

The concentration of cadmium in 2016 and nickel in 2017 is highest and found to be above the permissible drinking water limit of 0.003 and 0.02 mg/L respectively. The concentration of lead in 2003, 2014, 2016 and 2017 is highest and found to be above the drinking water limit of 0.01mg/L. These results indicated that the groundwater near the Ghazipur landfill site is heavily prone to contamination. These metals can pose an adverse health impact on human population living nearby the Ghazipur landfill site. Due to non-availability of liner system, the leachate can easily percolate into groundwater table, thus posing risk to human health.

4.2.6 Estimation of chronic daily intake (CDI) of heavy metals present in groundwater

To determine the daily intake of groundwater contaminated with heavy metals, chronic daily intake is calculated. The CDI values obtained for each heavy metal reported in following years is shown in Table 4.9. The results illustrated in figure 4.20 showed lead accounted for the highest value among all the heavy metals intake. The daily intake of lead was found to be higher in adults as compared to children in all of the following years. Lead, being a highly toxic element can cause neurological disorders or brain damage.

Table 4.9: CDI values calculated for heavy metals in a particular year

Year	Cd (mg/L)		Cr(mg/l)		Ni (mg/L)		Pb (mg/L)	
	Adult	**Child**	**Adult**	**Child**	**Adult**	**Child**	**Adult**	**Child**
2003	7.045E-06	3.28767E-06	3.41E-05	1.59E-05	4.81E-05	2.25E-05	1.81E-04	8.44E-05
2012	2.3483E-06	1.09589E-06	1.08E-04	5.04E-05	4.7E-05	2.19E-05	1.29E-05	6.03E-06
2014	NA	NA	4.7E-05	2.19E-05	2.94E-05	1.37E-05	7.98E-04	3.73E-04
2015	NA	NA	1.40-04	6.52E-05	5.99E-05	2.79E-05	8.22E-05	3.84E-05
2016	5.5773E-05	2.60274E-05	2.88-04	1.34-04	4.16E-05	1.94E-05	6.16E-04	2.88E-04
2017	NA	NA	1.14-04	5.32E-05	2.77E-04	1.29E-04	1.83E-04	8.55E-05
2019	6.8102E-06	3.17808E-06	1.47E-05	6.85E-06	2.09E-04	9.75E-05	6.81E-05	3.18E-05

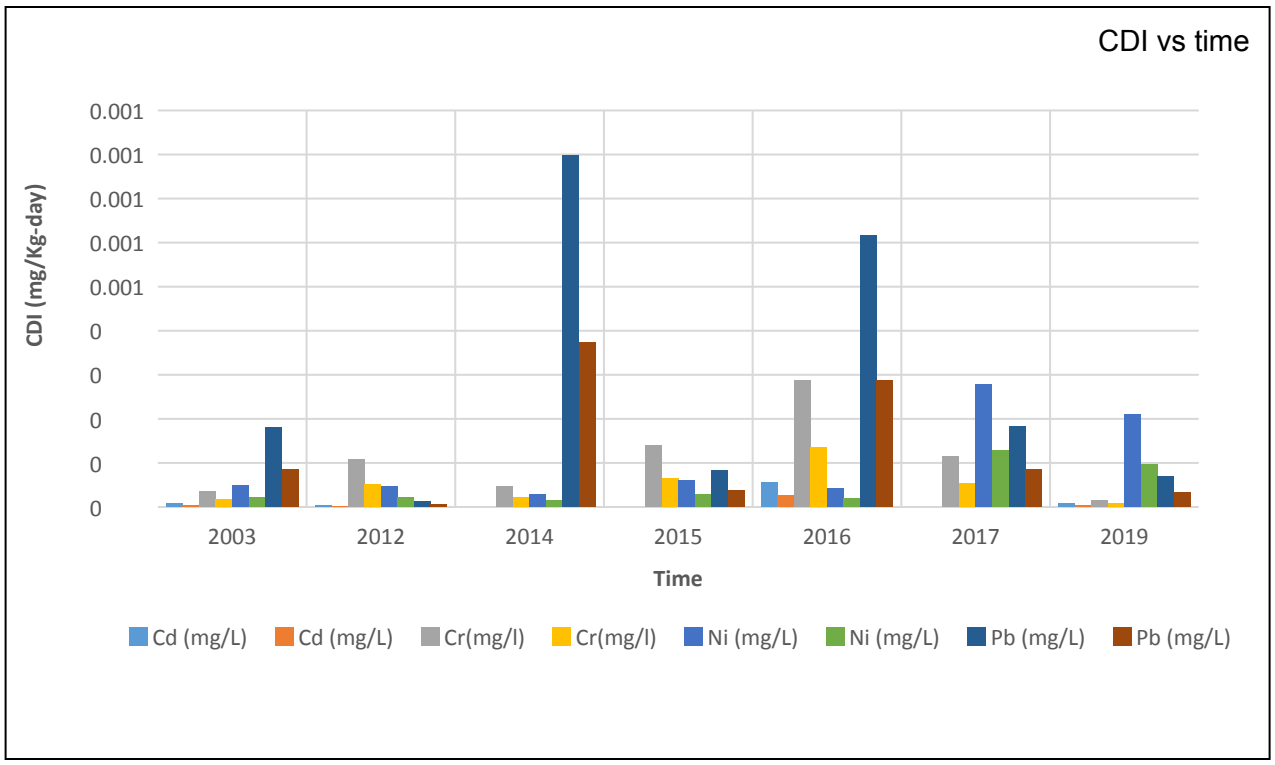

Figure 4.20: Chronic Daily Intake value for heavy metals in year wise manner

4.2.7 Comparison of carcinogenic risk of Adult and Children

The carcinogenic risk values for both adult and children were calculated by multiplying chronic daily intake value of heavy metals with their respective slope factors. Slope factors determine the carcinogenic risk on exposure to a carcinogenic pollutant. The trend of CR (Cancer risk) values are presented in Table 4.10. The variation in cancer risk due to heavy metals for adult and child with time is presented in figure 4.21. Risk posed by cadmium, chromium and nickel in case of adults is more as compared to children and it is found to be above the safe limit of 10^{-6}. Whereas, it was observed that the risk posed by lead in some years is found to be below the permissible limit i.e. in year 2003, 2015, 2017 and 2019 the risk value is less than 10^{-6} for children whereas for adults it was less in the year 2012 2015 and 2019. The results showed that out of all the metals studied for risk estimation, cadmium was found to have a high potential of causing cancer risk. Cadmium can cause a damage in DNA and is responsible for oxidative stress. These heavy metals can have an instant adverse effect on immune system and can advance the risk of cancer in human beings. The variation in risk observed in the following years is because of the variation in the metal concentration (C_m). Because of the change in concentrations of heavy metals present in groundwater, the risk also varies. However, the

concentrations of these metals in leachate depends upon the temperature conditions and the amount of rainfall occurring in the area.

Table 4.10: Cancer risk values for different metals

Year	Cd (mg/L)		Cr(mg/l)		Ni (mg/L)		Pb (mg/L)	
	Adult	**Child**	**Adult**	**Child**	**Adult**	**Child**	**Adult**	**Child**
2003	1.06E-04	4.93151E-05	1.7E-05	7.94521E-06	4.38E-05	2.04E-05	1.53699E-06	7.1726E-07
2012	3.5225E-05	1.64384E-05	5.4E-05	2.52055E-05	4.27E-05	1.99E-05	1.09785E-07	5.12329E-08
2014	NA	NA	2.35E-05	1.09589E-05	2.67E-05	1.25E-05	6.78669E-06	3.16712E-06
2015	NA	NA	6.99E-05	3.26027E-05	5.45E-05	2.54E-05	6.9863E-07	3.26027E-07
2016	8.37E-04	3.90E-04	1.44E-04	6.71233E-05	3.78E-05	1.77E-05	5.23973E-06	2.44521E-06
2017	NA	NA	5.69E-05	2.65753E-05	2.52E-04	1.18E-04	1.55695E-06	7.26575E-07
2019	1.02E-04	4.76712E-05	7.34E-06	3.42466E-06	1.90E-04	8.88E-05	5.78865E-07	2.70137E-07

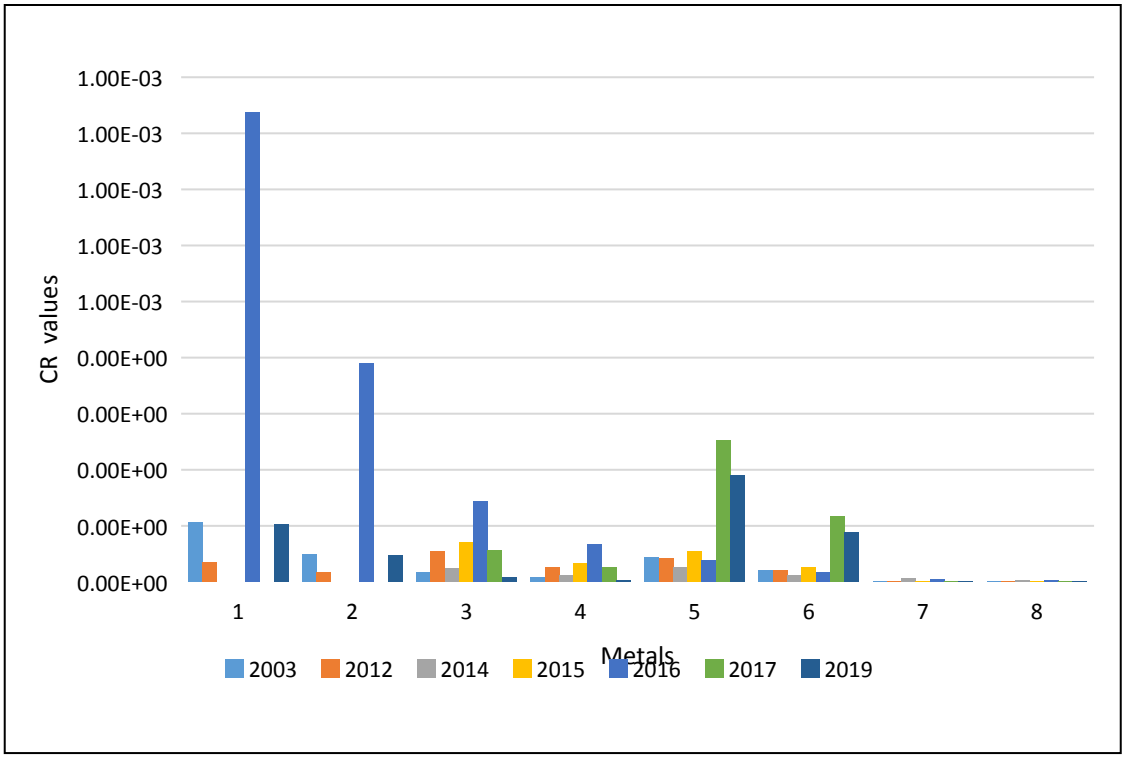

Figure 4.21: Cancer risk variation in adult and child for different heavy metals

4.2.8 Assessment of heavy metals present in leachate with surrounding temperature and rainfall pattern

Heavy metals present in leachate can become a potent source of groundwater pollution. The metals percolating down the landfill site have the immense potential to reach the groundwater table. The concentration of these metals is also dependent on the temperature and rainfall patterns in the surrounding area. The heavy metals such as lead, cadmium, nickel and chromium can pose a serious threat to human health. Human beings can become a point of contact by drinking leachate contaminated groundwater through handpumps. The metals studied for Ghazipur landfill and their variation with temperature and precipitation near the site area is shown in figure 4.22. Also, the correlation between metals concentration and temperature as well as precipitation is shown in figure 4.23. The correlation coefficient values between temperature of the area and Cd, Cr, Ni and Pb are -1, -0.782 ($p = 0.038$), -0.091 ($p = 0.846$) and -0.491 ($p = 0.263$) respectively. This shows that chromium shows a significant strong negative relation with temperature (℃). Whereas the correlation values between precipitation of the area and Cd, Cr, Ni and Pb are -0.33 ($p = 0.667$), -0.964 ($p = 0$), -0.091 ($p = 0.846$), and -0.2 ($p = 0.667$)

respectively. The results showed that out of these studied metals only chromium showed a significant strong relationship with amount of rainfall(mm).

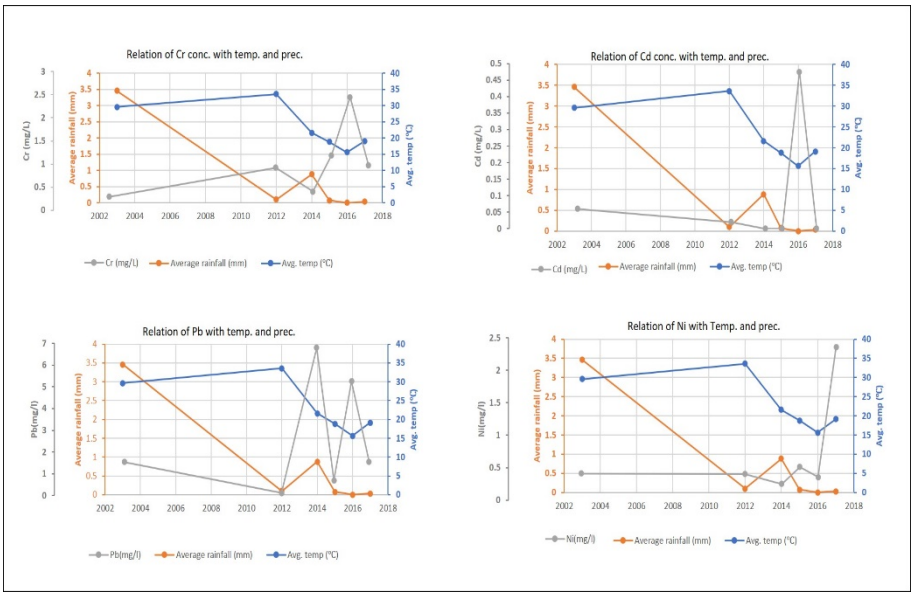

Figure 4.22: Variations of metal concentration with temperature and rainfall

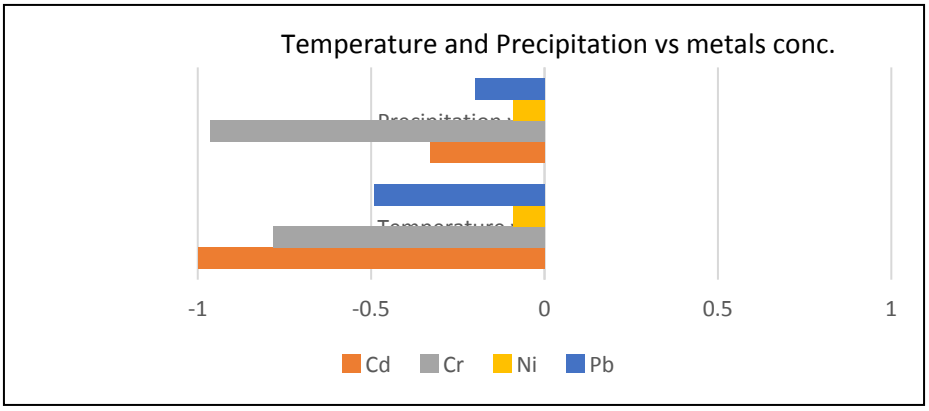

Figure 4.23: Correlation analysis of heavy metals with temperature and rainfall

4.2.9 Analysis of inorganic constituents present in leachate with respect to elevation

The inorganic constituents characterized in Ghazipur leachate were pH, TDS (total dissolved solids), TKN (total Kjeldhal nitrogen) and NH_3-N (ammonical nitrogen) and these constituents were compared with with respect to their discharge standard limits.

4.2.9.1 pH

Throughout the year-long observation of a landfill site exhibit distinctive trends in pH levels across different months—June, March, September and December were noted across various elevations (S1 to S5) of the landfill site.

March indicated lower pH values across all elevations, ranging from 6.97 to 7.91. At various heights, the pH readings were as follows: S1 (186.23 meters) - 6.97 to 7.35, S2 (175.33 meters) - 7.24 to 7.62, S3 (160.74 meters) - 7.36 to 7.7, S4 (159.94 meters) - 7.24 to 7.62, and S5 (156.77 meters) - 7.6 to 7.91(Fig. 4.24 a). These readings signify the initial stages of landfill operation characterized by acid formation from organic decomposition. Interestingly, despite differences in elevation, all sampling points uniformly displayed lower pH levels in March, emphasizing the early operation phase with acid-forming processes.

In June, a phase marked by advanced landfill maturity (Kumar & Singh, 2019), the pH values ranged from 7.8 to 9.5. Notably, at higher elevations like S1 (186.23 meters) and S2 (175.33 meters), the pH values were consistently elevated, ranging from 8.3 to 9.4. In contrast, lower elevations such as S5 (156.77 meters) displayed pH values closer to 9 (Fig.4.24 b), emphasizing more pronounced waste stabilization and biochemical activity in the final stages, aligning with the general trend of advanced maturity at lower levels due to earlier waste deposition.

Moving to September, the pH values varied from 7.72 to 8.43 across different elevations. At distinct heights: S1 (186.23 meters) -8.3 , S2 (175.33 meters) - 7.7 to 7.8, S3 (160.74 meters) – 7.9 to 8.2, S4 (159.94 meters) - 8 to 8.4, and S5 (156.77 meters) - 8.1 to 8.4 (Fig.4.24 b). These relatively higher pH values compared to March indicated increased biological activity owing to warmer temperatures influencing waste decomposition.

Finally, in December, the pH values decreased across elevations, ranging from 6.53 to 7.1. Notably, at different heights: S1 (186.23 meters) - 6.53 to 6.73, S2 (175.33 meters) - 6.68 to 6.88, S3 (160.74 meters) - 6.72 to 6.92, S4 (159.94 meters) - 6.75 to 6.95, and S5 (156.77 meters) - 6.9 to 7.1 (Fig.4.24 b). These lower pH readings indicate reduced biological activity owing to colder temperatures, with higher elevations experiencing a more pronounced decline, emphasizing the impact of colder temperatures on biological activity.

4.2.9.2 TDS

The data reflects the fluctuating Total Dissolved Solids (TDS) measurements across various sites (S1 to S5) over several years and sampling periods. In March Site1 showed consistent growth from 17479.8 mg/L (2020) to 23101.6 mg/L (2022) while maintaining a height of 186.23 m (Fig 4.25 a). Similarly, S2 displayed continuous increases reaching 19215.6 mg/L (2022) from 15087.9 mg/L (2020) at a height of 175.33 m. Site S3 experienced fluctuations over the years fluctuating from 15215.2 mg/L (2020) to 15142.05 mg/L (2022) at a height of 160.74 m. Conversely, Site S5 showcased a notable rise from 8341 mg/L (2020) to 13467 mg/L (2022) at a height of 156.77m. By June, there were decreases observed; S1 dropped to 24213.1 mg/L (2022), S2 to 20327.1 mg/L (2022), S3 to 16253.55 mg/L (2022), S4 to 15868.3 mg/L (2022) and S5 to 14578.5 mg/L (2022), indicating a potential decline in inorganic material presence. This trend continued by December, with further reductions observed across all sites – S1 to 16159.3 mg/L (2020), S2 to 13767.4 mg/L (2020), S3 to 13894.7 mg/L (2020) and S4 to 13585.7 mg/L (2020) in Fig 4.25 b, reinforcing the pattern of decreasing TDS values as a potential indicator of diminishing inorganic material content within the samples over time.

4.2.9.3 TKN

Across March and June from 2020 to 2022, the " TKN" parameter fluctuated significantly across sites and heights. In March 2020, Site S1 reported the highest value (2217 mg/L) at 186.23m in height, contrasting with the lowest (1872 mg/L) at Site S5 with height 156.77m in Fig 4.26 a. June 2020 maintained the trend with Site S1 registe ring the highest (2200 mg/L) and Site S5 the lowest (1763 mg/L) values. In June 2021, Site S1 recorded the high (2200 mg/L) while Site S4 reported the low (1742 mg/L) in Fig 4.26 a. September data over the years showed varied trends: In 2020, high at Site S1 (2129 mg/L) and low at Site S5 (1810 mg/L), 2021 high at Site S1 (2150 mg/L) and low at Site S5 (1818 mg/L) and in 2022 high again at Site S1 (2010 mg/L) with a low at Site S5 (1890 mg/L). Notably, December values spiked in 2020 (2226.1 mg/L) and 2021 (2330.1 mg/L), both at Site S1 in Fig 4.26 b, indicating that it can be due to household wastes. The presence of this component shows the presence of reducing environment (Bag et al., 2016).

4.2.9.4 Ammonical Nitrogen

The NH3-N concentration variations observed across sites S1 to S5, concerning different months and years, might be linked to the varying heights at which these measurements were taken. In

March, there is a consistent declining trend across sites, with S1 and S5 displaying decreases from 1216 mg/L to 972 mg/L and 1082 mg/L to 862 mg/L, respectively (Fig.4.27 a). However, June data exhibits more fluctuations: S1 decreases from 1115 mg/L in 2020 to 962 mg/L in 2021 before a slight rise to 985 mg/L in 2022, while S4 drops from 1110 mg/L in 2020 to 950 mg/L in 2021, sharply declining to 801mg/L in 2022 (Fig.4.27 b). September data also presents diverse trends among sites based on their heights, with S1 and S2 following a decreasing pattern from 1240 mg/L to 947 mg/L and 1210 mg/L to 927 mg/L, respectively. S3 initially rises to a peak of 1150 mg/L in 2021 before decreasing to 887 mg/L in 2022, reflecting S4 decline from 1190 mg/L in 2020 to 852 mg/L in 2022. However, S5 shows minor fluctuations between 820 mg/L and 837 mg/L (Fig.4.27 b). Moreover, in December, NH3-N levels across all sites tend to increase from 2020 to 2021: S1 rises from 1255 mg/L to 1335 mg/L, S2 from 1216 mg/L to 1296 mg/L, S3 from 1201mg/L to 1281 mg/L , S4 from 961mg/L to 1241 mg/L, and S5 from 1121 mg/L to 1201 mg/L (Fig.4.27 b). These variations, possibly due to the deamination of amino acids during the decomposition of organic compounds, might also reflect the influence of height-related environmental factors impacting the rates of organic matter breakdown and subsequent ammonia nitrogen concentrations at different elevations.

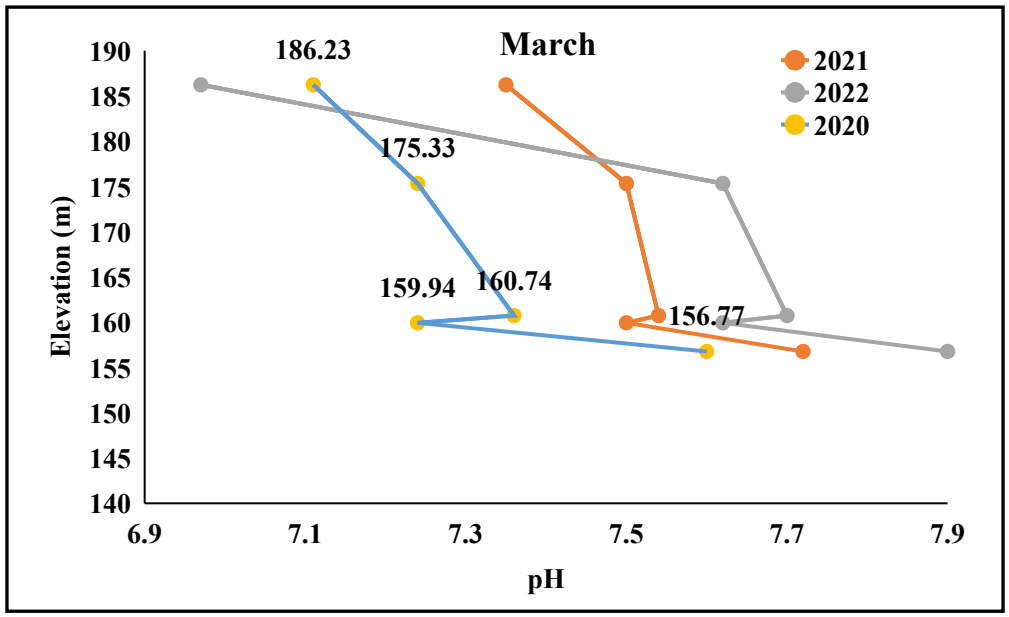

Figure 4.24 a) pH Variability Across elevation in March at different sites

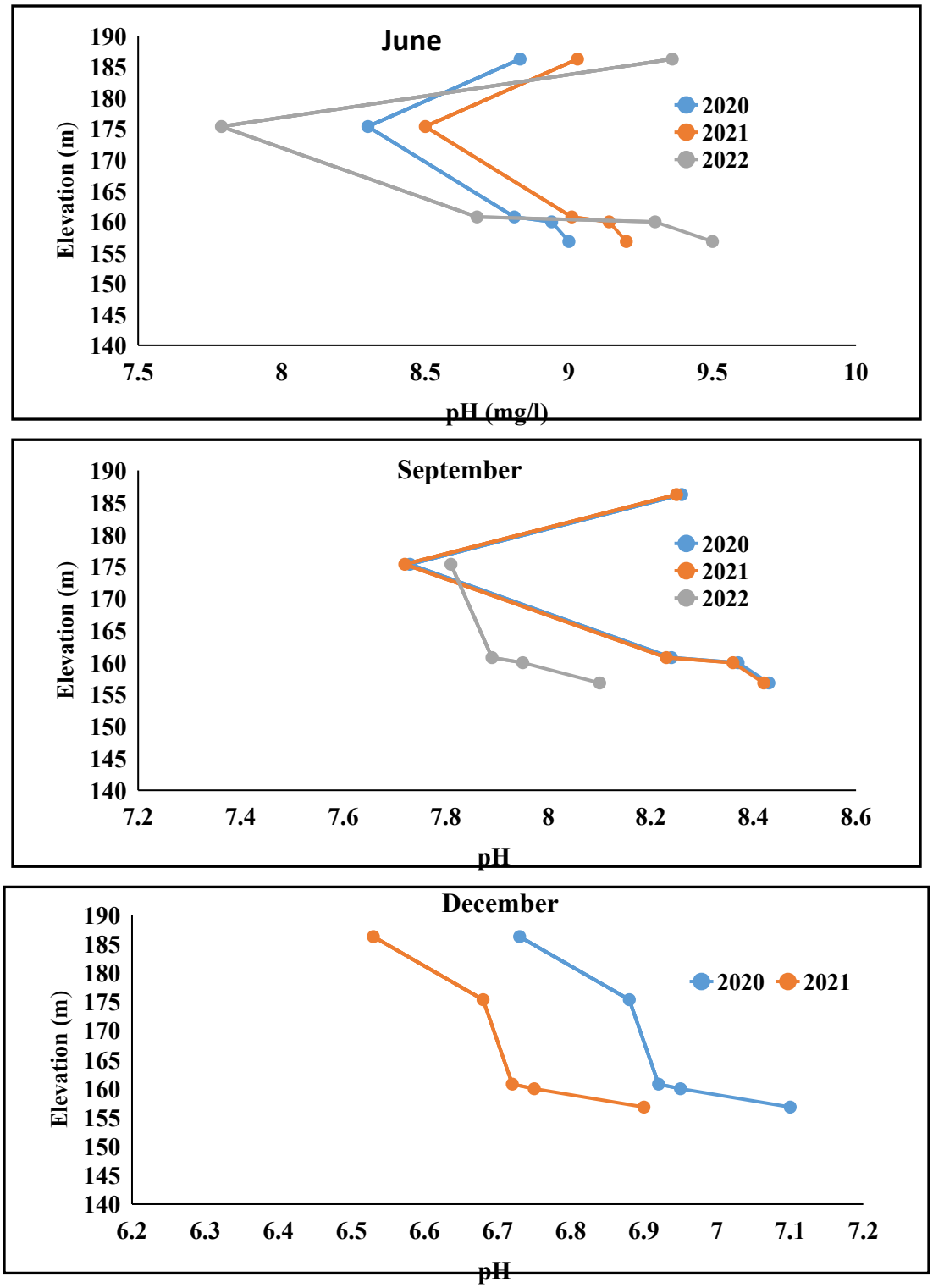

Figure 4.24 b) pH Variability across Elevations in June, September & December at different site

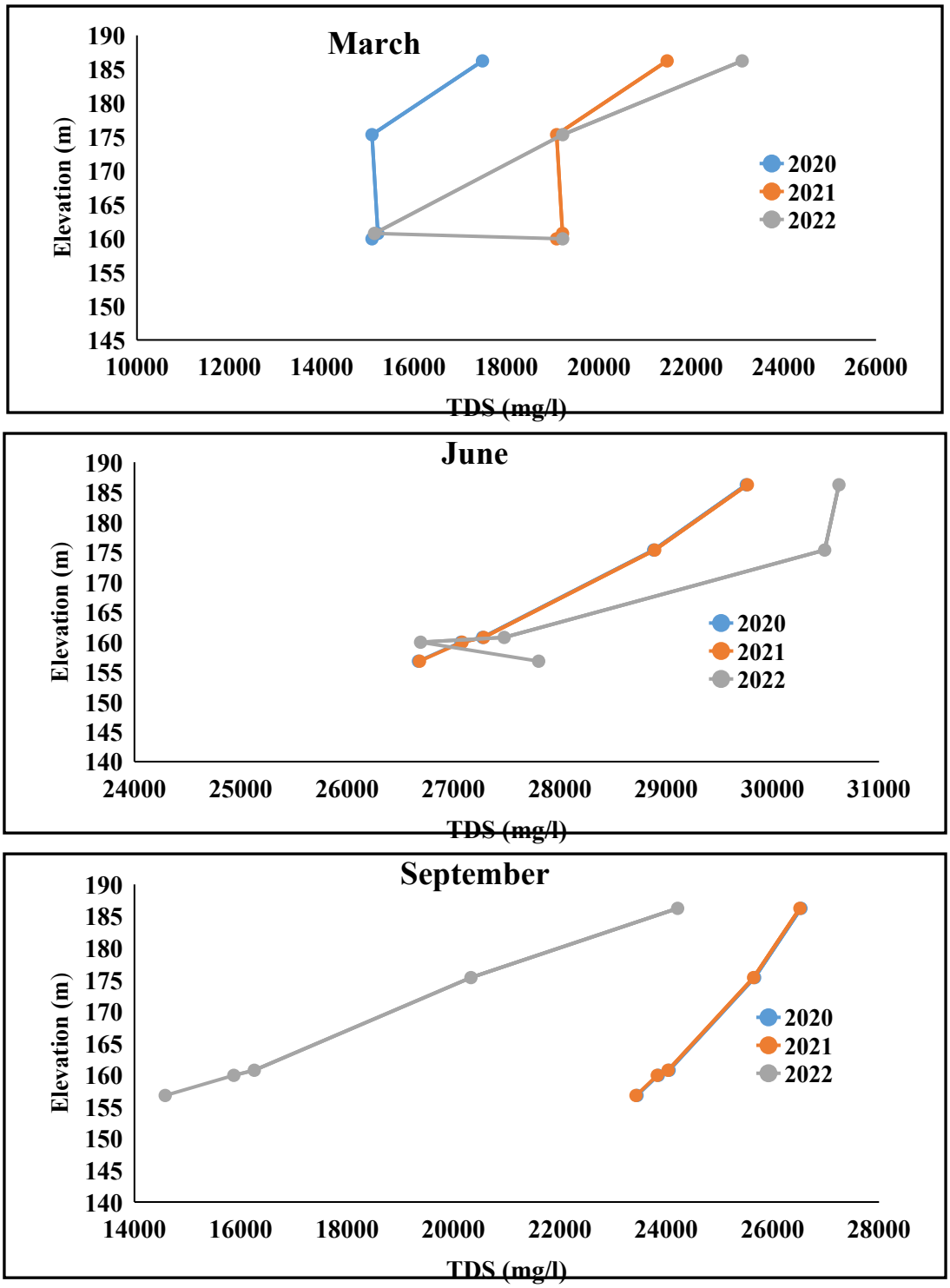

Figure 4.25 a) TDS Variability across Elevations in March, June & September at different site

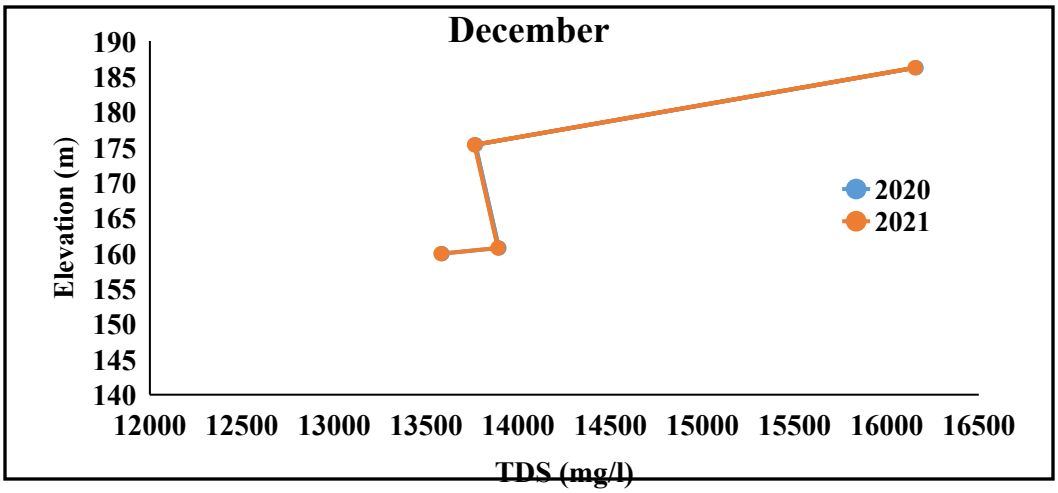

Figure 4.25 b) TDS Variability across Elevations in December at different site

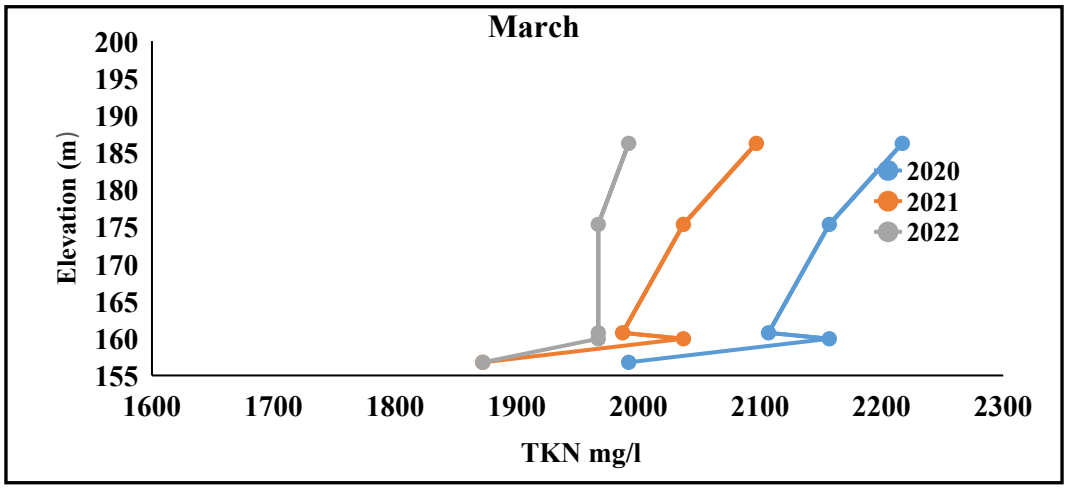

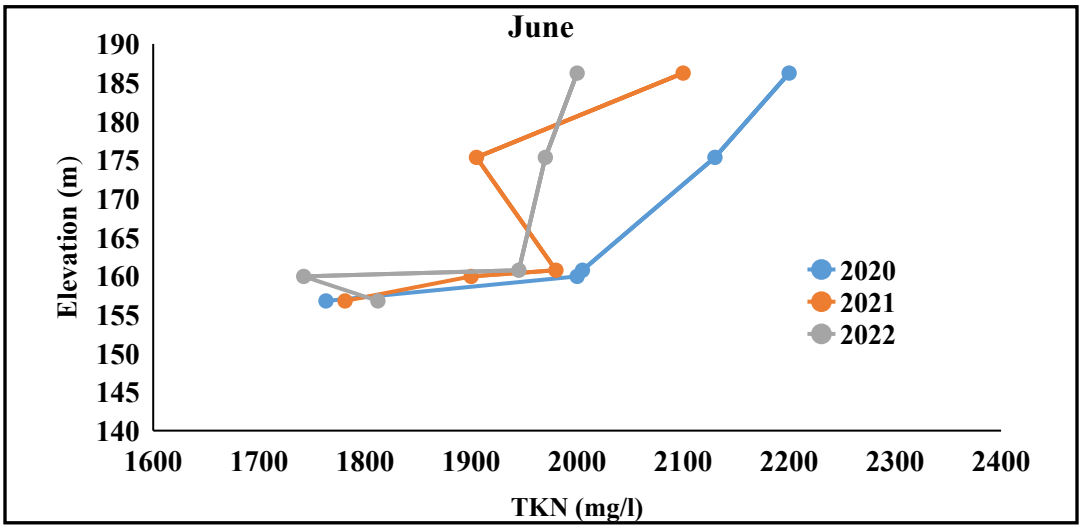

Figure 4.26 a) TKN Variability across Elevations in March & June at different site

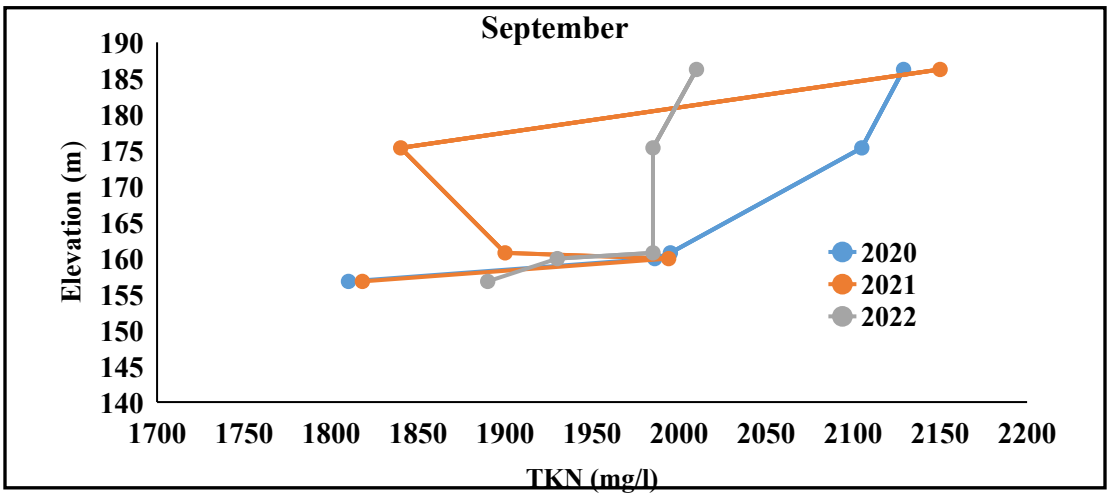

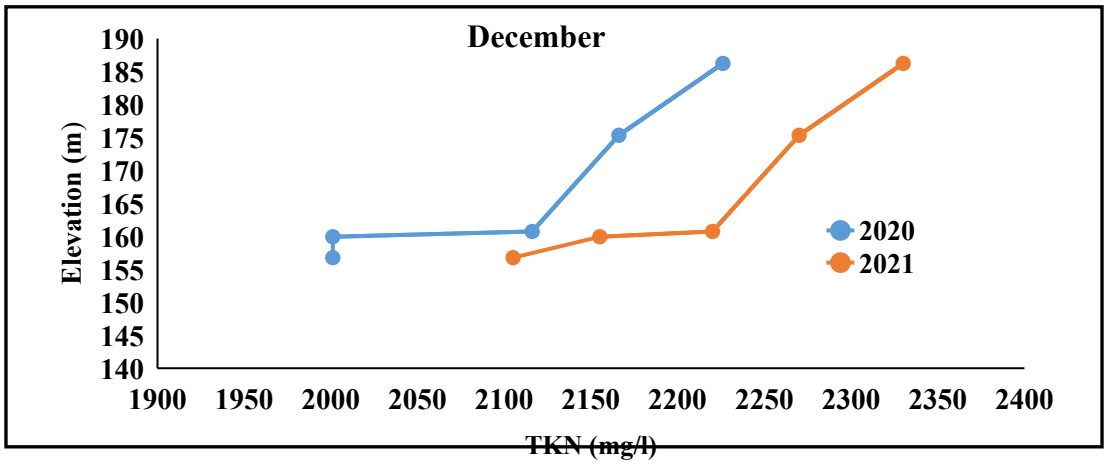

Figure 4.26 b) TKN Variability across Elevations in September & December at different site

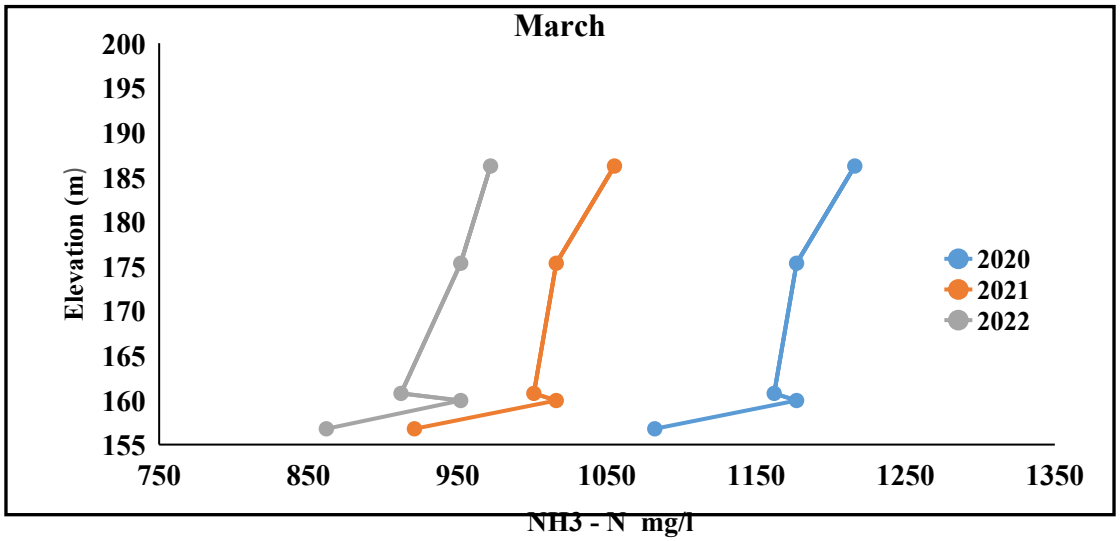

Figure 4.27 a) NH3-N Variability across Elevations in March at different site

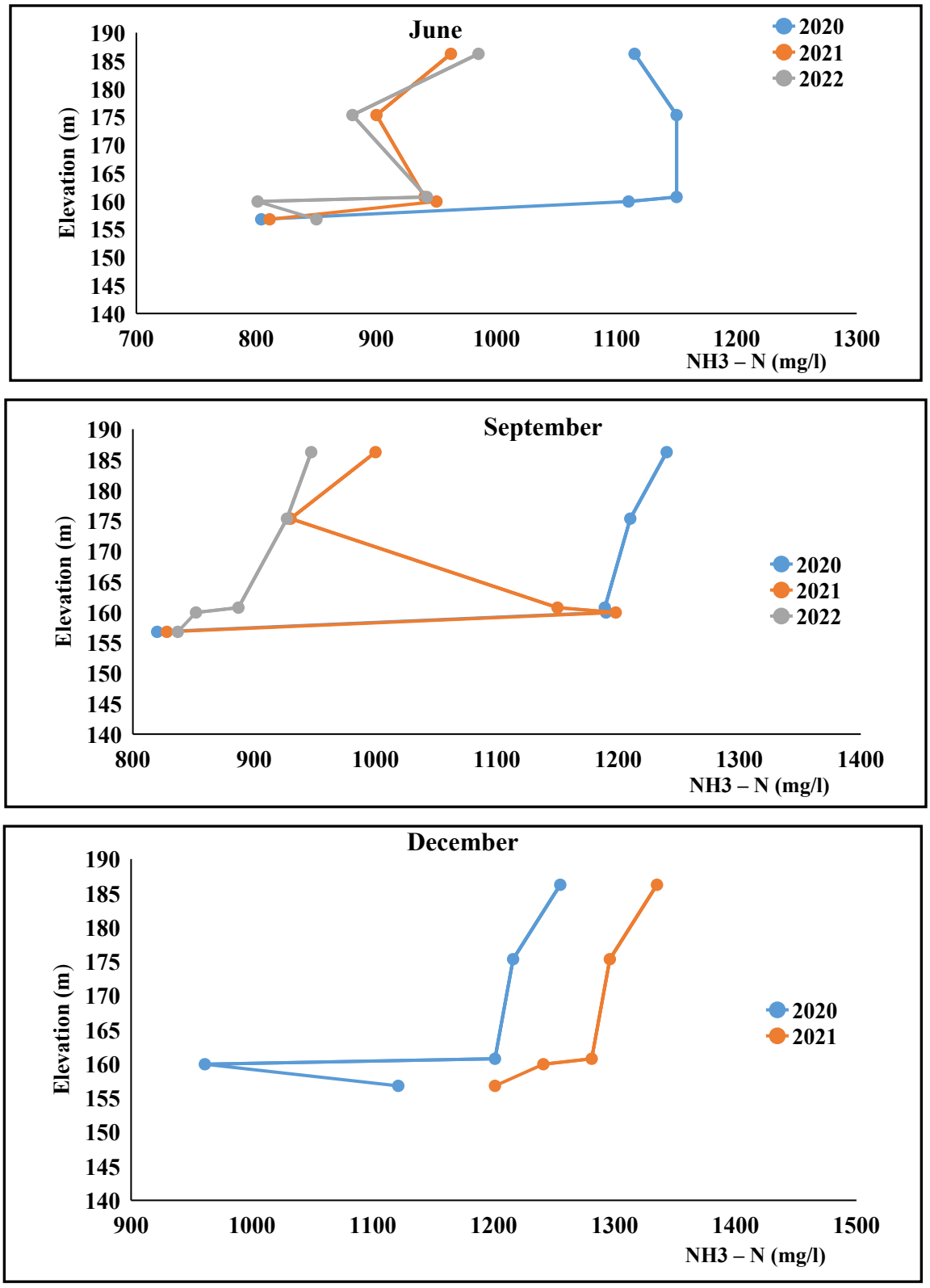

Figure 4.27 b) NH3-N Variability across Elevations in June, September & December at different site

4.2.10 Analysis of organic constituents present in leachate with respect to elevation

Variation of BOD and COD with increase in distance is shown in Fig. 4.28 & 4.29 the provided dataset of March illustrates the Biological Oxygen Demand (BOD) across five distinct sites (S1 to S5) over a three-year span from 2020 to 2022. Throughout this period, a consistent trend of decreasing BOD values is observed across most sites (Fig.4.28 a). In 2020, S1 started with a BOD of 563 mg/L, gradually declining to 476 mg/L by 2022. Similarly, S2 began at 547 in 2020, dropping to 446 mg/L in 2022. Site S3 commenced at 503 mg/L and ended at 441 mg/L over the same period, while S4 and S5 exhibited initial BOD values of 547 mg/L and 367 mg/L, respectively, decreasing to 446 mg/L and 376 mg/L by 2022. This downward trend suggests potential improvements in water quality.

In March, the Chemical Oxygen Demand (COD) concentration across five distinct sites (S1 to S5) during the years 2020, 2021, and 2022 (Fig.4.29 a). Each site, identified by its specific height measurement, demonstrates varying COD values across the three-year period. For instance, site S1 started in 2020 with a COD of 32,760 mg/L increased to 37,000 mg/L in 2021, and then decreased to 34,100 mg/L by 2022. Similarly, other sites like S2, S3, and S4 showed fluctuations in their COD values over the same timeframe, albeit with different starting and ending values. Interestingly, site S5 stands out significantly, initiating at 9,160 mg/L in 2020, escalating remarkably to 28,100 mg/L by 2022. This abrupt increase in COD at S5 might indicate a high organic strength.

In terms of BOD values for June, a varied pattern emerges across the sites. Site S1 experienced an increase from 500 mg/L in 2020 to 550 mg/L in 2022, indicating a rise in organic pollution or decomposition of organic matter in the water (Fig.4.28 a). Conversely, S2 showed a decline from 450 mg/L to 470 mg/L over the same period, suggestive of a potential improvement in water quality in this location. Sites S3 and S4 exhibited fluctuations in their BOD values, while S5 demonstrated a noticeable decrease from 452 mg/L in 2020 to 370 mg/L in 2022, possibly signaling a positive shift in the environmental conditions impacting this site.

Regarding the COD measurements for June, site S1 showed an increase from 51,850 mg/L in 2020 to 54,850 mg/L in 2022, indicating a potential rise in the concentration of organic compounds, chemicals, or pollutants in the water (Fig 4.29 b) . Site S2 experienced fluctuations, starting and ending at 51,850 mg/L in 2020 and 2022, respectively. S3 displayed a decline from

53,850 mg/L in 2020 to 49,850 mg/L in 2022, suggesting a potential improvement in water quality in this area. S4 displayed a similar pattern, with a decline from 52,850 mg/L to 49,980 mg/L. Remarkably; site S5 exhibited an increase in COD from 49,850 mg/L in 2020 to 50,000 mg/L in 2022, indicating a possible deterioration in water quality or an influx of organic compounds or pollutants.

In September, the data suggests that Site S3 likely sustained its historically low pollution levels, with BOD ranging between 382 mg/L to 475 mg/L and COD varying from 40080 mg/L to 52000 mg/L (Fig.4.28 a). S4 and S5, typically displaying lower pollution levels than S1 and S2, probably maintained BOD levels around 410 to 463 mg/L and COD between 36080 mg/L to 51000 mg/L (Fig.4.29 a).

Notable was Site S5 decreasing trend in BOD from 432 mg/L in 2021 to 410 mg/L in 2022, hinting at a potential reduction in organic pollution, which might have persisted into September (Fig.4.28 b) .Conversely, the increase in BOD at Site S3 from 382 mg/L in 2021 to 475 mg/L in 2022 might imply ongoing rising organic pollution possibly extending into September. Overall, the general decreasing trend in COD across all sites from 2021 to 2022 indicates a potential reduction in pollutants, which might have continued or stabilized by September, signifying positive strides in managing water quality.

In December, BOD (Biological Oxygen Demand) levels for the years 2020 and 2021. Site heights range from 156.77 to 186.23, while BOD levels show a decline across all sites from 2020 to 2021, indicating improved water quality. Across several sites labeled S1 through S5, their respective heights and recorded values for the years 2020 and 2021 are documented (Fig.4.28 b). Site S1, positioned at a height of 186.23, exhibited recorded values of 31770 mg/L in 2020 and 31650 mg/L in 2021 (Fig.4.28 b). Site S2, slightly lower at 175.33 in height, displayed values of 26970 mg/L in 2020 and 26850 mg/L in 2021. Site S3, at 160.74 in height, had recorded figures of 26470 mg/L in 2020 and 26350 mg/L in 2021. Site S4, with a height of 159.94, showcased values of 26170 mg/L in 2020 and 26050 mg/L in 2021. Site S5, at a height of 156.77, lacks recorded data for both 2020 and 2021.

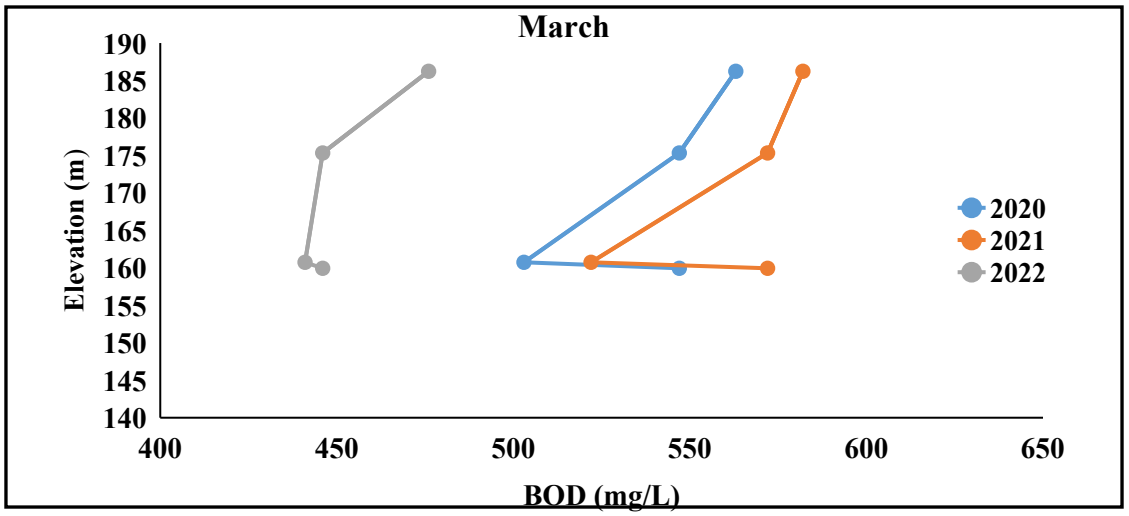

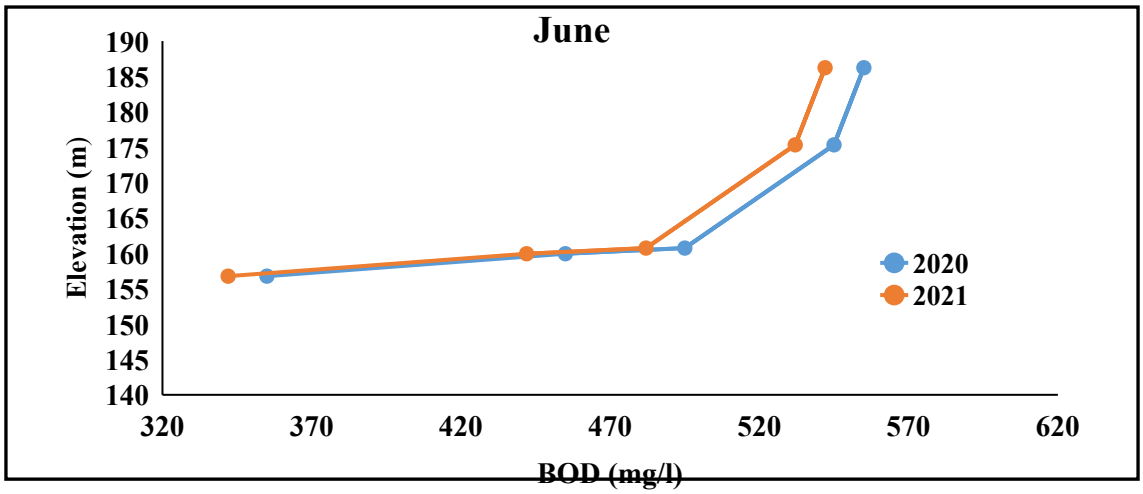

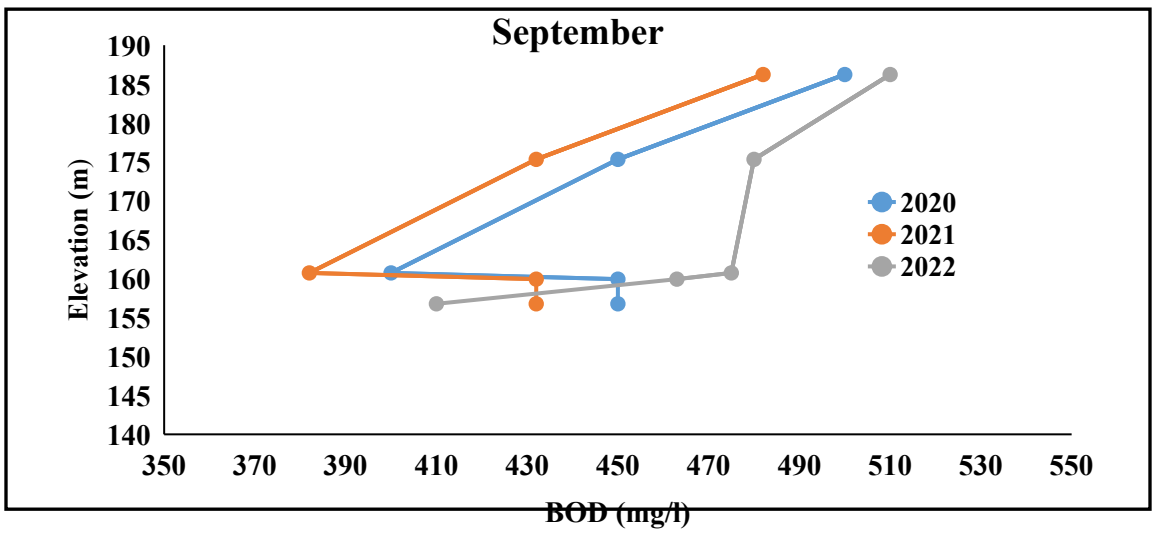

Figure 4.28 a) BOD Variability Across elevation in March, September & June at different sites

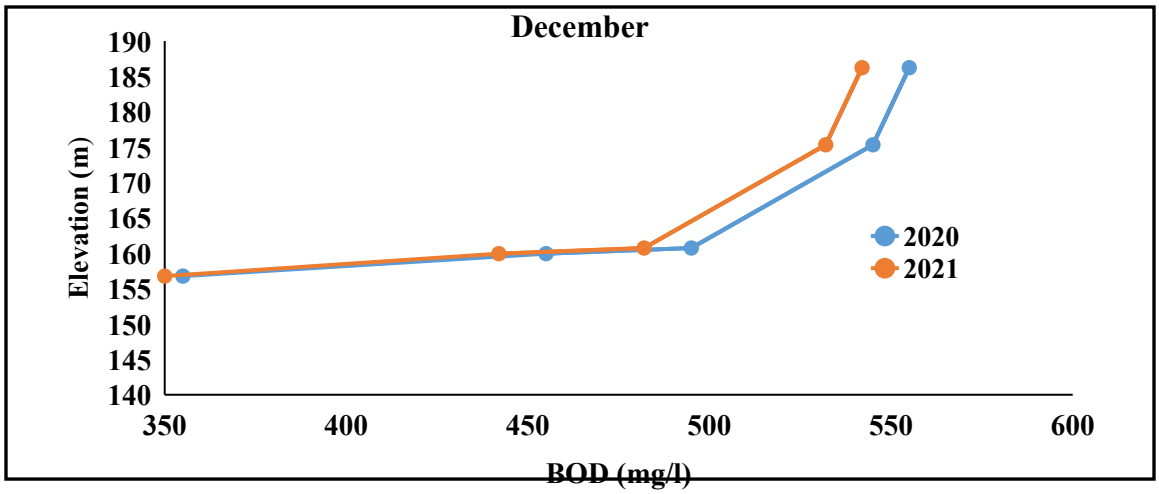

Figure 4.28 b) BOD Variability Across elevation in December at different sites

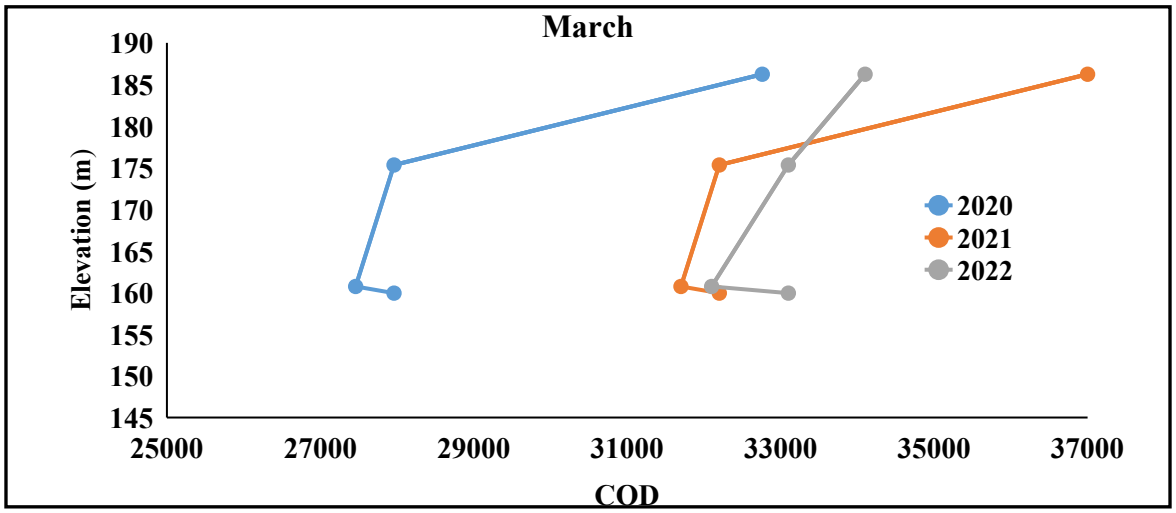

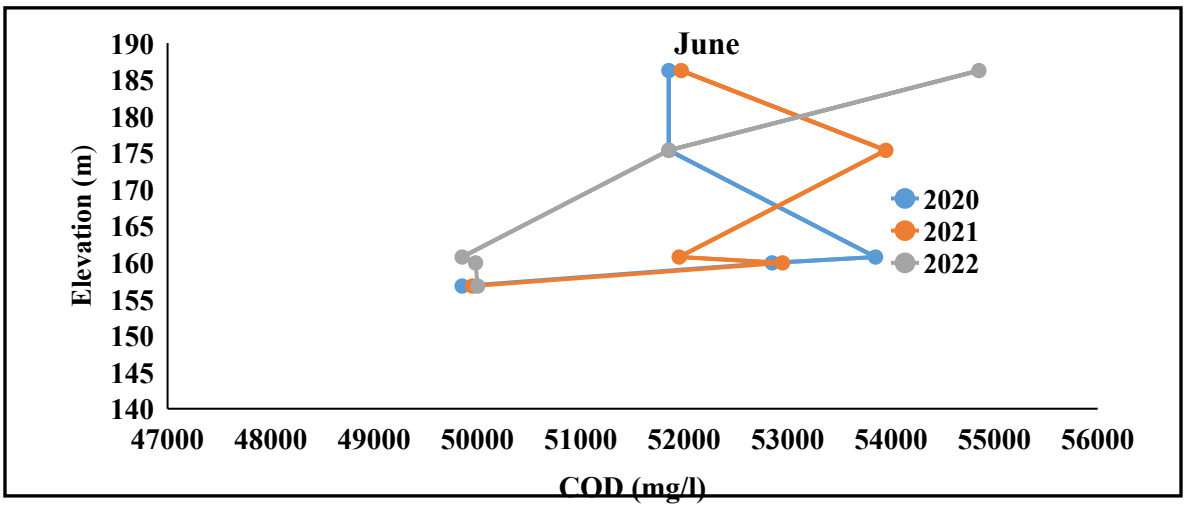

Figure 4.29 a) COD Variability Across elevation in March & June at different sites

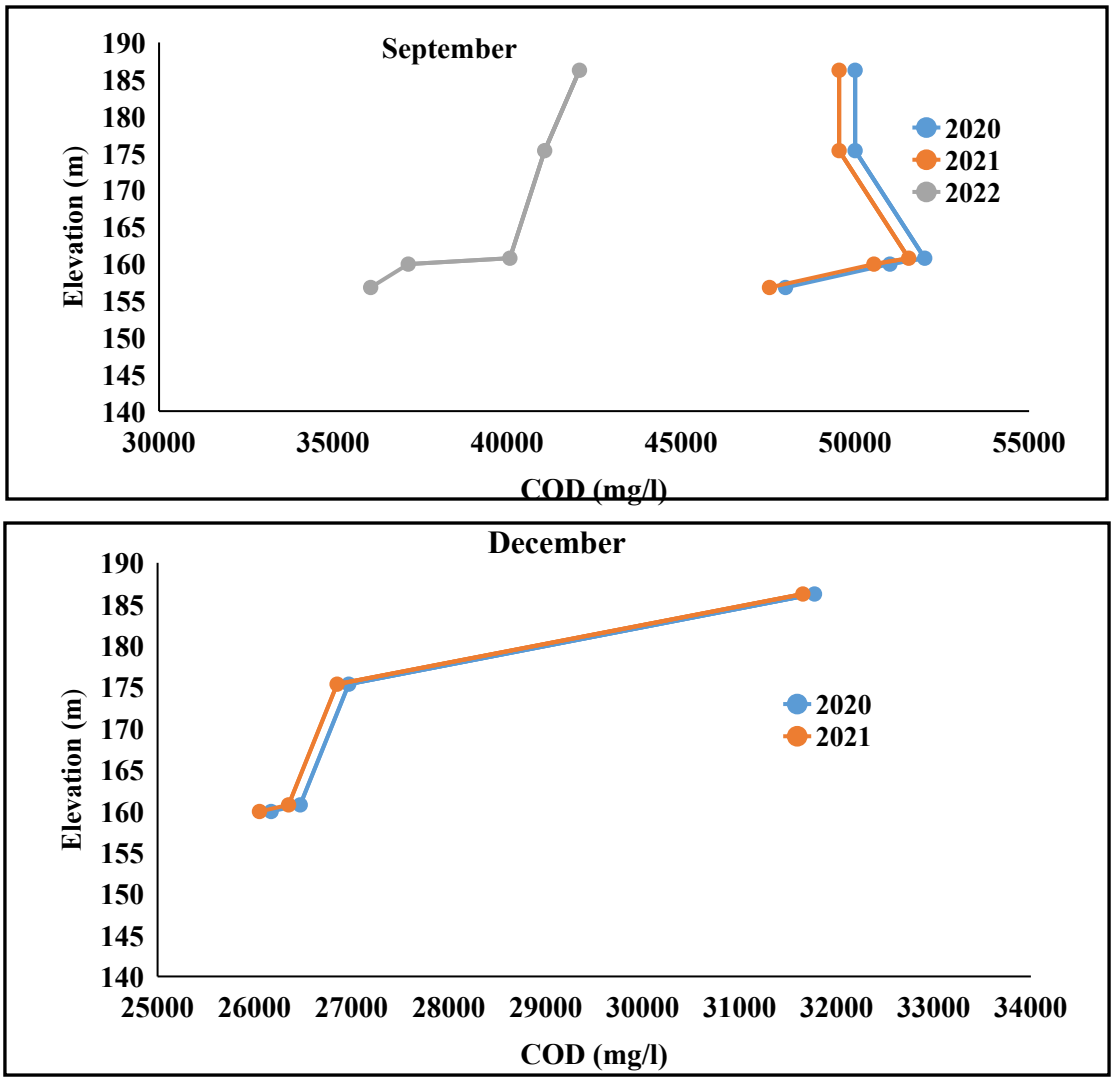

Figure 4.29 b) COD Variability Across elevation in September & December at different sites

4.2.11 Analysis of salts present in leachate with respect to elevation

The type of salts analyzed were cationic (Na^+ & K^+) and anionic (Cl^-, HCO_3^-, $NO_3^-$and F^-). The concentration of these salts present in Ghazipur leachate are present in figure 4.30 to 4.35.

4.2.11.1 Cation

In March, Over three years, spanning from 2020 to 2022, sodium and potassium concentrations were monitored at five sites, alongside their corresponding elevations. Sodium levels exhibited fluctuations across the sites: ranging from 272-262 mg/L at S1, 179-187 mg/L at S2, 164-177 mg/L at S3, 179-187 mg/L at S4, to 223-249 mg/L at S5 (Fig.4.30 a). Simultaneously, potassium concentrations varied between 408.46 mg/L -447.04 mg/L at S1, 243.6 mg/L - 263.9 mg/L at S2,

310.46 mg/L - 378.5 mg/L at S3, 243.6 mg/L -263.9 mg/L at S4, and 521.8-531 mg/L at S5 (Fig.4.31 a). These fluctuations were independent of microbiological activities within the landfill sites and likely originated from the decomposition of plant materials and household waste. Notably, heightened potassium levels in groundwater suggest the potential presence of leachate, pointing toward a probable contamination issue (Naveen et al., 2014).

In June, Site1 demonstrated a notable escalation of sodium concentration from 271 mg/L in 2020 to 362 mg/L in 2022, indicating a substantial increase over the observed period. Conversely, S2 began at 180 mg/L in 2020 and then declined to 171 mg/L by 2022, highlighting fluctuations with a subsequent decrease from its peak (Fig.4.30 a). Site S3 maintained a relatively consistent range, oscillating between 189-200 mg/L from 2020 to 2021 before slightly dropping to 185 mg/L by 2022. Site S4 exhibited an increase from 193 mg/L in 2020 to 279 mg/L in 2022, signifying a significant rise over the three years. Meanwhile, S5 displayed variations from 269 mg/L in 2020 to 268 mg/L in 2022, displaying minor changes over the observed timeframe.

The potassium concentrations across the various sites displayed distinctive ranges from 2020 to 2022 in june. Site S1 exhibited a considerable range, starting at 538 mg/L in 2020 and escalating to 813 mg/L by 2022 (Fig.4.31 a). Meanwhile, Site S2 showed a range from 263 mg/L in 2020 and then dropping to 172 mg/L in 2022. Site S3 demonstrated concentrations ranging from 355 mg/L in 2020 to 281 mg/L in 2022, displaying a notable decline over the observed period. Site S4 started at 429 mg/L in 2020, rose and then reached 548 mg/L in 2022, indicating an increase over time. Lastly, Site S5 maintained relatively consistent values, ranging from 543 mg/L in 2020 to 551 mg/L in 2022, with minimal variation.

In September, Sodium concentrations fluctuated across the sites over the three-year span. Site S1 experienced a gradual decline from 277.5 mg/L in 2020 to 270.3 mg/L in 2022 (Fig.4.30 a). In contrast, S2 displayed a fluctuating pattern, initially dropping from 186.675 mg/L in 2020 to 182.025 mg/L in 2021 but then rising to 195.45 mg/L in 2022. Site S3 exhibited a consistent decrease from 195.6 mg/L in 2020 to 172.3 mg/L in 2022, indicating a notable decline. S4 remained relatively stable, fluctuating marginally from 199.5 mg/L in 2020 to 193.8 mg/L in 2022. S5 displayed a gradual decrease from 275.25 mg/L in 2020 to 257 mg/L in 2022, showing a declining trend over time.

On the other hand, potassium concentrations demonstrated varying trends across the sites with changing elevations. Site S1 exhibited a significant drop from 532.535 mg/L in 2020 to 440.74 mg/L in 2022 (Fig.4.31 b). S2 displayed a slight decrease from 257.55 mg/L in 2020 to 257.6 mg/L in 2022. Conversely, S3 experienced a fluctuation, declining from 349 mg/L in 2020 to 343.5 mg/L in 2021, then increasing notably to 372.2 mg/L in 2022. Site S4 displayed an increase from 423 mg/L in 2020 to 444.6 mg/L in 2022. S5 exhibited a decreasing trend, declining from 537.5 mg/L in 2020 to 524.7 mg/L in 2022.

In December, over the observed period from 2020 to 2021, sodium concentrations exhibited consistent declines across the sites. Site S1 displayed a decrease from 261.5 mg/L to 251.3 mg/L, marking a slight reduction in sodium content (Fig.4.30 b). Similarly, Site S2 demonstrated a decline from 167.8 mg/L to 157.6 mg/L, reflecting a noticeable decrease in sodium concentration over the year. Site S3 echoed this trend, highlighting a reduction from 166.4 mg/L to 156.2 mg/L in sodium content. S4 mirrored these patterns, displaying a decline from 169.3 mg/L to 159.1 mg/L in sodium concentration. Lastly, Site S5 followed suit, registering a decrease from 211.6 mg/L to 201.4 mg/L in sodium levels.

Across the span of one year, from 2020 to 2021, potassium concentrations showed consistent declines across all observed sites. Site S1 illustrated a decrease from 408.26 mg/L to 388.26 mg/L (Fig.4.31 b). Similarly, Site S2 displayed a decline from 243.4 mg/L to 223.4 mg/L, indicating a significant drop in potassium concentration. Site S3 mirrored this trend, exhibiting a decrease from 310.26 mg/L to 290.26 mg/L in potassium levels. S4 demonstrated a decline from 427.13 mg/L to 407.13 mg/L in potassium concentration, following the decreasing pattern observed in other sites. Finally, Site S5 also experienced a reduction, declining from 521.6 mg/L to 501.6 mg/L in potassium content.

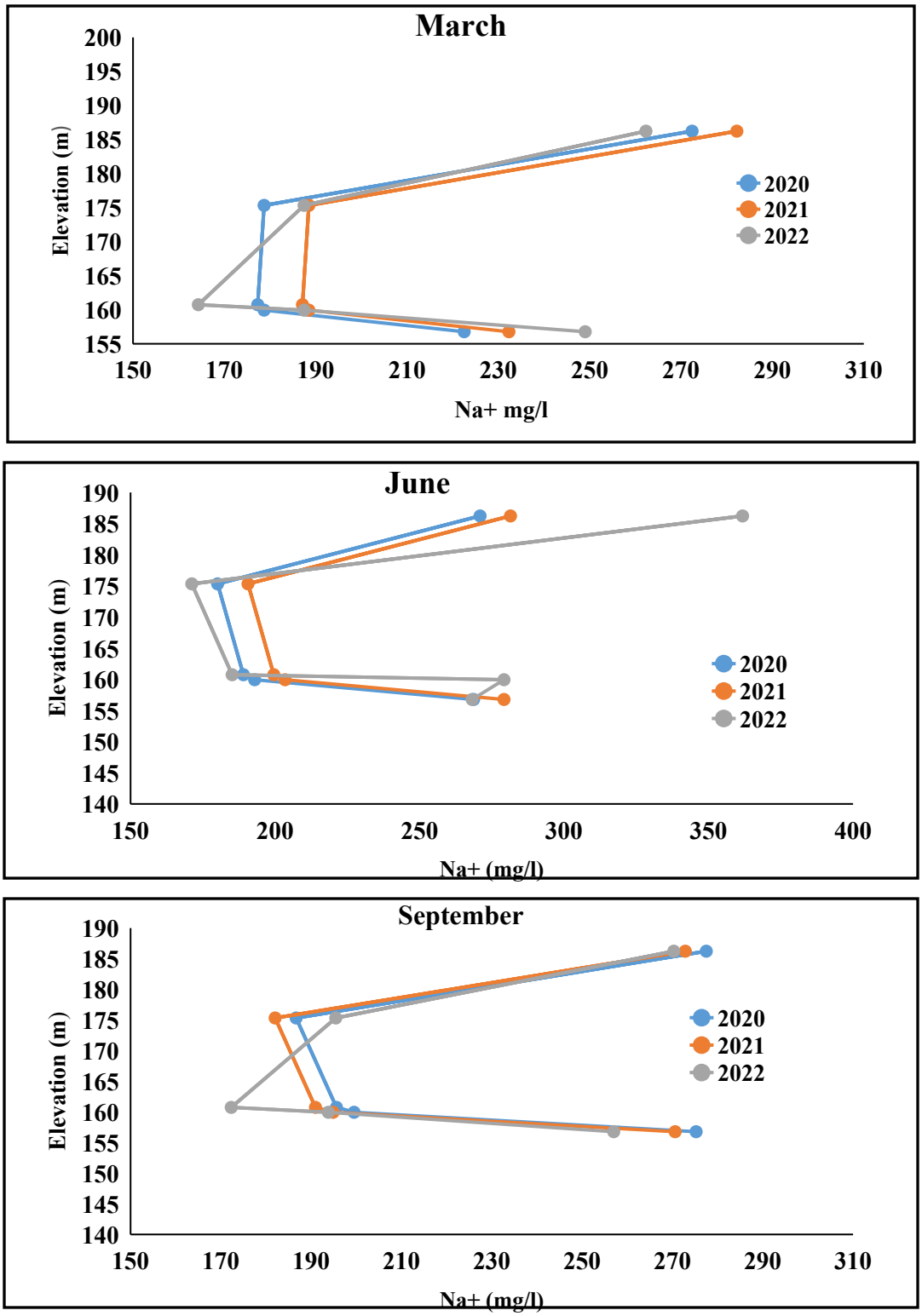

Figure 4.30 a) Sodium Variability Across elevation in March, June & September at different sites

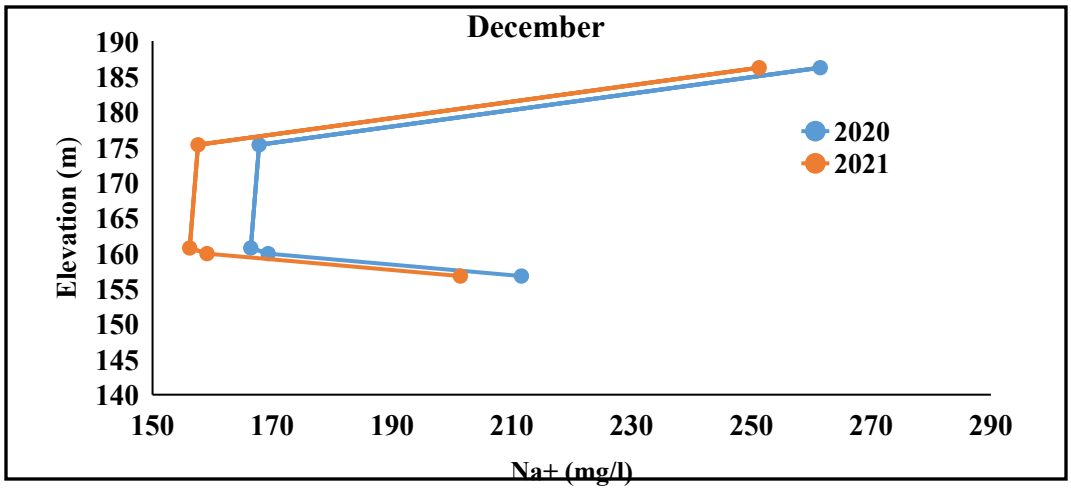

Figure 4.30 b) Sodium Variability Across elevation in December at different sites

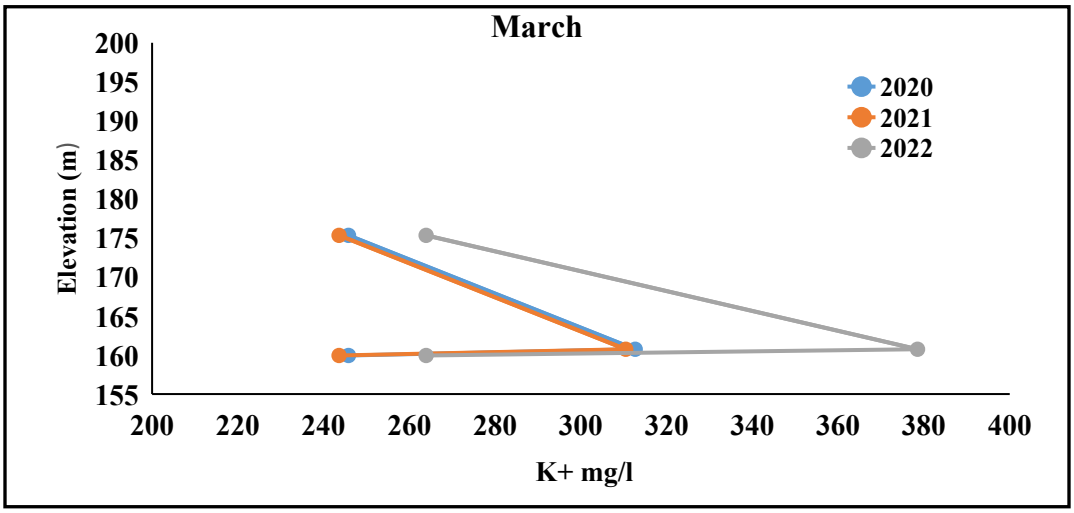

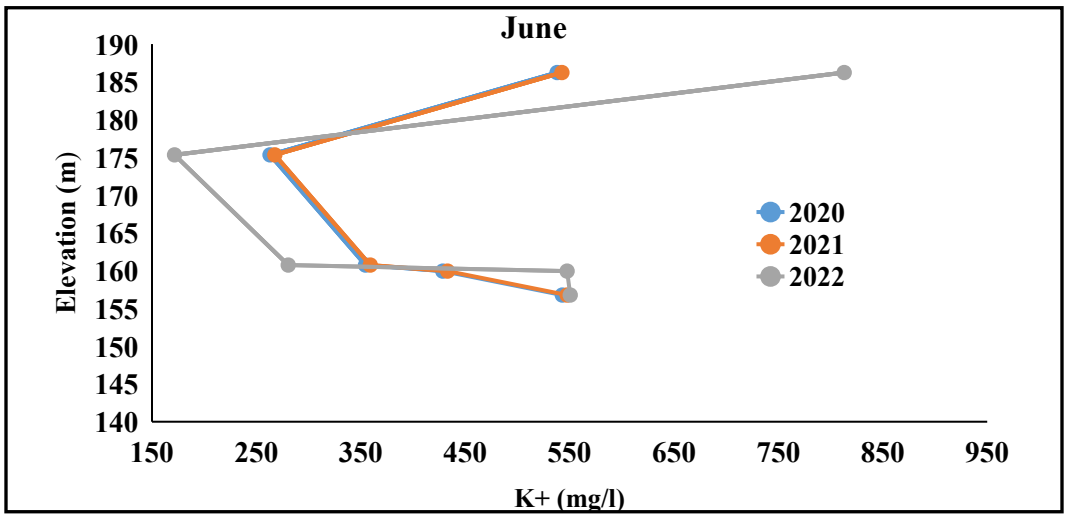

Figure 4.31 a) Potassium Variability Across elevation in March & June at different sites

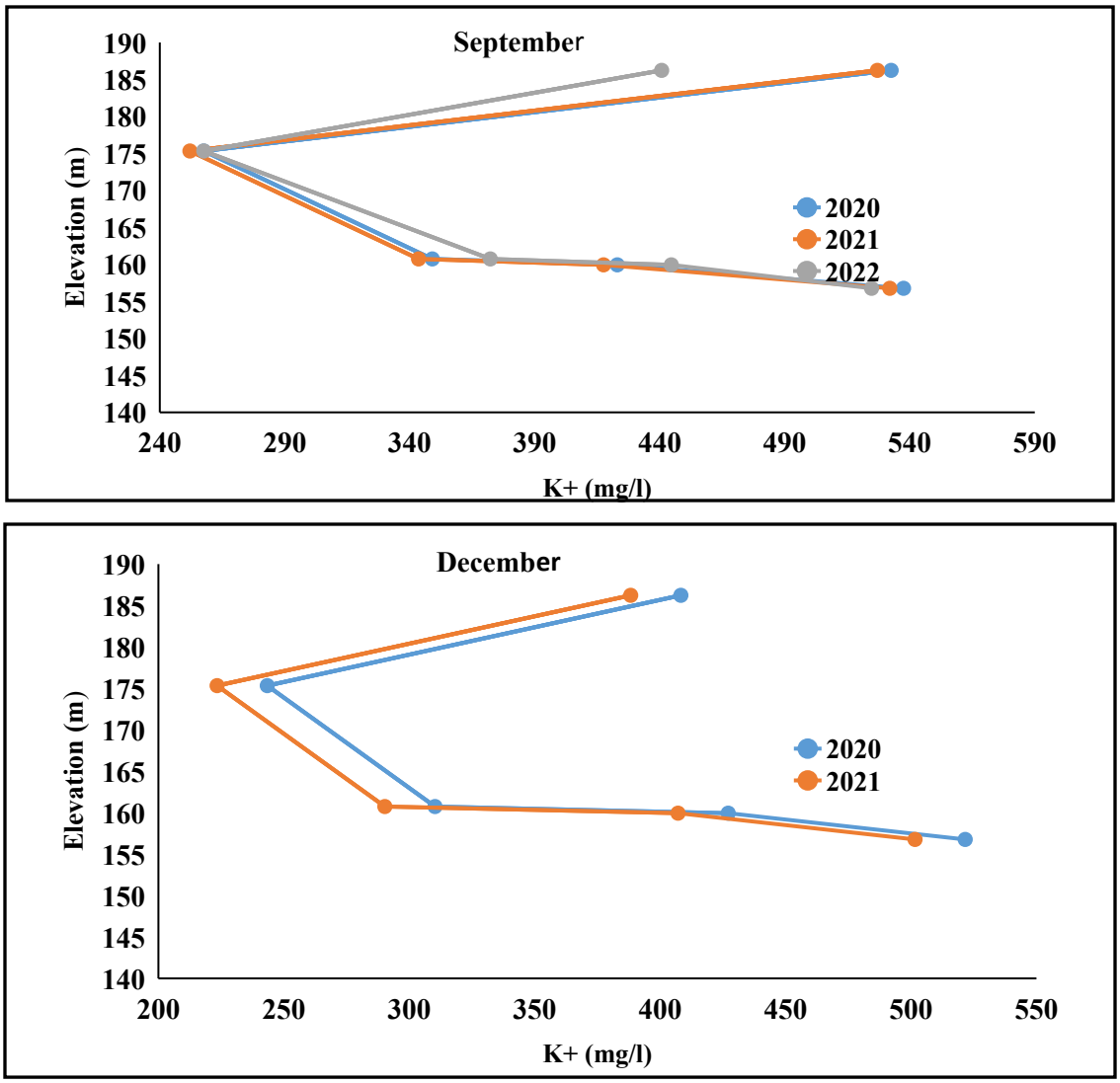

Figure 4.31 b) Potassium Variability Across elevation in September & December at different sites

4.2.11.2 Anion

In March, significant variations in chloride concentrations were evident across the sites and years, with the highest level detected at Site S5, reaching 5208.5 mg/L in 2022 (Fig.4.32 a). This notable peak was observed at an elevation of 156.77 meters, signaling substantial chloride presence at this specific location during that period. Chloride, characterized by negligible sorption, complexation, and precipitation reactions, stands as a conservative pollutant in the environment.

The range of nitrate concentrations showcased distinct fluctuations across various sites and years. The highest recorded nitrate concentration of 425.07 mg/L in 2021 was notably observed at Sites S2 and S4, situated at elevations of 175.33 m and 159.94 meters, respectively (Fig 4.33

a). Conversely, the lowest nitrate concentration, notably minimal at 37.4 in 2020, was identified solely at Site S5, positioned at an elevation of 156.77 meters. The presence of nitrates in leachate can be attributed to the oxidation process of ammonium, transitioning to nitrite and eventually forming nitrate.

HCO3 concentrations peaked at 12964 mg/L in 2022 at higher elevations (S2 and S4 at 175.33m and 159.94m), while reaching its lowest level of 9074 mg/L in 2022 at an elevation of 160.74m (S3) in Fig.34 a. The presence of bicarbonate may arise from organic waste decomposition or inert waste processes, contributing to its varying concentrations across these sites and elevations.

In June, variations in chloride concentrations were pronounced across different elevations and sites. The substantial peak of 8572 mg/L in 2022 at Site S3, positioned at 160.74 meters, highlighted a significant presence of chloride at this lower elevation in Fig 4.32 a . Conversely, Site S4, at 159.94 meters, exhibited the lowest chloride concentration of 2520 mg/L in 2020, indicating a marked decline in chloride levels at this slightly lower elevation.

Nitrate concentrations displayed diverse ranges across sites and years. Site S2 at 175.33 meters registered the highest nitrate concentration of 233.01 mg/L in 2022, indicating elevated levels at this higher elevation (Fig.4.33 a). In contrast, Site S1 at 186.23 meters showcased the lowest nitrate concentration of 167 mg/L in 2022, suggesting relatively reduced nitrate content at this higher elevation.

HCO3 concentrations exhibited notable disparities across sites and years. Site S2 at 175.33 meters displayed the highest concentration of 18540 mg/L in 2022, indicating elevated bicarbonate levels at this higher elevation (Fig 4.34 b). Conversely, Site S3 at 160.74 meters presented the lowest HCO3 concentration of 1910 mg/L in 2022, signifying a substantial decrease in bicarbonate content at this lower elevation.

In September, chloride concentrations displayed considerable variations. The highest concentration of 5394 mg/L in 2022 was found at Site S5, positioned at an elevation of 156.77 meters (Fig.4.32 a). This observation underscores a substantial presence of chloride specifically at this location during that year. Conversely, the lowest chloride level of 4160 mg/L in 2021 was recorded at Site S3, situated at an elevation of 160.74 meters, indicating notably reduced chloride content at this lower elevation.

Nitrate concentrations exhibited diverse ranges. The highest recorded nitrate concentration of 206.07 mg/L in 2022 was documented at Site S2 positioned at an elevation of 175.33 meters (4.33 b). This highlights elevated nitrate levels at this higher elevation during that specific year. On the other hand, the lowest nitrate concentration of 178.17 mg/L in 2021 was noted at Site S3 located at an elevation of 160.74 meters, indicating relatively lower nitrate content at this lower elevation.

HCO3 concentrations displayed notable variations across sites and years. The peak concentration of 13960 mg/L in 2021 was observed at Site S2, positioned at an elevation of 175.33 meters, indicating heightened bicarbonate levels at this higher elevation (Fig. 4.34 b). In contrast, the lowest HCO3 concentration of 8330 mg/L in 2020 was noted at Site S3, located at an elevation of 160.74 meters, showcasing a considerable decrease in bicarbonate content at this lower elevation.

In December 2021, the highest chloride concentration of 3185.2 mg/L was recorded at Site S1, positioned at an elevation of 186.23 meters. Conversely, Site S5 exhibited the lowest chloride concentration of 2533 mg/L in the same year, located at an elevation of 156.77 meters (Fig.4.32 b). Chloride, known for its negligible sorption, complexation, and precipitation reactions, typically maintains stability within the environment as a conservative pollutant.

During the same period, Site S2 documented the highest nitrate concentration of 358.6 mg/L at an elevation of 175.33 meters, while Site S1 displayed the lowest nitrate concentration of 277.3 mg/L at an elevation of 186.23 meters (Fig 4.33 b). The presence of nitrates in leachate can be attributed to the oxidation process of ammonium, transitioning to nitrite, and eventually forming nitrate.

Moreover, in 2021, Site S4 exhibited the highest HCO3 concentration of 14532 mg/L at an elevation of 159.94 meters (Fig.4.34 b). In contrast, Site S3 displayed the lowest bicarbonate concentration of 10286 mg/L in 2020, positioned at an elevation of 160.74 meters. The presence of bicarbonate might be linked to various processes, including organic waste decomposition or the breakdown of inert waste components, influencing its concentrations across different sites and elevations.

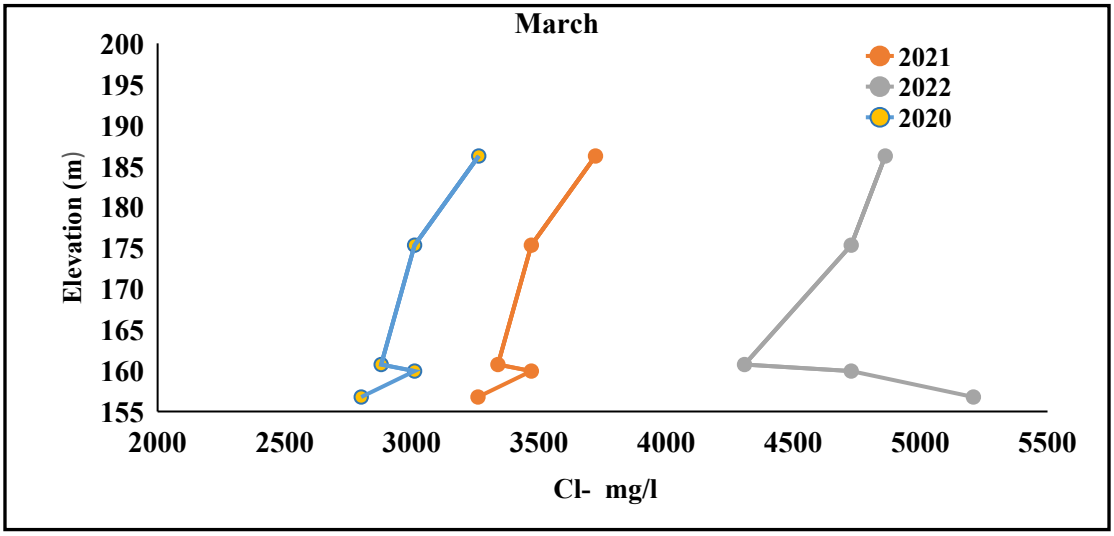
March
2021
2022
2020
Elevation (m)
200
195
190
185
180
175
170
165
160
155
2000
2500
3000
3500
4000
4500
5000
5500
Cl- mg/l

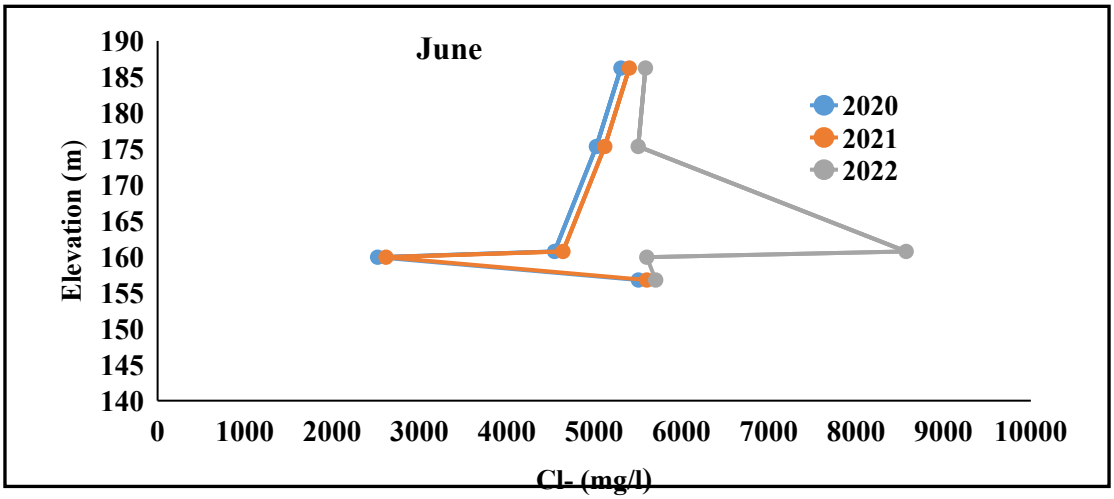
June
2020
2021
2022
Elevation (m)
190
185
180
175
170
165
160
155
150
145
140
0
1000
2000
3000
4000
5000
6000
7000
8000
9000
10000
Cl- (mg/l)

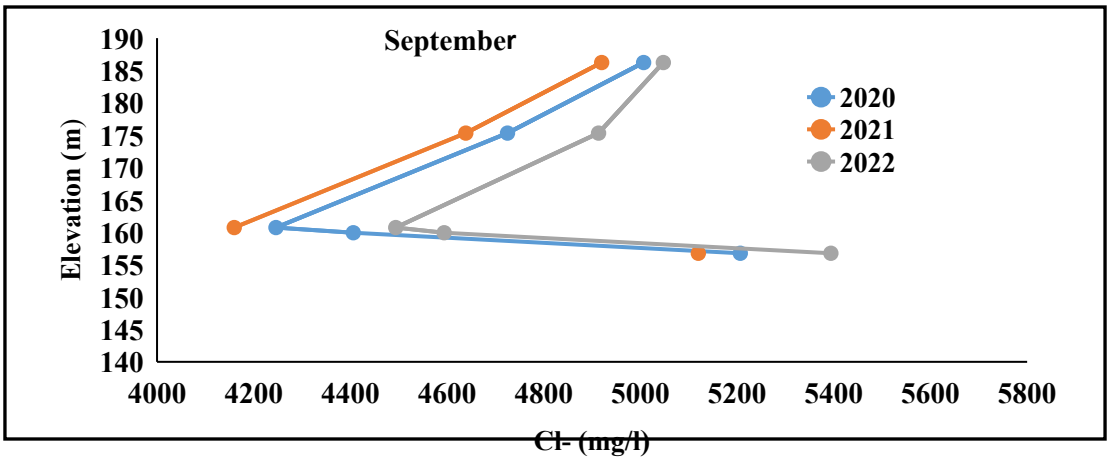

Figure 4.32 a) Chloride Variability Across elevation in March, June & September at different sites

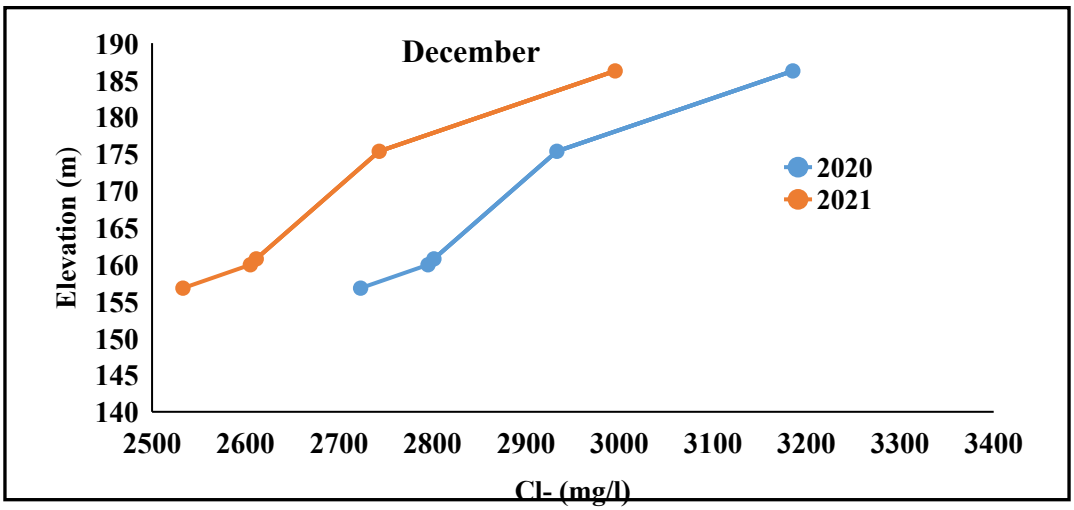

Figure 4.32 b) Chloride Variability Across elevation in December at different sites

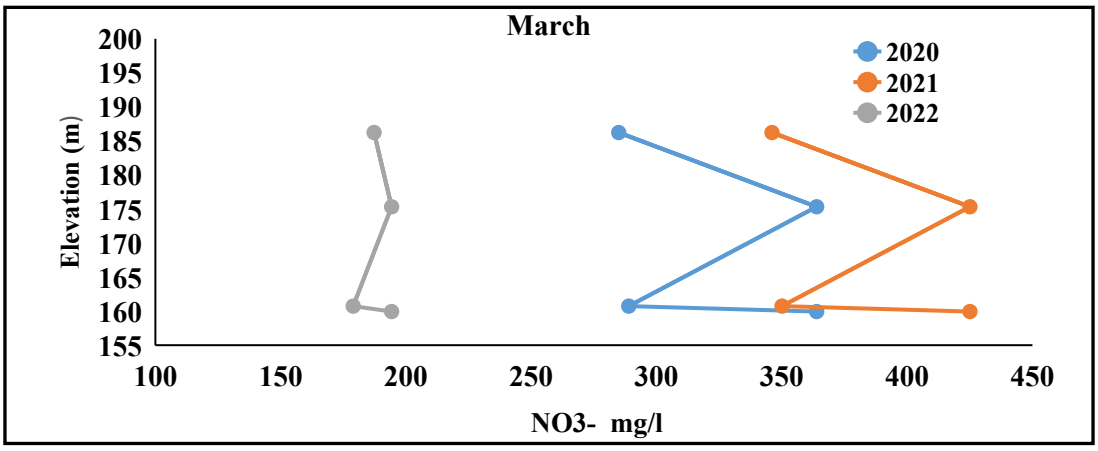

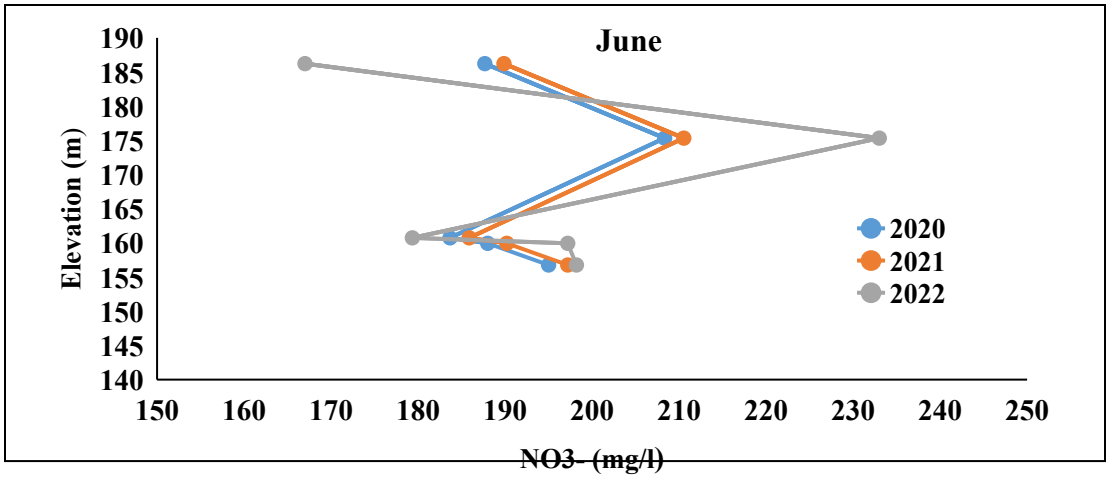

Figure 4.33 a) Nitrate Variability Across elevation in March & June at different sites

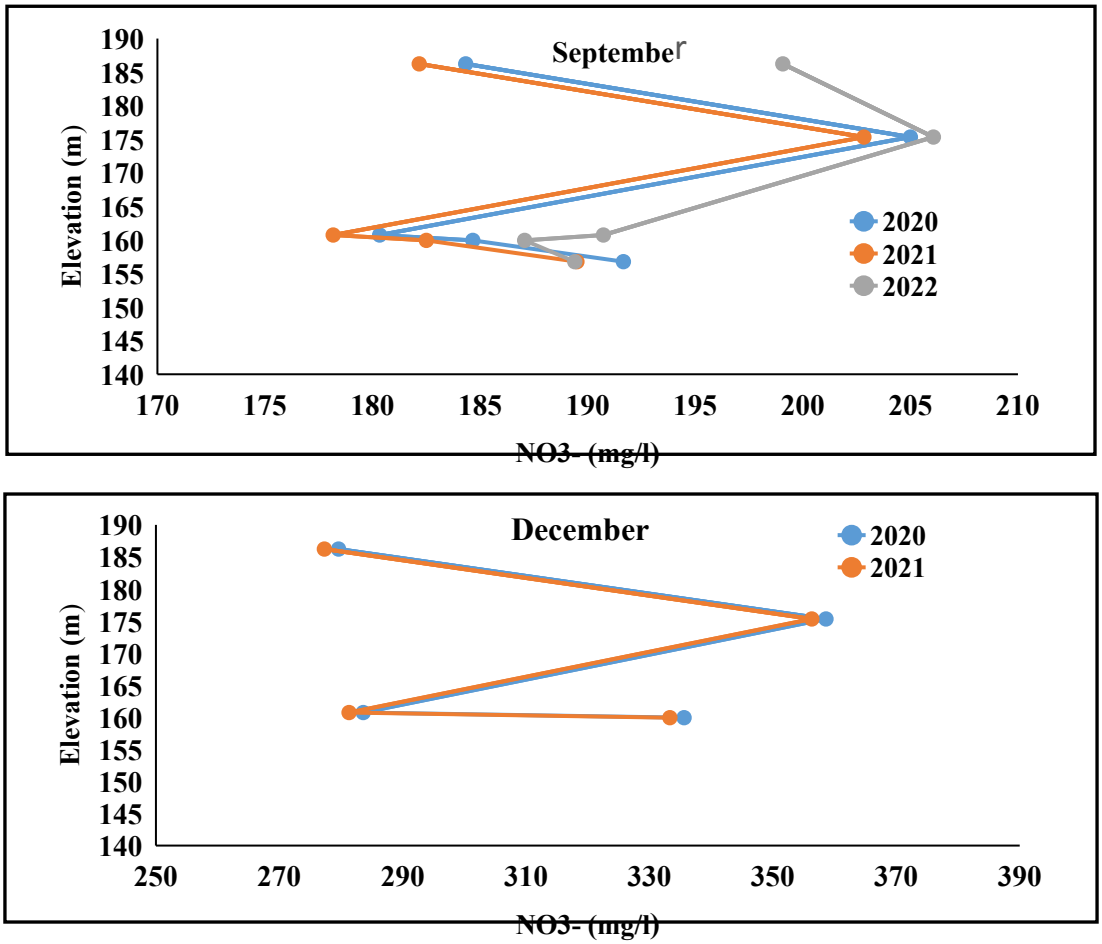

Figure 4.33 b) Nitrate Variability Across elevation in September & December at different sites

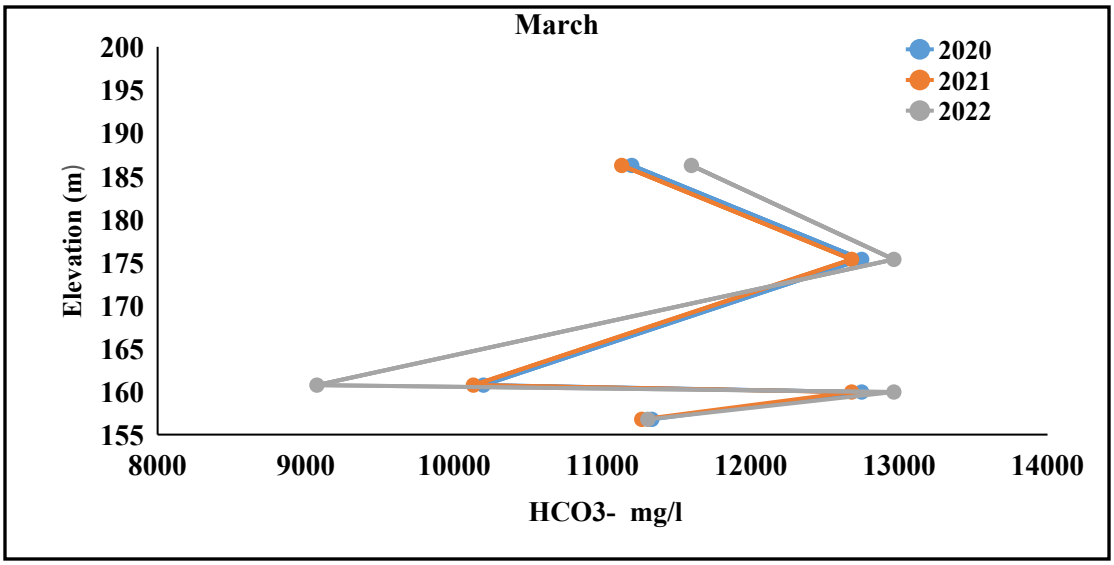

Figure 4.34 a) Bicarbonate Variability across elevation in March at different sites

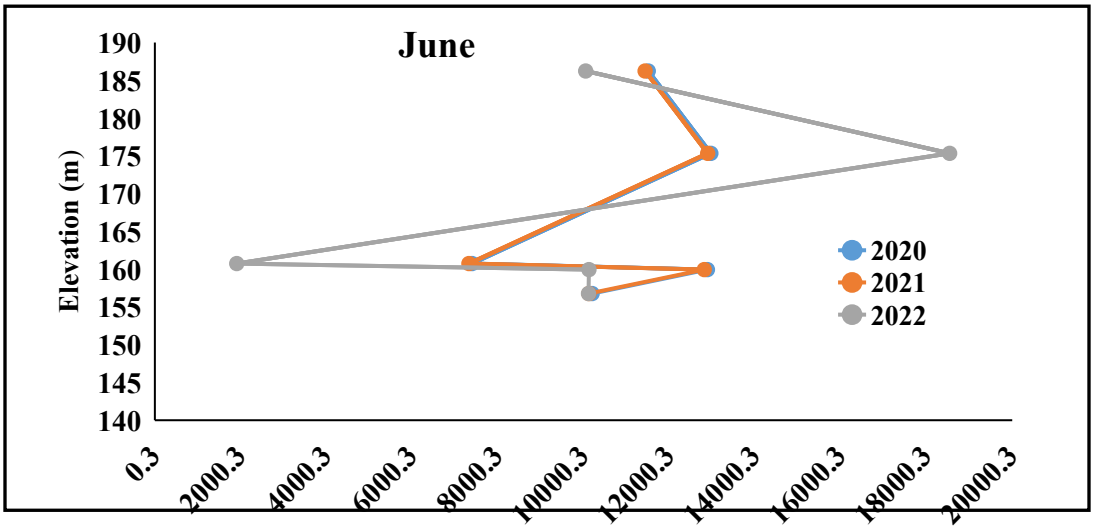

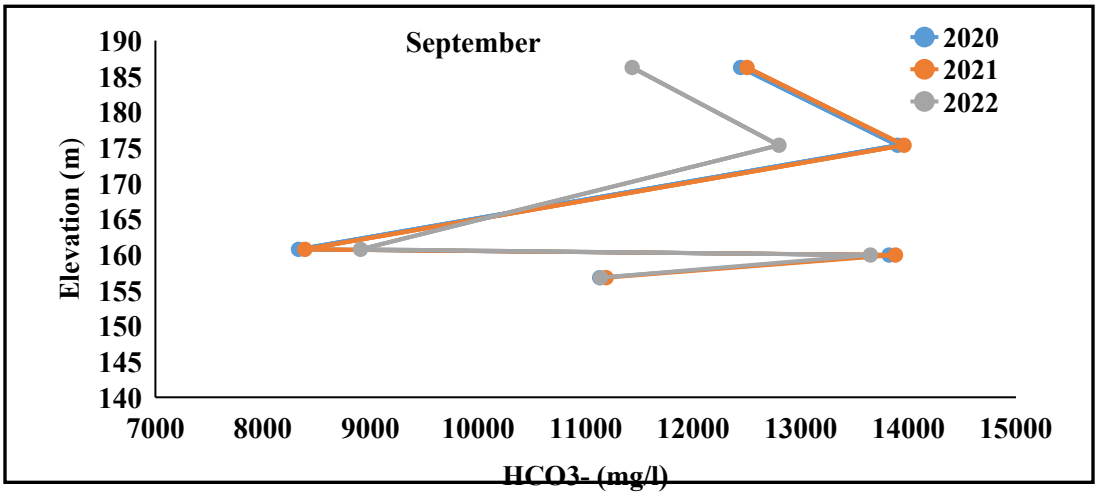

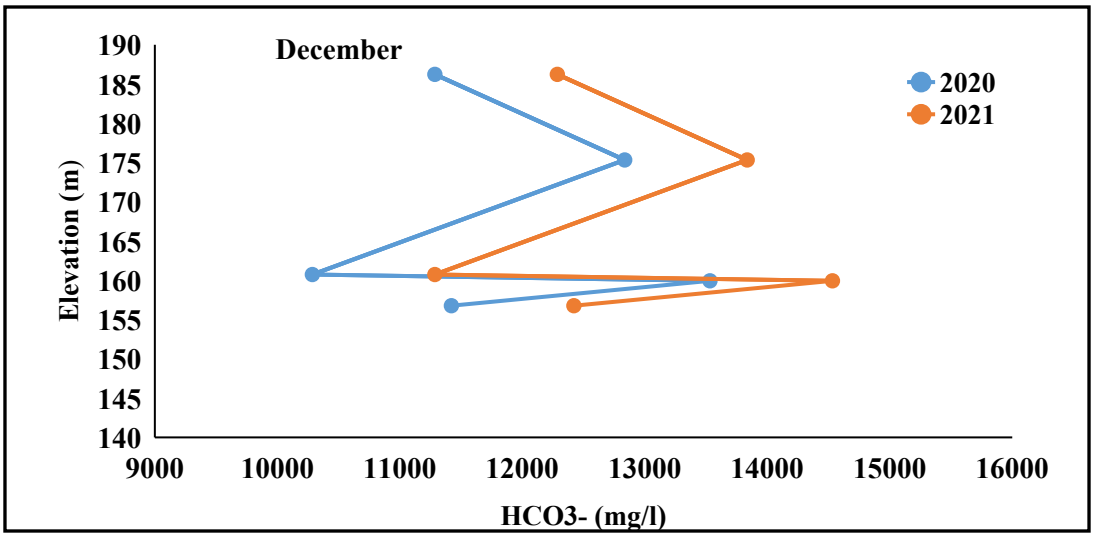

Figure 4.34 b) Bicarbonate Variability Across elevation in June, September & December at different sites

4.2.12 Analysis of heavy metal in leachate with respect to elevation

4.2.12.1 Iron

In March, Iron concentrations showed fluctuations across the sites. The highest Fe concentration was observed at Site S2 & S4, with S1 at 58.7 mg/L in 2020, declining to 12.23 mg/L in 2022 (Fig 4.35 a). Site S3, S4, and S5 displayed a significant decline from 57.4 mg/L, 58.7 mg/L, and 11.2 mg/L in 2020 to 6.43 mg/L, 12.23 mg/L, and 11.05 mg/L in 2022.

In June, the Fe concentrations showcased diverse patterns. Site S1 started at 17.253 mg/L in 2020, dropped to 13.253 mg/L in 2021, and slightly increased to 17.147 mg/L in 2022 (Fig.4.35 a). Site S2 demonstrated a decline from 17.359 mg/L in 2020 to 8.8 mg/L in 2022. Site S3 ranged from 16.94 mg/L in 2020, decreased to 12.94 mg/L in 2021, and rose again to 17.7198 mg/L in 2022. Site S4 showcased variations from 9.1586 mg/L in 2020, slightly decreased to 9.1186 mg/L in 2021, and increased to 15.11 mg/L in 2022. Meanwhile, Site S5 fluctuated from 11.17 mg/L in 2020 to 4.83 mg/L in 2022.

The September data highlighted varied Fe concentrations. Notably, Site S2 exhibited changes from 14.99 mg/L in 2020 to 12.16 mg/L in 2022 (Fig 4.35 a). Site S3 ranged from 11.08 mg/L in 2020 to 6.36 mg/L in 2022. Site S4 showed a decrease from 9 mg/L in 2020 to 4.76 mg/L in 2022. Site S5 fluctuated from 12 mg/L in 2020 to 16.98 mg/L in 2022.

In December, Fe concentrations displayed shifts across sites. Site S1 began at 49.9 in 2020, rising to 51.1 in 2021. Site S2 ranged from 60.9 in 2020 to 62.1 in 2021 (Fig 4.35 b). Site S3 showcased changes from 16.6 in 2020 to 17.8 in 2021. Site S4 exhibited variations from 55.9 in 2020 to 57.1 in 2021. Site S5 fluctuated from 12.2 in 2020 to 13.4 in 2021.

The presence of high Fe levels in the leachate samples suggests the disposal of iron and steel scrap in the landfill. The leachate's dark brown color primarily results from the oxidation of ferrous to ferric forms and the subsequent formation of ferric hydroxide colloids. These compounds form complexes with fulvic/humic substances, contributing to the overall coloration of the leachate.

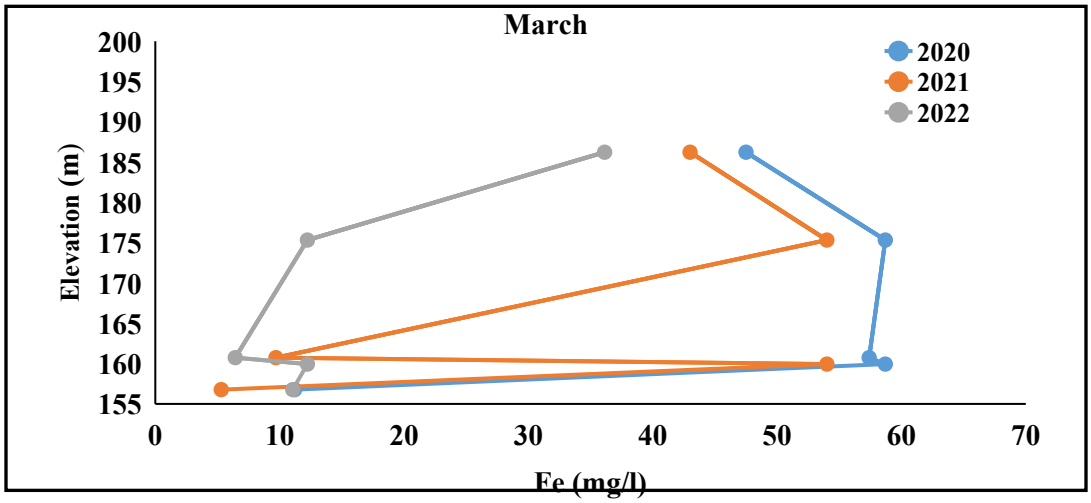

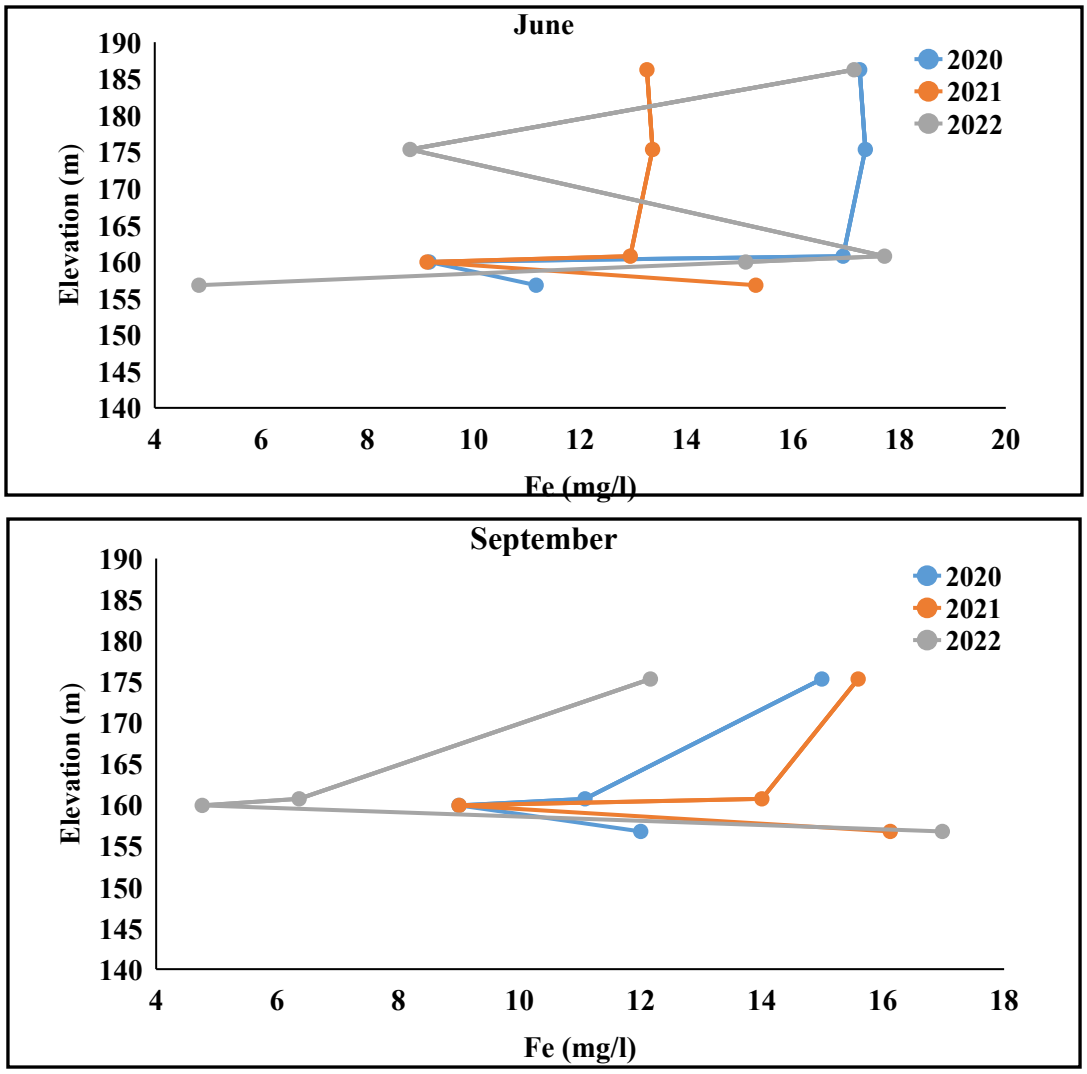

Figure 4.35 a) Iron Variability Across elevation in March, June & September at different sites

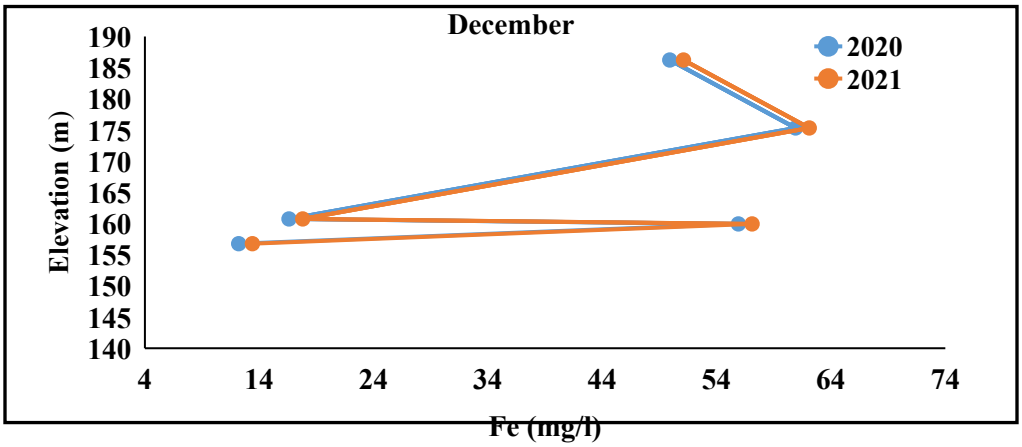

Figure 4.35 b) Iron Variability Across elevation in December at different sites

4.2.12.2 Zinc

In March, Zinc concentrations depicted variations across the sites. The highest Zn concentration was recorded at Site S1, S2, and S4 in 2020, decreasing notably to 5.39 mg/L in 2022 for S1, 1.55 mg/L for S2 and S4 (Fig.4.36 a). Site S3 exhibited a decrease from 7.07 mg/L in 2020 to 1.537 mg/L in 2022. Meanwhile, Site S5 displayed a decrease from 5.1 mg/L in 2020 to 3.86 mg/L in 2022.

The June data for Zn concentrations displayed varied patterns. Sites S1, S2, and S3 showcased decreases from 0.62355 mg/L, 0.67024 mg/L and 0.78555 mg/L in 2020 to 0.57686 mg/L, 0.55493 mg/L, and 0.8611 mg/L in 2022, respectively (Fig. 4.36 a). Site S4 showed a decrease from 0.71 mg/L in 2020 to 0.621 mg/L in 2022, while Site S5 decreased from 0.82 mg/L in 2020 to 0.5 mg/L in 2022.

In September, Zn concentrations exhibited fluctuations. Sites S1, S2, and S3 ranged from 0.50 mg/L (186.23 m), 0.55 mg/L (175.33 m), and 0.66 mg/L (160.74 m) in 2020 to 0.51 mg/L, 0.56 mg/L, and 0.68 mg/L in 2021, respectively (Fig 4.36 b). Site S4 showed an increase from 0.59 mg/L in 2020 to 2.03 mg/L in 2022, while Site S5 increased from 0.70 mg/L in 2020 to 3.23 mg/L in 2022.

The December Zn concentrations displayed varied trends. Sites S1 and S2 ranged from 11.78 mg/L (186.23 m) and 11.77 mg/L (175.33 m) in 2020 to 11.89 mg/L and 11.88 mg/L in 2021, respectively. Site S3 showcased changes from 7.75 mg/L in 2020 to 7.86 mg/L in 2021 (Fig 4.36 b). Site S4 exhibited variations from 8.45 mg/L in 2020 to 8.56 mg/L in 2021, while Site S5 fluctuated from 5.78 mg/L in 2020 to 5.89 mg/L in 2021. The presence of zinc in the leachate suggests that the landfill receives waste from batteries and fluorescent lamps, known for containing zinc compounds and Agro-chemicals like fertilizers and pesticides are the major sources of Zn.

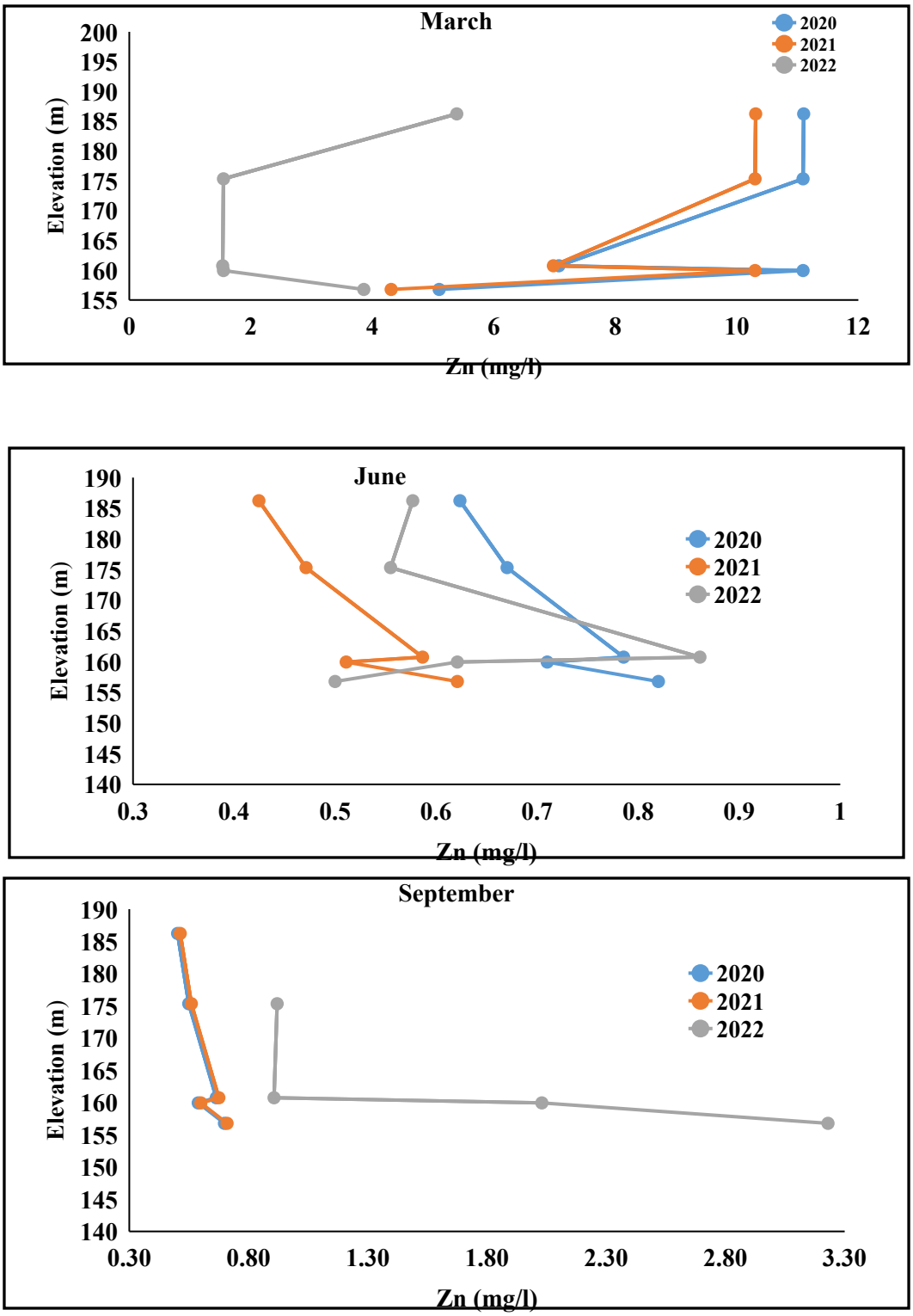

Figure 4.36 a) Zinc Variability Across elevation in March, June & September at different sites

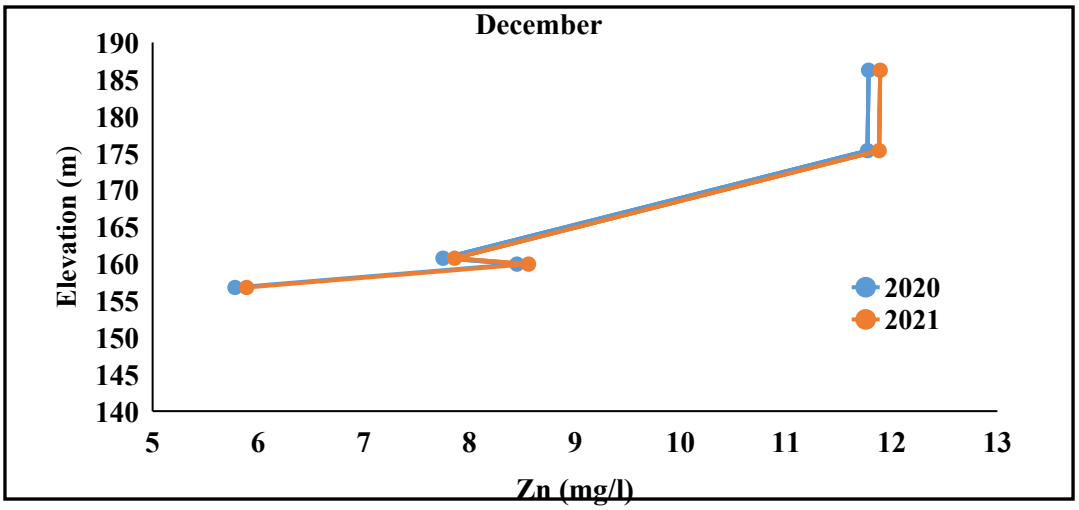

Figure 4.36 b) Zinc Variability Across elevation in December at different sites

4.2.12.3 Lead

In March, lead concentrations displayed varied patterns across the sites. The highest Pb concentration was observed at Site S1 in 2020 with 2.45 mg/L, decreasing notably to 0.124 mg/L in 2022. Sites S2 and S4 exhibited declines from 0.95 mg/L in 2020 to 0.0261 mg/L in 2022 (Fig 4.37 a). Site S3 showed a decrease from 1.74 mg/L in 2020 to 0.0267 mg/L in 2022, while Site S5 decreased from 0.552 mg/L in 2020 to 0.02 mg/L in 2022.

In June, data for Pb concentrations displayed diverse trends. Sites S1, S2, and S5 showcased decreases from 0.09661 mg/L, 0.1087 mg/L, and 0.1 mg/L in 2020 to 0.08452 mg/L, 0.16215 mg/L and 0.1 mg/L in 2022, respectively. Site S3 ranged from 0.05525 mg/L in 2020, increased to 0.06525 mg/L in 2021, and slightly decreased to 0.05321 mg/L in 2022 (Fig 4.37 a). Meanwhile, Site S4 ranged from 0.05729 mg/L in 2020, increased to 0.06729 mg/L in 2021, and then notably increased to 0.11 mg/L in 2022.

In September, Pb concentrations exhibited fluctuations. Sites S1, S2 and S5 ranged from 0.042 mg/L, 0.054 mg/L, and 0.045 mg/L in 2020 to 0.048 mg/L, 0.06 mg/L, and 0.051 mg/L in 2021, respectively. Site S3 increased from 0.000 mg/L in 2020 to 0.015 mg/L in 2022, while Site S4 ranged from 0.002 mg/L in 2020 to 0.089 mg/L in 2022 (Fig 4.37 a).

In December, Pb concentrations displayed varied changes. Sites S1 and S2 ranged from 2.519 mg/L and 1.019 mg/L in 2020 to 2.539 mg/L and 1.039 mg/L in 2021, respectively. Site S3 showcased changes from 1.809 mg/L in 2020 to 1.829 mg/L in 2021. Site S4 exhibited steady

concentrations of 1.109 mg/L in both 2020 and 2021, while Site S5 ranged from 0.62 mg/L in 2020 to 0.64 mg/L in 2021 (Fig 4.37 b).

The presence of Pb in the leachate samples suggests the disposal of Pb batteries, chemicals for photograph processing, Pb-based paints, and pipes at the landfill site.

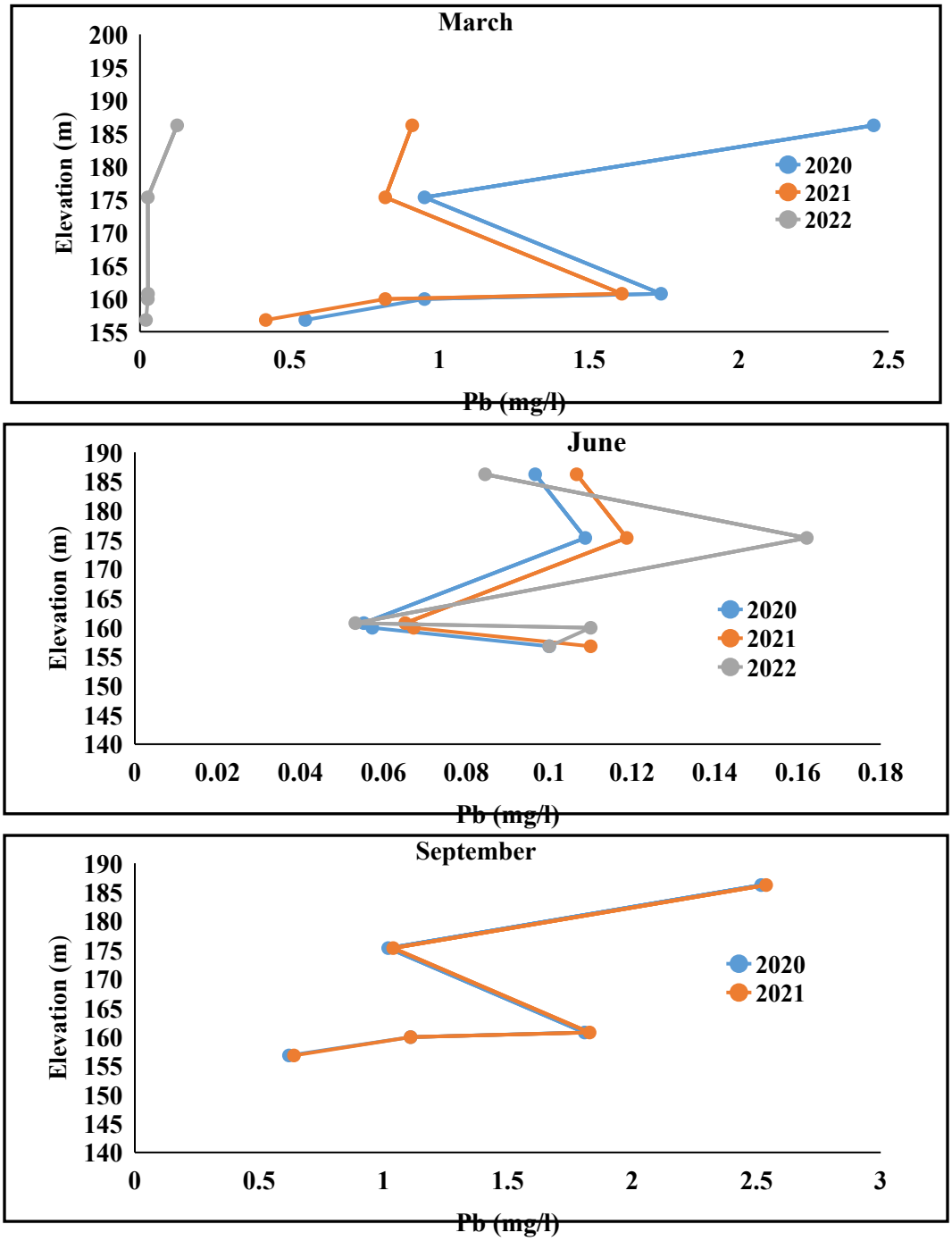

Figure 4.37 Lead Variability Across elevation in March, June & September at different sites

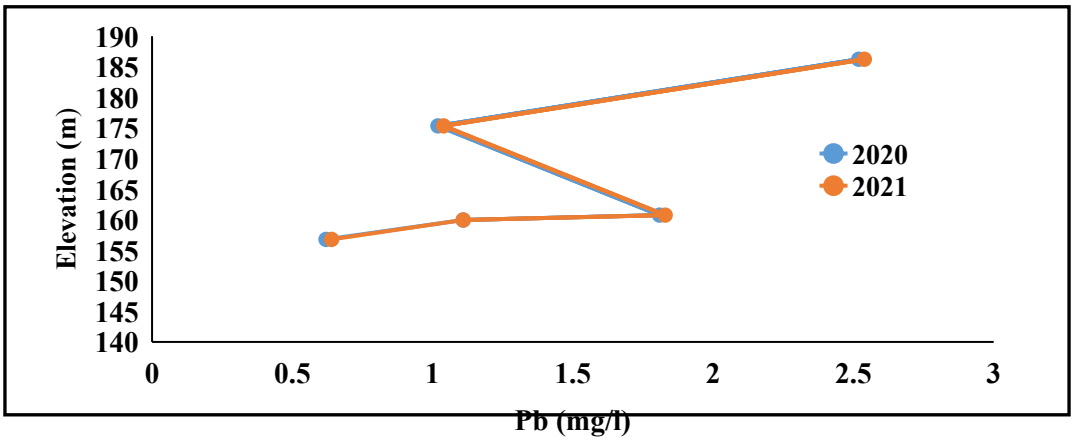

Figure 4.37 Lead Variability Across elevation in December at different sites

4.2.12.4 Chromium

In June, chromium levels remained relatively steady over the years, ranging between 0.4 mg/L in and 1.59 mg/L. However, at Site S2 & S3 showed variability, ranging from 0.63 mg/L in 2021 to 0.93 mg/L in 2022. S3 maintaining levels around 0.63 mg/L to 0.68 mg/L from 2020 to 2022. Conversely (Fig 4.38 a), Site S5 exhibited chromium levels ranging from 0.52 mg/L in 2021 to 0.81 mg/L in 2022.

In September, chromium concentrations showed variations across the sites. The highest Cr concentration was observed at Site S1 with 1.30 mg/L in 2020, declining to 0.52 mg/L in 2022. Site S2 ranged from 0.89 mg/L in 2020 to 0.97 mg/L in 2022 (Fig 4.38 a). Site S3 fluctuated from 0.74 mg/L in 2020 to 0.81 mg/L in 2022. Site S4 showed changes from 0.70 mg/L in 2020 to 0.91 mg/L in 2022. Meanwhile, Site S5 varied from 0.78 mg/L in 2020 to 0.43 mg/L in 2022.

In December Cr concentrations displayed varied changes. Sites S1 and S2 ranged from 0.443 mg/L and 0.386 mg/L in 2020 to 0.503 mg/L and 0.446 mg/L in 2021, respectively. Site S3 showcased changes from 0.464 mg/L in 2020 to 0.524 mg/L in 2021 (Fig.4.38 b). Site S4 exhibited steady concentrations of 0.532 mg/L in 2020 to 0.59 mg/L 2021, while Site S5 ranged from 0.43 mg/L in 2020 to 0.49 mg/L in 2021.

The presence of chromium in the leachate suggests the potential disposal of industrial waste, particularly from electroplating processes or other sources using chromium compounds.

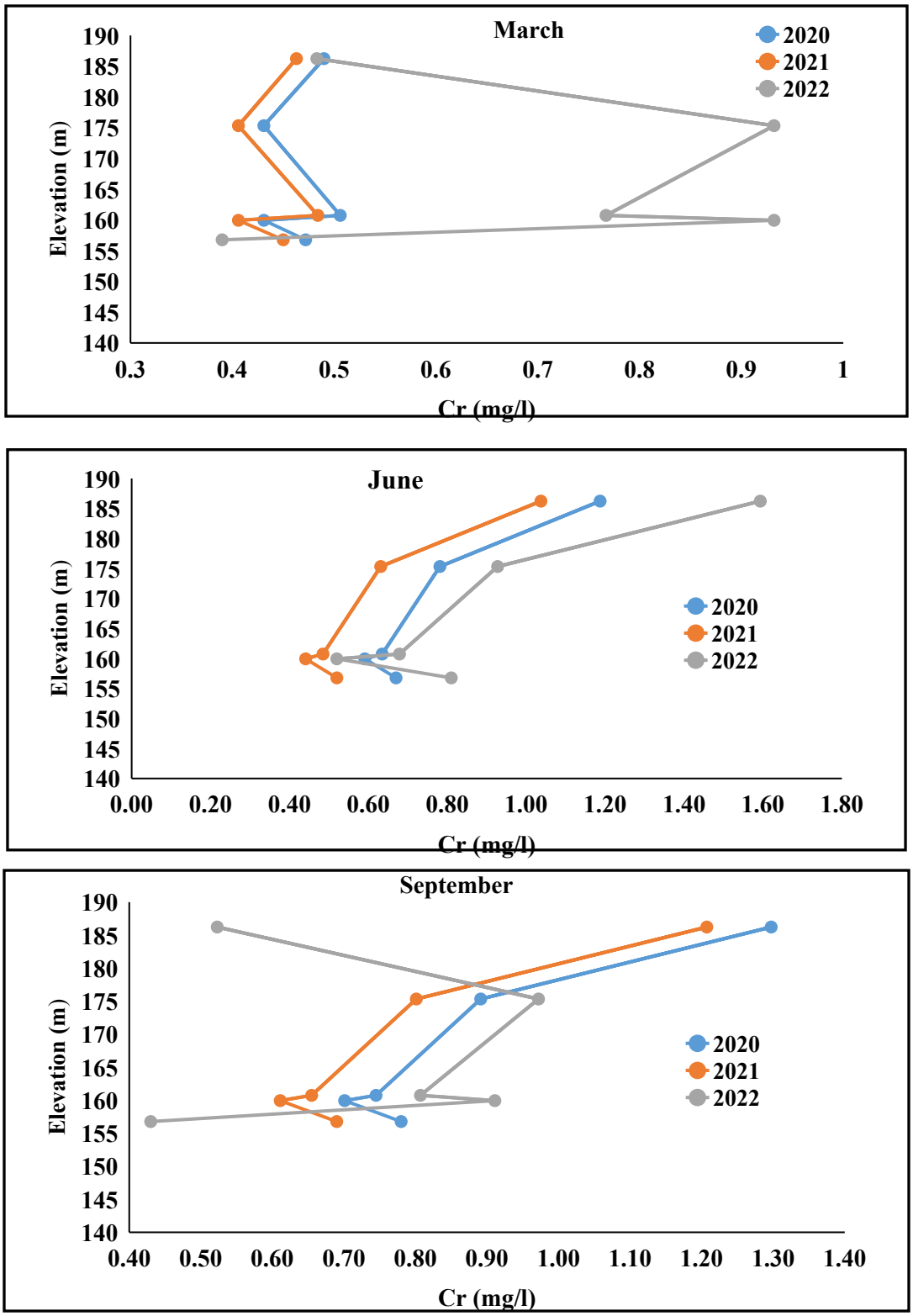

Figure 4.38 a) Chromium Variability Across elevation in March, June & September at different sites

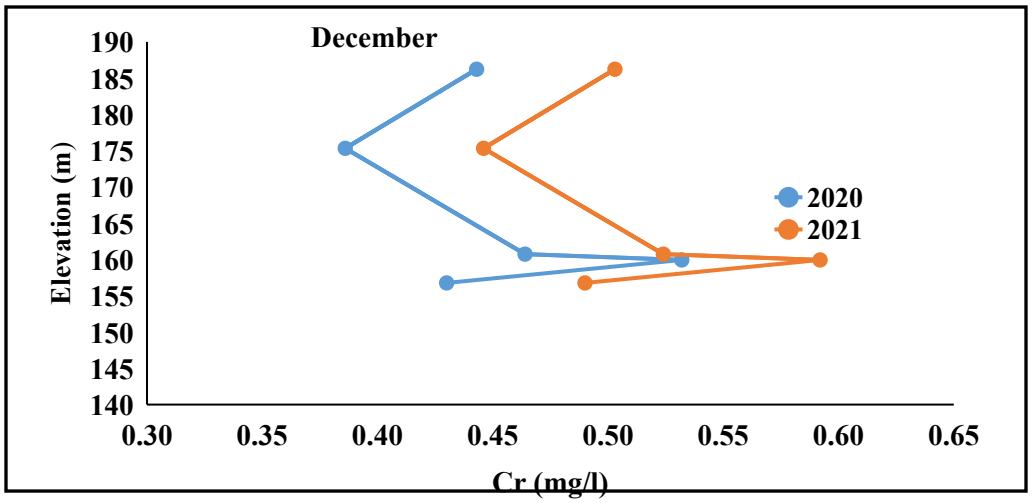

Figure 4.38 b) Chromium Variability Across elevation in March, June & September at different sites

4.2.12.5 Nickel

In March 2020, Site S1 began at a considerable height of 186.23 m and experienced a drastic decline in concentration 1.31 mg/L to 0.69 mg/L by 2022 (Fig. 4.39 a). Similarly, Site S2, 0.99 mg/L, and notably decreased to 0.452 mg/L by 2022, paralleling the trend of Site S4. Site S3, initially 1.05 mg/L by 2021 before slightly decreasing to 1.014 mg/L in 2022. Meanwhile, Site S5 started at 0.89 mg/L in 2020, declined to 0.73 mg/L, 2021 and experienced a significant drop to 0.102 mg/L by 2022.

Moving to June, Site S1 maintained its initial height of 186.23m in 2020, with concentrations fluctuating from 0.46 mg/L in 2020 to 0.49 mg/L in 2021 before dropping to 0.45 mg/L by 2022. Site 2 at 0.47 mg/L, remained at 0.49 mg/L in 2021, and increased to 0.56 mg/L in 2022 (Fig. 4.39 a). Site S3, starting at 160.74m, saw concentration changes from 0.37 mg/L in 2020 to 0.40 mg/L in 2021, slightly decreasing to 0.39 mg/L by 2022. Site S4 at 159.94m, exhibited concentrations of 0.36 mg/L in 2020, 0.38 mg/L in 2021, and rose to 0.43 mg/L by 2022. Site S5 at elevation 156.77m, displaying concentrations of 0.40 mg/L in 2020, 0.43 mg/L in 2021, and a rise to 0.52 mg/L by 2022.

By September, nickel concentrations varied among the sites. Sites S1 and S2 ranged from 0.57 mg/L to 0.84 mg/L and 0.58 mg/L to 0.60 mg/L in 2020 and 2022, respectively. Site S3 showcased changes from 0.48 mg/L to 1.16 mg/L in 2020 and 2021 (Fig.4.39 a). Site S4

maintained steady concentrations of 0.47 mg/L to 0.61 mg/L from 2020 to 2022, while Site S5 ranged from 0.51 mg/L to 0.25 mg/L in 2020 and 2021.

In December, nickel concentrations spanned from 0.9 to 2.0 mg/L across the sites, with Site S1 displaying the highest concentration and Site S5 indicating the lowest concentration of nickel (Fig 4.39 b).

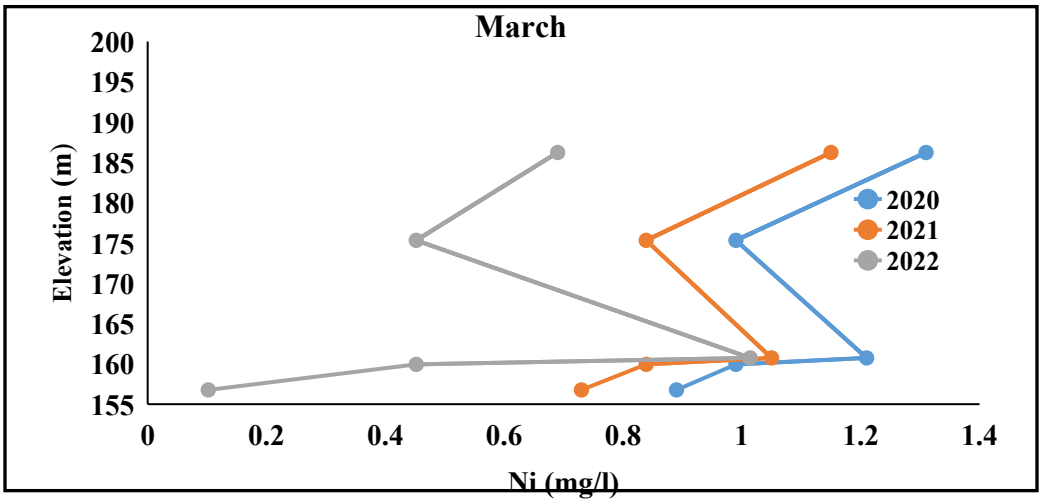

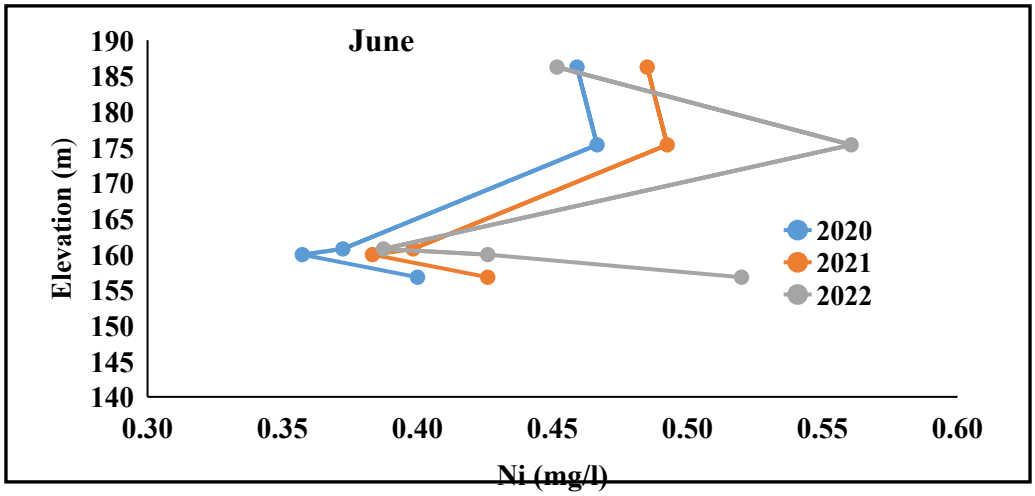

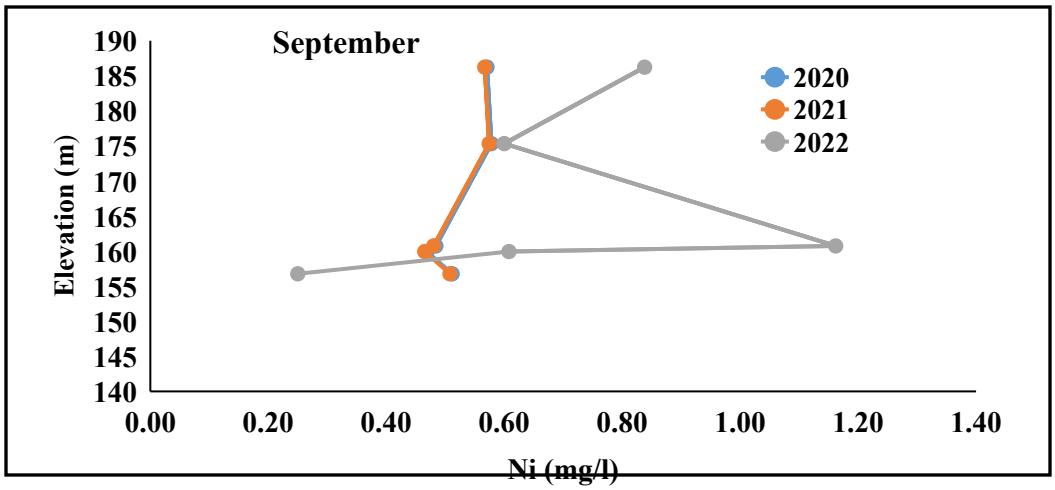

Figure 4.39 a) Nickel Variability Across elevation in March, June & September at different sites

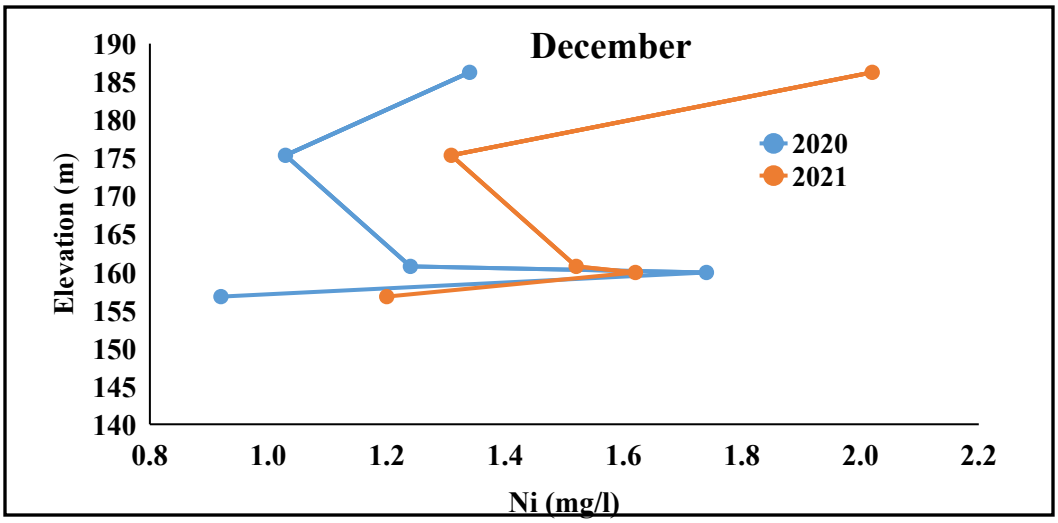

Figure 4.39 b) Nickel Variability Across elevation in December at different sites

4.2.12.6 Copper

In March, Site 1 commencing at an elevation of 186.23 m, had a concentration of 2.47 mg/L in 2020, which notably decreased to 1.29 mg/L in 2021, followed by a slight further decline to 1.242 mg/L by 2022 (Fig 4.40a). Meanwhile, Site S2, starting at 175.33 in height, exhibited a concentration of 3.26 mg/L in 2020, droping to 0.617 mg/L by 2022. Site S3, initiating at an elevation of 160.74 m, demonstrated a concentration of 3.36 mg/L in 2020 to 0.743 mg/L by 2022. Lastly, Site S5, beginning at an elevation of 156.77 m, displayed a concentration of 1.86 mg/L in 2020 and notably dropped to 0.196 mg/L by 2022.

In June, across sites S1 to S5, copper (Cu) concentrations varied over the years. Site S1, starting at 186.23 m in elevation, saw Cu levels at 0.41 mg/L (2020), 0.61 mg/L (2021), and 0.51 mg/L (2022). Site S2, at 175.33m elevation, showed 0.32 mg/L to 0.56 mg/L (2022) for Cu (Fig.4.40 a). Site S3 (160.74 elevation) had concentrations of 0.31 mg/L (2020) to 0.39 mg/L (2022). Site S4 (159.94 m elevation) exhibited levels of 0.23 mg/L (2020) to 0.29 mg/L (2022). Lastly, Site S5, starting at 156.77 m elevation, displayed 0.31 mg/L (2020), 0.29 mg/L (2021), and 0.26 mg/L (2022) for Cu concentration

In September, copper concentrations fluctuated at different elevations for sites S1 to S5. Site S1, starting at 186.23m in elevation, displayed Cu concentrations of 0.46 mg/L in 2020 to 0.56 mg/L in (2021). At 175.33m elevation, Site S2 showed 0.37 mg/L to a a notable increase 0.60 mg/L by 2022 (Fig. 4.40 b). Site S3, at 160.74 elevation, had concentrations of 0.71 mg/L and a slight increase to 0.73 mg/L in 2022. Site S4 (159.94 elevation) demonstrated Cu levels of 0.63 mg/L (2020), 0.73 mg/L (2021), and 0.67 mg/L (2022). Lastly, Site S5, starting at 156.77 elevation, provided values of 0.71 mg/L to 0.81 mg/L in 2021.

Over 2020 and 2021, copper (Cu) concentrations varied across sites S1 to S5 at different elevations. Site S1, beginning at 186.23m in elevation, showed a notable increase in Cu concentration from 2.71 mg/L (2020) to 4.56 mg/L (2021) (Fig. 4.40 b). At 175.33m elevation, Site S2 demonstrated concentrations of 3.5 mg/L (2020) and a slight increase to 3.8 mg/L (2021). Similarly, Site S3, at 160.74m elevation, displayed Cu concentrations of 3.6 mg/L (2020) and a slight rise to 3.9 mg/L (2021). Conversely, Site S4 (159.94m elevation) exhibited a decrease from 4.26 mg/L (2020) to 3.01 mg/L (2021) in Cu levels. Site S5, starting at 156.77m elevation, showed an increase in Cu concentration from 2.1 mg/L (2020) to 2.4 mg/L (2021).

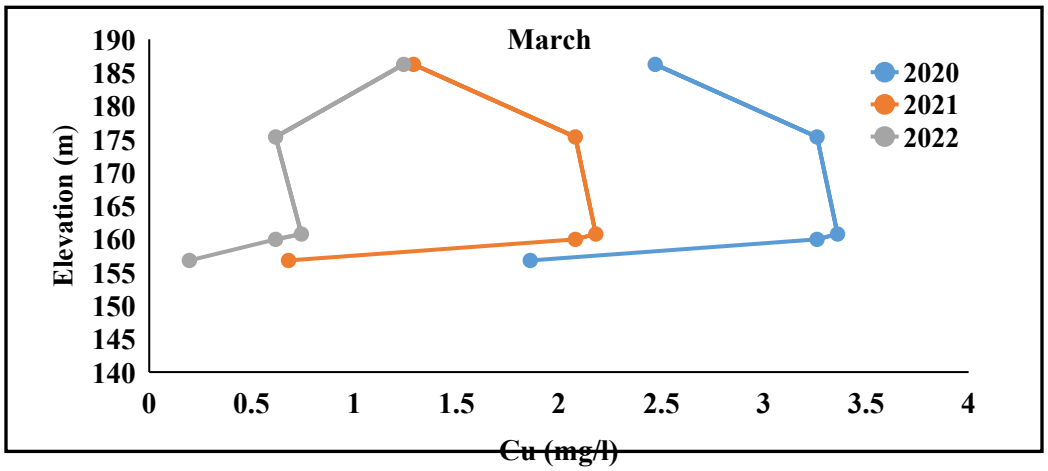

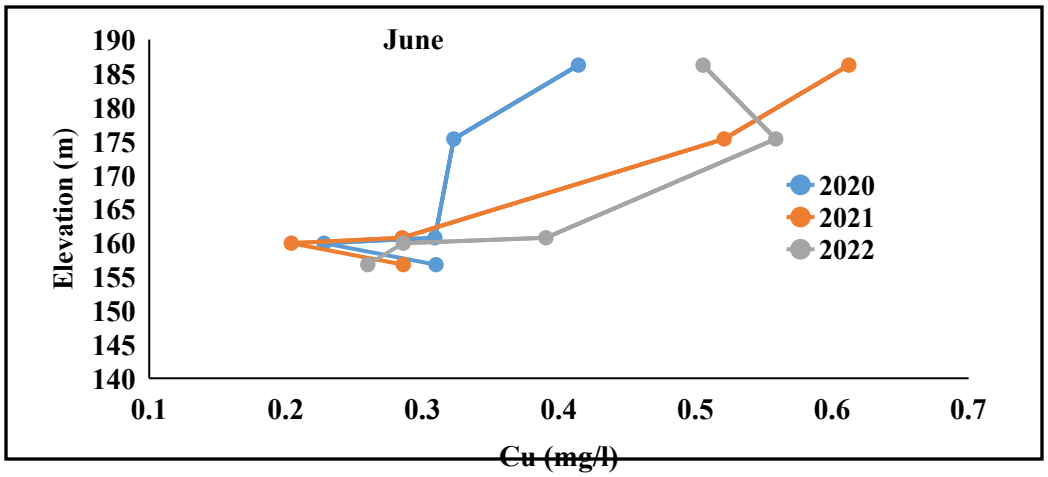

Figure 4.40 a) Copper Variability Across elevation in March & June at different sites

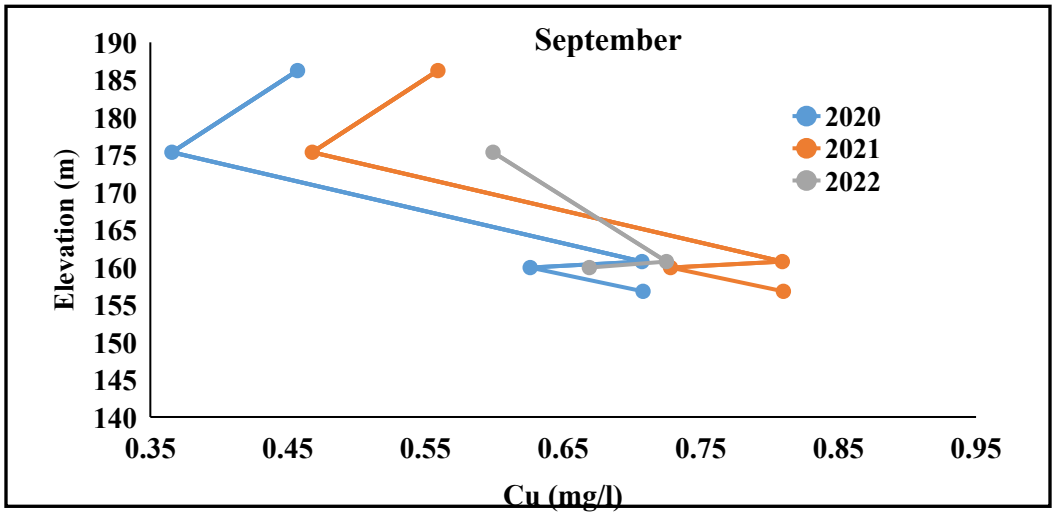

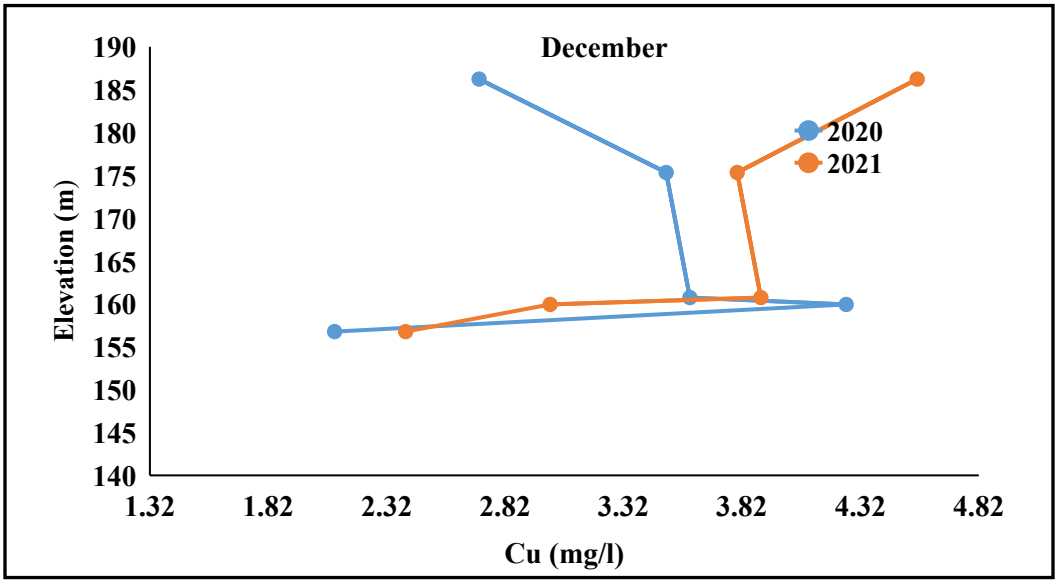

Figure 4.40 b) Copper Variability Across elevation in September & December at different sites

4.2.13 Characterization of Groundwater

The utilization of groundwater for various purposes, including drinking and domestic use, prompted an evaluation of its quality against the prescribed standards by the Bureau of Indian Standards (BIS). Assessing key parameters like pH, Electrical Conductivity (EC), and Total Dissolved Solids (TDS), Cation, Anion and Heavy metals across different sampling locations revealed significant variations and potential influences affecting water quality.

The pH levels varies from 6.6 to 7.8 with average value around 7.25, suggesting a slightly alkaline environment (Fig.4.41 a). All sampled locations adhered to regulatory standards, falling within the BIS-recommended range of 6.5–8.5. This ensured minimal impact on human health. Out of the wells surveyed, 24% were deeper while the rest were shallow. When combined these wells collectively displayed the highest and lowest pH values.

The Electrical Conductivity of groundwater ranges widely from 230 to 6800 µS/cm, averaging at 2173.99 µS/cm (Fig.4.41 a). As per WHO guidelines, the acceptable EC limit stands at 1500 µS/cm. Notably, only 31.4% of sampled groundwater met this standard, indicating that the majority, 68.6%, exceeded the permissible EC limit. The specific wells in close proximity to the Gazipur landfill site, namely G-36 (4400 µS/cm), G-37 (4500 µS/cm), G-44 (6800 µS/cm), and G-48 (6700 µS/cm), exhibited markedly elevated EC values. This spatial proximity suggests an influential correlation between the landfill and heightened EC levels within the groundwater. Furthermore, observations of EC levels around 4035 µS/cm and 4025 µS/cm in the urbanized area reinforce the impact of the Gazipur landfill on the groundwater composition. Notably, The lower EC values found in deeper wells, with G-128 at 1800 µS/cm and others like G-45 (900 µS/cm), G-125 (360 µS/cm), G-98 (1505 µS/cm), G-101 (2500 µS/cm), G-32 (1800 µS/cm), G-132 (2500 µS/cm), G-99 (2600 µS/cm), G-100 (2400 µS/cm), G-105 (900 µS/cm), and G-106 (2510 µS/cm), contrast starkly with the notably higher EC values observed in shallow wells. This suggests a proximity of shallow wells to potential sources of contamination.

The Total Dissolved Solids evaluated water quality by comparing it against the 2012 BIS standards with a safe threshold of 500 mg/L. Across all sampled sites, TDS levels varied from 147 to 4352 mg/L. Both shallow and deeper wells exceeded the acceptable TDS limits set by BIS 2012 (Fig. 4.41 a). Notably, shallow wells exhibited significant TDS variability, while deeper wells generally maintained lower to moderate values. Among the deeper wells, the outlier was well number 48, recording the higher TDS value at 4288 mg/L, compared to others below 1600 mg/L. Site G-44 near Bhati Chowk reported the

highest TDS (4352 mg/L), while sites like G-66 (256 mg/L) near Gazipur drain, G-125 (230.4 mg/L) near the Yamuna river, and G-137 (147.4 mg/L) near Park Sector-70 displayed notably lower TDS levels. The substantial differences in TDS levels, notably the higher values at G-44 compared to the lower levels at G-66, G-125, and G-137, might be attributed to dilution effects. Proximity to water bodies like Gazipur drain, Yamuna River, and Hindon could facilitate dilution processes resulting in lower TDS levels in these wells.

The analysis of groundwater chemistry highlighted specific ions including Chloride (Cl^-), Sodium (Na^+), Sulfate (SO_4^{2-}), Calcium (Ca^{2+}), Magnesium (Mg^{2+}) and Nitrate (NO_3^-). Chloride, a crucial indicator of organic matter in water, can significantly affect taste, health (specifically kidneys, heart, and oxidation-related issues) and water digestibility when present in excess. Recorded Chloride concentrations ranged from 30 to 6533 mg/L, averaging at 569 mg/L (Fig.4.41 a). Although 38% of samples met permissible limits, 61% surpassed the acceptable range of 200–600 mg/L. This increase is primarily attributed to percolation, leaching, contamination, and the discharge of industrial and domestic effluents, along with various sources like household waste and waste disposal sites.

Most of the deeper wells exhibited Chloride levels within a lower to moderate range. However, specific wells, including G-48, showcased concentrations around 1726 mg/L and G-5 shows the value is 6533 mg/L marking it as the highest among the deeper wells (Fig.4.41 b). Such variations emphasize the diverse impact of sources and infiltration patterns on the groundwater chemistry, especially in deeper aquifers.

The concentration of Sodium ions ranged from 28 to 2394.29 mg/L (Fig.4.41 b), with 44% of samples meeting the acceptable limit and 55% surpassing the WHO-recommended level in drinking water guidelines. Elevated Sodium content in groundwater significantly affects irrigation, contributing to increased water hardness and reduced soil permeability.

Sulfate concentrations, ranging from 3 (G-36) to 1787 mg/L and averaging at 260.93 mg/L (Fig.4.41 b), are notably elevated due to water percolation containing increased Sulfate levels from agricultural runoff. Among the deeper wells, most adhere to the acceptable limit of 200 mg/L set by BIS 2012. A few such as G-45, G-100, and G-101 register values within the low to moderate range. However, well like G-48 and G-5 records a significantly higher sulfate level at 737.68 mg/L & 1787 mg/L, marking it as the highest among the deeper wells.

The concentrations of Calcium ranging from 11 to 1597 mg/L and averaging at 173 mg/L, exhibit significant variability (Fig.4.41 c). Specifically, higher values observed at certain sites, such as G-5 (1597

mg/L) and G-8 (1094 mg/L), both of which are deeper wells covering the Ghaziabad area in the study, may be associated with agricultural activities. This could be attributed to practices like the use of lime in farming to modify soil acidity in the adjacent agricultural areas.

The range of Magnesium concentrations observed varies from 13 (G-125 mg/L) to 792 mg/L with averaging value 88.91 mg/L (Fig.4.41 c). The highest value of 792 mg/L in well G-97, categorized as a shallow well near an electric power station, stands out notably. The presence of this industrial facility could potentially influence this heightened concentration. Electric power stations commonly employ materials containing Magnesium, and their operational processes might result in the release of Magnesium ions into the surrounding environment, including groundwater

Potassium concentrations, varying between 2 to 81 mg/L with an average value of 12.8 mg/L, display considerable variability (Fig.4.41 c). The elevated levels, particularly exceeding the WHO 2011, recommended limit in some samples, may originate from agricultural activities. Clay particles prevalent in soils can retain potassium strongly, allowing it to persist and potentially leach into groundwater over time.

Nitrate concentrations range from 0 to 731 mg/L, with an average of 37.7 mg/L (Fig.4.41 d). Approximately 21.9% of the total wells exceed the acceptable limit of 45 mg/L as per BIS 2012, making them unsuitable for drinking purposes. Notably, 6% of the samples, including G-5, G-8, G-98, G-101, G-100, and G-102, originate from deeper wells, with G-5 (731.19 mg/L) and G-8 (515.02 mg/L) displaying the highest nitrate values. Conversely, the shallow wells exhibit lower nitrate concentrations overall.

Zinc levels fluctuate between 0 and 46.10 mg/L, surpassing the standard of 5 mg/L in 70% of the samples, indicating potential anthropogenic origins (Fig.4.41 d). Among these, seven samples recorded the highest Zinc values, with four wells among the deeper ones—namely G-101 (31.37 mg/L), G-99 (14.73 mg/L), G-102 (31.46 mg/L), and G-106 (5.88 mg/L). Additionally, three shallow wells, specifically G-107 (26.01 mg/L), G-109 (46.11 mg/L), and G-111 (6.60 mg/L), exhibited elevated Zinc levels. Notably, G-109 registered the highest Zinc concentration above the acceptable limit.

Iron presence varying widely from 0.7 to 93520 mg/L, exceeding acceptable limits in all samples and causing water discoloration, might primarily arise from geological factors (Fig.4.41 d). G-101, G-99, and G-106 are deeper wells and display elevated iron levels, notably G-101 registering a high concentration of 85063.90 mg/L. Meanwhile, G-107, G-109, and G-111 are shallow wells and exhibit considerable iron concentrations, with G-109 recording the highest among the shallow wells at 93520.07 mg/L. The deeper wells despite being fewer in number display high iron content emphasizing potential issues with iron levels in these deeper aquifers.

Lead concentration exhibit a range of values across the sampled wells, from 0 to 0.552 mg/L (Fig.4.41 e). Among these, wells G-100, G-101, and G-105, identified as deeper wells, highlight higher lead concentrations, with G-101 displaying the highest level at 0.305 mg/L. Shallow wells, including G-20, G-15, G-35, G-44, G-50, G-79, G-87, G-97, G-75, G-77, G-81, G-7, G-15, G-130, G-107, G-108, G-109 and G-111 present a varied range of lead concentrations, with G-109 registering the highest value of 0.55 mg/L near Lava International Limited.

Nickel concentrations in this dataset span from 0 to 0.062 mg/L, and the BIS 2012 standard sets an acceptable level at 0.02 mg/L (Fig.4.41 e). Among the deeper wells—G-99, G-106, and G-101—nickel levels range from 0.03 to 0.04 mg/L. Shallow wells like G-81, G-107, G-108, and G-109 exhibit a range of nickel concentrations, varying from 0.02 to 0.06 mg/L. While certain wells, like G-108 with a concentration of 0.02 mg/L, meet this threshold, others, notably G-107 among the shallow wells, surpass the acceptable limit, recording 0.06 mg/L.

Arsenic concentrations in the dataset ranging from 0 to 0.4 mg/L (Fig.4.41 e). Among the sampled wells, 28 samples exhibit values surpassing the acceptable limit of 0.01 mg/L according to the BIS 2012 standard. While G-101, G-99, and G-100 adhere to the specified standard at 0.01 mg/L, G-105 stands out with a notably higher nitrate level of 0.47 mg/L. This difference underscores that G-105, among the deeper wells, exceeds the nitrate concentration considered acceptable by BIS 2012.

Chromium concentrations in the dataset vary from 0 to 0.41 mg/L (Fig.4.41 f). Among the wells, G-101, classified as a deeper well, shows a chromium concentration of 0.06 mg/L. In contrast, both G-109 and G-111, categorized as shallow wells, display concentrations of 0.06 mg/L and 0.41 mg/L, respectively. These concentrations exceed the acceptable limit set by BIS 2012, which stands at 0.05 mg/L. Particularly, G-111 significantly surpasses this threshold, indicating a notable concern for elevated chromium levels in these wells.

Aluminum levels fluctuate between 0 and 6.47 mg/L, averaging at 0.25 mg/L (Fig.4.41 f). Several samples, including G-65, G-66, G-68, G-2, G-3, G-17, G-44, G-53, G-78, G-85, G-91, G-94, G-96, G-120, G-121, G-123, G-127, G-130, G-132, G-134, G-40, G-62, G-93, G-129, G-133, and G-136, meet the acceptable limit of 0.03. Both shallow and deeper wells exhibit the most significant variability in the dataset. However, there are outliers such as G-67, G-20, G-15, G-37, G-50, G-60, G-77, G-81, G-75, G-98, G-101, G-105, G-107, G-108, G-111, G-113, G-100, G-119, and G-138, which exhibit concentrations surpassing the permissible limit, indicating higher than accepted levels of aluminum in these samples. Notably, G-108 demonstrates the highest concentration of 6.48, significantly exceeding the acceptable limit.

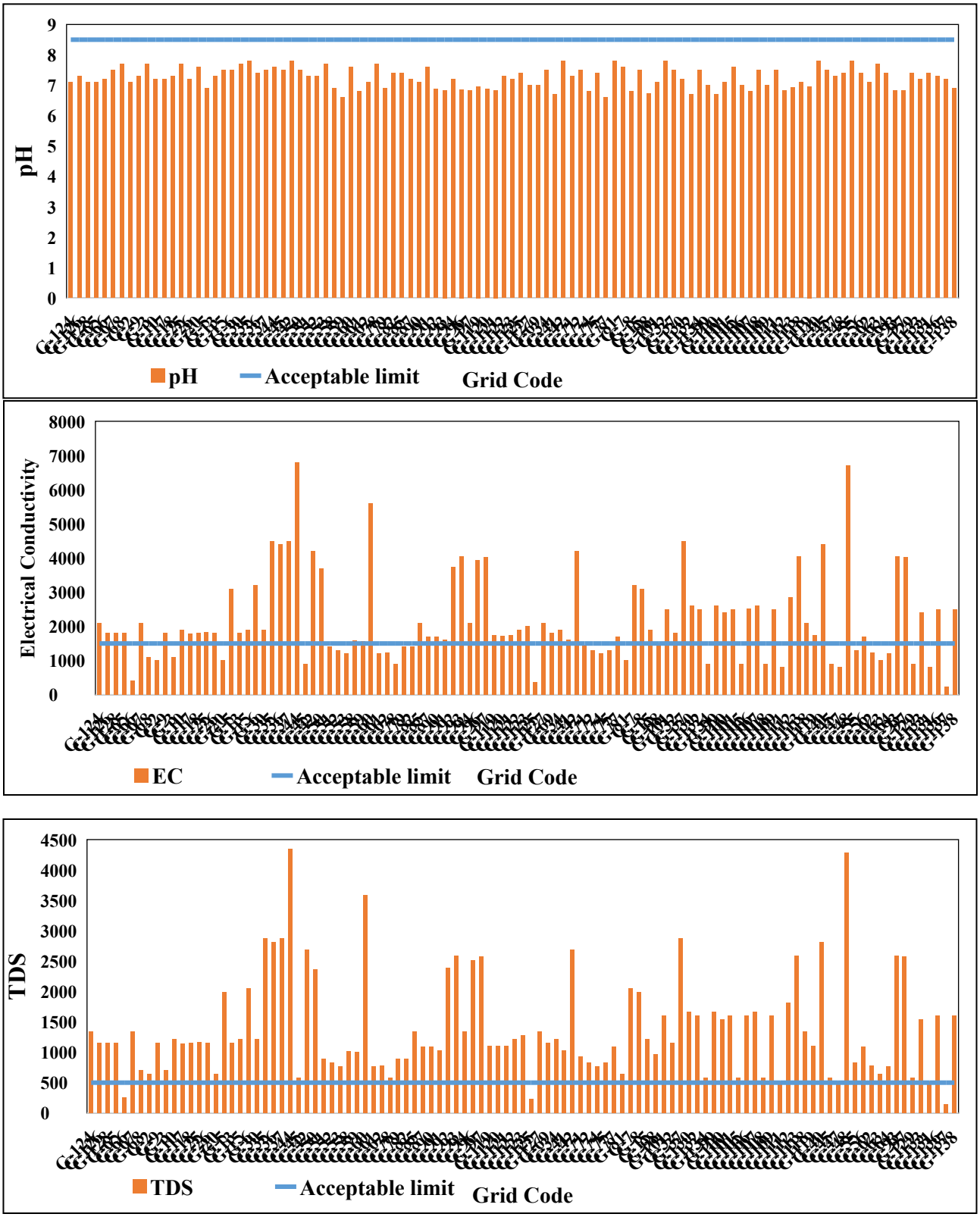

Figure 4.41 a) Variation of pH, EC & TDS in relation to the BIS 2012 Standard

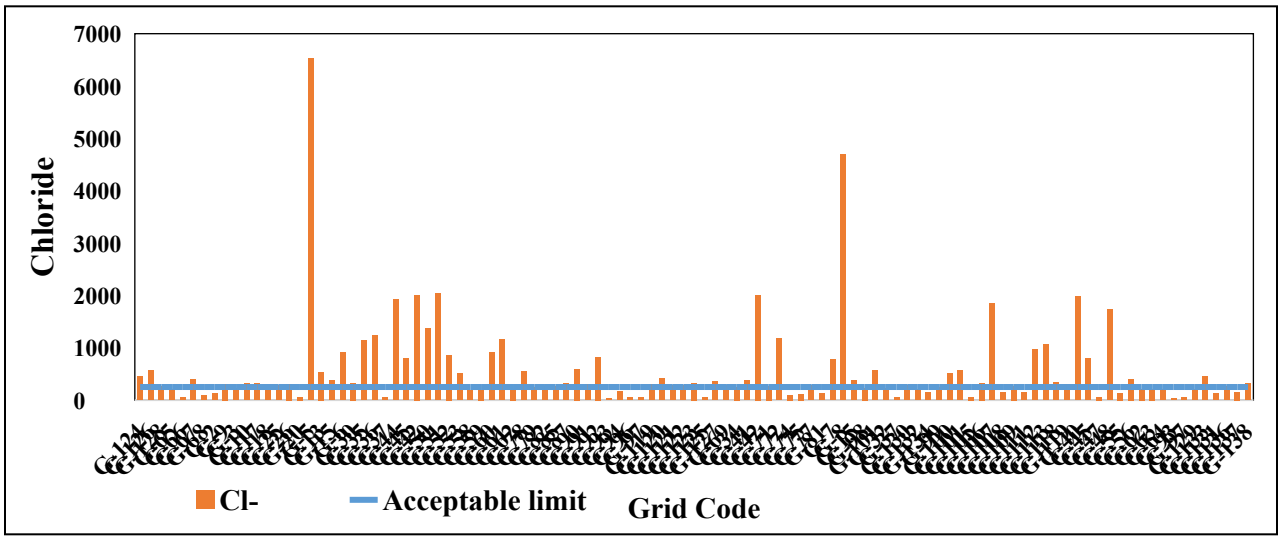
Chloride
7000
6000
5000
4000
3000
2000
1000
0
Cl-
Acceptable limit
Grid Code

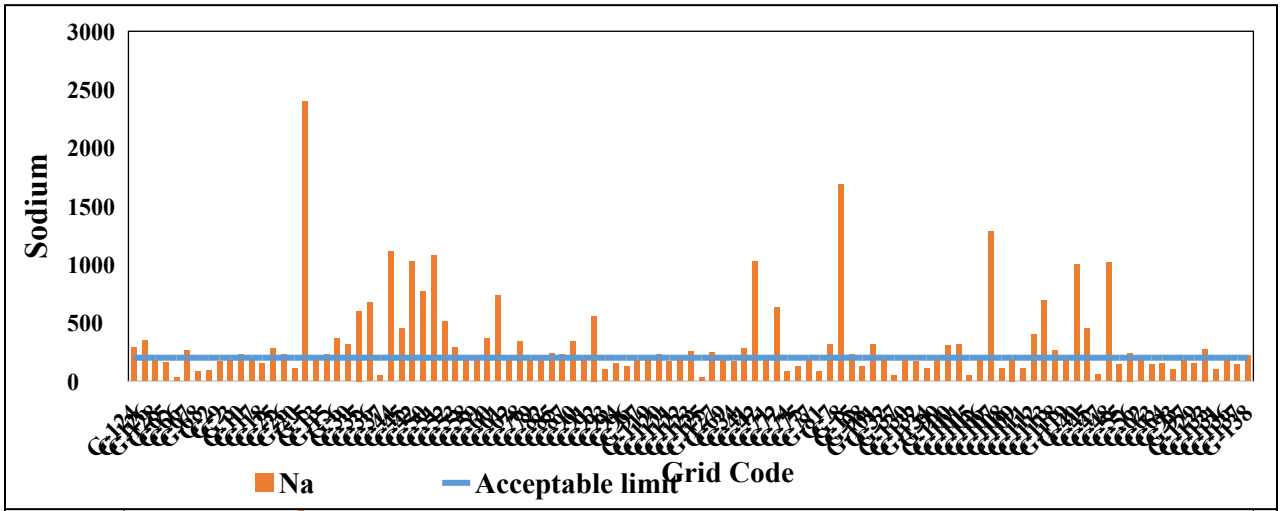
Sodium
3000
2500
2000
1500
1000
500
0
Na
Acceptable limit
Grid Code

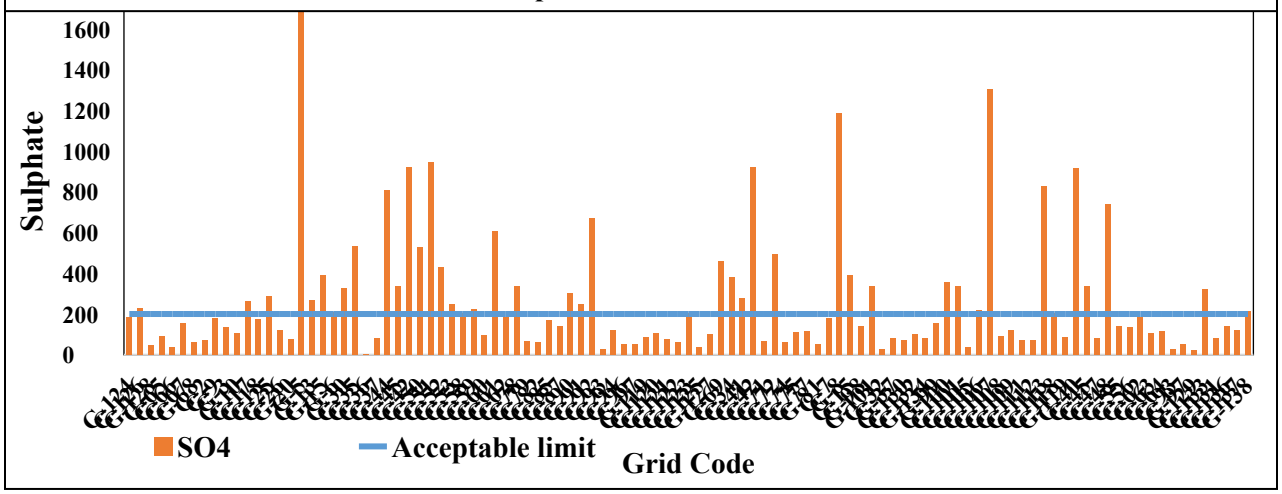
Sulphate
1600
1400
1200
1000
800
600
400
200
0
SO4
Acceptable limit
Grid Code

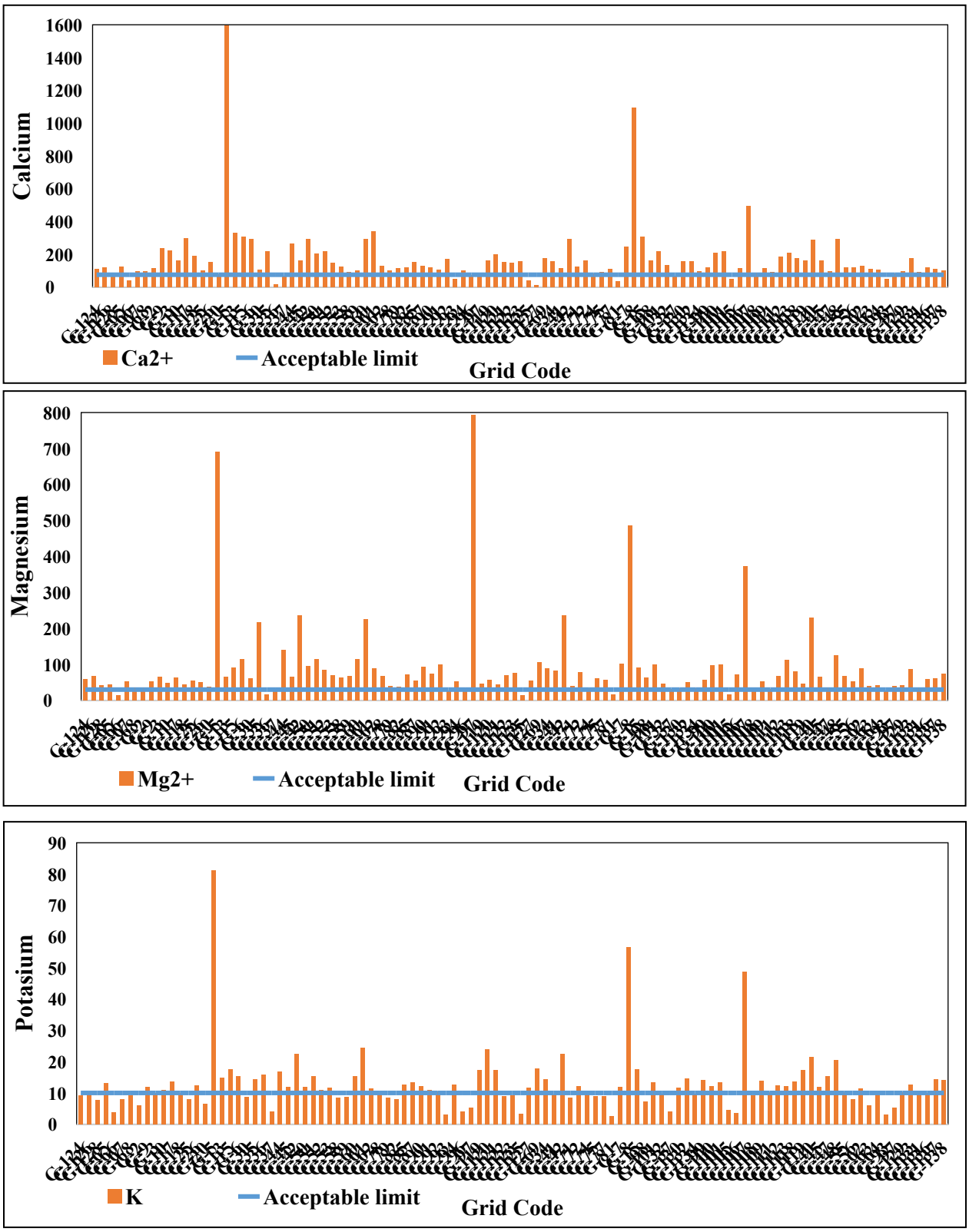

Figure 4.41 c) Variation of Ca^{2+}, Mg2+ & K+ in relation to the BIS 2012 Standard

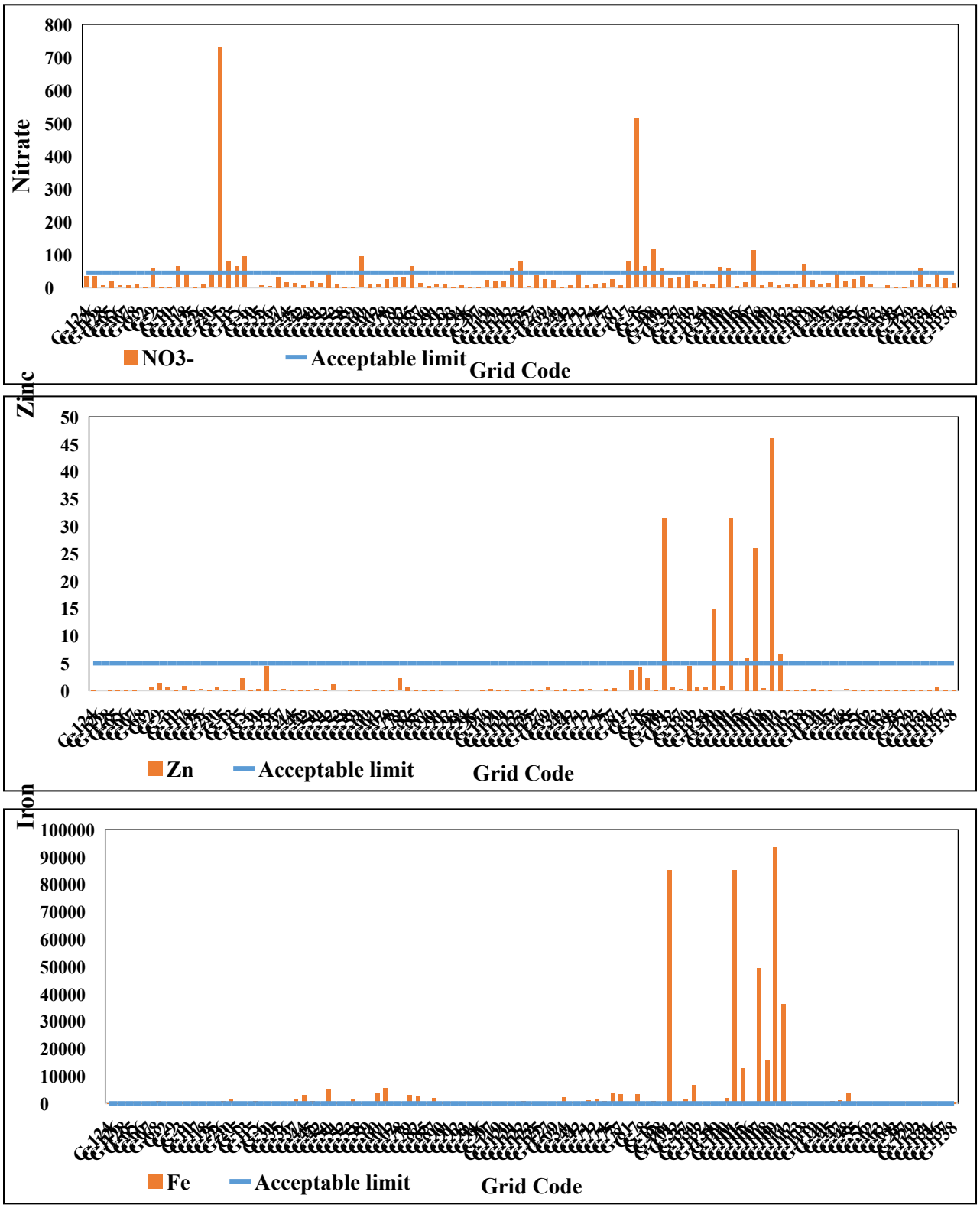
Nitrate
800
700
600
500
400
300
200
100
0
NO3-
Acceptable limit
Grid Code
Zinc
50
45
40
35
30
25
20
15
10
5
0
Zn
Acceptable limit
Grid Code
Iron
100000
90000
80000
70000
60000
50000
40000
30000
20000
10000
0
Fe
Acceptable limit
Grid Code

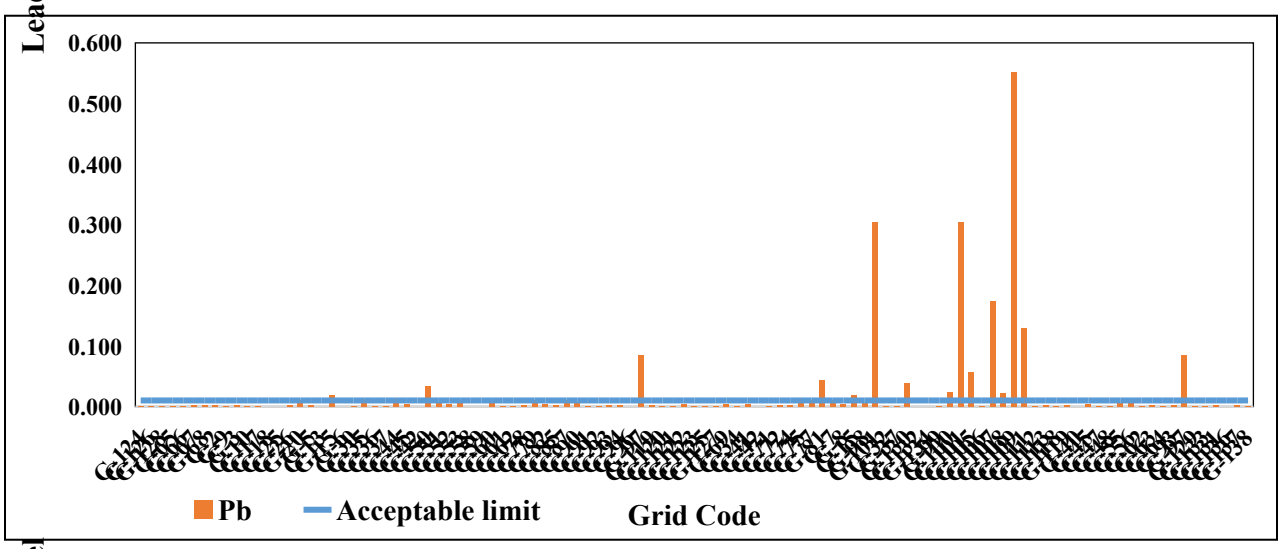
Lead
0.600
0.500
0.400
0.300
0.200
0.100
0.000
Pb
Acceptable limit
Grid Code

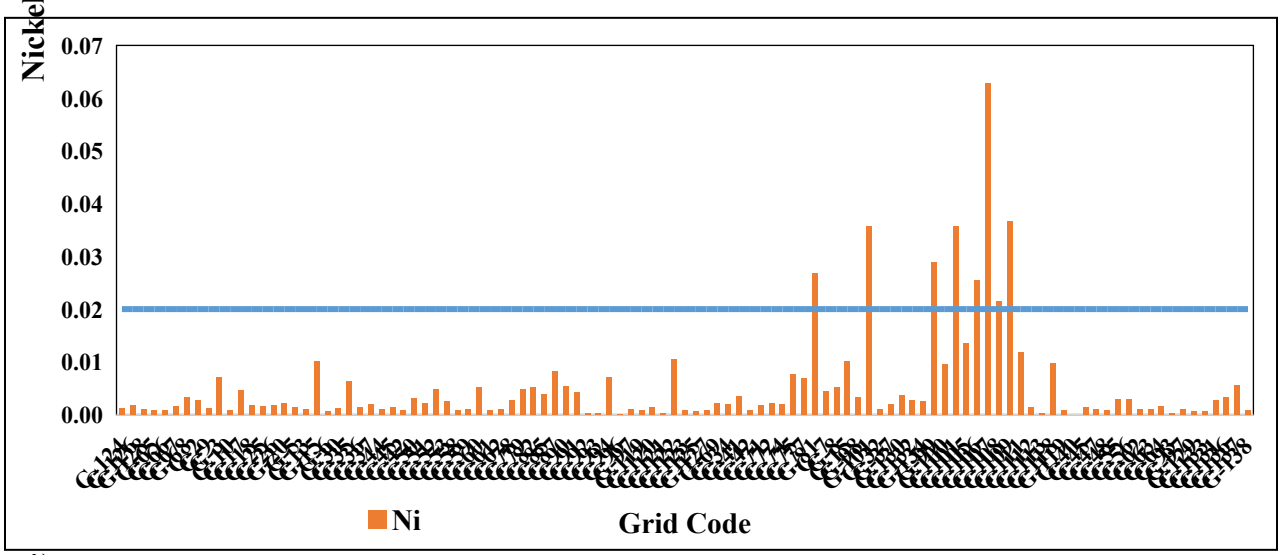
Nickel
0.07
0.06
0.05
0.04
0.03
0.02
0.01
0.00
Ni
Grid Code

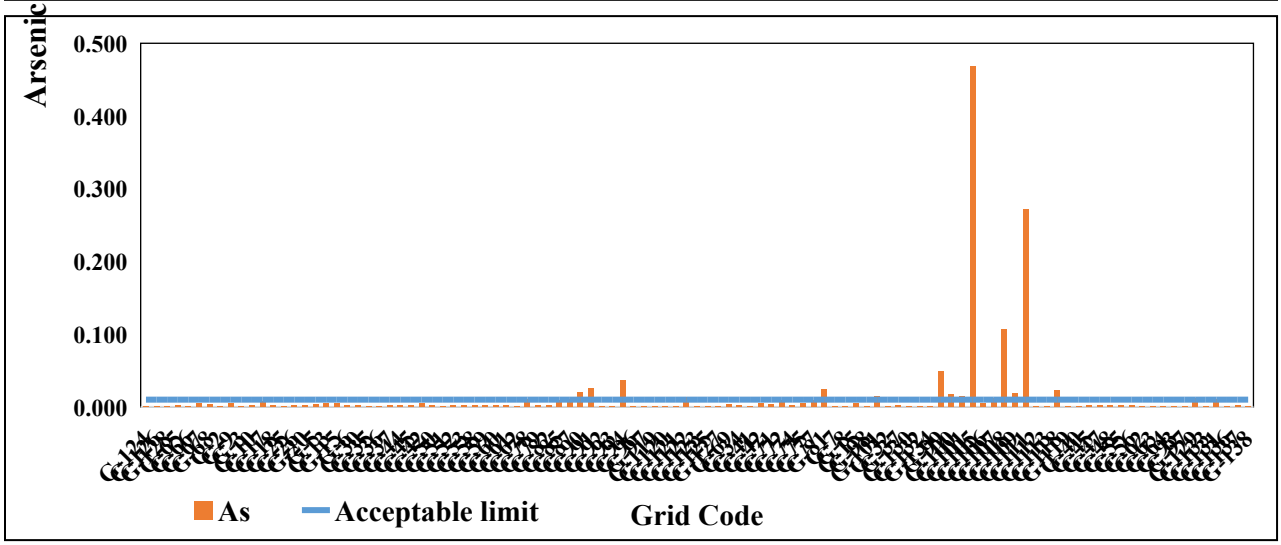
Arsenic
0.500
0.400
0.300
0.200
0.100
0.000
As
Acceptable limit
Grid Code

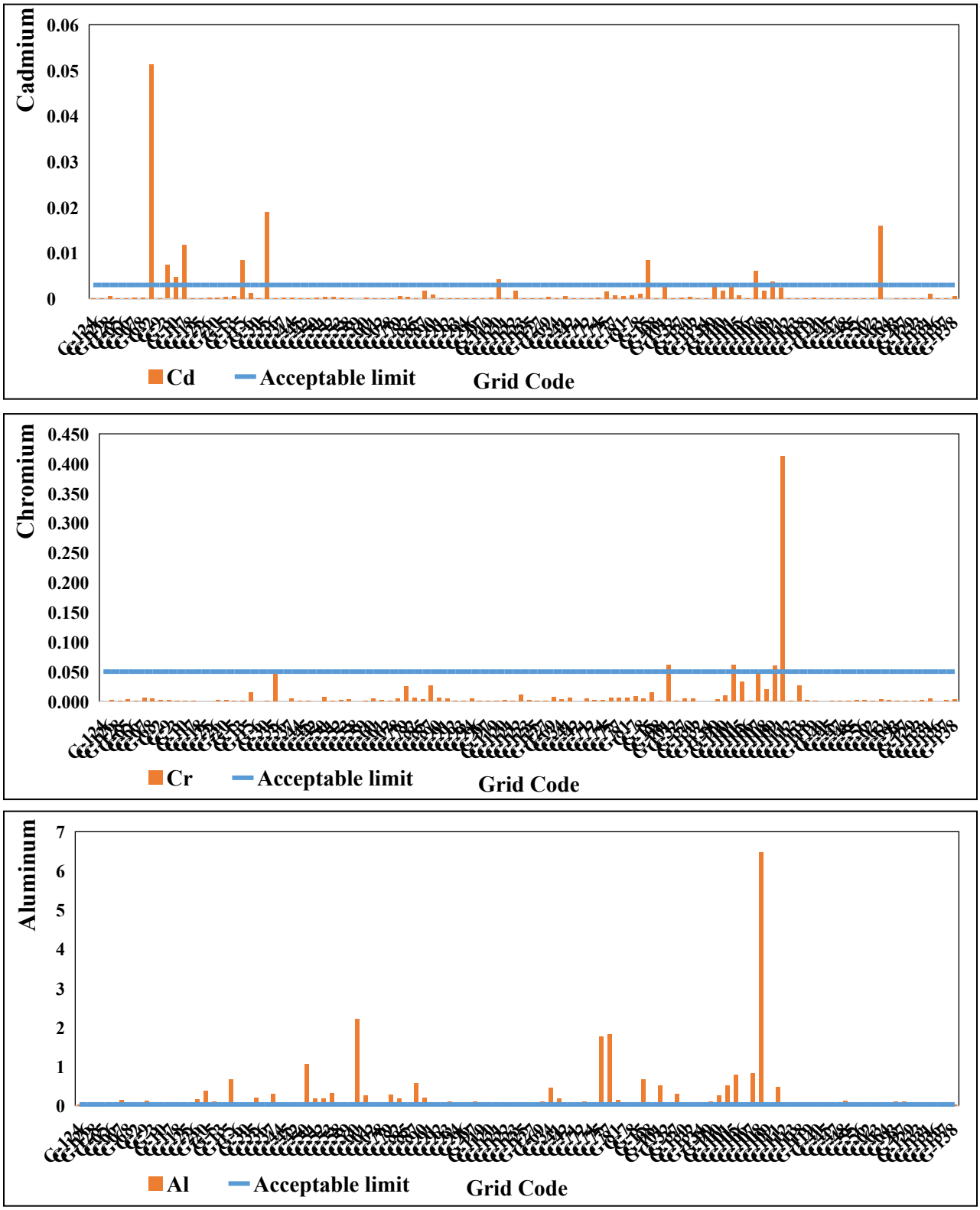

Figure 4.41 f) Variation of Cd, Cr & Al in relation to the BIS 2012 Standard

Chapter 5: Assessment of emerging contaminants in landfill leachate

5.1 Materials and methods

Leachate samples were systematically gathered following standardized protocols and procedures by environmental sampling experts affiliated with the National Institute of Hydrology, Roorkee. The pesticide solid waste utilized in preparing the leachate was obtained from the dumping site located at Ghazipur, Delhi, India. These samples were carefully transported to the laboratory for further analysis.

For the assessment of Contaminants of Emerging Concern (CECs) concentrations in the leachate samples, an analytical approach employing GC/MS (Gas Chromatography/Mass Spectrometry) methods was adopted (Masoner et al., 2014). Specifically, a method using full scan GC/MS analysis was employed to ascertain the concentrations of Emerging contaminants. The determination of pesticide concentrations followed the same protocol as the household/industrial method, utilizing sample extracts obtained through continuous liquid–liquid extraction (CLLE).

This comprehensive methodological approach enabled the thorough evaluation of CEC concentrations in the leachate samples and ensuring a comprehensive understanding of the presence and levels of various contaminants arising from the deposited dumping site.

5.2 Emerging contaminants

Emerging contaminants are substances that are recognized or suspected to pose potential risks to human health or the environment, but their full extent and impact are not yet fully understood or regulated (R. Kumar et al., 2022; Stefanakis & Becker, 2019). These contaminants can include a wide range of substances from various sources, such as:

- **Pharmaceuticals and Personal Care Products (PPCPs):** Compounds found in medications, cosmetics, and personal care items that make their way into water systems through human use and wastewater treatment plant discharge.
- **Perfluoroalkyl and Polyfluoroalkyl Substances (PFAS):** Chemicals used in various industrial processes, firefighting foams, and consumer products known for their persistence and potential health risks.

- **Pesticides and Herbicides:** Chemicals used in agriculture to control pests and weeds that might leach into water systems or soil, causing environmental concerns.
- **Industrial Chemicals:** Chemicals produced in manufacturing processes, some of which may have harmful effects on health and the environment.
- **Microplastics:** Tiny plastic particles from the breakdown of larger plastic items, found in water bodies and posing potential risks to aquatic organisms and possibly human health.
- **Hormone Disruptors:** Chemicals that can interfere with the endocrine system, affecting hormonal balance in living organisms.

The presence of various pesticides such as Monocrotophos, Phorate, BHC-alpha (benzene hexachloride), Isoproturon, Chlorpyrifos, DDE-o,p', Endosulfan I (alpha isomer) and DDT-o,p' has been identified within the leachate collected from the landfill site in Gazipur (Table 5.1).

5.2.1 Monocrotophos

Monocrotophos an organophosphate insecticide employed in agriculture to manage pests, presents significant concerns as a Contaminant of Emerging Concern (CEC) due to its potential adverse impacts on both human health and the environment.

The accepted safety level for monocrotophos in drinking water stands at 1 part per billion (ppb). A concentration of 413.0942 ppb represents a substantial deviation from this safety threshold (Table 5.1).

Physico-chemical properties reveal that monocrotophos exhibits high solubility in water, possesses a low partition coefficient, and demonstrates limited binding to sediment/soil. Although it's volatile, its low volatility from water is anticipated due to its low Henry’s law constant, calculated at 6.4 x 10-7 atm.m3 .mol-1.

Regarding its application and use, monocrotophos was registered for use across various crops such as cotton, apples, bananas, sunflowers, maize, sorghum, soybeans, potatoes, tomatoes, and others. It was predominantly used in sorghum and sunflowers to manage a broad spectrum of pests like aphids, caterpillars, mites, moths, and scale, as well as for locust control in Australia.

However, its usage was often as a secondary measure, especially during periods of high insect pressure or resistance levels. Notably, it wasn't employed by the Australian Plague Locusts Commission due to its perceived high toxicity levels (Chemicals, n.d.).

1. **Health Impact:** Exposure to monocrotophos above permissible levels in drinking water can pose serious health risks. Organophosphate pesticides like monocrotophos are neurotoxins and can cause acute and chronic health issues. Short-term exposure might lead to symptoms like nausea, dizziness, headaches, and respiratory issues. Long-term exposure could result in more severe effects on the nervous system, developmental problems in children, and even potential links to certain cancers.
2. **Environmental Concerns:** Monocrotophos, when present in water bodies due to runoff from agricultural fields or other sources, can have detrimental effects on aquatic life. It can harm fish, invertebrates, and other organisms, disrupting ecosystems and potentially impacting biodiversity.
3. **Regulatory Attention:** Contaminants like monocrotophos are increasingly garnering attention from regulatory bodies due to their potential risks. Such contaminants are being closely monitored, and regulatory limits might be updated based on new research and assessments of their impacts on health and the environment.
4. **Treatment and Mitigation:** Addressing contaminants like monocrotophos in water sources requires effective treatment methods. Advanced filtration techniques, such as activated carbon filtration or reverse osmosis are used to remove pesticides and other contaminants from drinking water.

5.2.2 Phorate

Phorate, an organophosphate insecticide, is among the compounds monitored in drinking water due to its potential health and environmental impacts. Its concentration of 32.1695 parts per billion (ppb) compared to the permissible limit of 2 ppb for drinking water indicates an exceedance of the accepted safety level (Table 5.1).

Here is a detailed discussion regarding its significance:

Health Concerns: Organophosphate pesticides like phorate are known neurotoxins. Exposure to levels beyond permissible limits in drinking water can pose serious health risks to humans. Short-term exposure might cause symptoms such as nausea, dizziness, headaches, and respiratory issues. Long-term exposure could lead to more severe effects on the nervous system, developmental problems in children, and potential links to certain health conditions.

Environmental Impact: Phorate, when present in water sources due to agricultural runoff or other means, can harm aquatic life and disrupt ecosystems. Its presence in water bodies may negatively impact fish, invertebrates, and other organisms, affecting the balance of aquatic ecosystems.

Regulatory Attention: Compounds like phorate fall under the category of contaminants of concern due to their potential risks. Regulatory bodies monitor and set permissible limits for such substances in drinking water to safeguard public health. The established limits may change based on evolving scientific understanding and risk assessments.

Mitigation and Treatment: Dealing with contaminants like phorate in water sources requires effective treatment methods. Advanced water treatment processes, including activated carbon filtration, oxidation, or reverse osmosis, are employed to remove pesticides and other contaminants from drinking water.

5.2.3 BHC-alpha (Benzenehexachloride)

The presence of BHC-alpha (Benzenehexachloride) at a concentration of 4.4094 parts per billion (ppb) in drinking water, compared to the extremely low permissible limit of 0.01 ppb, is a cause for concern, given its toxicity and historical use as an agricultural insecticide (Table 5.1).

Here is an elaboration on this issue:

1. **Health and Environmental Risks:** BHC, including its alpha isomer is highly toxic and poses significant health risks to humans and the environment. Prolonged exposure to even trace amounts can lead to severe health issues, including neurological, reproductive and developmental problems. BHC compounds are also harmful to aquatic life and can persist in the environment for extended periods, leading to bioaccumulation in the food chain.

2. **Government Ban:** The ban imposed by the Indian government on the manufacture and use of BHC, effective from April 1, 1997, indicates recognition of the severe risks associated with this chemical (https://www.downtoearth.org.in/news/commotion-over-a-ban-23709). The ban aimed to prevent further environmental contamination and protect public health from the detrimental effects of BHC exposure.

3. **Water Quality Concerns:** Even though there is a ban on its production and use, the detection of BHC-alpha in drinking water above the permissible limit raises concerns about

potential sources of contamination. It might indicate past usage, improper disposal, or residual contamination that persists despite regulatory actions.

4. **Monitoring and Compliance:** Monitoring BHC levels in drinking water remains crucial, especially in areas historically associated with its use. Regular surveillance is necessary to ensure compliance with regulatory standards and to prevent public exposure to this hazardous compound.

5. **Remediation and Public Awareness:** Efforts toward remediation of contaminated sites and public awareness campaigns regarding the dangers of BHC exposure are vital. Remediation strategies and education programs can aid in preventing inadvertent exposure and mitigating the risks associated with past contamination.

5.2.4 Isoproturon

The detection of Isoproturon at a concentration of 3109.1386 parts per billion (ppb) in drinking water, compared to the permissible limit of 9 ppb (BIS, 2012), raises significant concerns due to its use as a phenyl urea herbicide and potential health and environmental risks associated with its elevated presence (Table 5.1).

Here is a detailed discussion regarding its significance:

1. **Health Impacts:** Isoproturon is an herbicide used in agriculture to control weeds. Exposure to levels exceeding permissible limits in drinking water could pose health risks to humans. Chronic exposure to Isoproturon has been associated with potential adverse effects on the endocrine system, reproductive health, and developmental problems. Ensuring levels stay within the permissible limit is crucial to avoid these health concerns.

2. **Environmental Concerns:** Isoproturon can persist in the environment, potentially contaminating water sources via runoff from agricultural fields. Its presence in water bodies can harm aquatic organisms, disrupt ecosystems, and affect biodiversity.

3. **Regulatory Considerations:** The permissible limit for Isoproturon in drinking water is set to protect public health. Exceeding this limit indicates potential contamination and raises alarms for immediate action, including investigation into the sources of contamination and measures to mitigate further exposure.

4. **Monitoring and Mitigation:** Continuous monitoring of Isoproturon levels in water sources is essential to ensure compliance with safety standards. Efforts to mitigate contamination involve implementing best agricultural practices, proper disposal of unused chemicals, and employing effective water treatment technologies to remove or reduce Isoproturon levels.

5. **Public Awareness and Education:** Educating farmers, communities, and stakeholders about the proper use, handling, and disposal of Isoproturon and similar chemicals is crucial to prevent accidental contamination of water sources and to promote responsible agricultural practices.

5.2.5 Chlorpyrifos

The detection of Chlorpyrifos at a concentration of 719.9573 parts per billion (ppb) in drinking water, compared to the permissible limit of 30 ppb (BIS, 2012), raises concerns due to its classification as an insecticide and potential risks associated with elevated exposure (Table 5.1).

Here is a detailed discussion regarding its significance:

1. **Health Impacts**: Chlorpyrifos is an organophosphate insecticide used in agriculture. Exposure to levels exceeding permissible limits in drinking water can pose health risks to humans. Acute exposure to Chlorpyrifos can cause symptoms such as nausea, dizziness, respiratory issues, and in severe cases, it can lead to neurotoxic effects. Long-term exposure may result in chronic health issues, particularly affecting the nervous system and potentially influencing developmental processes, especially in children.
2. **Environmental Concerns:** Chlorpyrifos, when present in water bodies due to runoff from agricultural areas or other sources, can harm aquatic life and disrupt ecosystems. Its presence may adversely affect fish, invertebrates, and other organisms, leading to ecological imbalances.
3. **Regulatory Guidelines:** The permissible limit for Chlorpyrifos in drinking water is established to protect public health. Detection above this limit signifies potential contamination and necessitates immediate action, including investigating the sources of contamination and implementing measures to mitigate further exposure.

4. **Monitoring and Mitigation:** Regular monitoring of Chlorpyrifos levels in water sources is essential to ensure adherence to safety standards. Efforts to mitigate contamination include adopting integrated pest management practices in agriculture, proper disposal of unused pesticides, and employing effective water treatment technologies to reduce Chlorpyrifos levels.
5. **Awareness and Education:** Educating farmers, communities and stakeholders about the responsible use, handling, and disposal of Chlorpyrifos and similar chemicals is crucial to prevent accidental contamination of water sources and promote safer agricultural practices.

5.2.6 DDE-o,p'

DDE-o,p' stands for Dichlorodiphenyldichloroethylene - ortho, para isomer. The detection of DDE-o,p' at a concentration of 1.9719 parts per billion (ppb) in drinking water, compared to the permissible limit of 1 ppb (BIS, 2012), raises concerns regarding its presence as a breakdown product of DDT and potential implications for human health and the environment (Rogers et al., 2021) (Table 5.1).

Here is a detailed discussion regarding its significance:

1. **Source and Formation:** DDE-o,p' is a metabolite formed when DDT, an organochlorine pesticide, breaks down in the environment. It is one of the several breakdown products of DDT and is known to persist in the environment.

2. **Health Impacts:** DDE-o,p' is considered toxic and, similar to DDT, is classified as an endocrine disruptor. Exposure to levels beyond permissible limits in drinking water may pose health risks to humans. Chronic exposure to DDE-o,p' has been associated with various health issues, including potential impacts on the reproductive system and hormone regulation.

3. **Environmental Persistence:** DDE-o,p', being a persistent organic pollutant, can accumulate in the food chain, affecting various organisms and potentially causing harm to wildlife and ecosystems .

4. **Regulatory Standards:** The permissible limit for DDE-o,p' in drinking water is established to minimize human exposure and potential health risks. Detection above this

limit prompts actions to investigate sources of contamination and implement measures to mitigate further exposure.

5. **Mitigation and Treatment:** Monitoring DDE-o,p' levels in water sources is crucial to ensure compliance with safety standards. Employing effective water treatment technologies is essential to reduce or remove DDE-o,p' concentrations in drinking water.

6. **Preventive Measures:** Preventing contamination sources, such as the proper disposal of DDT and other organochlorine pesticides, as well as educating about their risks, is vital to prevent further environmental pollution and human exposure.

5.2.7 Endosulfan I (alpha isomer)

The detection of Endosulfan I (alpha isomer) at a concentration of 4.05 parts per billion (ppb) in drinking water, compared to the permissible limit of 0.04 ppb (Table 5.1), raises significant concerns due to its classification as an agricultural insecticide and potential risks associated with elevated exposure.

Endosulfan indeed presents significant concerns due to its persistence and high toxicity to aquatic life. Its extensive use, environmental spread, and lasting presence have raised alarms globally. Given its persistence and harmful effects, endosulfan has been classified as a hazardous substance, prompting stringent regulations for the disposal of endosulfan-containing waste by federal authorities (M. Kumar & Philip, 2007).

Despite numerous countries enforcing bans on endosulfan production and usage due to its detrimental impact, it remains a significant component of pest control strategies in India. The continued utilization of endosulfan in India highlights its status as a priority pollutant for pest management, despite its known risks to the environment and organisms within it.

Here is a detailed discussion regarding its significance:

1. **Health Risks:** Exposure to Endosulfan I can pose health risks to humans as well, especially to agricultural workers handling the chemical and individuals living in proximity to areas where it is used. It can cause acute and chronic health issues, including neurotoxic effects.
2. **Environmental Concerns:** Endosulfan I can persist in the environment and contaminate water sources through various means, primarily through runoff from agricultural areas

where it is used. Its presence in water bodies can harm aquatic life, impact biodiversity, and disrupt ecosystems.

3. **Bioaccumulation:** Endosulfan I has the potential to bioaccumulate in organisms. This means that as it moves up the food chain, higher-level predators can accumulate larger concentrations of the chemical, leading to more severe impacts on top-level consumers and predators.
4. **Regulatory Guidelines:** The permissible limit for Endosulfan I in drinking water is established to safeguard public health. Detection above this limit signifies potential contamination and warrants immediate action, including investigating sources of contamination and implementing measures to reduce further exposure.
5. **Monitoring and Mitigation:** Regular monitoring of Endosulfan I levels in water sources is essential to ensure adherence to safety standards. Employing effective water treatment technologies is crucial to reduce or eliminate Endosulfan I concentrations in drinking water.
6. **Preventive Measures:** Preventing contamination sources, such as the regulated and careful use, application, and disposal of Endosulfan I and similar insecticides, as well as educating about their risks, is vital to prevent further environmental pollution and human exposure.

5.2.8 DDT-o,p'

DDT-o,p' stands for Dichlorodiphenyltrichloroethane - ortho, para isomer. The detection of DDT-o,p' at a concentration of 3.4717 parts per billion (ppb) in drinking water, compared to the permissible limit of 1 ppb (BIS, 2012), raises concerns due to its classification as a pesticide and potential risks associated with elevated exposure (Rafati et al., 2022).

Here is a detailed discussion regarding its significance:

1. **Health Impacts:** DDT-o,p' is a breakdown product of DDT, an organochlorine pesticide. Exposure to levels above permissible limits in drinking water can pose health risks to humans. Chronic exposure to DDT-o,p' has been associated with various health issues, including potential impacts on the nervous system, hormonal disruptions, and reproductive health concerns.

2. **Environmental Persistence:** DDT-o,p', being a persistent organic pollutant, can remain in the environment for extended periods. It can accumulate in the food chain, potentially causing harm to wildlife and ecosystems (Haarstad, 2008).

3. **Regulatory Standards:** The permissible limit for DDT-o,p' in drinking water is established to minimize human exposure and potential health risks. Detection above this limit indicates potential contamination and calls for actions to investigate sources of contamination and mitigate further exposure.

4. **Monitoring and Mitigation:** Regular monitoring of DDT-o,p' levels in water sources is crucial to ensure compliance with safety standards. Employing effective water treatment technologies is essential to reduce or remove DDT-o,p' concentrations in drinking water.

5. **Preventive Measures:** Preventing contamination sources, such as the proper disposal of DDT and other organochlorine pesticides, and educating about their risks is vital to prevent further environmental pollution and human exposure.

Table 5.1: List of Pesticides detected in Gazipur Landfill Leachate

Compound	Conc (ppb)	Permissible limit in drinking water (ppb)
Monocrotophos	413.0942	1
Phorate	32.1695	2
BHC-alpha (benzene hexachloride)	4.4094	0.01
Isoproturon	3109.1386	9
Chlorpyrifos	719.9573	30
DDE-o,p'	1.9719	1
Endosulfan I (alpha isomer)	4.0499	0.04
DDT-o,p'	3.4717	1

References

BIS. (2012). Indian Standard Drinking Water Specification (Second Revision). *Bureau of Indian Standards*, *IS 10500*(May), 1–11. http://cgwb.gov.in/Documents/WQ-standards.pdf

Chemicals, V. (n.d.). *Review of MONOCROTOPHOS - Environmental Assessment*.

Haarstad, K. (2008). Long-term leakage of DDT and other pesticides from a tree nursery landfill. *Ground Water Monitoring and Remediation*, *28*(4), 107–111. https://doi.org/10.1111/j.1745-6592.2008.00217.x

Kumar, M., & Philip, L. (2007). Biodegradation of endosulfan-contaminated soil in a pilot-scale reactor-bioaugmented with mixed bacterial culture. *Journal of Environmental Science and Health - Part B Pesticides, Food Contaminants, and Agricultural Wastes*, *42*(6), 707–715. https://doi.org/10.1080/03601230701465940

Kumar, R., Qureshi, M., Vishwakarma, D. K., Al-Ansari, N., Kuriqi, A., Elbeltagi, A., & Saraswat, A. (2022). A review on emerging water contaminants and the application of sustainable removal technologies. *Case Studies in Chemical and Environmental Engineering*, *6*(May), 100219. https://doi.org/10.1016/j.cscee.2022.100219

Masoner, J. R., Kolpin, D. W., Furlong, E. T., Cozzarelli, I. M., Gray, J. L., & Schwab, E. A. (2014). Contaminants of emerging concern in fresh leachate from landfills in the conterminous United States. *Environmental Science: Processes and Impacts*, *16*(10), 2335–2354. https://doi.org/10.1039/c4em00124a

Rafati, L., Services, H., Ehrampoush, M. H., & Sedighi-khavidak, S. (2022). *Chlorpyrifos bioremediation in the environment : A review article of Environmental Environmental Health of Health and Sustainable Development (JEHSD) Sustainable Development Chlorpyrifos Bioremediation in the Environment : A Review Article*. *December*.

Rogers, E. R., Zalesny, R. S., & Lin, C. H. (2021). A systematic approach for prioritizing landfill pollutants based on toxicity: Applications and opportunities. *Journal of Environmental Management*, *284*(October 2020), 112031. https://doi.org/10.1016/j.jenvman.2021.112031

Stefanakis, A. I., & Becker, J. A. (2019). A review of emerging contaminants in water: Classification, sources, and potential risks. *Waste Management: Concepts, Methodologies,*

Tools, and Applications, *June*, 177–202. https://doi.org/10.4018/978-1-7998-1210-4.ch008

Chapter 6: Understanding of hydrodynamics of groundwater flow in the study area

6.1 Groundwater Hydrodynamics

The Central Ground Water Board and WAPCOS undertook an extensive hydrodynamic exploration in Ghazipur area, Eastern Delhi (CGWB, 2017). Their focus was on drilling 42 exploration wells that probed both shallow and deep aquifers (Fig.6.1). These wells delved to a maximum depth of 320 meters allowing for an in-depth understanding of the groundwater resources in the region.

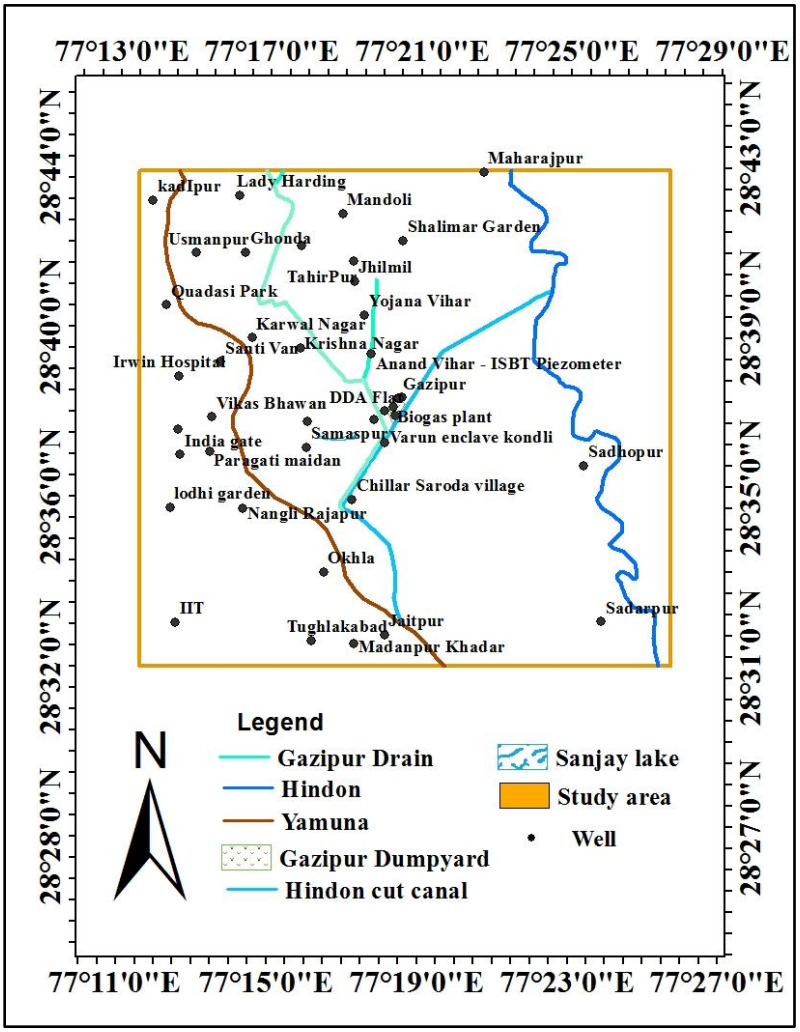

Figure 6.1: Location of exploratory wells constructed for Data Generation in study area

6.1.1 Aquifer Disposition

The study aimed to understand the area aquifer layout using well logs and geophysical methods. By analyzing these records from wells drilled by the Central Ground Water Board and WAPCOS VES survey, different aquifer zones with varied resistivity were identified. This integrated data was used to create an aquifer map, detailing the regional aquifer structure in the study area. Principal aquifers were categorized based on sand types, while surface materials like topsoil, silty clay and bedrock formations were classified for a comprehensive understanding.

The findings revealed the presence of a two-tiered aquifer system which generally characterizes the groundwater structure in this area. However, it is worth noting that Aquifer-III was also identified in specific locations suggesting a nuanced and varied groundwater distribution. To provide a visual representation and detailed information about the locations of these exploration boreholes reference was made in Figure 6.1, which presumably contains a map or illustration depicting the positions of these wells within the region. This mapping provides insight into the strategic positioning and spatial distribution of drilled wells optimizing the exploration of groundwater resources.

The granular zones in Aquifer Group–I are generally thick-bedded, very large, and made up of relatively coarser material than the deeper Aquifer Groups–II and III are thin-bedded sometimes lens-shaped and made up of finer sediments mostly silty and clayey material.

6.1.2 Eastern district

The eastern district of the study area, bordering Ghaziabad and Noida in Uttar Pradesh and situated between the Yamuna and Hindon rivers, spans an area of 64 sq km. It lies about 6 km eastward from the Delhi border, encompassing the space between these two rivers. Along the Yamuna floodplain and the eastern border near the Hindon river, the sub-surface consists of a substantial layer of fine sand at shallower depths, around 60–70 meters below ground level. Finer sediments like clay, clayey-silt, and silty-clay separate these granular zones as indicated in Figure 6.2.

Deeper zones beyond 70 meters showcase finer materials intermixed with silt, kankar, and clay. The basement rock condition in the East district features a moderately uneven terrain sloping gently toward the east. At specific locations like Yojana Vihar, Anand Vihar, and Nangli Rajapur, the basement has been encountered at depths ranging from 145 to 159 meters below ground level. In Ghazipur, a mound-shaped basement rock exists within the depth range of 54 to 79 meters below

ground level. Underlying the Yamuna floodplain, the basement rock in East Delhi varies in depth from 28 to 204 meters below ground level.

6.1.3 New Delhi District

The New Delhi district within NCT Delhi spans 35 sq km and centrally located displaying varied surface altitudes due to the presence of the Delhi Ridge. Approximately 10 sq km lies within the ridge area, with altitudes ranging between 225 to 255 meters above mean sea level (amsl). The surface slopes gently towards the east, reaching an altitude of 210m amsl near the Yamuna river course.

The sub-surface landscape depicted in Figure 6.2, exhibits significant variations. The western part, adjacent to the Delhi Ridge is characterized by marginal alluvium where a 0 to 30-meter thick layer covers weathered and fractured quartzite rocks. The alluvium thickness increases eastward from the ridge. Depths to the bedrock fluctuate ranging from 5 meters below ground level (bgl) at Mahavir Banasthali to 91 meters bgl at Pragati Maidan. At Lodi Garden, bedrock is encountered at 74 meters bgl. The overlying alluvium comprises clay, silt, and fine to medium sand, often mixed with kankar.

The topsoil primarily consists of silty-clay, occasionally interspersed with clay, sand, and silt layers. Sand, silt, and kankar strata form favorable aquifer zones. Towards the western part encompassing Rashtrapati Bhavan, Chanakyapuri, Shantipath, South and North Avenue, and Connaught Place, alternate bands of clay, silt, and kankar were found at India Gate in a tubewell drilled to 150 meters depth (Fig.6.2).

The eastern extremity bound by the Yamuna River, represents a linear plain of the river. Groundwater occurs under the water table and semi-confined conditions in alluvium. Tubewells commonly access kankar zones mixed with silt and sand aquifers, encountered alternately beyond 10 meters bgl, extending to the basement rock. The groundwater quality is typically fresh within the quartzite, with a fresh-saline interface observed at 40 meters depth in Pragati Maidan.

6.1.4 North East District

The North-East district, situated east of the Yamuna River and bordering Ghaziabad and Meerut districts of Uttar Pradesh to the east and north respectively, spans an area of 60 sq km below the surface lies a substantial layer of fine sand and silt extending to depths of about 70 meters below

ground level (bgl). Finer sediments like clayey silt, silty clay, buff-colored clay and kankars exist separating granular zones. Clay content increases moving eastward from the Yamuna floodplain.

The basement rock depth along the Yamuna floodplain in this district is shallower due to the Delhi central ridge which diminishes at the Wazirabad Barrage and extends further in the same direction, resulting in a shallower subsurface basement condition. Depths to bedrock range from 54 meters bgl at Mandaoli to 67 meters bgl at Ushmanpur. Moving further east, the depth of the basement rock increases as depicted in Figure 6.2. The depth of the fresh-saline water interface in the Yamuna floodplain varies from 26 meters at Sonia Vihar to 56 meters bgl at Dilshad Garden.

6.1.5 South District

The South district covers 45.2 sq km and showcases mountainous, undulating terrain with visible exposures of Delhi quartzite. Central to this region lies a saucer-shaped alluvial field, filled with alluvium and underlain by quartzitic basement rock. At Madanpur Khadar, the freshwater zone is limited, and bedrock has been discovered at a depth of 300 meters (Fig.6.2). Boreholes drilled in quartzitic formations like Jaunapur, Asola, Mandi, and Tughlakabad indicate moderately fractured zones within the 30 to 90-meter depth range, diminishing gradually with increased depth. A weathered zone consistently appears above the hard rock, albeit with varying thicknesses across different locations.

6.1.6 Central District

The Central district spans from a hard rock area of Delhi quartzite to alluvium underlain by the same rock. Bounded by the Yamuna River in the east, the region primarily consists of unconsolidated Quaternary alluvium atop Pre-Cambrian Meta sediments of the Delhi system. Due to limited exploratory well data within the Central district, aquifer disposition has been inferred from neighboring areas like North East, West, New Delhi, and East (refer to Fig. 6.2). The Quaternary alluvium comprises fine sand, silt, clay, and occurrences of kankars. Its aquifer system consists of fine to medium-grained yellowish sand, accompanied by medium to high-grade kankars. Water quality remains fresh down to a depth of 31 meters below ground level.

6.1.7 Ghaziabad District

The 3-D multi-log and fence graphic clearly demonstrates that the quality of aquifers is good in

the eastern portion of the district and poor in the western portion. The alluvial formation in the Ghaziabad district contains important aquifers that are less than 100 metres deep. This subsurface aquifer is large, and its thickness varies throughout the district. The aquifer sand layers get thinner as one moves deeper, with conspicuous interbeds of clay and finer sediments (Fig.6.2). The shallow occurrences of brackish/saline groundwater are located in the westernmost portion of the region between the rivers Yamuna and Hindon, as observed in the boreholes at Pancharya and Shalimar Garden, where the depth to brackish/saline groundwater is 74 and 58 m, respectively.

6.1.8 Gautam Buddha Nagar District

The lithological variation and aquifer disposition of Gautam Buddha Nagar are depicted using a fence diagram and a three-dimensional multi-log (Fig. 6.2). The 3-D multi-log and fence shows that in the northern western portion at Sadarpur, the saline zone begins in the first aquifer at a depth of 58 mbgl, whereas in the northern eastern portion at Sadhopur, it begins in the third aquifer at a depth of 329 mbgl. The Bedrock was seen at 310 mbgl at Sadarpur and 444 mbgl at Sadhopur.

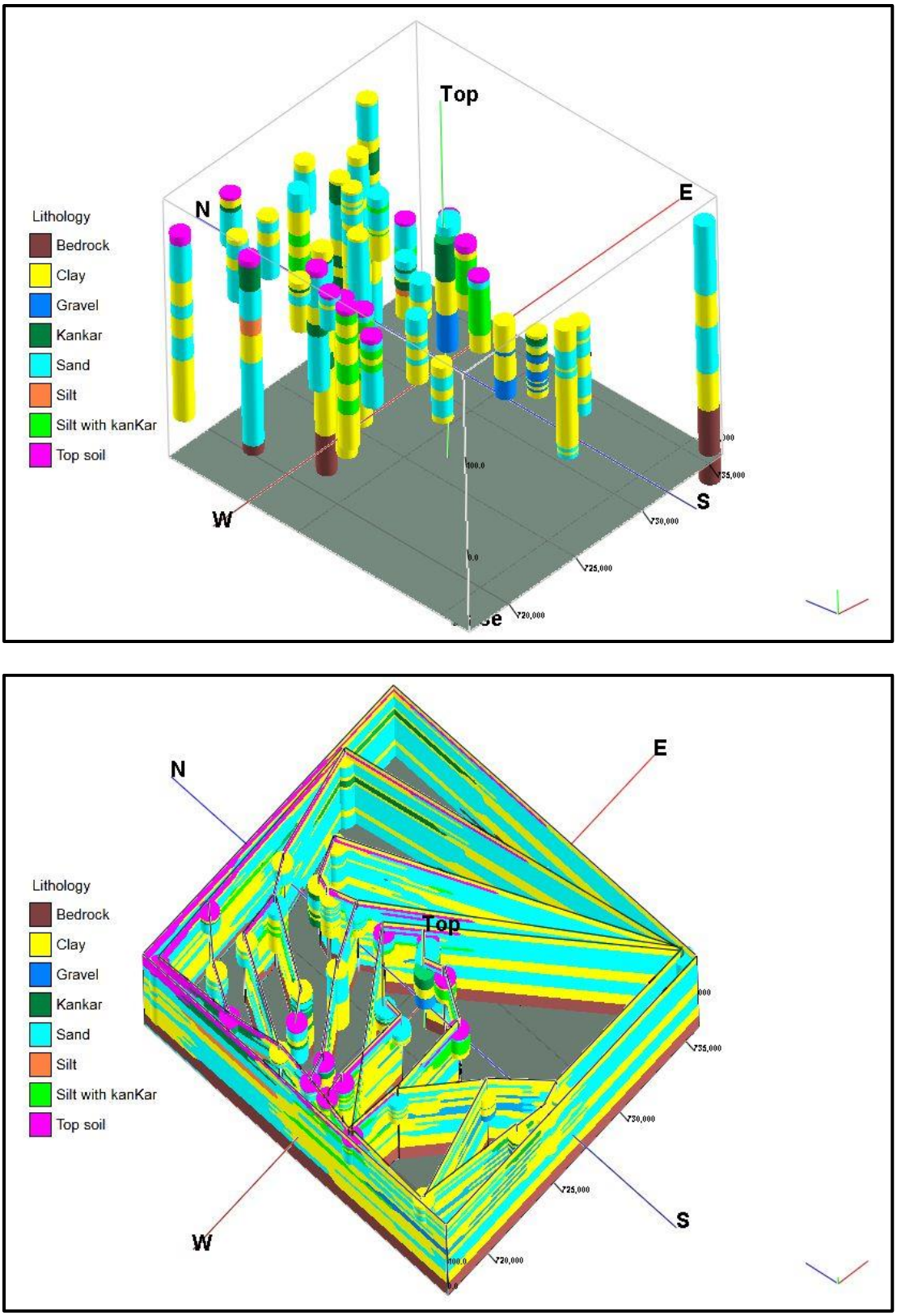

Figure 6.2 3-D Multi-log of aquifer disposition and lithological variation in the study area

6.2 Aquifer Parameters

During the groundwater exploration by CGWB, pumping tests were performed to assess aquifer parameters, computing transmissivity and Hydraulic Conductivity values. WAPCOS conducted slug tests in bore wells to determine the hydraulic conductivity of aquifers.

6.2.1 Hydraulic Conductivity

Hydraulic conductivity values derived from the Hvorslev (1951) and Bouwer & Rice (1976) methods for various wells are summarized in Table 6.1. In South Delhi, the Hvorslev method yielded K values ranging from 1.31 to 1.69 m/day, averaging at 1.5 m/day, while Greater Kailash showed values from 1.26 to 1.63 m/day, averaging at 1.45 m/day, and Bhatti Khurd exhibited values from 1.2 to 1.55 m/day, averaging at 1.38 m/day.

Moving to the East district, Ferojsah Kotla displayed values from 3.01 to 3.92 m/day, averaging at 3.47 m/day. Meanwhile, in North East at Jagatpur, values varied from 7.01 to 9.33 m/day. Notably, Hvorslev method-derived values tended to be slightly higher compared to Bouwer & Rice Method.

In Gautam Buddha Nagar, values ranged from 2.03 to 2.63 m/day, while in Ghaziabad, they spanned from 6.15 to 8.99 m/day. Jagatpur and Ghaziabad exhibited relatively higher average hydraulic conductivity (K) values, while Bhatti Khurd and Khanpur sites in Greater Kailash showed lower K values (Table 6.1).

6.2.2 Specific Yield

Specific yield represents the water volume a soil or rock can release through gravity drainage after saturation, relative to its own volume (Todd & Mays, 2005). This data is obtained through extensive field studies like prolonged pumping tests or dry season groundwater assessments, especially in hard-rock regions. Alternatively, it is derived from recommendations by GEC-1997 based on water balance studies conducted by CGWB, SGWD and academic institutions. Table 6.2 presents the GEC-1997 recommended specific yield ranges for various geological formations.

- **Unconsolidated formations (e.g., Alluvium):** These formations, such as loose sands, gravels, and silts found in river valleys or floodplains, typically exhibit higher specific yield values ranging from 0.04 to 0.22. Their loosely packed nature allows for greater

storage of water and relatively easier movement, enabling higher yields.

- **Semi-consolidated formations (e.g., Sedimentary rocks):** These formations like sandstones or certain sedimentary rocks show moderate specific yield values ranging from 0.01 to 0.15. They have some level of compaction but still possess porosity that allows water storage and movement, albeit at lower rates than unconsolidated formations.
- **Consolidated formations (e.g., Crystalline and hard rocks):** Formations like crystalline rocks (granite, basalt) or hard metamorphic rocks typically have very low specific yield values, ranging from 0.002 to 0.04. These formations have extremely low porosity and permeability, restricting water storage and movement, resulting in limited groundwater availability and extraction rates.

Table 6.1: Estimated hydrological parameters derived from the slug tests

Site Name	Latitude	Longitude	Hydraulic Conductivity K (m/day)		Average K m/day
			Hvorslev Method	Bouwer & Rice Method	
Khanpur	28° 30' 46.681" N	77° 13' 26.161" E	1.69	1.31	1.5
Greater Kailash	28° 33' 33.597" N	77° 13' 57.480" E	1.63	1.26	1.45
Bhatti Khurd	28° 26' 15.896" N	77° 12' 0.900" E	1.55	1.2	1.38
Ferojsah Kotla	28° 38' 17.823" N	77° 14' 28.980" E	3.92	3.01	3.47
Jagatpur	28° 44' 28.261" N	77° 12' 54.661" E	9.33	7.01	8.17
Gautam Buddha Nagar	28°21'32.19"N	77°33'2.63"E	2.63	2.03	2.33
Ghaziabad	28°40'8.85"N	77°27'13.44"E	8.99	6.15	7.57

Table 6.2: Specific Yields for Different Formations recommended by GEC 1997

Formation		Range of Specific Yield
Unconsolidated formations	**Alluvium**	0.04 to 0.22
Semi-consolidated formations	**Sedimentary rocks**	0.01 to 0.15
Consolidated formations	**Crystalline and other hard rocks**	0.002 to 0.04

6.2.3 Transmissivity

Transmissivity is a measure that describes the capacity of an aquifer to transmit water. In this context, the variations observed in transmissivity across different geological formations highlight the differing abilities of these formations to transmit water. The Delhi Quartzite, for instance, demonstrates a transmissivity range from 5 to 135 m2/day, indicating its varied permeability.

Older Alluvium, with transmissivity values spanning 130 to 400 m2/day, shows a relatively higher capacity to transmit water compared to Delhi Quartzite. Conversely, the Younger Alluvium exhibits even greater transmissivity estimated between 1300 and 2000 m2/day indicating its significantly higher permeability.

These variations are particularly pronounced in certain regions, like the Yamuna floodplain and parts of the North West district, where notably higher transmissivity values are observed. In contrast, the rest of the state displays lower transmissivity values indicating differing groundwater movement and storage capacities across the region geological formations.

6.3 Water level behaviour

The Arc GIS 10.3 software was utilized to analyze the groundwater level data facilitating the creation of groundwater level maps. These maps visually depict the variations in water levels between the pre and post-monsoon periods, covering observation wells over the span of 2005 to 2015. Comparative plots and the precise locations of wells were integrated to showcase the seasonal variations over five years (Fig. 6.3). In 2005 (Fig. 6.5 a & b), the depth to groundwater level ranged between 1.33 meters to 26.04 meters across the wells. This range notably expanded to 28.79 meters in 2010 (Fig. 6.6 a & b) and further increased to 32.19 meters in 2015 (Fig. 6.8 a & b), portraying a substantial rise in groundwater depth over the years.

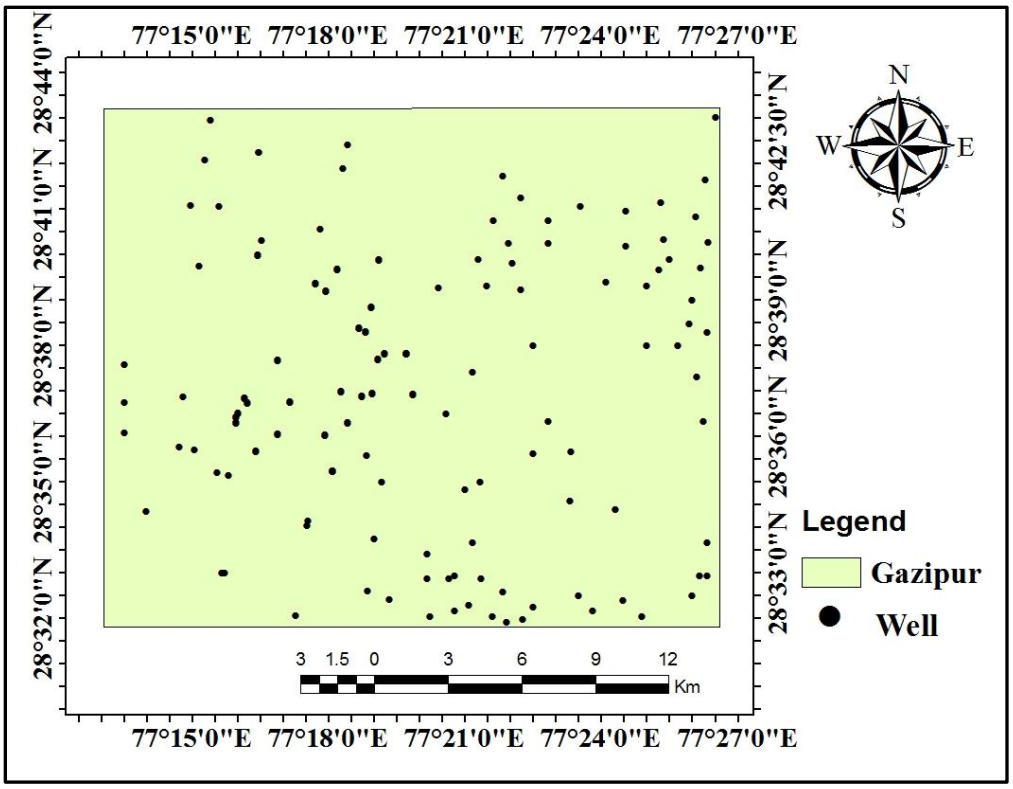

Figure 6.3 Location of well in the study area

6.3.1 Depth to water level during Pre-monsoon (May, 2005)

The groundwater depth in Ghazipur Delhi, recorded in May 2005, spans from 1.33 to 25.64 meters below ground level (mbgl). An analysis of 105 observation wells district-wise reveals a distinct pattern the eastern part exhibits declining groundwater levels while the western section shows relatively shallower water tables (Fig 6.4). In the eastern zone, approximately 8% of wells indicate GWL below 1.33 to 4.5 mbgl, with around 42% registering levels between 5 to 10 mbgl and 50% of the wells exhibit groundwater levels ranging from 10 to 25.64 mbgl (Fig 6.5a). The pre-monsoon 2005 data across different locations highlights significant variations in groundwater levels. Commencing with CIPL at 22 mbgl, followed by a marginal increase at C.G.O. Complex (22.4 mbgl), Govt. Nursary in Kavinagar recorded 23 mbgl, and further escalated at Vijay Nagar to 24.3 mbgl. The highest groundwater level observed was at Chaudhary Turning peaking at 25.64 mbgl, displaying a progressive deepening trend during this period in these specific locations.

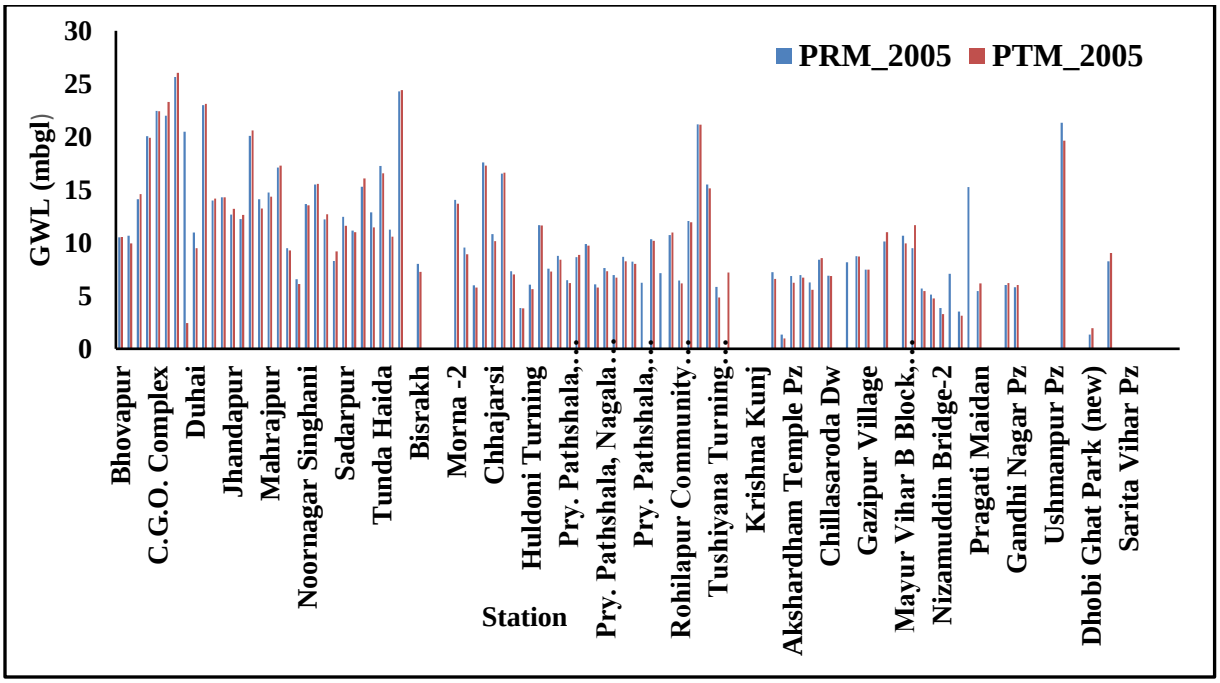

Figure 6.4 Comparison of pre and post monsoon groundwater levels at different station in 2005

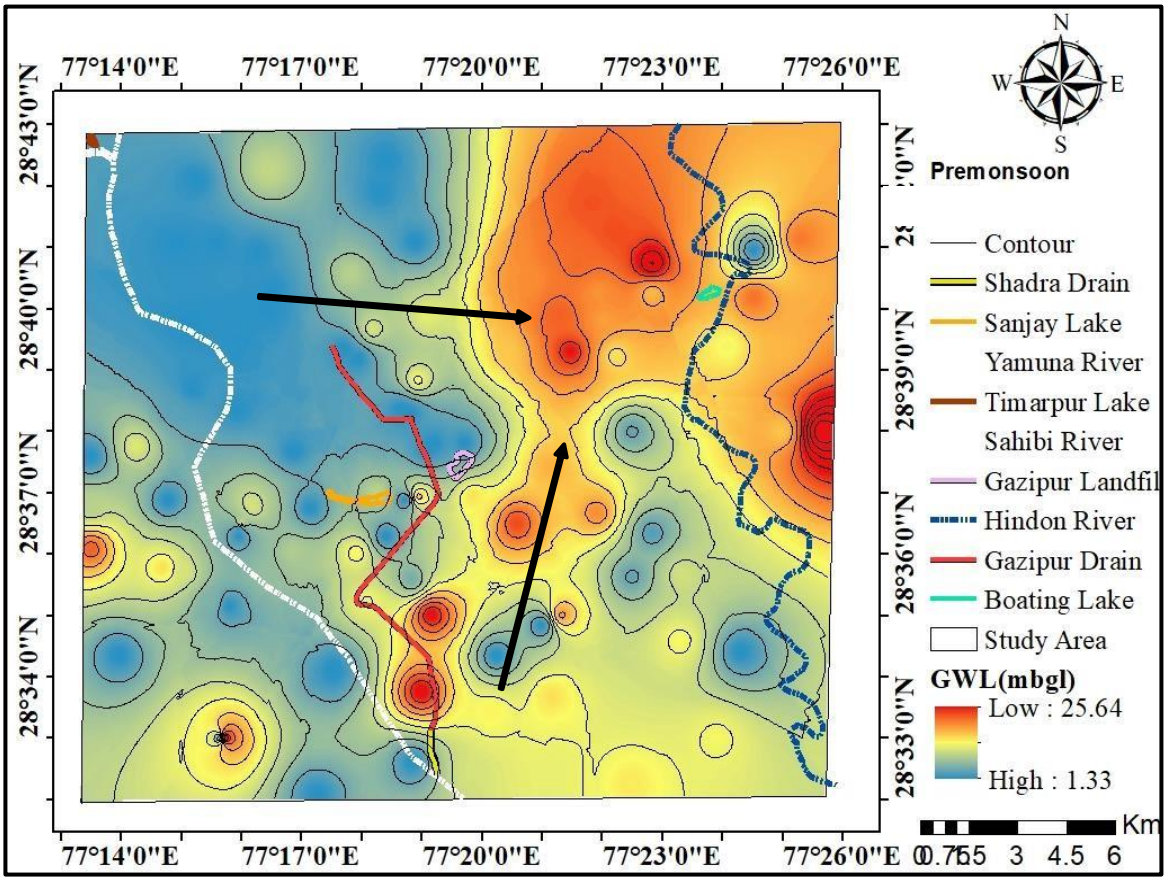

Figure 6.5 a) Groundwater level variations in meters below ground level (mbgl) during the pre-monsoon 2005

6.3.2 Depth to water level during Post-monsoon (November, 2005)

The recorded depth to the water level in November 2015 varied between 1.63 to 26.04 mbgl. Specifically, Chaudhary Turning exhibited an increase in water level, reaching 26.04 mbgl, rising by 0.41 meters compared to the pre-monsoon period (Fig 6.4a). Similarly, CIPL showed an increment, reaching 23.28 mbgl, rising by 1.28 mbgl compared to the previous reading.

Among the monitored wells, 72% displayed water levels between 1.33 to 10.45 mbgl, while the rest recorded levels above this range. The closely spaced contours on the eastern ridge indicate a steep slope and higher groundwater flow, contrasting with widely spaced contours on the western side, indicating a gentler slope. The directional arrow within the study area illustrates the movement of groundwater in the Northeast and Southeast directions (Fig 6.5 b).

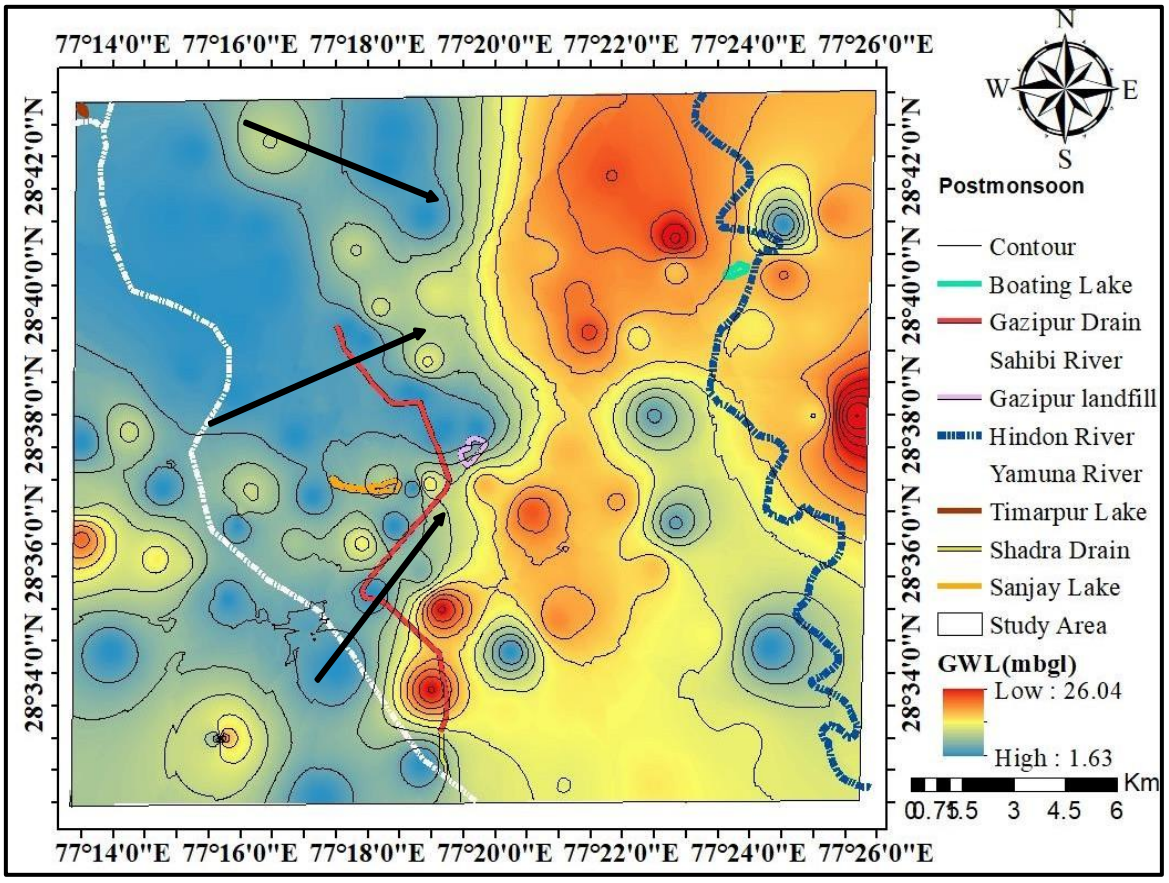

Figure 6.5 b) Groundwater level variations in meters below ground level (mbgl) during the post-monsoon 2005

6.3.3 Depth to water level during Pre-monsoon (May, 2010)

The groundwater levels varied significantly across different sites. At Chaudhary Turning, the water table was notably deep at 28.79 mbgl, indicating considerable depth in that specific region (Fig 6.6). Conversely, areas such as Bumhaita Shahpur, Civil Line Police, Makanpur, and Zila Ganna Adhikari recorded the highest groundwater levels at 1.09 mbgl. Mayur Vihar B Block, Ph-II, and Mayur Vihar Flood Plain demonstrated relatively similar groundwater levels at 5.4 mbgl and 5.5 mbgl, respectively, suggesting similar water table depths in these adjacent areas (Fig 6.7a). Meanwhile, locations like Nagali Rajapur Pz, Nizamuddin Bridge-1 and Nizamuddin Bridge-2 exhibited lower ground water levels, ranging from 3.49 mbgl to 3.68 mbgl, indicating potentially shallower water tables in these specific regions. In contrast, Patpargunj Industrial Area stood out with a significantly higher groundwater level of 7.89 mbgl, indicating a relatively deeper water table compared to the others. Conversely, the northeastern parts showed moderate depths in their groundwater levels.

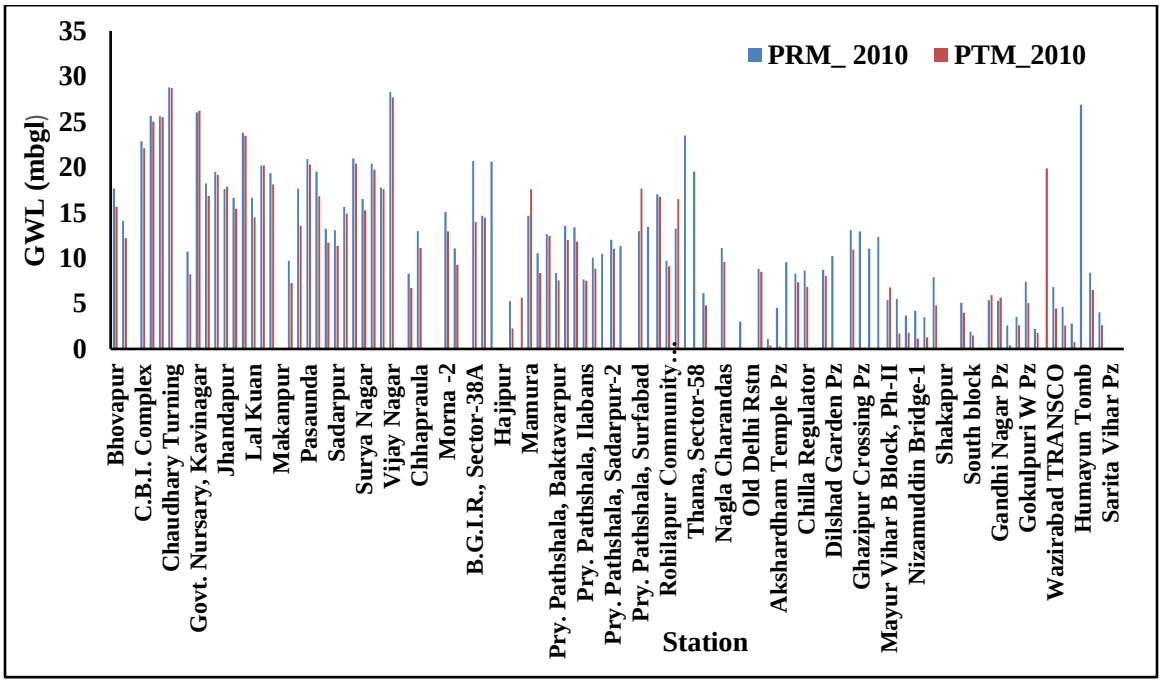

Figure 6.6 comparison of pre and post monsoon groundwater levels at different station in 2010

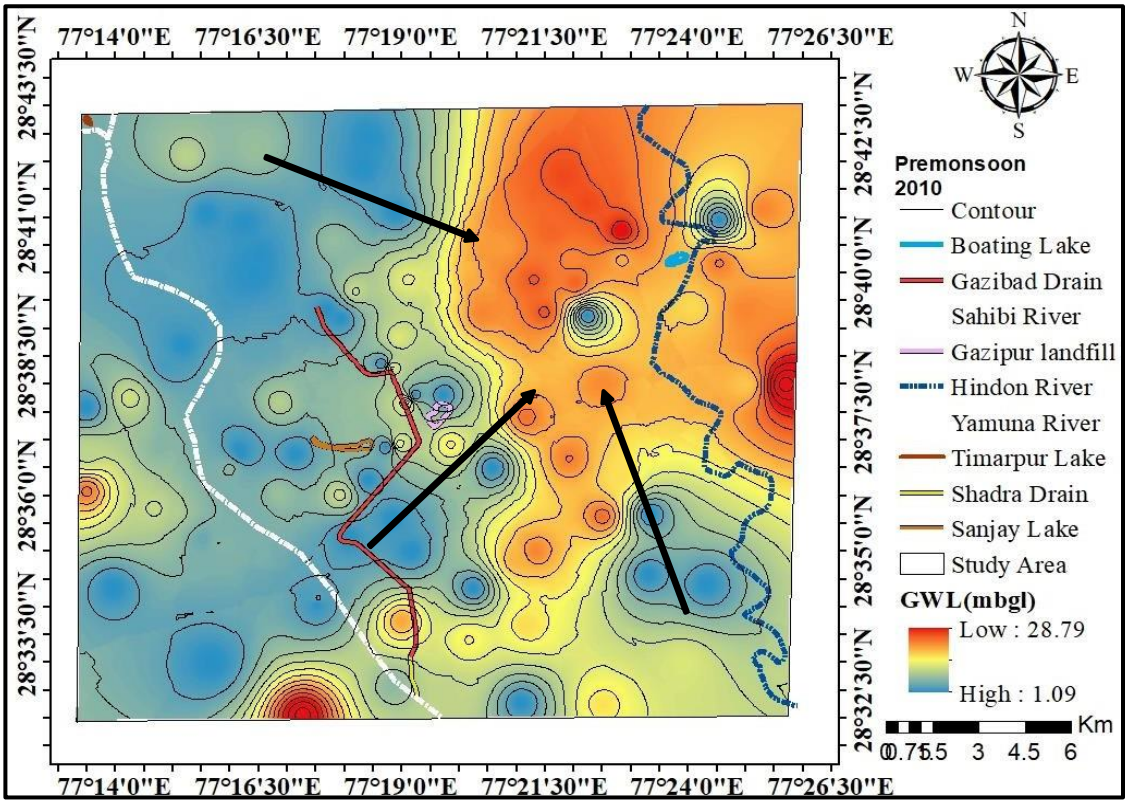

Figure 6.7 a) Groundwater level variations in meters below ground level (mbgl) during the pre-monsoon

6.3.4 Depth to water level during Post-monsoon (November, 2010)

During the post-monsoon analysis, fluctuations in groundwater levels became apparent. Chaudhary Turning maintained a high level of 28.69 mbgl, signaling relative stability compared to its pre-monsoon reading (Fig 6.7 b). In contrast, Govt. Nursary, displayed a slight increase from 26.05 mbgl to 26.23 mbgl, indicating a minor rise in the water table post-monsoon. Notably, Vijay Nagar experienced a decrease from 28.3 mbgl to 27.7 mbgl, highlighting a noticeable decline in groundwater levels after the monsoon season. For instance, Bhovapur displayed signify drop from 17.66 mbgl pre-monsoon to 15.65 mbgl post-monsoon while in Biharipur 14.09 mbgl declining to 12.18 mbgl post-monsoon (Fig 6.6).

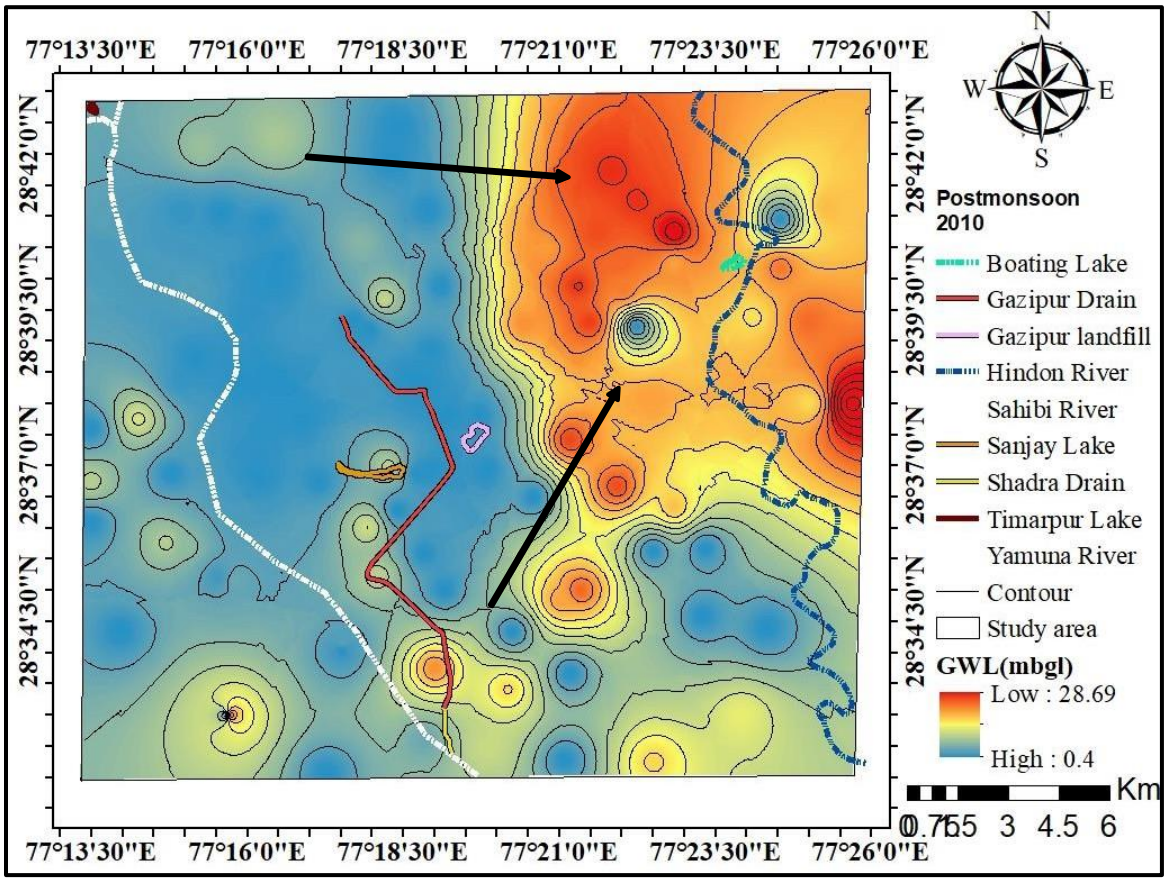

Figure 6.7 b) Groundwater level variations in meters below ground level (mbgl) during the post-monsoon 2010

6.3.5 Depth to water level during Pre-monsoon (May, 2015)

The pre-monsoon groundwater depth in May 2015 varied widely, ranging from 1.23 to 31.39 mbgl (Fig 6.9 a). A comprehensive analysis of observation wells across districts revealed a distinct trend: the northeast portion showed a consistent decline in groundwater levels, while the southeast exhibited a partial decline in the study area (Fig 6.8). Notably, the eastern region covering 58.26% of Ghaziabad and Gautam Buddha Nagar areas displayed the most substantial decline ranging from 7 mbgl to 31.39 mbgl. In specific locations, Vijay Nagar at 31.39 mbgl, Zila Ganna Adhikari at 30.22 mbgl, and Govt. Nursary in Kavinagar at 28.95 mbgl indicated notably deeper water tables, potentially due to increased stress on these resources. Conversely, several spots like Chaudhary Turning, Civil Line Police, Jhandapur, Makanpur, Surya Nagar, and Vaishali displayed shallow water tables. Moderate variations in groundwater levels were evident across various places, including Bhovapur at 23.35 mbgl, Biharipur at 21.63 mbgl, C.B.I. Complex at 24.27 mbgl, and

several others, underscoring the diverse groundwater distribution before the monsoon.

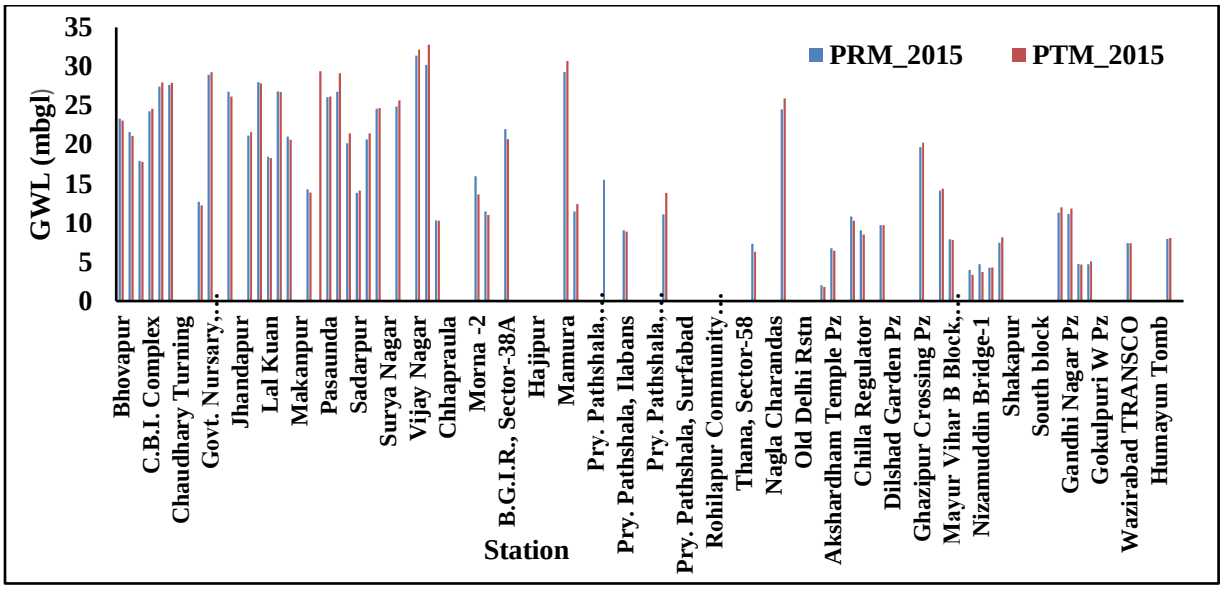

Figure 6.8 Comparison of pre and postmonsoon groundwater levels at different station in 2015

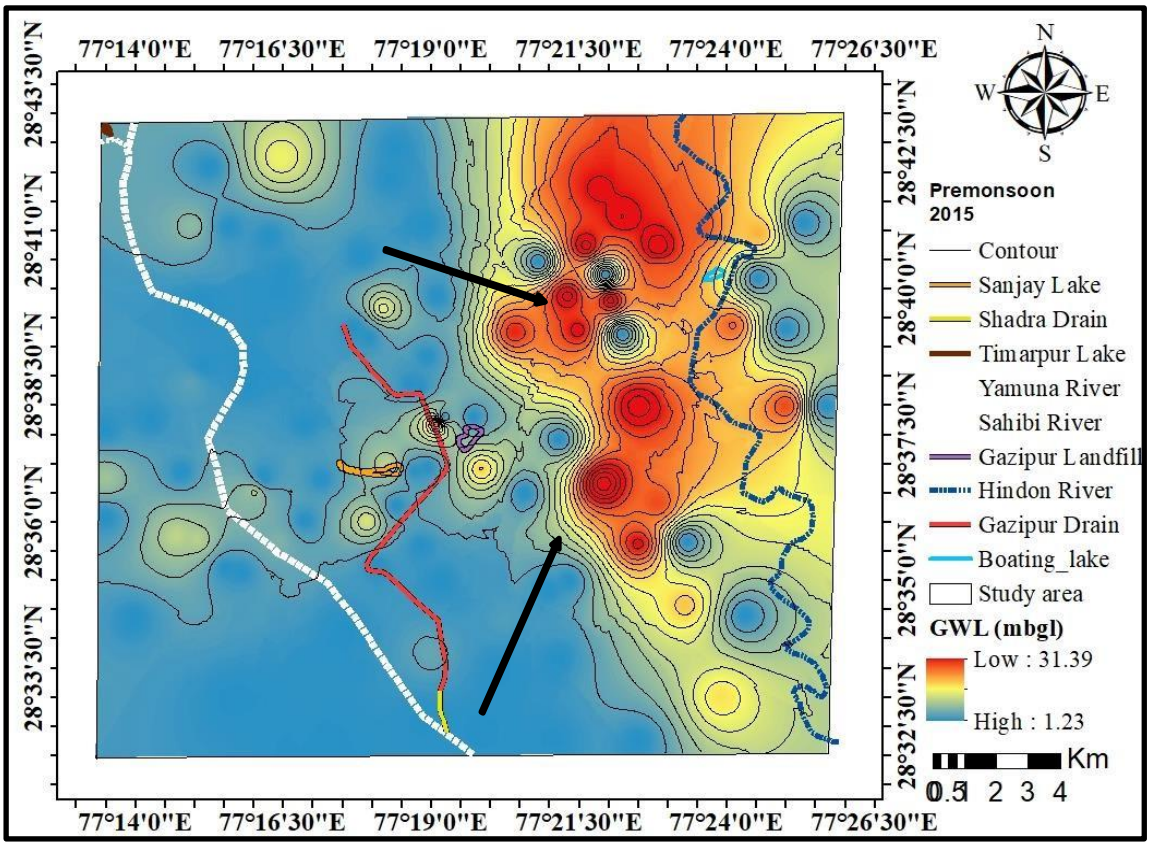

Figure 6.9 a) Groundwater level variations in meters below ground level (mbgl) during the pre-monsoon 2015

6.3.6 Depth to water level during Post-monsoon (November, 2015)

The groundwater level (GWL) data pre-monsoon and post-monsoon reflects interesting trends across various locations. For instance, in areas like Vijay Nagar, the GWL increased from 31.39 mbgl to 32.19 mbgl post-monsoon, indicating a substantial rise and robust recharge (Fig 6.6 b). Similarly, Zila Ganna Adhikari displayed an increase from 31.22 mbgl to 31.8 mbgl, marking significant post-monsoon groundwater recharge. Govt. Nursary, Kavinagar maintained a substantial level of 28.95 mbgl in pre-monsoon and increased to 29.27 mbgl post-monsoon, showcasing a noteworthy rise. Conversely, Bhovapur declined from 23.35 mbgl to 23.07 mbgl post-monsoon, indicating a reduction in groundwater levels. Biharipur also showcased a decrease from 21.63 mbgl to 21.11 mbgl post-monsoon, signaling a slight decline. Locations such as C.G.O. Complex and C.I.P.L. exhibited increases from 27.42 mbgl to 27.96 mbgl and 27.62 mbgl to 27.91 mbgl, respectively, highlighting robust post-monsoon recharge. Meanwhile, areas like Nandgram saw a decrease from 14.27 mbgl to 13.87 mbgl, and Sadarpur displayed a decline from 13.85 mbgl to 14.12 mbgl, indicating mild reductions in post-monsoon GWL. These variations underscore the diverse impacts of the monsoon season on groundwater levels, illustrating patterns of recharge and depletion in the region.

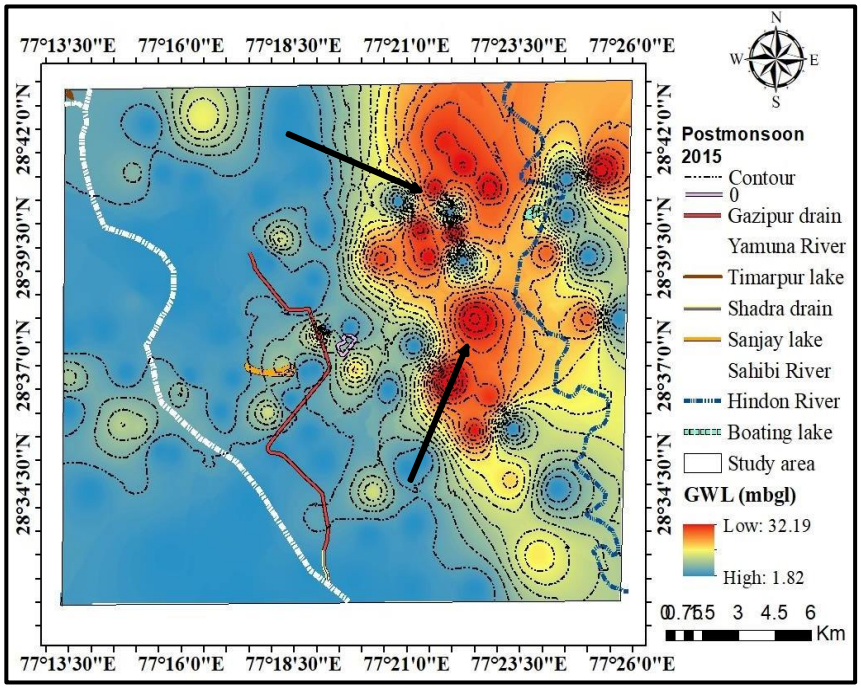

Figure 6.9 b) Groundwater level variations in meters below ground level (mbgl) during the post-monsoon 2015

Chapter 7: Modelling of leachate migration pattern in groundwater in space and time

7.1 Methodology

In this study the flow in an unsaturated medium are detailed. A summary of the modeling of unsaturated fluid movement is provided. The following section provides a comprehensive description of the Hydrus software, including its initial and boundary conditions, potential evapotranspiration, solute transport, and solution process. The final sections describe the conceptualization of the model for this investigation; the sensitivity analysis of several parameters involved; the model parameters employed in this study; and the process of model calibration and validation.

7.1.1 Flow in an unsaturated medium

Municipal solid waste is a complicated mix of mostly connected solid, liquid, and gaseous phases. The location and shape of each phase, as well as the movement of solutes between phases, are controlled by physical, chemical, and biological processes. The unsaturated zone is restricted by the surface of the liner and combines with groundwater at the capillary fringe. Fluids are held in place in an unsaturated medium by capillary and adsorption forces. Unsaturated flow is mostly controlled by how the particles of the medium are arranged in relation to the water and air phases in the pore space of the medium, which is determined by the pore-size distribution and the amount of water in the pores, or the volumetric water content. The gradient in total water potential is the driving force for water to flow in the unsaturated zone. The sum of all probable component potentials, such as osmotic, matric, gravitational, and hydrostatic pressure potentials, may be represented as the total potential of bulk soil water. The matric pressure head is the pressure head equivalent of the combined adsorptive and capillary forces in soils. The water potential in unsaturated soils is negative when compared to the reference potential of free water. As the soil moisture content falls, the matric potential decreases or becomes more negative. The relationship between the amount of water held by the soil and the controlling soil matric, or suction forces, is determined by the soil water retention function. Typically, these suction forces are denoted by the soil water matric head (strictly negative) or soil suction (strictly positive). The soil water retention curve is fairly soil specific and very nonlinear because the matric forces are regulated by the pore-size distribution, specific surface area, and type of physico-chemical interactions at the solid–liquid interfaces. The soil water retention curve displays hysteresis, meaning that the value differs during wetness and drying. Various papers provide laboratory and field procedures for measuring the soil water retention curve, as well as functional models that match the obtained

soil water retention data, such as the van Genuchten and Brooks and Corey models. Also, the size distribution of the particles could tell us something about the shape of the soil water retention curve. The relationship between the unsaturated hydraulic conductivity of the soil, K, and its volumetric water content is the second basic soil hydraulic characteristic required to characterize unsaturated soil water flow. K is a function of the water and soil matrix characteristics, governs water infiltration and drainage rates, and is greatly influenced by water content and maybe hysteresis. The hydraulic conductivity (K) characterizes the bulk soil's capacity to transfer water and is measured in terms of the amount of water flowing per unit area of bulk soil per unit time. Functional models for unsaturated hydraulic conductivity are based on pore-size distribution, pore shape, and connectivity, and analytical formulations for unsaturated hydraulic conductivity need to include soil water retention functions(Brooks & Corey, 1964a; Hopmans, 2011; Hopmans & Dane, 2002; Mualem, 1976a; van Genuchten, 1980a).

7.1.2 Modelling of unsaturated solute movement

In several investigations, Richard's equation has been used to numerically simulate unsaturated water flow. It is an equation for the dynamic fluid flow that combines the Darcy expression with a mass balance formulation. The subsurface area of interest is discretized into finite-size elements using different solution techniques to solve for temporal variability in matric potential, volumetric water content, or water flow, for each element at each time t. The Richards equation is often solved numerically using a finite element, Picard time-iterative approach in multidimensional soil water flow models. Since the water content and unsaturated hydraulic conductivity of soil are highly nonlinear functions of the soil water matric head, the partial differential equation proposed by Richards is particularly difficult to solve numerically. This equation cannot be solved unless the unsaturated hydraulic conductivity and soil moisture retention relationships are known in advance. It will require the slope of the soil water retention curve in particular.

Many physical, chemical, and biological soil factors influence dissolved solutes as they travel through layers of media. Additional factors that affect the destiny of subsurface compounds include solid-phase sorption and biological changes, as well as diffusion and dispersion. Diffusion and dispersion of the delivered chemical are dependent on the distribution of pore size and water content. Mechanical or hydrodynamic dispersion results from the mixing of fluids inside and between pores due to differences in pore fluid velocity. Increasing dispersivity values lead the chemical to disperse farther, hence reducing its peak concentration. Because

sorbed chemicals travel through the vadose zone more slowly than non-interacting chemicals, mineral type, specific surface area of the solid phase, and organic matter percentage all have a role in sorption. Radioactive decay, as well as biogeochemical processes such as cation exchange or mineral precipitation and dissolution, as well as reactions like complexation and oxygen–reduction chemistry, all have an effect on contaminant concentration. The convection–dispersion equation is often used to describe the solute transport equation. This equation is used to model and predict how the concentration of solutes in the soil changes over time within the simulation domain(Ferré & Warrick, 2005; Hopmans, 2011).

7.1.3 Hydrus Software

Hydrus is software for modeling the transport of water, heat, and solutes in one-dimensional, variable-saturated systems. To solve the Richard's equation for water flow with different saturation levels and advection-dispersion type equations for heat and solute transport, the HYDRUS software uses numerical methods. Water absorption by plant roots is taken into consideration in the flow equation by including a sink element. Additionally, dual-porosity type flow, in which some water is mobile and some is not, or dual-permeability type flow, in which the matrix and macropores are both mobile areas, may be taken into account in the flow equation. Thermal conduction and water convection are considered using the heat transfer equation. Transport of water, vapor, and energy may also be discussed. Advective-dispersive transport in the liquid phase and diffusion in the gaseous phase are both taken into account by the solute transport equations. Nonlinear nonequilibrium processes between the solid and liquid phases, linear equilibrium reactions between the liquid and gaseous phases, zero-order production, and two first-order degradation reactions: one that is independent of other solutes, and one that offers coupling between solutes participating in sequential first-order decay reactions, are all included in the transport equations. Moreover, physical nonequilibrium solute movement may be accounted for by adopting a two-region, dual-porosity formulation that divides the liquid phase into mobile and immobile parts. Additionally, kinetic attachment/detachment of solute from the solid phase may be included in the transport equations to model viral, colloidal, or bacterial transportation.

There are additional carbon dioxide and main ion solute transport simulation modules included in the HYDRUS software suite. Transport processes for CO2 include diffusion and convection in the liquid and gas phases, respectively. The model for CO2 generation is given. Alkalinity and CO2 are two of the most important factors in the chemical system. The model takes into consideration chemical interactions such as complexation, cation exchange, and precipitation-

dissolution equilibrium between these components. Both equilibrium and multicomponent kinetic expressions incorporate both forward and reverse processes for modeling the precipitation-dissolution of calcite and the dissolution of dolomite, respectively. The model includes both the modified Debye-Hückel and Pitzer expressions as ways to figure out the activity of a single ion. This is because the ionic strength of soil solutions can change a lot over time and space and often reaches high values.

Water and solute flow in porous media, whether unsaturated, slightly saturated, or completely saturated, may be studied using this application. Non-uniform soils may be encountered in the flow area. Vertical, horizontal, or generally angled flow and transport are all possible. Modeling water flow is capable of handling boundary conditions that are regulated by meteorological variables as well as free drainage circumstances. Galerkin-type linear finite element techniques are used to solve the governing flow and transport equations numerically. With HYDRUS's Marquardt-Levenberg type parameter optimization technique for transient or steady-state flow and transport data, the hydraulic transport and response parameters of the soil can be estimated backwards(by J. Šimůnek et al., 2013; J. Šimůnek et al., 2012b).

By assuming that the entrapped air has no role in fluid transfer and neglecting the fluid flow due to thermal gradients the modified form of Richards equation is:

$$\frac{\partial \theta}{\partial t} = \frac{\partial}{\partial x}\left[K\left(\frac{\partial h}{\partial x} + \cos\alpha\right)\right] - S \qquad (1)$$

Where h is the water pressure head[L], θ is the volumetric water content[L^3L^{-3}], t is time[T], x is spatial coordinate[L] (positive upward), S is the sink term[$L^3L^{-3}T^1$], $\propto$ is the angle between the flow direction and the vertical axis ($\propto = 0^0$ for vertical flow and 90^0 for horizontal flow) and K = unsaturated hydraulic conductivity function [LT^{-1}].

The unsaturated hydraulic conductivity function(K) is given as:

$$K(h, x) = K_s(x)K_r(h, x) \qquad (2)$$

Where K_r is the relative hydraulic conductivity [-] and K_s = saturated hydraulic conductivity [LT^{-1}].

The unsaturated media hydraulic properties $\theta(h)$ and $K(h)$ in equation (1) are non linear functions of pressure head. In HYDRUS we have 5 analytical models to define the hydraulic properties of medium:

- Brooks and Corey(Brooks & Corey, 1964b).

- Van Genuchten(van Genuchten, 1980b).
- Vogel and Cislerova(Vogel & Cislerova, 1988).
- Kosugi(Kosugi, 1996).
- Durner(*Durner*, 1994).

For this study we are using the Van Genuchten soil hydraulic function. Van Genuchten incorporated the statistical pore size distribution model of Mualem(Mualem, 1976b) to get expression for the unsaturated hydraulic conductivity function in terms of soil water retention parameters. The equations given by Van Genuchten are:

$$\boldsymbol{\theta(h)} = \begin{cases} \boldsymbol{\theta_r + \frac{\theta_s - \theta_r}{[1+|\alpha h|^n]^m}} & \boldsymbol{h < 0} \\ \boldsymbol{\theta_s} & \boldsymbol{h \geq 0} \end{cases} \qquad \textbf{(3)}$$

$$\boldsymbol{K(h) = K_s S_e^l \left[1 - \left(1 - S_e^{1/m}\right)^m\right]^2} \qquad \textbf{(4)}$$

here,

$$\boldsymbol{m = 1 - \frac{1}{n} \;\; ; \;\; n > 1}$$

The independent parameters in above equations are: θ_r is the residual water content, θ_s is the saturated water content, α is the inverse of air entry value, n is the pore size distribution index, K_s is the saturated hydraulic conductivity and l is the pore connectivity parameter (estimated to about 0.5 as an average for many soils).

7.1.3.1 Initial Conditions:

The initial distribution of pressure head and water content is required for solving equation (1):

$$\boldsymbol{h(x,t) = h_i(x)} \qquad \boldsymbol{t = t_0}$$

$$\boldsymbol{\theta(x,t) = \theta_i(x)} \qquad \boldsymbol{t = t_0}$$

Where h_i[L] is the prescribed function of x and t_0 is the simulation start time.

7.1.3.2 Boundary Conditions:

Hydrus allows us to choose from a wide range of boundary conditions which are broadly classified as system dependent and independent boundary conditions. They deal with recommended head and flux boundaries, boundaries dictated by atmospheric conditions and free drainage or seepage face boundary conditions.

7.1.3.3 Potential Evapotranspiration:

HYDRUS-1D allows us to calculate the potential evapotranspiration using 2 methods:

- Penman Monteith combination equation(Smith et al., 1998).
- Hargreaves equation(George Hargreaves, 1994).

In this study we are using Hargreaves formula for calculating the potential evapotranspiration, which is described as:

$$\boldsymbol{ET_P = 0.0023R_a(T_m + 17.8)\sqrt{TR}} \qquad \textbf{(5)}$$

Where R_a is the extraterrestrial radiation [having same units as ET_P e.g., mm d^{-1} or J m^{-2} s^{-1}], T_m is the daily mean air temperature [^{0}C] and T_m is the daily mean air temperature [^{0}C] and TR is the temperature range between the mean daily maximum and minimum air temperatures[^{0}C].

The extraterrestrial radiation, R_a is calculated as:

$$\boldsymbol{R_a = \frac{G_{sc}}{\pi} d_r(\omega_s \sin\varphi \sin\delta + \cos\varphi \cos\delta \sin\omega_s)} \qquad \textbf{(6)}$$

Where G_{sc} is solar constant [$Jm^{-2}s^{-1}$], φ is the site latitude[rad], ω_s is sunset hour angle[rad], d_r is the relative distance between earth and sun [-] and δ is solar declination[rad].

The last 3 values are calculated as:

$$\boldsymbol{\omega_s = \arccos(-\tan\varphi \tan\delta)} \qquad \textbf{(7)}$$

$$\boldsymbol{d_r = 1 + 0.033\cos\left(\frac{2\pi}{365}J\right)} \qquad \textbf{(8)}$$

$$\boldsymbol{\delta = 0.409\sin\left(\frac{2\pi}{365}J - 1.39\right)} \qquad \textbf{(9)}$$

Where J are the number of days in the year [-].

7.1.3.4 Solute Transport:

HYDRUS 1-D uses Galerkin finite element method to solve the solute transport equation. In liquid phase the solute movement is assumed to be due to convection and dispersion and in gaseous phase due to diffusion. Appropriate boundary conditions need to be defined for the solution. The boundary conditions which can be applied to upper and lower boundaries are Dirichlet type and Cauchy type. They are described as:

- Dirichlet type: It describes the concentration at the boundary:

$$c(x,t) = c_o(x,t) \quad \text{at } x = 0 \text{ or } x = L$$

- Cauchy type: It describes the concentration flux at the boundary:

$$\theta D \frac{\partial C}{\partial x} = 0 \quad \text{at } x = 0 \text{ or } x = L$$

7.1.3.5 Solution process:

In HYDRUS the solution process at each time step proceeds with an iterative process which gives the solution of Richards' equation (1). After achieving the solution, in next step Darcy's law is applied to find out the fluid flux at each node (as defined in the nodal discretization) from the corresponding values of pressure heads at each node which ultimately gives us the solution of the transport equation. The nodal values of water content and fluid flux obtained at each time step is used as an input of transport equation for the subsequent time step which leads to the formation of a system of linear algebraic equations. The iterative procedure for solute transport is similar to that of solute flow and continues in the same manner. This iterative process continues until the absolute variation in fluid flux and concentration at each node comes out to be less than the predefined values of relative and absolute fluid flow and concentration tolerances which in turn leads to a satisfactory degree of convergence(Rassam et al., 2018; by J. Šimůnek et al., 2013).

7.2 Model conceptualization

Determining the content of a simulation model is one of the most challenging aspects of simulation modeling. The role of the modeler is to comprehend the actual system that is the focus of the simulation research and to create an acceptable simulation model from this understanding. In other words, model conceptualization is the abstraction of a simulation model from the portion of the actual world that it represents.

In this study, the modeling technique is largely utilized to examine the spatial and temporal fluctuations of leachate constituents as they migrate from the top to the bottom of a landfill. Hydrus-1D, a Windows-based simulation program, is utilized for this purpose. In Hydrus, the simulation is conducted in two stages: the first is the preprocessing stage, and the second is the postprocessing stage. As seen in the Figure 7.1 below, the primary window of the software's graphical user interface contains two sections: the preprocessing portion on the left and the post-processing area on the right. The preprocessing component is separated into numerous subsections, including main processes, geometry and time information, print information, etc. In the preprocessing stage, we must define the model inputs and conceive the model so that

executing it after entering the needed input data yields the intended simulation results. The results are displayed in the post-processing phase. The post-processing component is further divided into numerous sections based on application, including observation points, profile information, run time information, etc. For our research, we began with the preprocessing phase and conceptualized the model by providing it with inputs. In the main processes section, we opted to simulate water flow and solute transport using the option for standard solute transport. In the geometry information, the length unit was set to centimeters, the number of soil materials was set to four, the depth of the soil profile was set to 3261.40 cm, the decline from the vertical axis was set to one because we are only simulating a one-dimensional vertical flow, and the number of layers for mass balances was set to one. In the time information, we ascertained the time units to be days, the initial simulation time to be 0 days and the final simulation time to be 509 days, with the initial simulation time corresponding to the day of the first sampling on September 21, 2020, and the final sampling day falling on February 11, 2022. The initial time step of sampling is 0.001 days, the minimum time step is 10-5 days, and the maximum time step is 5 days. In time-variable boundary conditions, the number of precipitation records and meteorological records are both maintained at 509. For estimating the potential evapotranspiration, the Hargreaves formula was selected. In print information, the number of print times was set to 5, and site sampling events were also included in the same print times. All other values were left at their default settings. In the iteration criteria, the maximum number of iterations was set to 100, while the remaining entries were left as default. The soil hydraulic model selected was a van Genuchten-Mualem model with a single porosity and no hysteresis. The water flow parameters were developed from prior literature by integrating the material density and initial water content values collected from East Delhi Municipal Corporation bore log reports and interpolation techniques. The upper water flow boundary condition was determined to be an atmospheric boundary condition with surface runoff, whereas the lower water flow boundary condition was determined to be free drainage. The initial conditions were evaluated based on their water content. For solute transport, the time weighing scheme was set to Crank-Nicholson, the space weighing scheme was set to Galerkin finite elements, mass units were set to milligrams, the solute transport model was set to equilibrium model, the Millington and Quirk approach was used for tortuosity factor, the pulse duration was set to 509 days, and the rest of the options were left at their default values. The solute transport boundary condition was maintained as the concentration boundary condition for the upper boundary, while a concentration gradient of zero was maintained for the lower boundary. The initial condition selected for solute concentration was the liquid phase. In time variable boundary conditions,

precipitation records for 509 days were entered, the top boundary solute concentrations were kept as concentrations of leachate parameters to be modeled as measured in the laboratory for samples collected in the field, and the bottom concentration was kept at zero. The data for the maximum and minimum temperatures were collected and entered into the meteorological conditions field.

In the model's graphical editor, the entire vertical section of the landfill has been subdivided into 100 discrete divisions, with a total of 101 nodes. All nodes are equally spaced along the depth, with the top node at the surface and the bottom node at a depth of 3261.40 cm below the surface. In material distribution, the entire profile is subdivided into four layers that indicate variations in the qualities of municipal solid waste along its depth as shown in Figure 7.2 below.

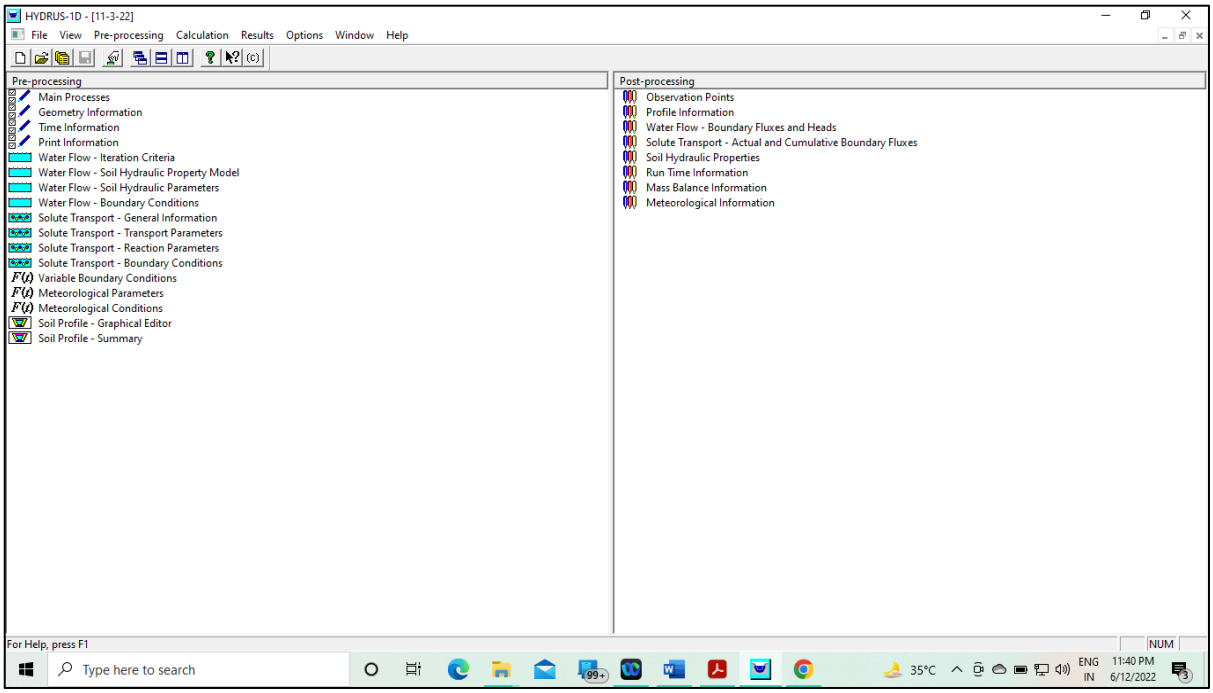

Figure 7.1 : Hydrus-1D software graphical user interface

The default scaling factors are maintained. Initial water content, temperature, and solute concentrations are entered into the graphical editor based on measurements made in the field and laboratory and received from the bore log data report. So that concentration fluctuations can be monitored at the same locations, five observation nodes were added to the profile discretization at the same depths from which leachate samplers were collected on-site. After inputting the essential inputs in the preprocessing area of the Hydrus application, the post-processing section was executed to obtain the appropriate outputs.

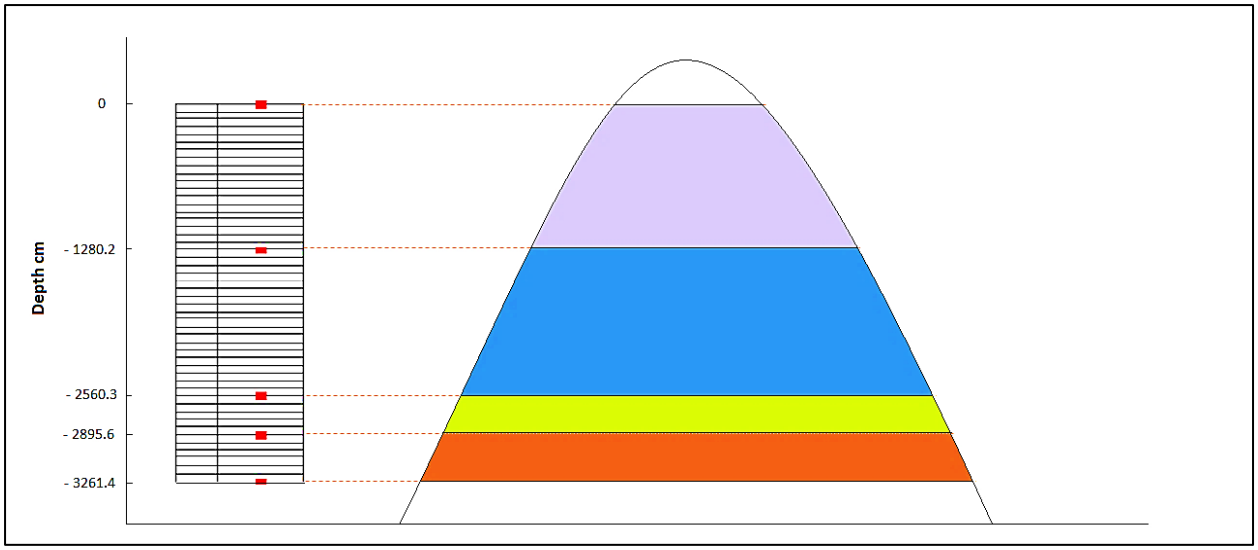

Figure 7.2: Material discretization and nodes defining

7.3 Model parameters

Principal model inputs include precipitation records, atmospheric temperature records, municipal solid waste qualities such as bulk density, moisture content, temperature, and van Genuchten parameters at varying depths. The precipitation records were retrieved from the Indian Meteorological Department website (https://www.imdpune.gov.in/Clim Pred LRF New/Gridded Data Download.html) and the daily maximum and minimum temperature records were retrieved from the Power Data Access Viewer website (https://power.larc.nasa.gov/data-access-viewer/) for 509 days beginning on September 21st, 2020 and ending on February 11th, The intrinsic qualities of municipal solid waste were gathered from the East Delhi Municipal Corporation bore log data report (Spectro Analysis Report). The hydraulic conductivity of municipal solid waste at various depths was estimated using the equation (Reddy et al., 2009).

$$k(cm/s) = 4.64\, exp\left(-7.53\frac{r_d}{\gamma_w}\right)$$

Here, γ_w is the unit weight of water and r_d is the dry unit weight of municipal solid waste material. The van Genuchten parameters for the waste were obtained from previous literatures which are listed in the Table 7.1 below.

Table 7.1: Van Genuchten parameters for municipal soild wastes from various studies

Source	α(1/kPa)	n	θr	θs	γ_d (kN/m^3)	ρ_d(Kg/m^3)
(Korfiatis et al.,1984)	0.9	1.6	0	0.55	6	611.6208
(Benson and Wang,1998)	2.6	2.2	0.11	0.53	6.2	632.00815
(Jang et al.,2002)	0.07	1.7	0.12	0.52	7.8	795.10703
	0.37	1.2	0.05	0.4	9.8	998.98063
	0.37	1.1	0	0.3	11.8	1202.8542
(Soltz and Gourc.,2007)	0.19	2.38	0.27	0.62	5.3	540.26504
	0.05	2.43	0.34	0.45	7.6	774.71967
(Kazimoglu et al.,2006)	1.4	1.6	0.14	0.58	6.5	662.58919
	0.66	1.95	0.17	0.58	6.5	662.58919
(Stoltz et al., 2012)	3	1.64	0.2	0.69	4.5	458.7156
	2.9	1.56	0.2	0.62	5.3	540.26504
	2.3	1.47	0.2	0.59	6.1	621.81448
	0.57	1.33	0.2	0.45	7.6	774.71967
	2	1.33	0.35	0.64	4.5	458.7156
	3	1.19	0.15	0.55	5.2	530.07136
	2	1.12	0.15	0.52	5.7	581.03976
	3.5	1.37	0.15	0.68	3.7	377.16616
(Breitmeyer & Benson, 2014)	3.07	2.32	0.21	0.58	5.5	560.6524
	1.95	2.82	0.25	0.53	6.2	632.00815
	1.11	1.38	0.01	0.41	7.8	795.10703
	2.72	2.01	0.21	0.58	5.5	560.6524
	2.06	1.95	0.25	0.53	6.2	632.00815
	1.18	1.33	0.03	0.41	7.8	795.10703
(Breitmeyer et al., 2020)	3.38	1.85	0.21	0.6	5.2	530.07136
	2.92	1.58	0.22	0.53	6.2	632.00815
	1.18	1.33	0.03	0.41	7.8	795.10703
	22.2	1.1	0	0.68	5.2	530.07136
	5.22	1.11	0	0.62	6.2	632.00815
	2.51	1.07	0	0.52	7.8	795.10703
	49.3	1.1	0	0.6	6.2	632.00815

	0.92	1.95	0.28	0.57	7.8	795.10703
	11.35	1.22	0	0.67	6.2	632.00815
	5.35	1.21	0	0.58	7.8	795.10703
(Wu et al., 2012)	1.18	1.59	0.2	0.69	6.98	711.51886
	0.98	1.51	0.25	0.61	12.65	1289.5005
	0.71	1.49	0.27	0.53	14.32	1459.735
(Stoltz et al., 2007)	1.85	2.42	0.27	0.62	5.2974	540
	0.5	2.29	0.33	0.45	7.5537	770
(Stoltz et al., 2011)	1.75	1.37	0.35	0.64	4.5126	460
(Staub et al., 2010)	3.5	1.37	0.15	0.77	3.7278	380
	0.9	1.34	0.15	0.68	5.6898	580

Note: This table is adapted from (Breitmeyer et al., 2020; Breitmeyer & Benson, 2014; Stoltz et al., 2012; Wu et al., 2012).

The values of municipal solid waste properties were adapted for our study by using concepts averaging and interpolation to obtain the desired results for our modelling.

7.4 Parameter sensitivity analysis

Sensitivity analysis in a numerical model is a technique for determining how variability in one or more input variables influences the output variables. This analysis is beneficial because it enhances or decreases the model's prediction by evaluating qualitatively and quantitatively the model's reaction to input variable changes or by comprehending the phenomena researched through the investigation of interactions between variables. This means that evaluating the resilience, i.e., "sensitivity," of the findings and identifying the values beyond which the results dramatically change may be done using the predicted value of different parameters involved. Priority requirements are identified by doing sensitivity analysis. As a result of this analysis, it is possible to make conclusions regarding the phenomena under investigation with less uncertainty about the assessment's parameters(Pichery, 2014).

Many parameters are involved in this study, including bulk density of municipal waste, saturated hydraulic conductivity of waste (K_s), residual water content of waste (θ_r), saturated water content of waste (θ_s), inverse of air entrance value (α) and pore size distribution index (n). Bulk density of garbage, residual water content of waste, and saturated water content of waste are inherent qualities of waste material that are often measured in a laboratory. As a result, these three parameters cannot be changed for model calibration and validation.

Therefore, no sensitivity analysis is conducted on these three parameters. In contrast, the inverse of air entrance value (α) and the pore size distribution index (n) are empirical parameters that can be adjusted for model calibration. Also, the waste's saturated hydraulic conductivity (K_s) is not tested in the laboratory for our scenario, so we must alter it for model calibration. As a result, parameter sensitivity analysis is performed in our work for the parameters α, n and K_s.

7.5 Model calibration and validation

Calibrating models means adjusting their input parameters, initial conditions, and boundary conditions until the simulated model outputs closely match the observed variables. When calibrating a model, the typical strategy is to choose an objective function that measures the degree of agreement between observed and modeled data and that is either directly or indirectly connected to the parameters under consideration. By minimizing this objective function, the best fit parameters may then be identified and used. Trial and error or automated minimization or parameter estimation strategies may be used to accomplish model calibration. When a model can reproduce data with a level of accuracy that is good enough, it is said to have been calibrated well. The movement of chloride and nitrate is modelled in this study. To calibrate the model for this investigation, known chloride and nitrate values from a prior measurement in 2020 were used, as shown in Figure 7.3 below for the same sample locations. The trial-and-error method was used to adjust the most sensitive parameters learned from the sensitivity analysis, in order to obtain output from the model that is close to the 2021 sampling concentrations at the same observation points, until the calibration run gives a satisfactory level of accuracy.

The model was validated after it has been calibrated and reached the required level of precision. The 2021 sample concentrations for the sampling locations were used as inputs for the model's validation, along with additional inputs for which calibration data was obtained. The model was run to obtain concentration output values at the same observation sites over the simulation period up to the sampling time of 2022. The validation model's output concentrations were then compared to the concentrations measured in the laboratory, and the model's validity was assessed.

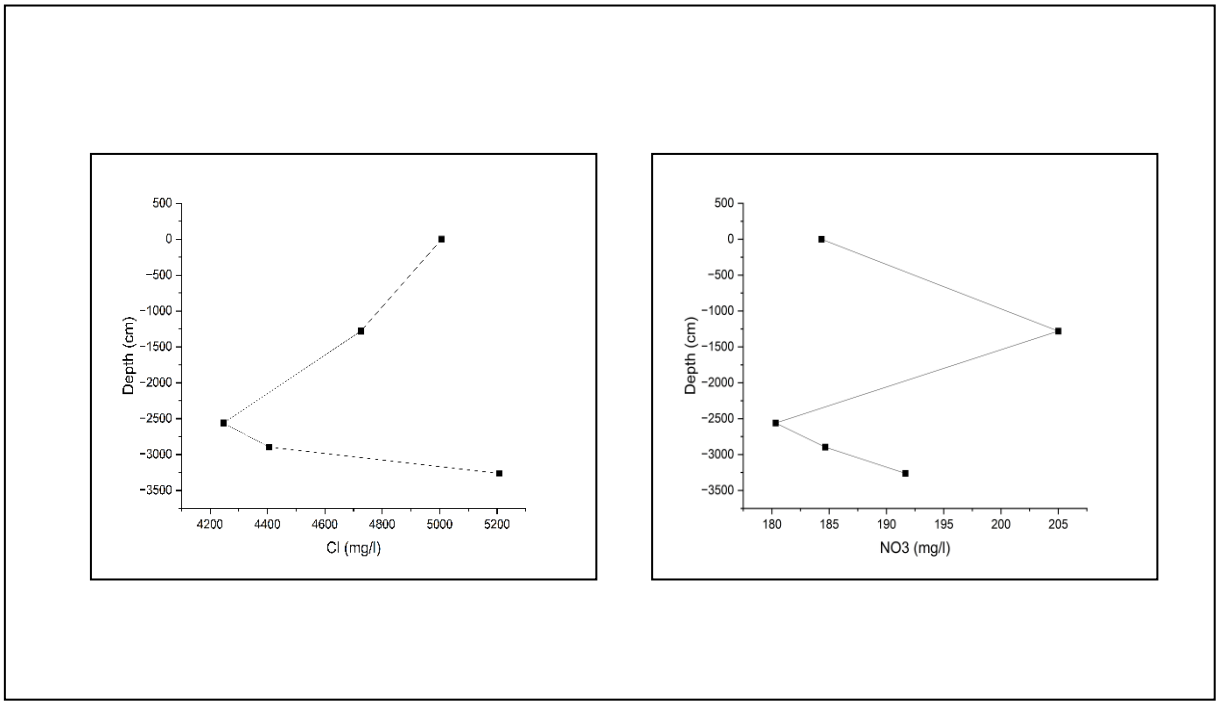

Figure 7.3: Chloride and Nitrate Variation for 2020 sampling

7.2 Result

7.2.1 Parameter sensitivity analysis results

7.2.1.1 Sensitivity analysis of parameter K_s

For checking the sensitivity of model output with respect to saturated hydraulic conductivity (K_s) of municipal solid waste material, only the value of K_s is varied and all other parameters are kept constant. Now the variation of output parameter concentration of solute with depth is observed. It is observed that when K_s is increased from 10 cm/day to 61 cm/day and time is varied from T_0 to T_1 then the peak in concentration vs depth curve which was occurring at a depth between 1000 to 1500 cm having concentration intensity of about 130 mg/cm^3 from the top surface has moved more quickly and now in the same time the plume has advanced more rapidly and the peak is now occurring at a depth of about 1800 cm from the top surface and its intensity also has decreased significantly. Same pattern is observed when K_s is increased further as shown in the Figure 7.4 below. Hence it can be concluded that K_s is a sensitive parameter for this study.

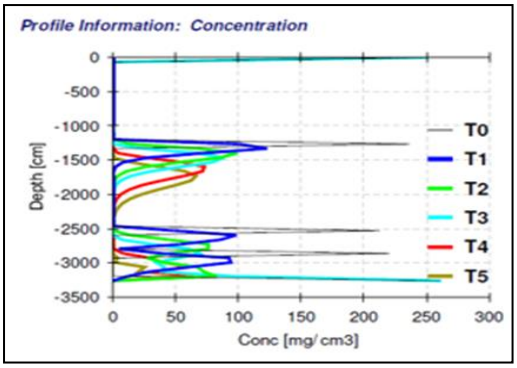

K_s= 10 cm/day

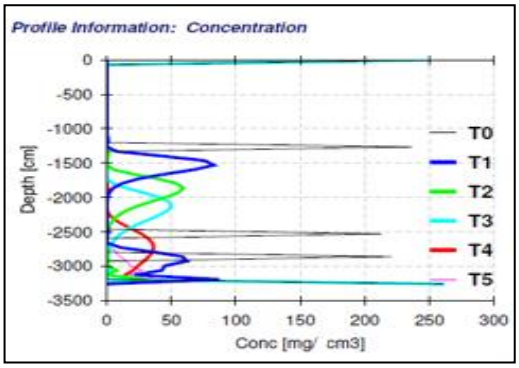

K_s= 30 cm/day

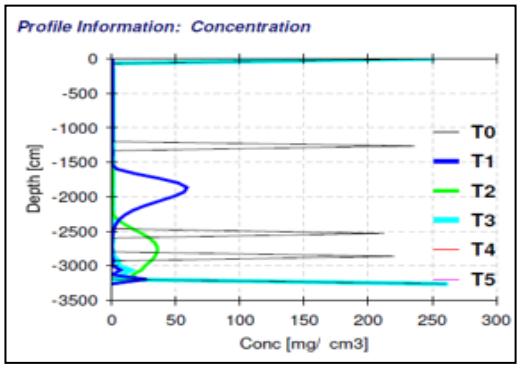

K_s= 61 cm/day

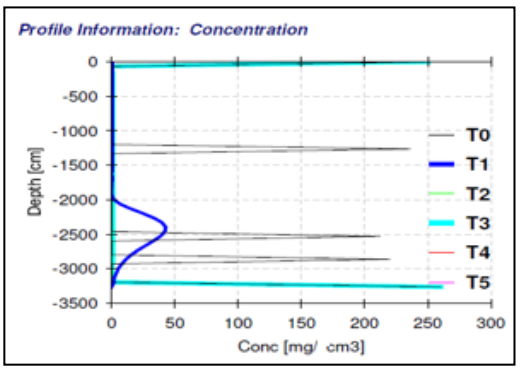

K_s= 100 cm/day

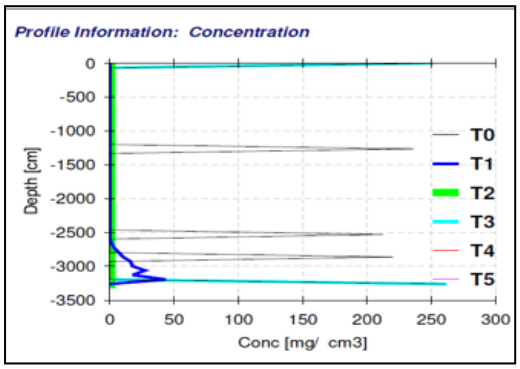

K_s= 150 cm/day

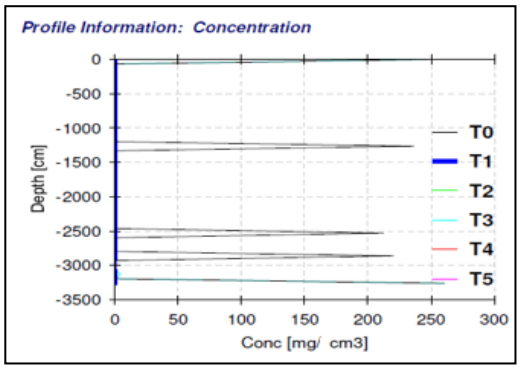

K_s= 200 cm/day

Figure 7.4: Sensitivity analysis of parameter K_s

7.2.1.2 Sensitivity analysis of parameter α

For checking the sensitivity of model output with respect to inverse of air entrance value (α), only the value of α is varied and all other parameters are kept constant. Now the variation of output parameter concentration of solute with depth is observed. It is observed that when α is increased from 0.1 to 0.25 and time is varied from T_0 to T_1 then there is no significant change in the concentration plume movement with depth and it appears more or less same. Same pattern is observed when α is increased further as shown in the Figure 7.5 below. Hence it can be concluded that α is a less sensitive parameter for this study.

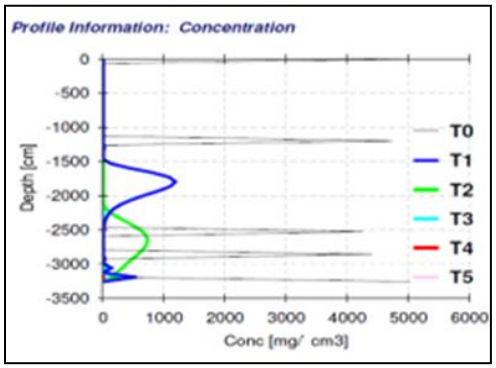

α= 0.10

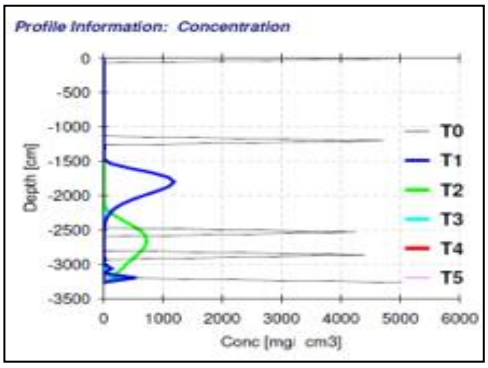

α= 0.15

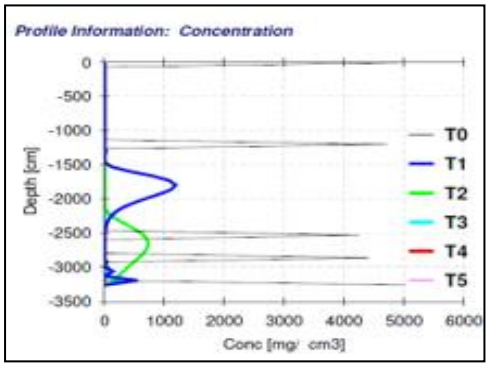

α= 0.20

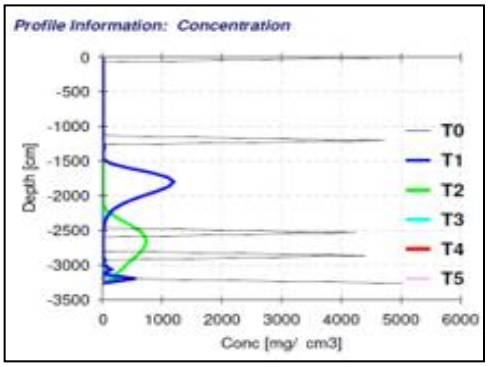

α= 0.25

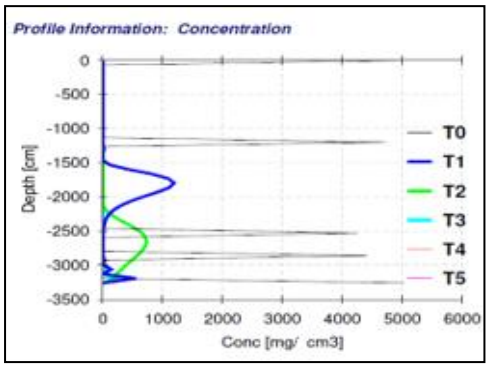

α= 0.30

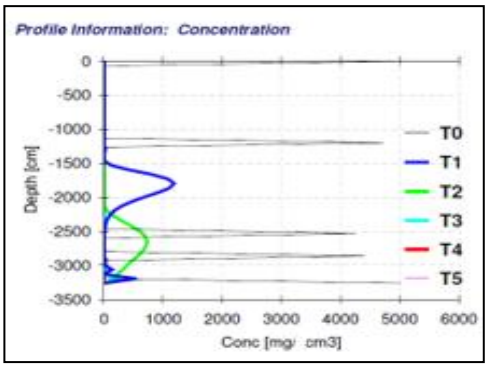

α= 0.40

Figure 7.5: Sensitivity analysis of parameter α

7.2.1.3 Sensitivity analysis of parameter n

For checking the sensitivity of model output with respect to pore size distribution index (n) only the value of n is varied and all other parameters are kept constant. Now the variation of output parameter concentration of solute with depth is observed. It is observed that when value of n is increased from 1.2 to 1.75 and time is varied from T_0 to T_1 then the peak in concentration vs depth curve which was occurring at a depth between 1000 to 1500 cm having concentration intensity of about 3000 mg/cm^3 from the top surface has moved more quickly and now in the same time the plume has advanced more rapidly and the peak is now occurring at a depth of about 2250 cm from the top surface and its intensity also has decreased significantly. Same pattern is observed when n is increased further as shown in the Figure 7.6 below. Hence it can be concluded that n is a sensitive parameter for this study.

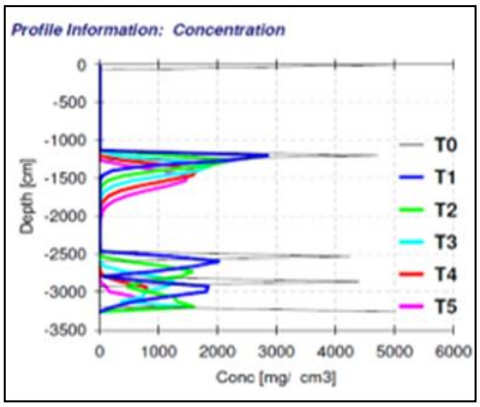

***n*= 1.2**

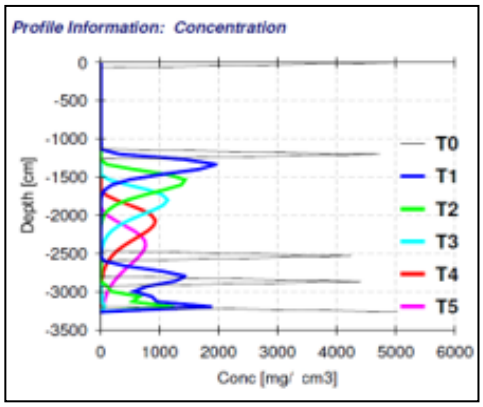

***n*= 1.3**

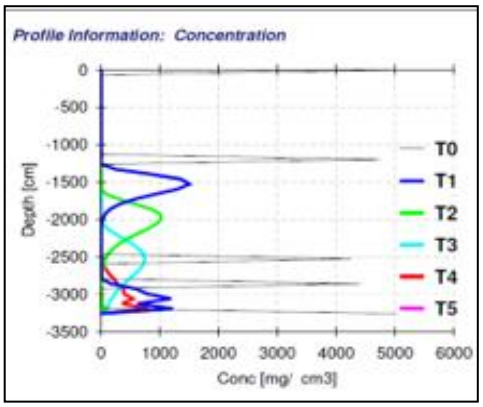

***n*= 1.4**

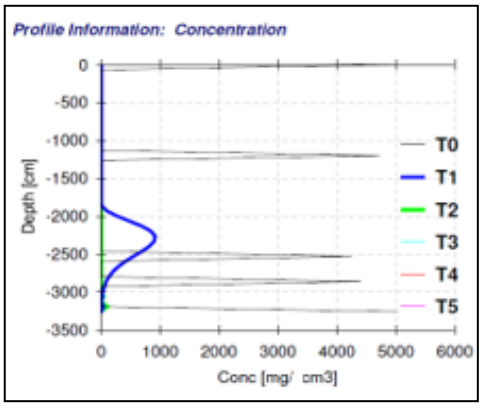

***n*= 1.75**

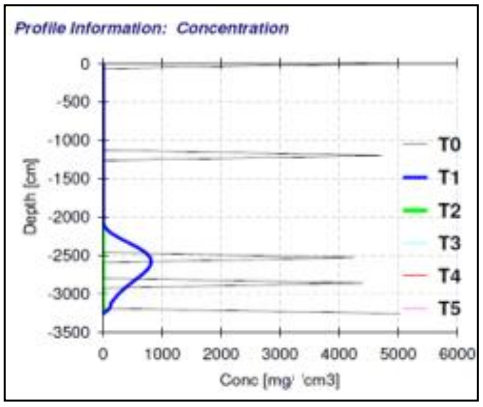

***n*= 1.9**

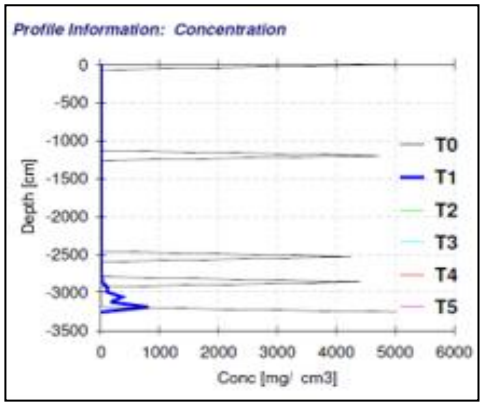

***n*= 2.5**

Figure 7.6: Sensitivity analysis of parameter n

From the sensitivity analysis it is known that saturated hydraulic conductivity (K_s) and pore size distribution index (n) are the most sensitive parameters for our study and we need to vary them for calibrating the model and get the desired results.

7.2.2 Modelling results

7.2.2.1 Calibration results

During model calibration, the results of 2020 chloride and nitrate sampling analyses at observation locations were entered into the model. In addition, the solid waste properties were taken from previous studies related to municipal solid waste landfills around the world and integrated with the Gazipur landfill reports obtained from East Delhi Municipal Corporation. After that, the concepts of interpolation, averaging, and variation of the sensitive parameters were used to derive the input parameters for the Gazipur landfill municipal solid waste required for the model. The final calibration-derived values are displayed in Table 7.2 below.

Table 7.2: Municipal Solid Waste Properties used in this study

Sl. No.	Depth of sample (cm)	Bulk Density (Kg/cum)	α (1/kPa)	n	θr	θs	K (cm/day)
1	0 - 5	0.835	0.653	1.225	0.046	0.395	236.677
2	5-12.5	0.859	0.429	1.167	0.029	0.361	144.458
3	12.5-20	0.876	0.493	1.218	0.064	0.400	123.701
4	20-32.614	0.846	0.37	1.156	0.028	0.356	120.728

Figure 7.3 in the preceding section depicts the chloride and nitrate analysis findings from 2020 that were used as input for the calibration simulation conducted during model calibration. At the same observation stations in 2021, chloride and nitrate concentrations were simulated using the model. Figure 7.7 displays the chloride simulated and actual values for the year 2021.

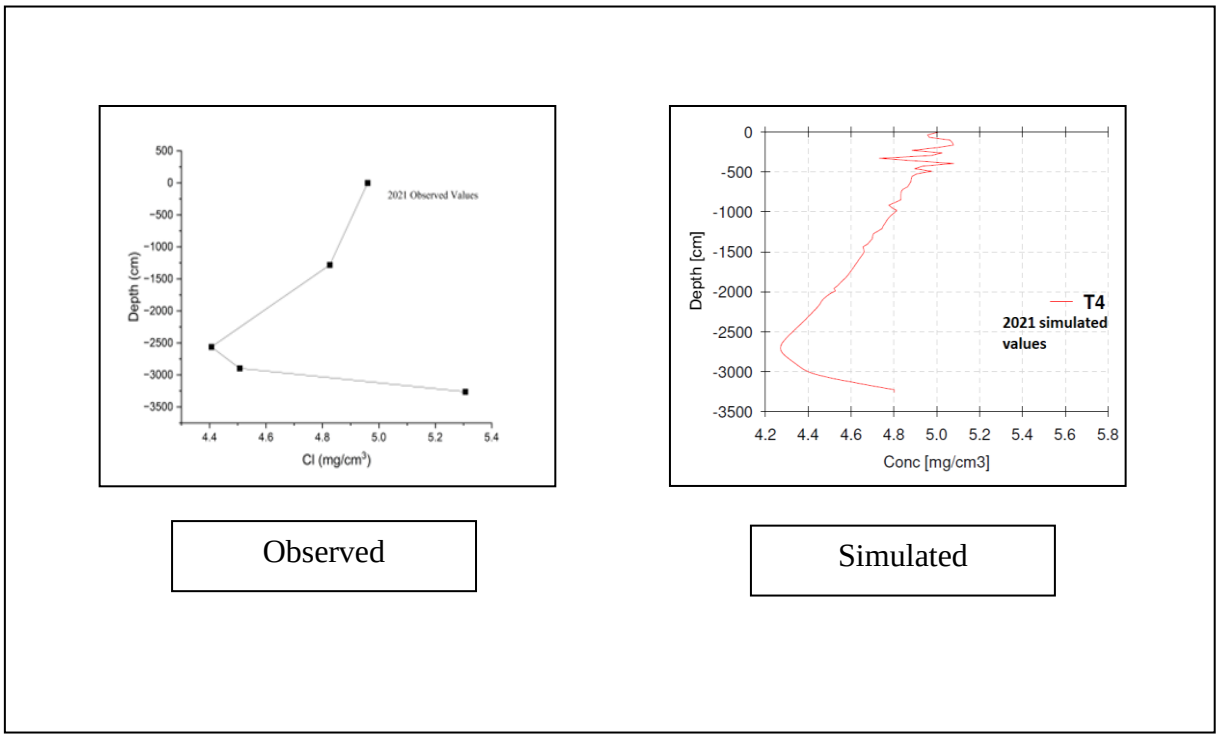

Figure 7.7: Chloride calibration observed and simulated results

As shown in Figure 7.8, the R^2 value for the trendline between simulated and observed Hydrus values for 2021 sampling at the observation stations for chloride calibration was 0.8652.

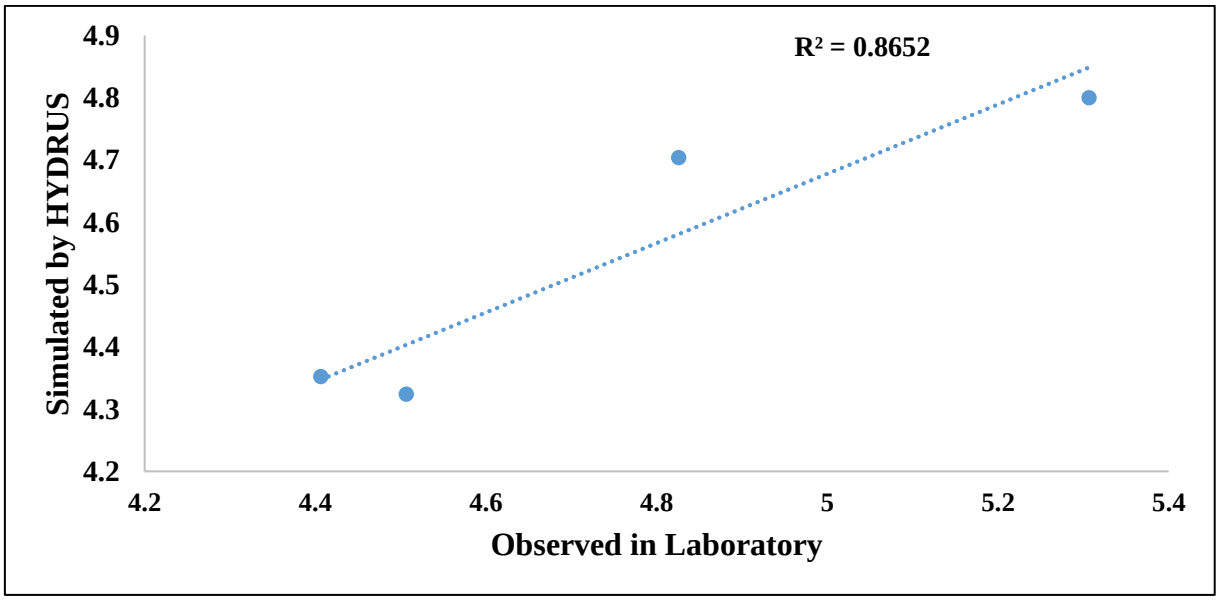

Figure 7.8: Chloride calibration

The simulated and observed nitrate values for 2021 are displayed in Figure 7.9 below.

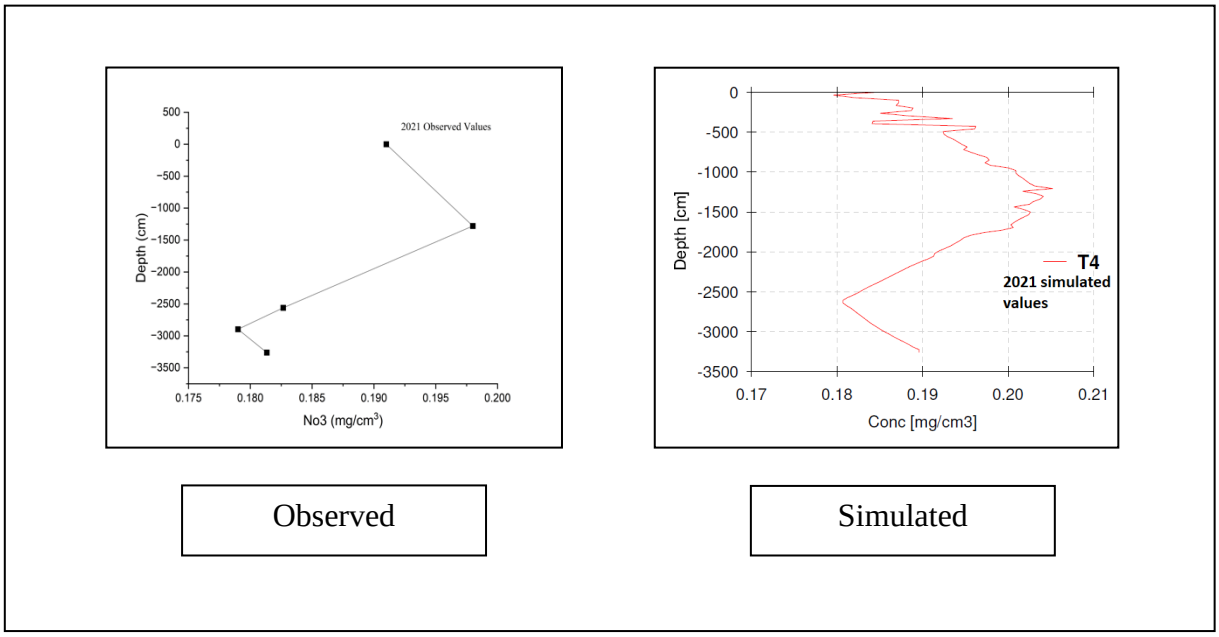

Figure 7.9: Nitrate calibration observed and simulated results

As shown in Figure 7.10, the R^2 value for the trendline between simulated and observed Hydrus values for 2021 sampling at the observation stations for nitrate calibration was 0.8516.

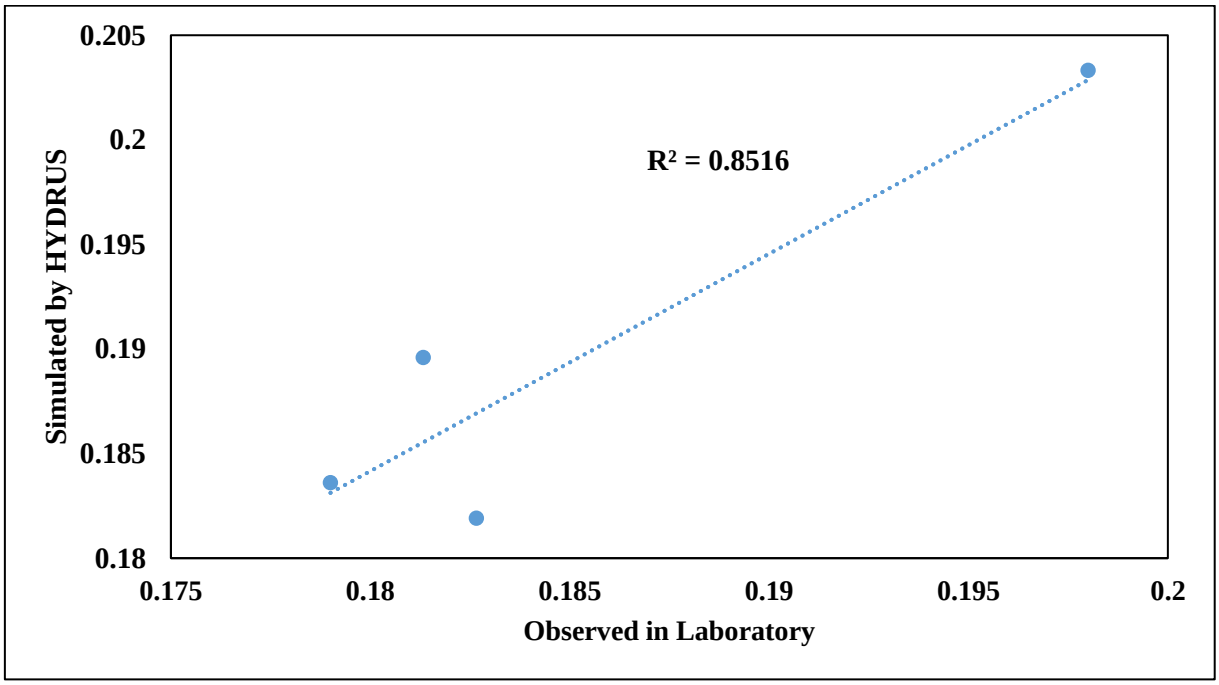

Figure 7.10: Nitrate calibration

7.2.2.2 Validation results

After completing the calibration and achieving an acceptable level of precision, the same inputs were used to validate the model for observed and simulated values in 2022. Figure 7.11 illustrates the chloride validation simulated and observed values for 2022.

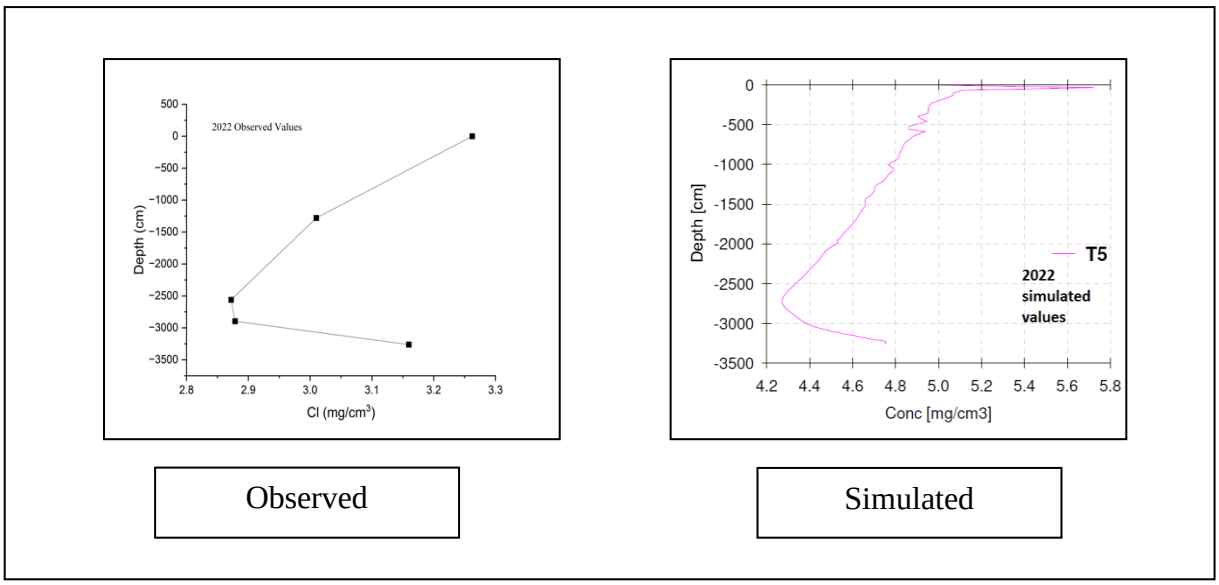

Figure 7.11: Chloride validation observed and simulated results

As illustrated in Figure 7.12, when we plotted the trendline between observed and simulated concentration levels at observation points for chloride validation, we obtained an R^2 value of 0.858.

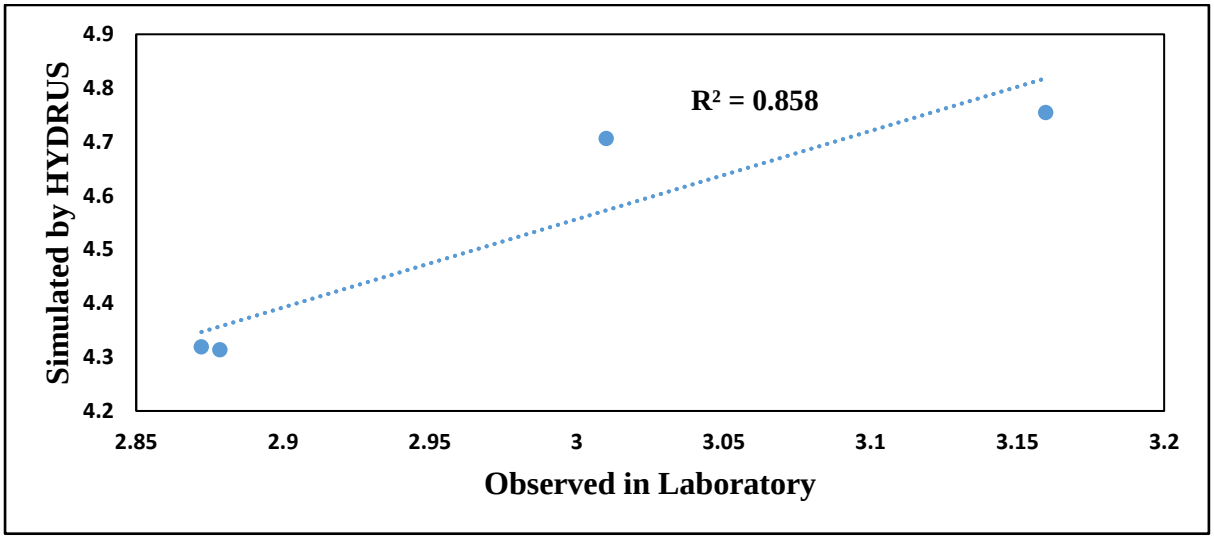

Figure 7.12: Chloride validation observed and simulated results

The Nitrate validation simulated and observed values for 2022 are shown in the Figure 7.13 below

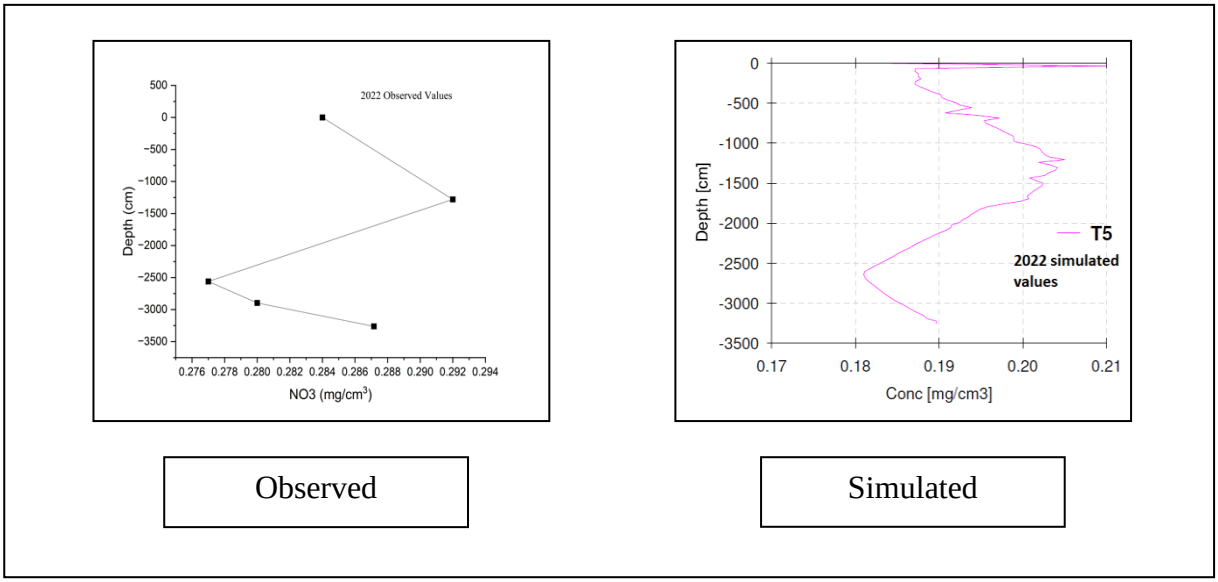

Figure 7.13: Nitrate validation observed and simulated results

As shown in Figure 7.14, when we plotted the trendline between observed and simulated concentration values for nitrate validation, we obtained an R^2 value of 0.8934.

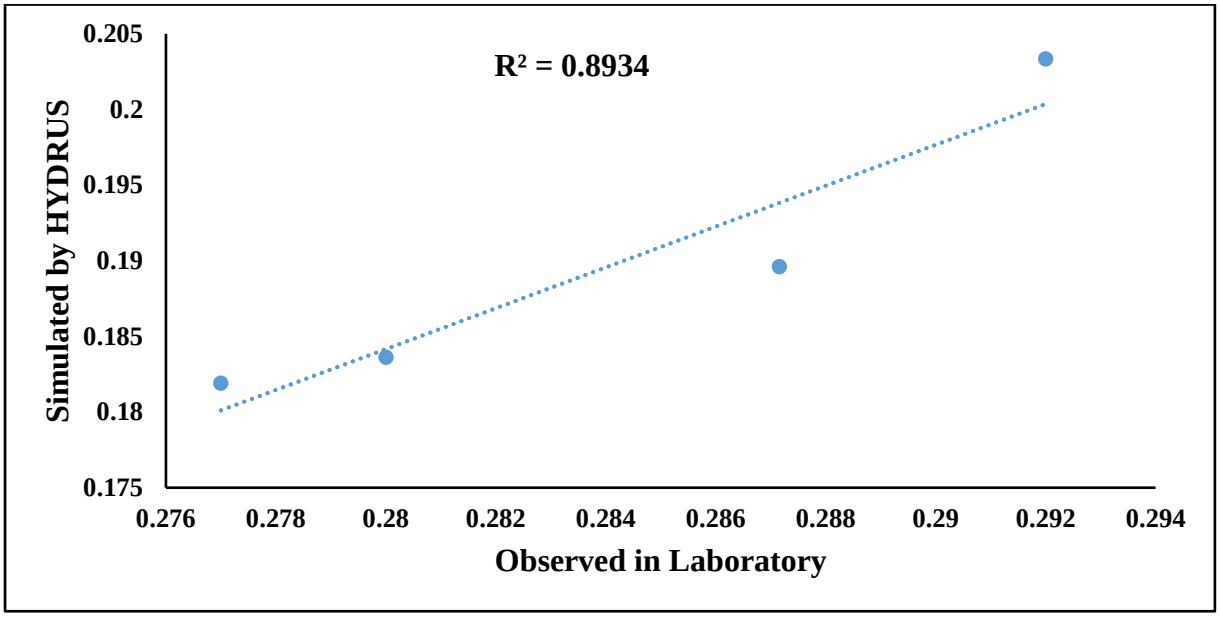

Figure 7.14: Nitrate validation

The Hydrus-1D model was shown to be accurate in predicting the concentrations of chloride and nitrate in Gazipur landfill leachate, as demonstrated in model validation. However, the findings diverge from the reported values due to a lack of information on the waste's water retention qualities. The real flow of leachate is three-dimensional, although only one-

dimensional movement was taken into account in this research. Municipal solid waste is a porous medium comprised of macropores and a matrix in which preferential flows occur frequently and accelerate percolation and waste heterogeneity, and in which the permeability changes continually owing to compaction. Several simplifications were made for the leachate flow, and the majority of calculations were performed by assuming the leachate to be water. However, the true nature of leachate is vastly different from that of water, making it much more challenging to monitor its movement and model the concentration of its elements. No chemical reactions were examined for nitrate, despite the fact that its concentration is changed by a number of chemical processes. Hydrus software provides a soil catalog for modeling in soil medium, but no direct computation for municipal solid waste can be done. Extensive laboratory and field experiments must be conducted in order to conduct simulations that are more accurate. The inverse estimation approach may be used to determine medium hydraulic parameters; however, empirical information and computations are required to achieve convergence of the solution.

Chapter 8: Source apportionment of Groundwater

8.1 Sample collection and Analysis

The study involved the collection of five leachate samples from Ghazipur landfill site at different seasons: pre-monsoon, monsoon, post-monsoon and winter. Additionally, groundwater samples were collected from hand pumps, open wells and bore wells within a buffer zone of 5 to 10 km from the landfill site on 6 June 2022. Surface water samples from various sources such as Sanjay Lake, Yamuna River, Hindon Cut Canal, Ghazipur Drain, and Hindon River were collected on 2-3 September 2021 to assess their impact on the surrounding area and vice versa. All samples were stored in 1-liter plastic bottles and transported to the water quality laboratory of the groundwater division of NIH Roorkee.

8.2 Source apportionment

The study examined the characteristics of leachate, groundwater and surface water. Hierarchical cluster analysis, principal component analysis and positive matrix factorization, utilized Origin 2022 and EPA PMF 5.0 software to ascertain contamination sources in the groundwater. This comprehensive approach enabled the differentiation and quantification of various pollution sources contributing to the studied groundwater.

8.2.1 Hierarchical Cluster Analysis

HCA is a powerful statistical technique that organizes data points, such as wells, into clusters by evaluating their similarities via distance measurements. This method aims to uncover distinct characteristics within these clusters, emphasizing the grouping of objects with high similarity while distinguishing those with lower similarity into separate clusters. The fundamental objective of HCA is twofold: to minimize the variance within each cluster while maximizing the differences between clusters. This process involves gradually forming clusters from pairs of objects that are most similar and merging them iteratively until all samples belong to a single encompassing cluster.

Step 1: Distance Measurement

The process begins by calculating distances between pairs of objects (wells) using a similarity metric like the squared Euclidean distance formula:

$$(\mathbf{X}, \mathbf{Y}) = \sum_{\mathbf{i=1}}^{\mathbf{n}} (\mathbf{X_i} - \mathbf{Y_i})^2$$

This computes the similarity between two samples based on the squared differences across their attributes or dimensions (Nathan et al., 2018) . Here is a breakdown:

- *X* and *Y* are two points in an *n*-dimensional space.
- *Xi* and *Yi* are the *i*th attributes (or coordinates) of points *X* and *Y* respectively.
- The formula calculates the sum of squared differences between corresponding attributes of the two points across all dimensions.

Step 2: Linkage Methods

After obtaining distance measurements, the method for merging or linking objects into clusters (linkage) is chosen. Different linkage methods include simple linkage (nearest neighbor), complete linkage (farthest neighbor), average between-group linkage, centroid linkage, and notably, Ward's method (Mohapatra et al., 2011) . Ward's method minimizes the increase in variance within clusters using the formula:

$$\Delta\mathbf{SS}(\mathbf{AB}) = \mathbf{SS}(\mathbf{A} \cup \mathbf{B}) - \mathbf{SS}(\mathbf{A}) - \mathbf{SS}(\mathbf{B})$$

- ΔSS (*AB*) is the increase in sum of squares resulting from merging clusters *A* and *B*.
- SS ($A \cup B$) represents the total sum of squares for the merged cluster *A* and *B*.
- SS (A) and SS (*B*) are the individual sums of squares for clusters *A* and *B*, respectively.

Step 3: Formation of Clusters

Hierarchical Cluster Analysis then sequentially forms clusters, starting with the most similar pairs and iteratively merging them into higher clusters. This process continues until all samples belong to a single encompassing cluster. The linkage method chosen guides the merging process, determining how objects are grouped together based on their distances.

Step 4: Squared Euclidean Distance

The squared Euclidean distance formula plays a pivotal role in measuring similarities across samples, representing variance in analytical values. It computes the sum of squared differences

between corresponding attributes of two points across all dimensions, aiding in assessing the similarity or dissimilarity between pairs of samples.

Step 5: Z-score Standardization

To ensure fair variable comparisons, variables undergo standardization to Z scores using formula given below:

$$\mathbf{Z = \frac{X - \mu}{\sigma}}$$

Where:

- Z represents the Z score.
- X is the value of the variable.
- μ is the mean of the variable.

8.2.2 Principal Component Analysis

The study employed Principal Component Analysis (PCA) to discern sources of pollution within the dataset, providing comprehensive insights into spatial patterns and the origins of environmental contaminants (Subba Rao et al., 2007). This analysis utilized standardized data to create new variables known as principal components, effectively illustrating interrelationships among diverse chemical variables.

These components were derived through a linear combination of the original data, streamlining the dataset by emphasizing crucial parameters, primarily based on their highest loading values (Herojeet et al., 2016) .The initial principal component predominantly accounted for the total variance, while subsequent components captured the remaining variance. Prior to conducting PCA to explore underlying relationships, the suitability of selected sampling points was verified via the Kaiser–Meyer–Olkin (KMO) test, requiring a KMO value surpassing 0.5 (Krishan et al., 2023).

Following the KMO test a varimax rotation was applied to produce score plots. Employing Origin software, an effective PCA was conducted, integrating diverse indicators to simplify complexity and pinpoint pollutant origins in Gazipur. A range of techniques, including scree-plots, observed data Eigenvalues, or randomly generated Eigenvalues, were utilized to extract vital insights (Banda & Kumarasamy, 2020). Furthermore, component rotation using varimax aimed to enhance

interpretability, aligning with findings from (Baluch et al., 2019). The following equation is used to express the principal component analysis:

$$Z_{ij} = a_{ij}x_{ij} + a_{i2}x_{2j} + \ldots\ldots\ldots\ldots + a_{im}x_{mj}$$

In this equation, Z symbolizes the score of the component, where 'a' represents the component loading, and 'x' stands for the measured value of the variable. The indices 'i', 'j', and 'm' respectively signify the component sample, and the total count of variables involved. Factor loadings show crucial relationship between variables and components. High factor loadings, nearing ±1, indicate robust relationships (either positive or negative) between the variable and the component (Cloutier et al., 2008).

This study observed that within each cluster, three to four primary components emerged based on Eigenvalues surpassing 1.0. These components, taken together, accounted for an extensive portion, ranging from 80% to 90%, of the total variation within the dataset (Banda & Kumarasamy, 2020; Mohammad Salim Moyel, 2015). Various factors, including lithological characteristics, leachate absorption, anthropogenic influences, Farmland, Urbanization, Boating Lake and several other controlled variables were discerned from the scores obtained through principal component analysis. The influence exerted by these identified factors across different sampling locations was visually depicted through the creation of distinct sets of plots, shedding light on their varying impacts and spatial distributions.

8.2.3 Positive Matrix Factorization (PMF)

Receptor Models are statistical approach for quantifying the contributions of different sources based on chemical fingerprint of the sources. The main aim of the receptor models is to solve chemical mass balance (CMB) between measured species concentration and source profile (EPA, 2014). The different receptor models are CMB, Unmix and PMF.

Positive Matrix Factorization (PMF) is a multivariate factor analysis tool that separate the sample data into (a) Source Contribution and (b) Source Profile. The PMF Model determines the source contribution and profile by minimizing the objective function represented by the formula:

$$Q = \sum_{i=1}^{n}\sum_{j=1}^{n}\left[\frac{x_{i,j} - \sum_{k=1}^{p} g_{i,k} f_{k,j}}{u_{i,j}}\right]^2$$

Where, i represents the number of samples, j is the number of species analysed, $x_{i,j}$ is the measured species in the groundwater sample , p is the number of sources or factors, f represents the species profile for each sample, g is the amount of mass contribution by each factor to each individual sample, $e_{i,j}$ is the residual for each sample species and $u_{i,j}$ is the uncertainty in sample analysis. The equation based uncertainty in the samples is calculated by;

$$\boldsymbol{Unc = \frac{5}{6} \times MDL}$$ When, concentration ≤ MDL

$$\boldsymbol{Unc = \sqrt{(\sigma + c)^2 + MDL^2}}$$ When, concentration > MDL

Where, *Unc* is the uncertainty, *MDL* is the Method detection limit, $\boldsymbol{\sigma}$ represents the relative standard deviation and *c* is the concentration of water quality parameters. The calculated uncertainty is represented in Table 8.1 to Table 8.5.

8.3 Result

8.3.1 Source Characterization

The physio-chemical characteristics of surface water sample are listed in Fig.8.2. The Hindon River displayed a substantial organic pollution load, as evidenced by its COD value of 1000 mg/l (Fig.8.2 a). The dominant surface water chemistry in the river comprised Ca^+ (38.2 mg/L), HCO_3^- (157.38 mg/L) & Cl^- ions with concentration 28.5 mg/L (Fig.8.2 b) with Fe & Al being the most abundant heavy metals at concentrations of 1.53 mg/l & 1.47 mg/l (Fig.8.2 c), respectively. Nitrate concentration in the Hindon River was notably high reaching 16.6 mg/l. In contrast, the Hindon Cut Canal exhibited a similar heavy metal dominance pattern with Fe being the most prevalent followed by Al and Mn in the order of 1.18 > 0.65 mg/L. The Yamuna River covering the western part of the study area had acidic pH value of 6.65 within an acceptable range for aquatic ecosystems. It was characterized by dominant ions in the sequence of $HCO_3^- > Cl^- > Na^+$ ions with concentrations of 87, 64 and 24 mg/l (Fig.8.2 b), respectively.

The Ghazipur Drain is situated between a landfill on its right and Sanjay Lake on its left and a comparison of the water chemistry among three sites, namely Ghazipur Landfill leachate, Ghazipur Drain, and Sanjay Lake indicates noteworthy differences in their pollutant levels. The Ghazipur Landfill leachate exhibits high contamination levels with COD measured at 37,000 mg/l (Fig 8.2 a) and Zn at 4.04 mg/l (Fig 8.2 d). In comparison, the Ghazipur Drain shows lower

contamination with COD at 800 mg/l and Zinc is 0.2 mg/L. Sanjay Lake located further away from the landfill appears to be less affected by pollutants with COD at 420 mg/L and Zn at 2.3 mg/l (Fig.8.2c). It is evident that the Ghazipur Drain, which receives runoff from the nearby landfill, still demonstrates some contamination though at a reduced level compared to the leachate. In contrast, Sanjay Lake, being situated farther from the landfill experiences lower levels of COD.

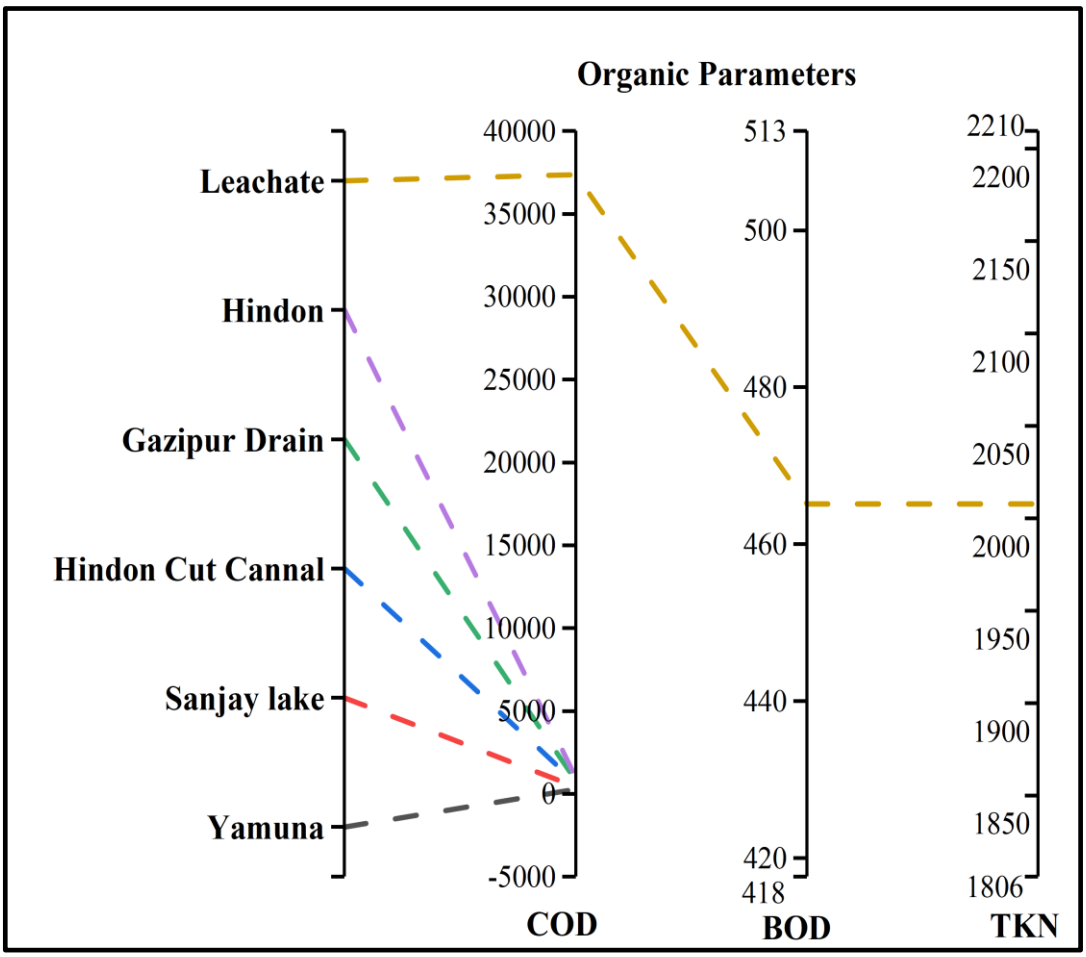

Figure 8.2 a) illustrates a comparison between organic parameters of surface water bodies along with Gazipur drain and landfill site

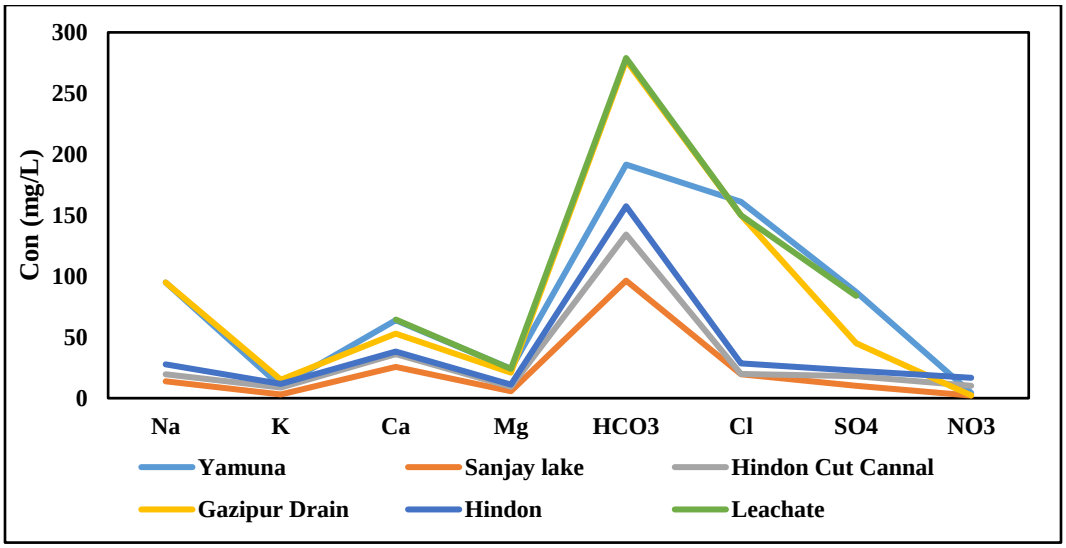

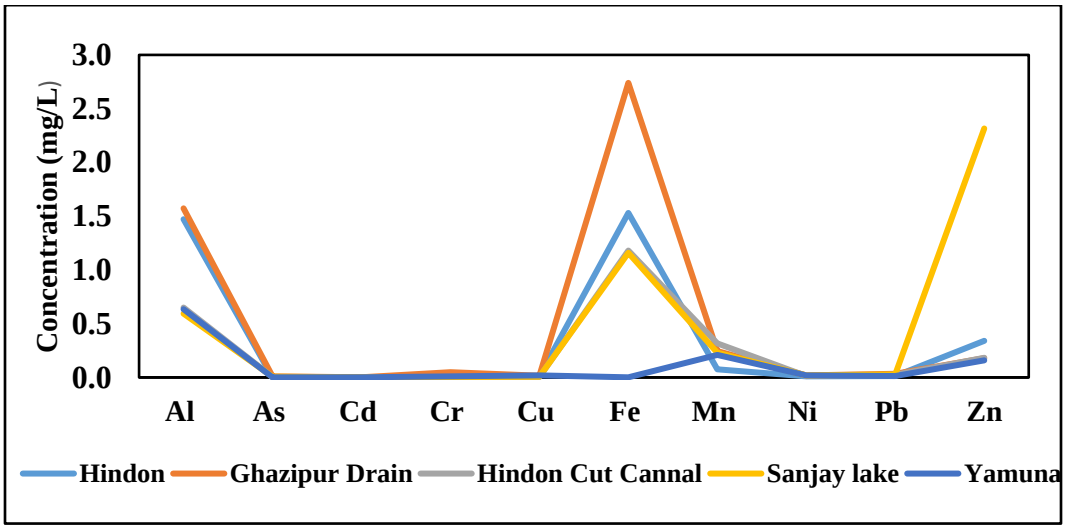

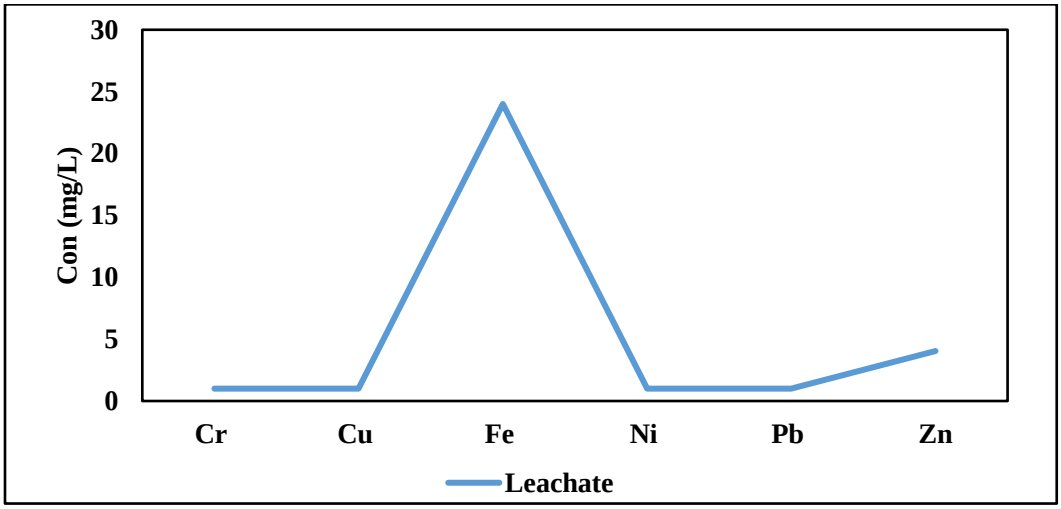

Figure 8.2 b) Illustrates a comparison of In- Organic Parameters , c) Heavy metal concentrations in various surface water bodies & d) Heavy metal concentration of Landfill leachate

8.3.3 Hierarchical cluster Analysis

The Hierarchical Cluster Analysis was utilized to group groundwater samples based on their geochemical similarities. Ward's method with Euclidean distance linkage was employed for this purpose, resulting in a dendrogram displaying the classifications of the sampling sites (Fig.8.3). The HCA yielded five major clusters namely C1, C2, C3, C4 and C5, which showed distinct features and natural backgrounds possibly influenced by similar pollution sources (Fig 8.3).

Cluster C1 covered about 46% of the wells surrounding the Ghazipur Landfill and the central part of study area. The water in this cluster had slightly acidic to slightly alkaline nature, with pH values ranging from 6.6 to 7.8. Additionally, C1 exhibited variations in COD and TDS levels with mean values of 156 mg/l and 1463 mg/l, respectively. Some wells within C1 showed high variability suggesting possible localized contamination sources. The Stiff diagram based on mean values for each cluster revealed the dominance of major ions, where samples in C1 were characterized by $Cl^{-}>Na^{+}>SO_4^{2-}$. In terms of heavy metals, cluster C1 exhibited lower quantities compared to other clusters with Fe>Mn>Zn being the observed order of dominance and recorded high COD concentration of 220 mg/L in the groundwater near Ghazipur landfill indicates severe contamination with organic pollutants.

Cluster C2, constituting 8% of the wells proximate to the Yamuna River, exhibited a pH range slightly leaning towards neutral acidity, measuring between 6.8 to 7.4. This cluster showcased a prevalent presence of sulfate and chloride in its anion composition coupled with cations primarily composed of sodium and calcium. Notably, C2 deviated in terms of heavy metal compositions, particularly with elevated levels of Fe, Mn and Zn where an outlier in manganese, raising concerns regarding potential health hazards.

Within Cluster 2, specific parameters such as sodium ranging from 28 to 251.7 mg/l, calcium ranging from 11.68 to 201.3 mg/L, iron ranging from 3.84 to 698.4 mg/L, sulfate ranging from 37.6 to 202.14 mg/L, and manganese ranging from 0.01 to 40.62 mg/L surpassed acceptable thresholds, indicating a heightened potential for pollution. These exceedances highlight the increased risk posed by certain elements within this cluster and signal a higher probability of adverse environmental impacts.

Cluster 3, encompassing 7% of the sampled wells, demonstrates a pH range between 6.6 to 7.8, signifying a spectrum from slightly acidic to slightly alkaline conditions. The water within this cluster exhibits moderate organic pollution, indicated by a mean COD (Chemical Oxygen Demand) value of 138 mg/L. Furthermore, it displays notably high mineral content, with Total Dissolved Solids averaging at 1116.8 mg/L.

Analyzing the chemical composition, samples from Cluster 3 notably feature dominant levels of sodium, ranging from 82.4 to 1023.8 mg/L, potassium ranging from 2.66 to 22.37 mg/L, chloride ranging from 98.7 to 2008.12 mg/L, and sulfate ranging from 51.88 to 922.76 mg/L .

Moreover, this cluster demonstrates elevated concentrations of heavy metals, particularly iron ranging from 3.6 to 3566.24 mg/L and manganese ranging from 0 to 5.27 mg/L. These concentration ranges reflect the extremities observed within the datasets for Cluster 3.

Cluster 4, representing 10% of the wells located in the northeastern part of the study area, demonstrates a pH range spanning from 6.70 to 7.8. The water within this cluster shows moderate organic pollution, evidenced by an average Chemical Oxygen Demand (COD) value of 162 mg/L. Furthermore, it displays a notably high mineral content, with an average Total Dissolved Solids (TDS) level reaching 2880 mg/L. Within this cluster, the predominant ions are characterized by their concentrations in the following order: $Cl^- > Na^+ > SO_4^{2-} > Ca^{2+}$ .Chloride levels range from 53 to 4691 mg/L, while sodium ranges from 50 to 1690 mg/L. Sulfate concentrations varied from 28.56 mg/L to 1186.29 mg/L, with the highest value recorded at well G-8. Moreover, calcium concentrations ranged from 66 to 1095 mg/L within this cluster.

Within Cluster 5, the pH levels observed among the sampled data spanned from 6.7 to 7.8 range typical indicate moderately acidic to neutral conditions. The variability in Total Dissolved Solids (TDS) ranged widely from 147 to 4288 mg/L. Chemical Oxygen Demand (COD) values were noted within the range of 100 to 200 mg/L. The primary ions prevalent in Cluster 5 were dominated in the following order: $Cl^- > SO_4^{2-} > Na^+$. Chloride levels showed a range from 30.59 to 1975 mg/L, indicating considerable fluctuations. Sulfate content demonstrated variability within the range of 23 to 1306 mg/L, while sodium concentrations varied between 48.60 and 1281.06 mg/L. Regarding heavy metal concentrations, iron, manganese, zinc, and chromium emerged as the most abundant heavy metals within this cluster.

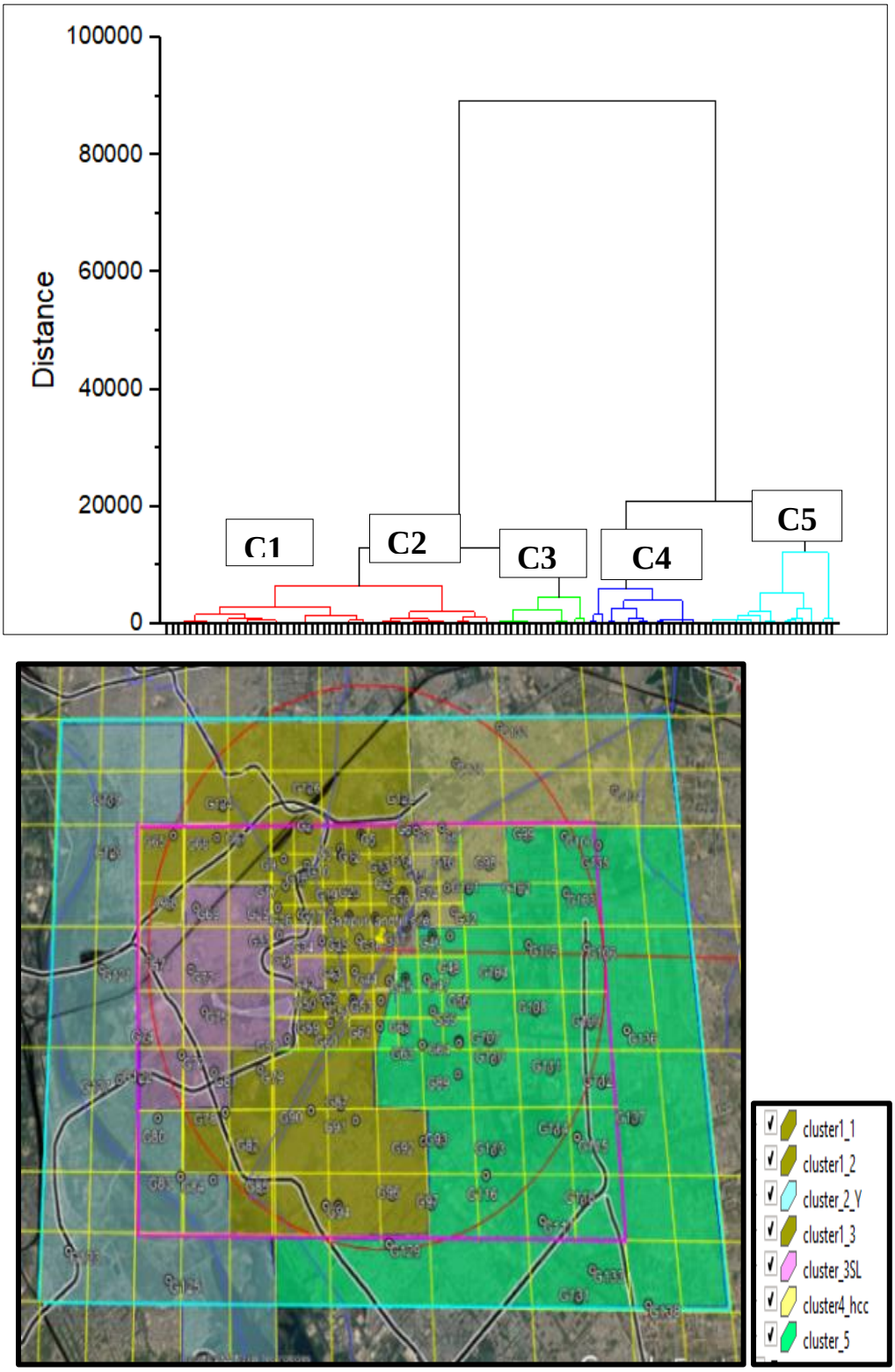

Figure 8.3 Hierarchical cluster analysis for the groundwater samples and Google Earth image to superimpose the location of each cluster and highlight the grids belonging to each cluster using different colors provided a visual representation of the clustering results

8.3.4 Cluster-1

The study area was divided into five clusters for source apportionment analysis. The Principal Component Analysis and EPA-PMF analysis were used to identify and attribute pollutant contributions from different sources within each cluster. Cluster 1 comprises five significant principal components (PC1, PC2, PC3, PC4 & PC5) explaining 85.65% variance. Two primary sources of pollution have been identified within the study area.

Source 1 attributed to the Gazipur Drain, contributing significantly to the variance in pollution at 42.83% with an Eigen value of 8.57 (Fig.8.4 a). This source is marked by elevated levels of Cr & Zn commonly found in sewage discharge due to their presence in human waste (Fig 8.4b & c). Accounting for 14% of the overall sewage-related contamination (Fig 8.4 e), Source 1 geographical spread covers both the northern and southern regions consistent with the findings of PC1 and F3 in the PCA and PMF models (Fig.8.4f, a & III).

Source 2 also associated with the Ghazipur Drain, predominantly influences cluster 1, explaining 20.92% of variance with an Eigen value of 4.18 (Fig 8.4 a & b). The significant presence of NH_4^+ & F^- in the Ghazipur Drain suggests that agricultural runoff and industrial effluents might be major contributors to the pollution in this area. In this cluster, Source 2 accounts for 14% of the overall groundwater pollution, making it a critical (Fig 8.4 e). This aligns with similar spatial patterns indicating high pollution levels in the northeast and northwest, consistent with the findings derived from PC2 and F2 (Fig 8.4 f, b & II).

Leachate absorption, specifically representing Source 3. This source explains 9.47% of the pollution variance with an Eigen value of 1.89, primarily influenced by Fe and Mn originating from waste introduced into the landfill (Fig 8.4 a & b). The presence of Fe in leachate samples, signifies a range of contributors including municipal waste, construction debris, industrial processes, electronic waste, natural soil, and deteriorating infrastructure. Source 3 significantly contributes to pollution, accounting for roughly 25% of groundwater contamination (Fig 8.4 e), particularly impacting PC3 & F4 and affecting the northeastern part of the study area (Fig 8.4 f, c & IV).

The landfill as Source 4, explaining 7.21% of the pollution variance with an Eigen value of 1.44 (Fig 8.4 a). This cluster is characterized by strong positive correlations between Cl^-, NO_3^-, and

SO_4^{2-} (Fig.8.4 b). Notably, the landfill leachate investigation revealed a significant increase in Cl^- concentration, indicating leachate disposal as a major contributor to elevated groundwater chloride levels (Fig.8.4 c, d &e). The heightened nitrate levels in February and March are associated with increased winter water infiltration and leachate percolation. This source accounting 24% of groundwater pollution impact (Fig.8.4 e), especially in areas near the landfill aligns with PC4 and F1 (Fig 8.4f, d & I).

Leachate absorption from Landfill marked as Source 5, explains 5.22% of the variance (Eigen value 1.04) and is primarily influenced by pH and COD (Fig.8.4 a & b). These elements likely originate from annual waste deposition in the landfill. Notably, all collected leachate samples exhibit COD values exceeding 37,000 mg/l, while groundwater COD levels remain below 200 mg/l, indicating the presence of macrobiotic contaminants in landfill leachate, making it a notable contamination source. F5 is characterized by high pH and COD levels, contributing 70% and 75% to this factor (Fig.8.4 c). Leachate absorption emerges as a critical factor affecting groundwater hydrochemistry in the region, contributing 23% to overall pollution (Fig.8.4 e). This aligns with spatial patterns reflecting elevated pollution levels in the eastern part of the study area (Fig.8.4 f, e & V), further supported by the PC5 and F5 findings detailed in Table 4.6.

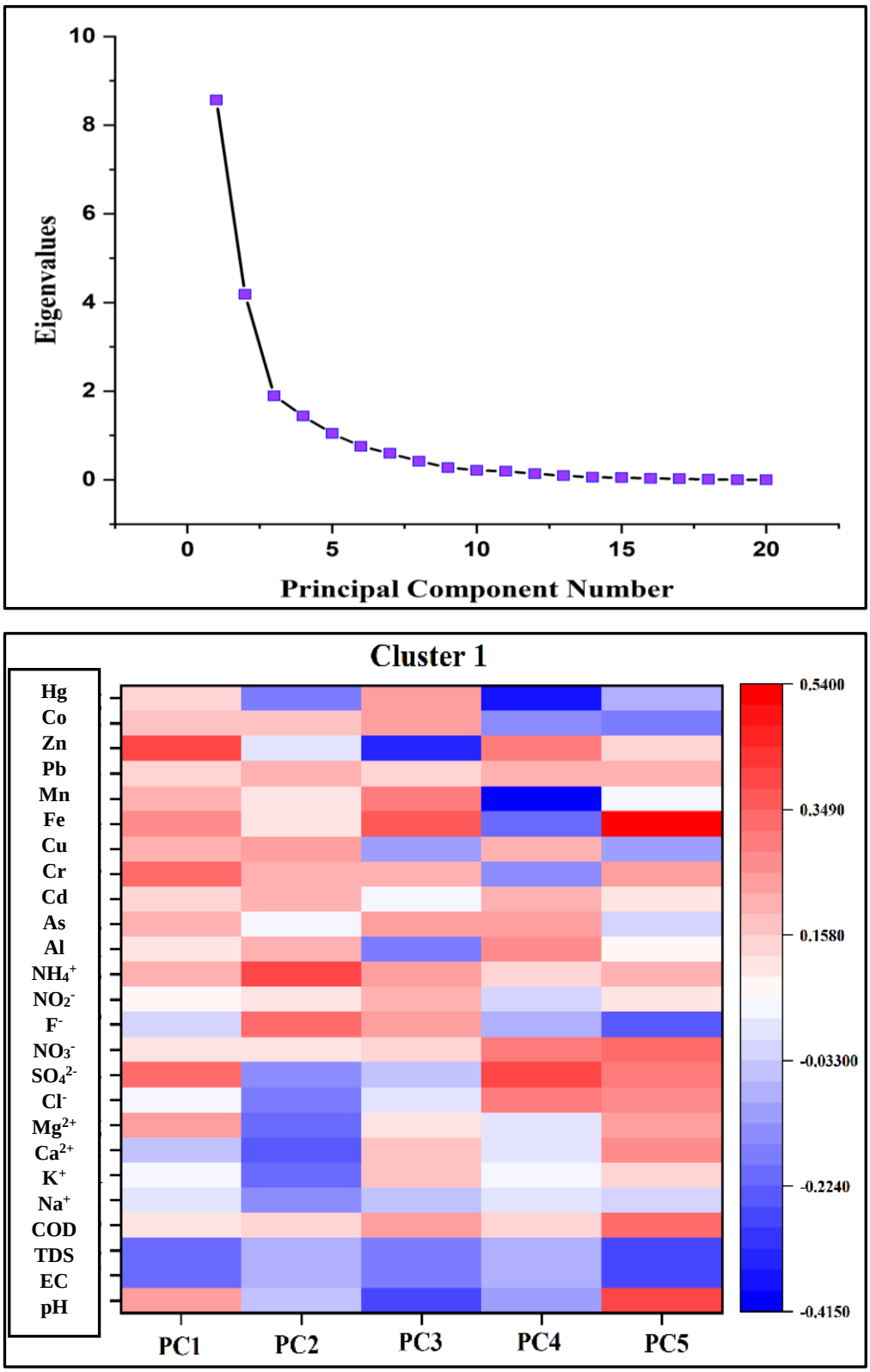

Figure 8.4 For Cluster 1 a) Eigenvalues of principal components are depicted in the Scree plot & b) Principal component profiles obtained using the PCA model

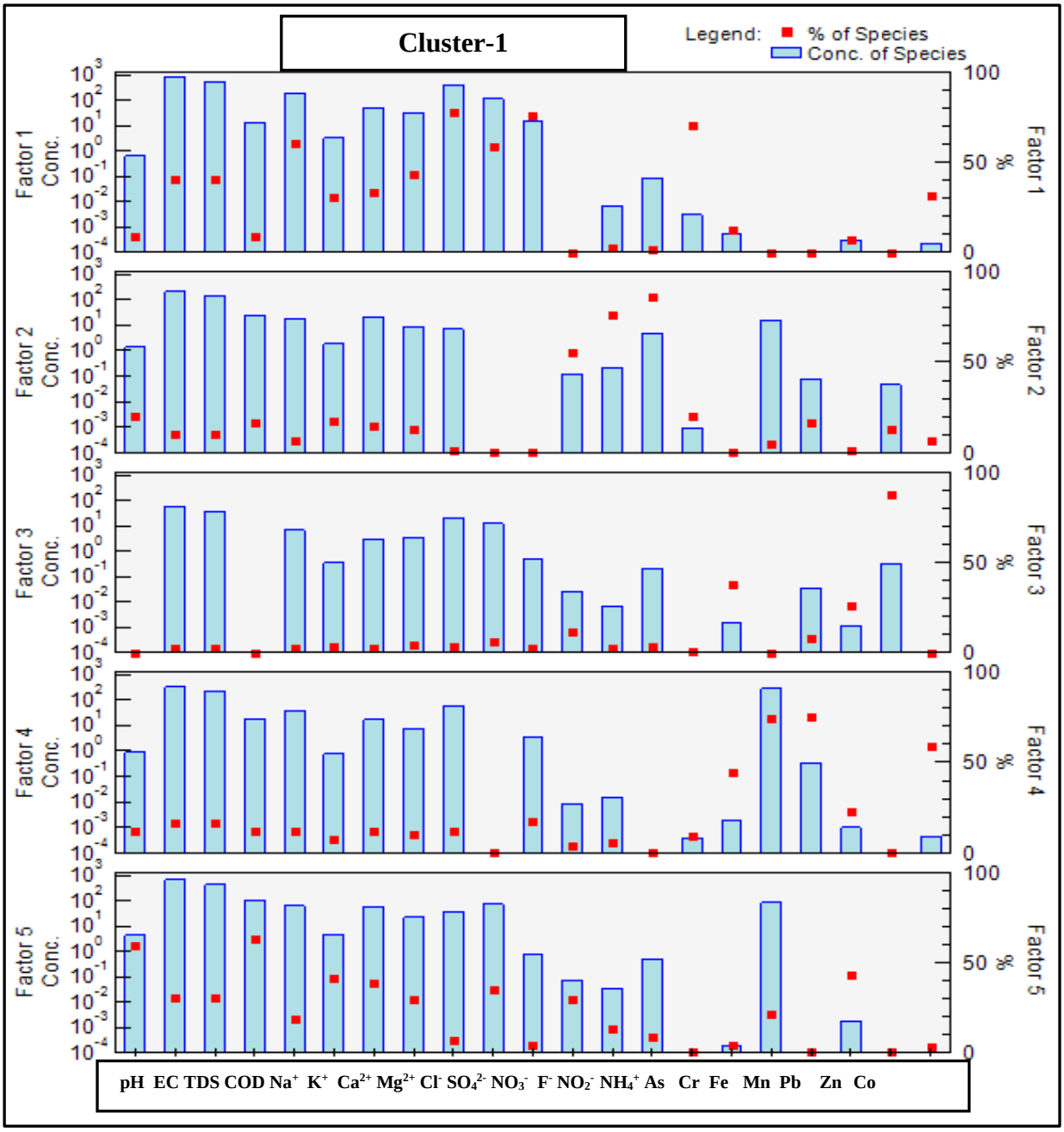

Figure 8.4 c) Factor Contribution profile

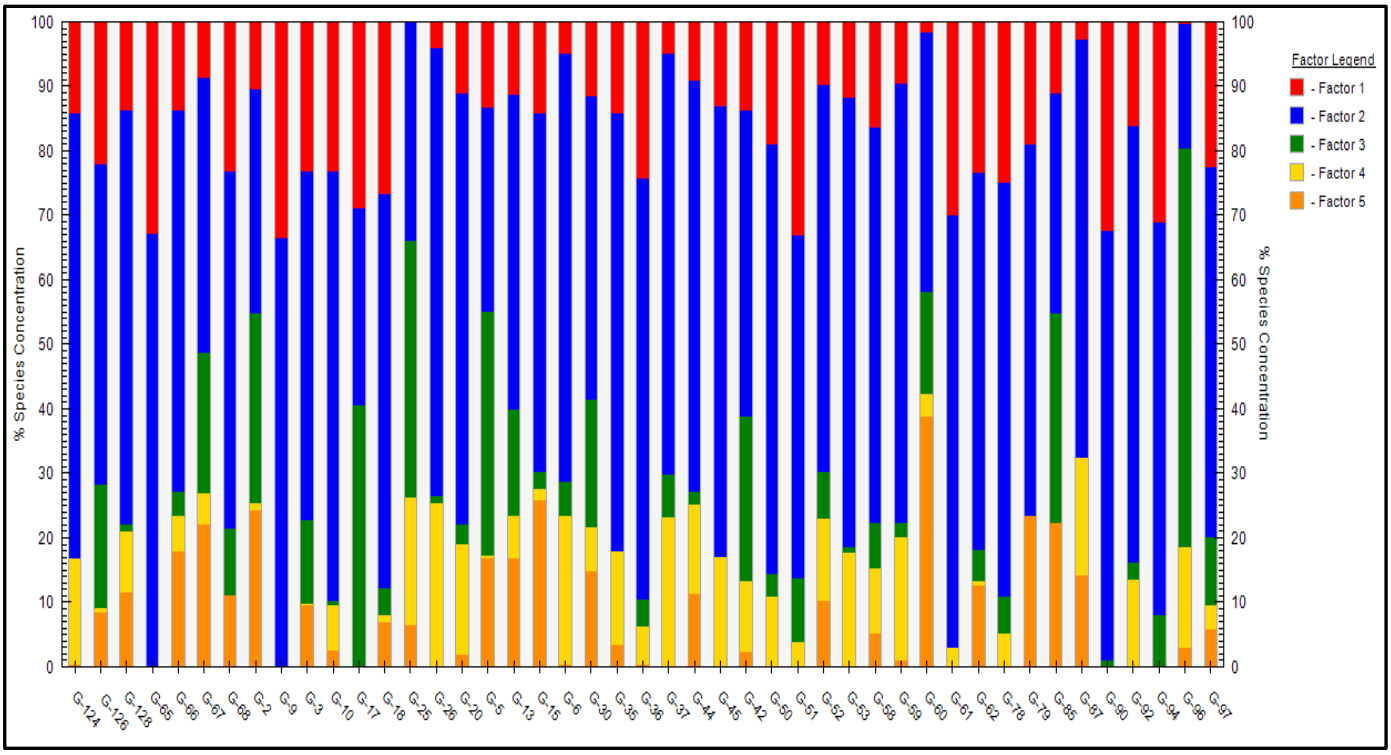

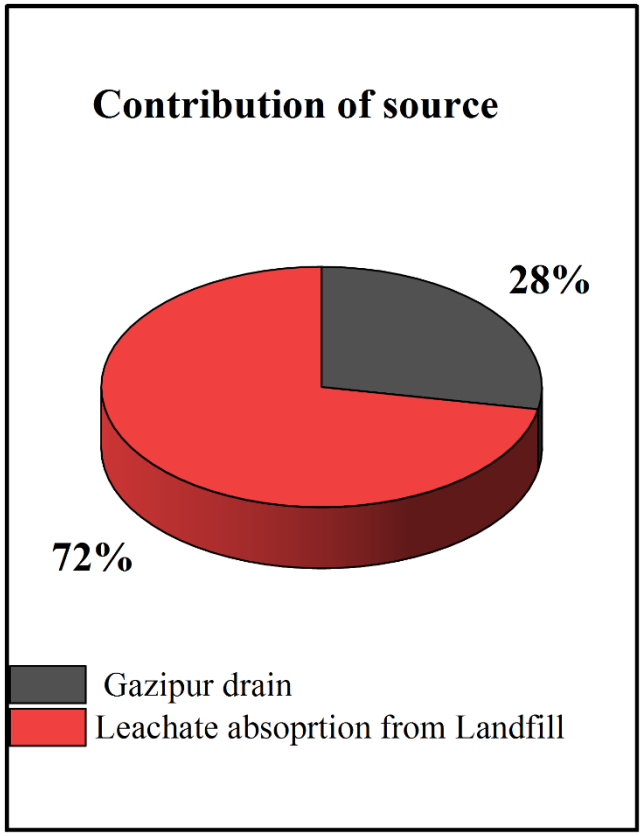

Figure 8.4 d) Factor Contribution profile of each well & e) Overall Contribution

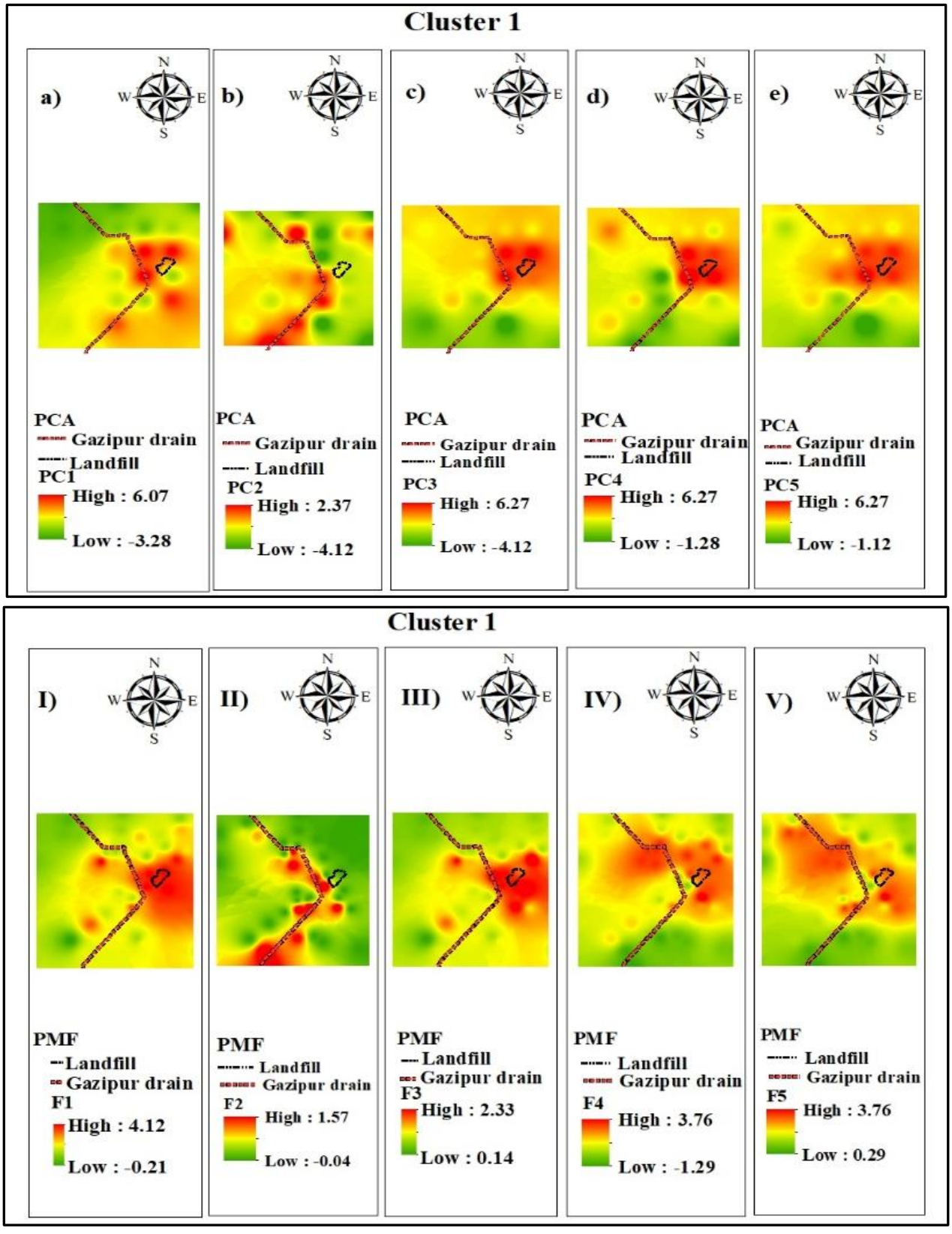

Figure 8.4 f) Spatial distribution of PCA and PMF analysis

8.3.5 Cluster 2

Cluster 2 analysis revealed four key components, with PC1 explaining 43.03% of the variance and an Eigenvalue of 10.76. PC1 prominently displayed substantial levels of K^+, Ca^{2+}, and Na^+ (Fig.8.5 a & b). Robustness analysis confirmed a strong association, especially for K^+ and Ca^{2+} ($R2 > 0.95$). F4 significantly contributed to K^+ and Ca^{2+} (Fig.8.5 c &d). Recharge from the soil significantly enhanced groundwater enrichment with essential elements like Ca^{2+}, K^+, and Na^+. The wells in urban locales like G-123, 125, and G-119, where paved surfaces limit infiltration, element levels remain low (Fig.8.5f, f & IX). In contrast, G-122 in agricultural land benefits from rainwater permeating the soil, dissolving and leaching nutrients from underground minerals, resulting in elevated Ca^{2+}, K^+, and Na^+ levels, contributing approximately 24.4% to the overall concentration (Fig.8.5 e).

Farmland demonstrates its significant influence through PC2 and F3 in Source 2, explaining 30.56% of the variance with an Eigen value of 7.64. These factors exhibit a robust correlation ($r = 0.7$) with NO2 and $NH_4^{+,}$ primarily linked to agricultural fertilizer usage (Fig.8.5 a, b & c). Factor 1 prominently shows substantial contributions of NO_2^- (72%) and NH_4^+ (50%), especially around wells like G-120 and G-121 in agriculturally intensive areas, indicating contamination of groundwater due to fertilizer application. Furthermore, a slight discrepancy in spatial distribution showed different heavily polluted areas between PCA (eastern and western part) and PMF (western part) models (Fig.8.5 f, g & VIII), signifying extensive fertilizer-related pollution, collectively contributing 24.2% to groundwater degradation (Fig.8.5e).

Older Alluvium, represented by PC3, accounts for 14.44% of the variance with an Eigenvalue of 3.61, there is a conspicuous presence of significant Zn and Fe loadings demonstrating a robust correlation coefficient ($r = 0.9$) (Fig.8.5a & b). Elevated heavy metal levels (Zn, Pb, Mn, Co, Fe) in Yamuna River sediments, especially in older alluvium, accumulate from nearby geology. This makes the alluvium a key source of Zn and Fe groundwater contamination, affecting local water quality. F1 also exhibits noteworthy loadings of Zn, contributing significantly with 78% (Fig.8.5c). PC3 and F1 jointly contribute 15.5%, revealing concentration hotspots near wells G120, 122, and G-127 in the northeast and southeast areas (Fig.8.5f, h & VI).

In Yamuna Sediments, the variance attributed is approximately 5.74%, featuring strong and positive loadings of Mn, Pb and Co (Dalai et al., 2004). This suggests that the Yamuna river sediments are indeed enriched with these ions and serve as a prominent source. F2 stands out with

substantial loadings for Mn and Co contributing 100% and 82%, respectively (Fig 8.5 c). The spatial distribution underscores this, with wells closest to the Yamuna Rivers exhibiting the highest loading values (Fig.8.5f, i & VII)

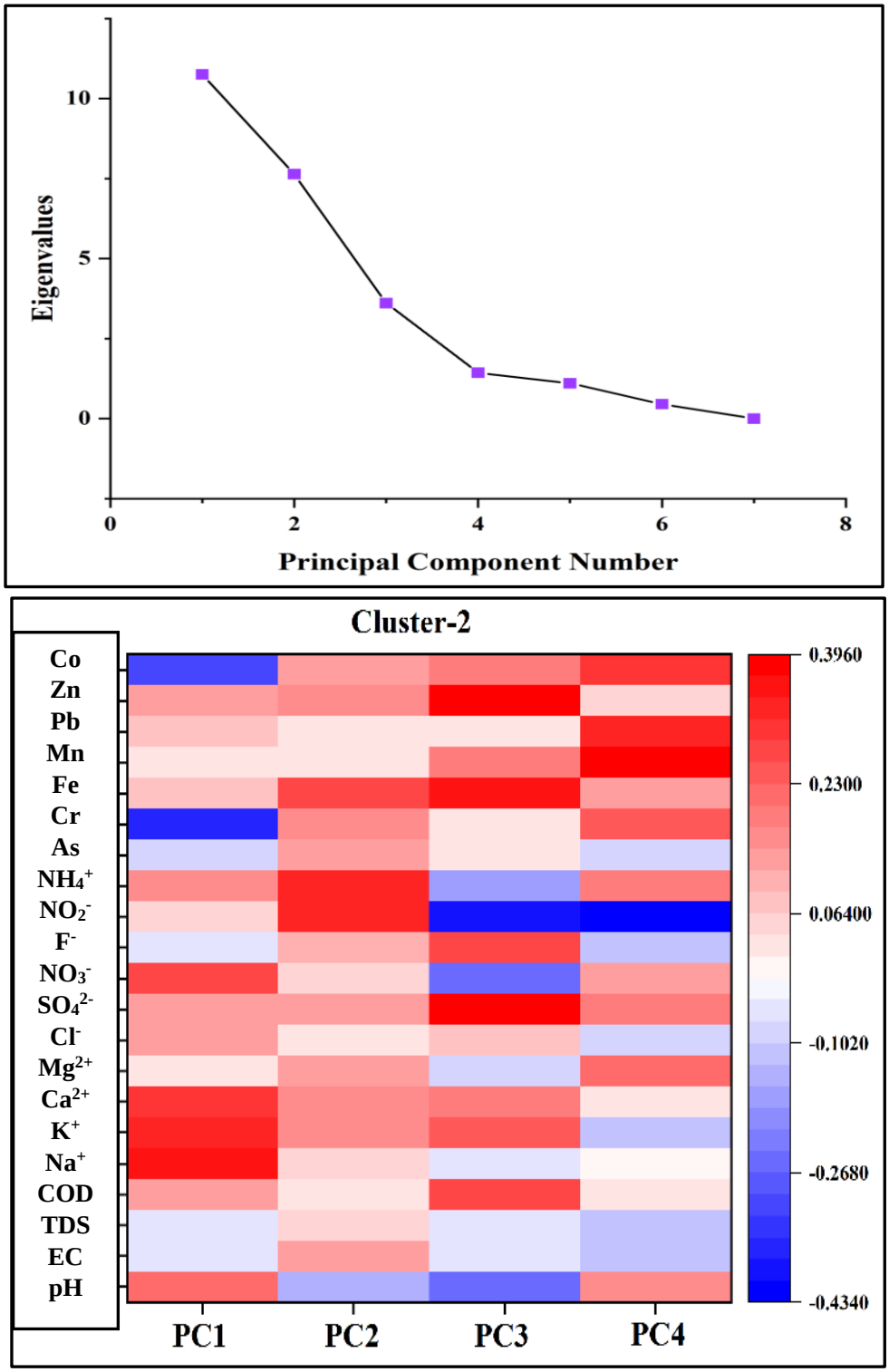

Figure 8.5 for Cluster 2 a) Eigenvalues of principal components are depicted in the Scree plot & b) Principal component profiles obtained using the PCA model

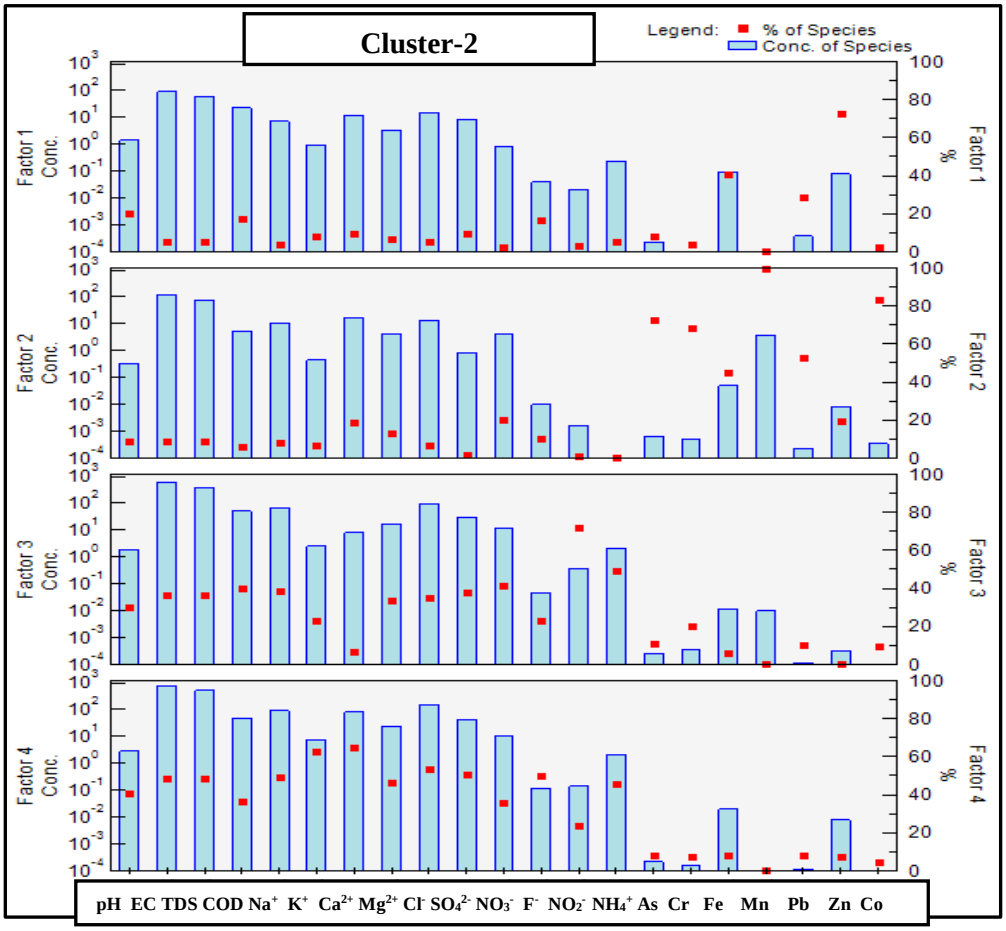

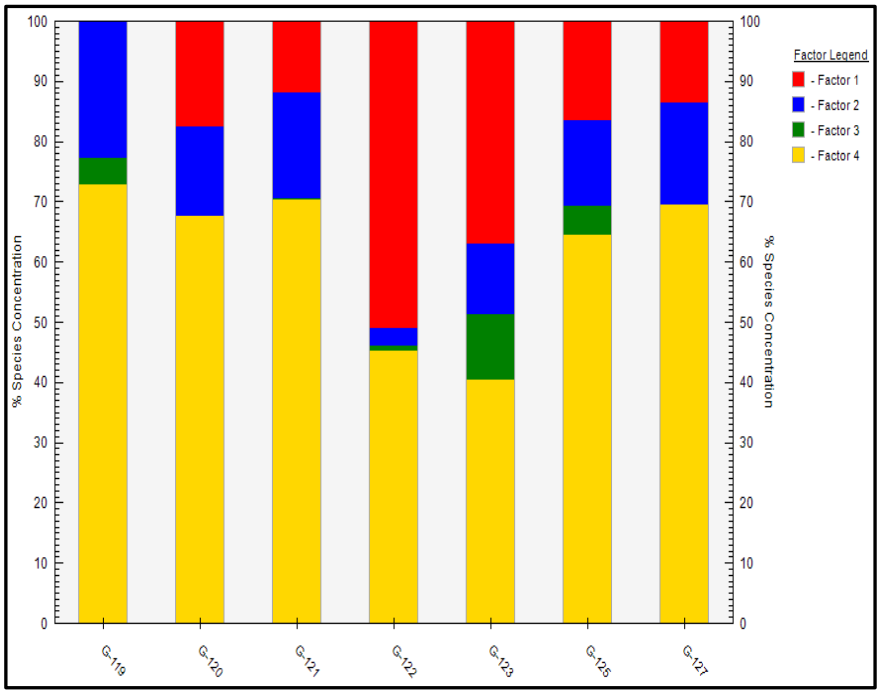

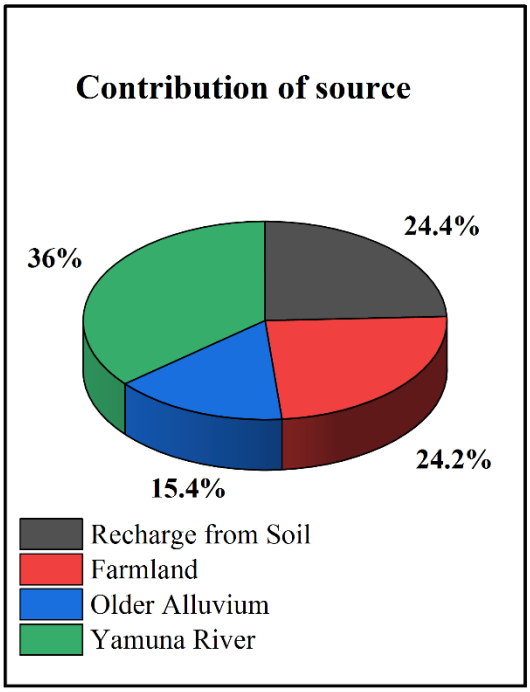

Figure 8.5 c) Factor Contribution profile , d) Factor Contribution profile of each well & e) Overall Contribution

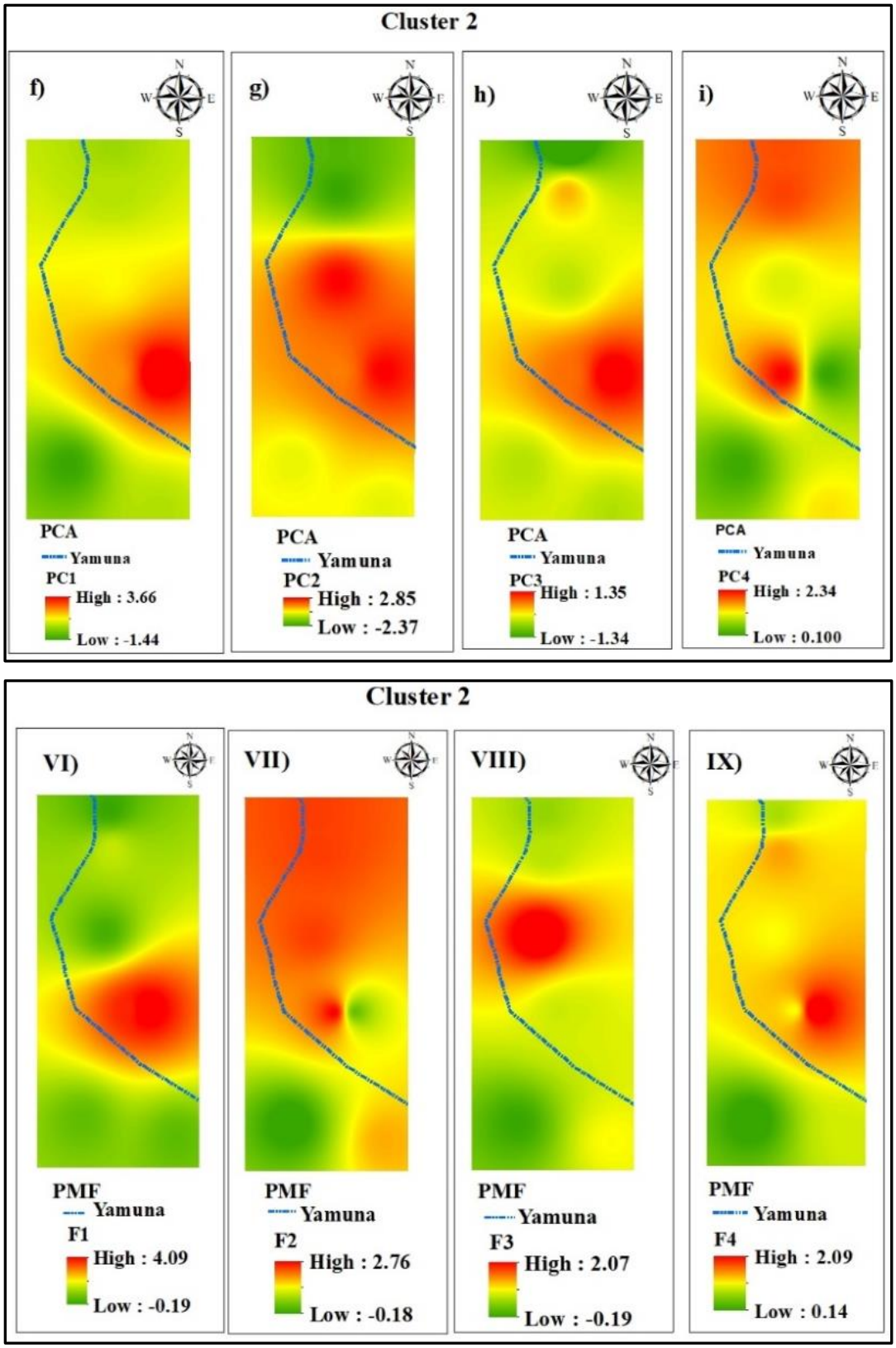

Figure 8.5 f) Spatial distribution of PCA and PMF analysis

8.3.6 Cluster-3

In Cluster 3, five principal components were observed, with Sanjay Lake serving as a key marker of Source 1, where PC1 explains 52.40% of the variance and features high loadings of toxic metals (Mn & Fe) impacting drinking water quality (Fig. 8.6 a & b). These heavy metals likely migrate from Sanjay Lake to groundwater, influencing its quality, supported by a robust model fit (Q value ratio = 1.19). Factor 1 exhibits the highest loading of Mn and Fe (Fig. 8.6 c & d), reinforcing Sanjay Lake role as the primary source of these metals. Detailed analysis reveals significantly higher metal levels in Sanjay Lake compared to groundwater, contributing 20% (Fig.8.6e). Spatial distribution highlights consistently polluted areas in both PCA and PMF models (central parts) (Fig. 8.6f, j & X).

Farmland, represented as Source 2, is characterized by PC2, explaining 17.61% of the variance with an Eigenvalue of 3.52 (Fig.8.6 a & b). It displays significant loadings of Cl^-, K^+, and SO_4^{2-}, indicating the presence of these elements within the agricultural environment. These elements are commonly associated with fertilizers and irrigation practices in farmland areas, suggesting that agricultural activities contribute to their presence in groundwater, potentially affecting water quality. F4 is also dominated by Cl^-, K^+, and SO_4^{2-} (Fig.8.6c), aligning with the influence of "Agriculture activities," as observed in PC2 from the PCA results. Both PC2 and F4 indicate high pollution levels in the southwest part of the study area, surrounded by farmland (Fig. 8.6f, k & XIII), contributing significantly at 25% (Table 8.6).

Medical waste represent as Source 3, explains 9.69% of the variance with an Eigenvalue of 1.94, displaying significant F^- and K^+ loadings, indicative of a strong correlation coefficient (r = 0.82) (Fig. 8.6a & b). Hospitals and dental clinics can elevate groundwater ion levels, such as fluorine (F^-) and potassium (K^+), through improper waste disposal and the use of fluoride-containing products. Inadequate handling of waste materials and runoff from healthcare facilities may introduce these ions into the environment, potentially affecting groundwater quality. F2 also shows noteworthy loadings of F^- and K^+, contributing significantly at 40% and 37% (Fig.8.6 c). Together, PC3 and F2 contribute 14% and reveal concentration hotspots near wells G75, G42, and G-41 in the northeast and southwest areas (Fig. 8.6f, l & XI).

Source 4, representing power plants, is characterized by PC4, explaining 6% of the variance with an Eigenvalue of 1.2. Both PC4 and F3 prominently exhibit significant levels of NO_2^- and NO_3^- (Fig.8.6a &b). This is particularly relevant to two different power plants in close proximity to specific wells: Newton Power Plant and Kshitiz Solar Energy near G-75, and Smart Grid Power Plants near G-72. These power plants release effluents with high concentrations of these elements, which can significantly affect groundwater quality in their respective areas. Both PC4 and F3 share similar spatial distributions in the

Northwest part (Fig.8.6f, m & XII), indicating heavily polluted areas and contributing 16% to groundwater degradation (Fig.8.6e).

Source 5 representing urbanization, is characterized by PC5 and F5, explaining 5.45% of the variance with an Eigenvalue of 1.09, and notable loadings of As and Pb (Fig. 8.6a & b). Urbanization in Gazipur, Delhi, has led to elevated levels of Pb and As in groundwater, primarily due to construction, population growth, and industrial activities. Infrastructure development disturbs natural layers, potentially releasing these elements into groundwater. Increased urban and industrial material usage further contributes to Pb and As contamination, exemplified by the influence of "Urbanization." Notably, both PC5 and F5 indicate significant pollution levels in the northwest and northeast regions of the study area, surrounded by residential and industrial areas (Fig. 8.6 f, n & XIV), serving as major contamination sources (Table 8.6).

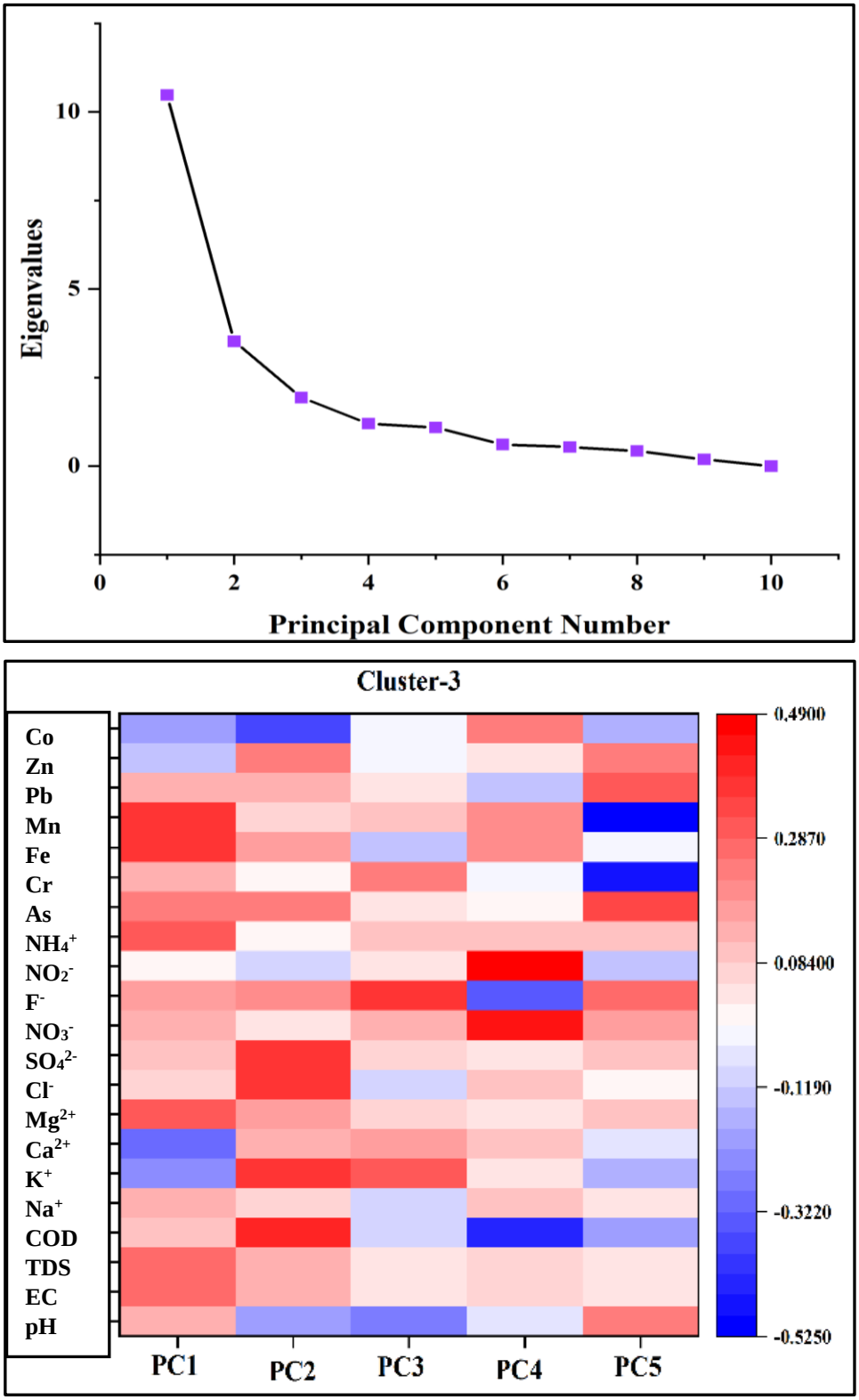

Figure 8.6 Cluster 3 a) Eigenvalues of principal components are depicted in the Scree plot & b) Principal component profiles obtained using the PCA model

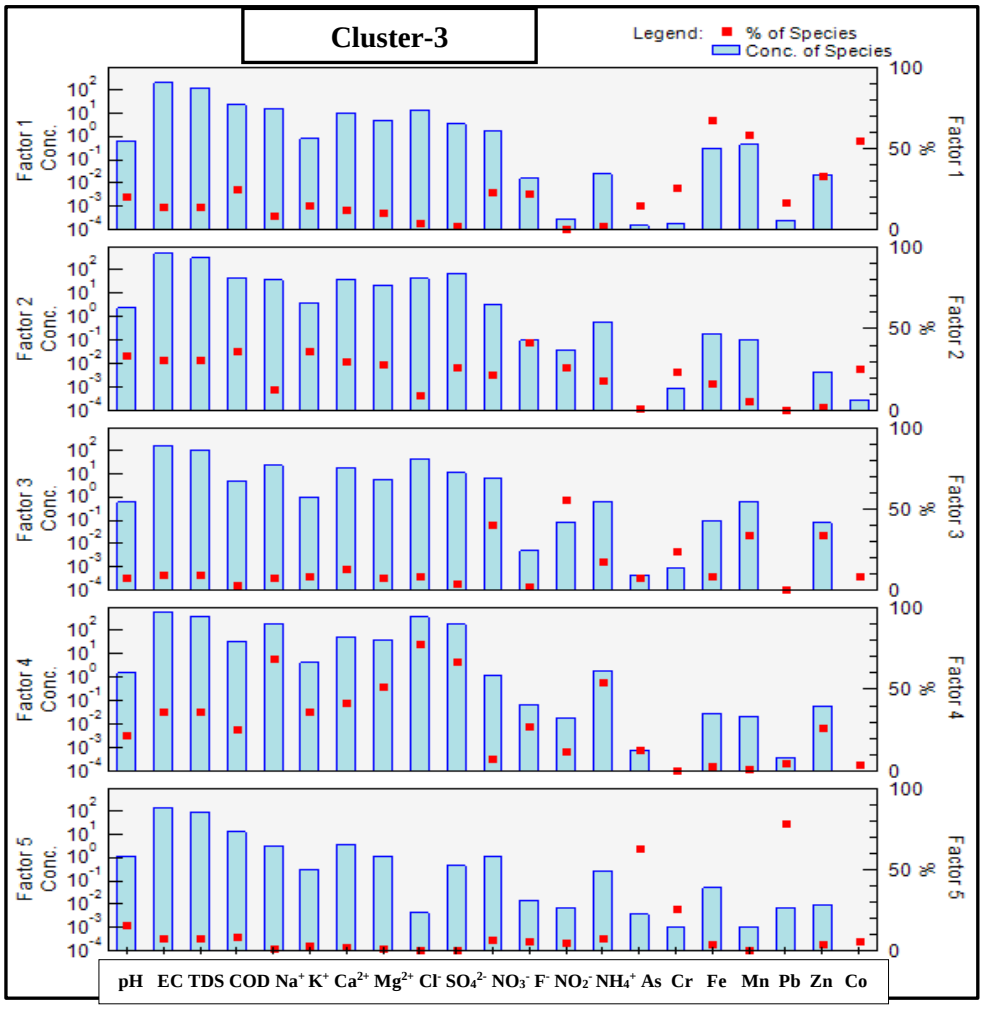

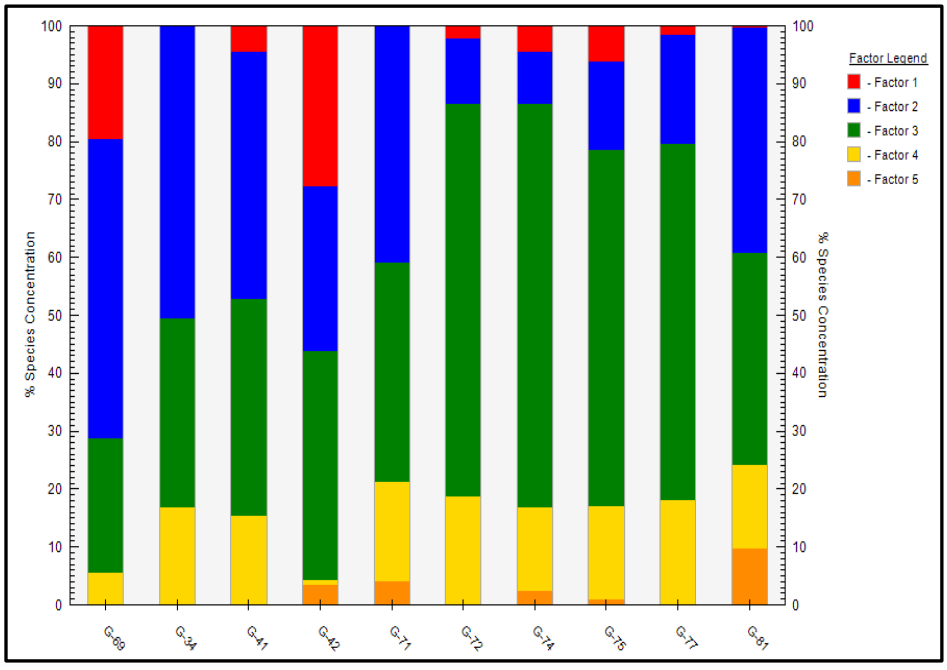

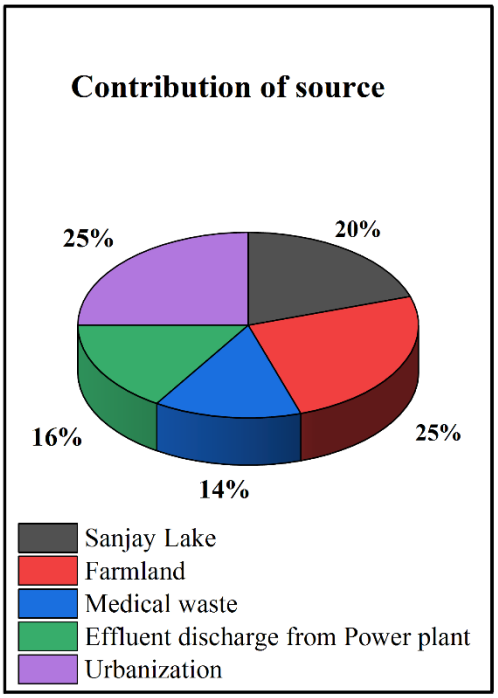

Figure 8.6 c) Factor Contribution profile , d) Factor Contribution profile of each well & e) Overall Contribution

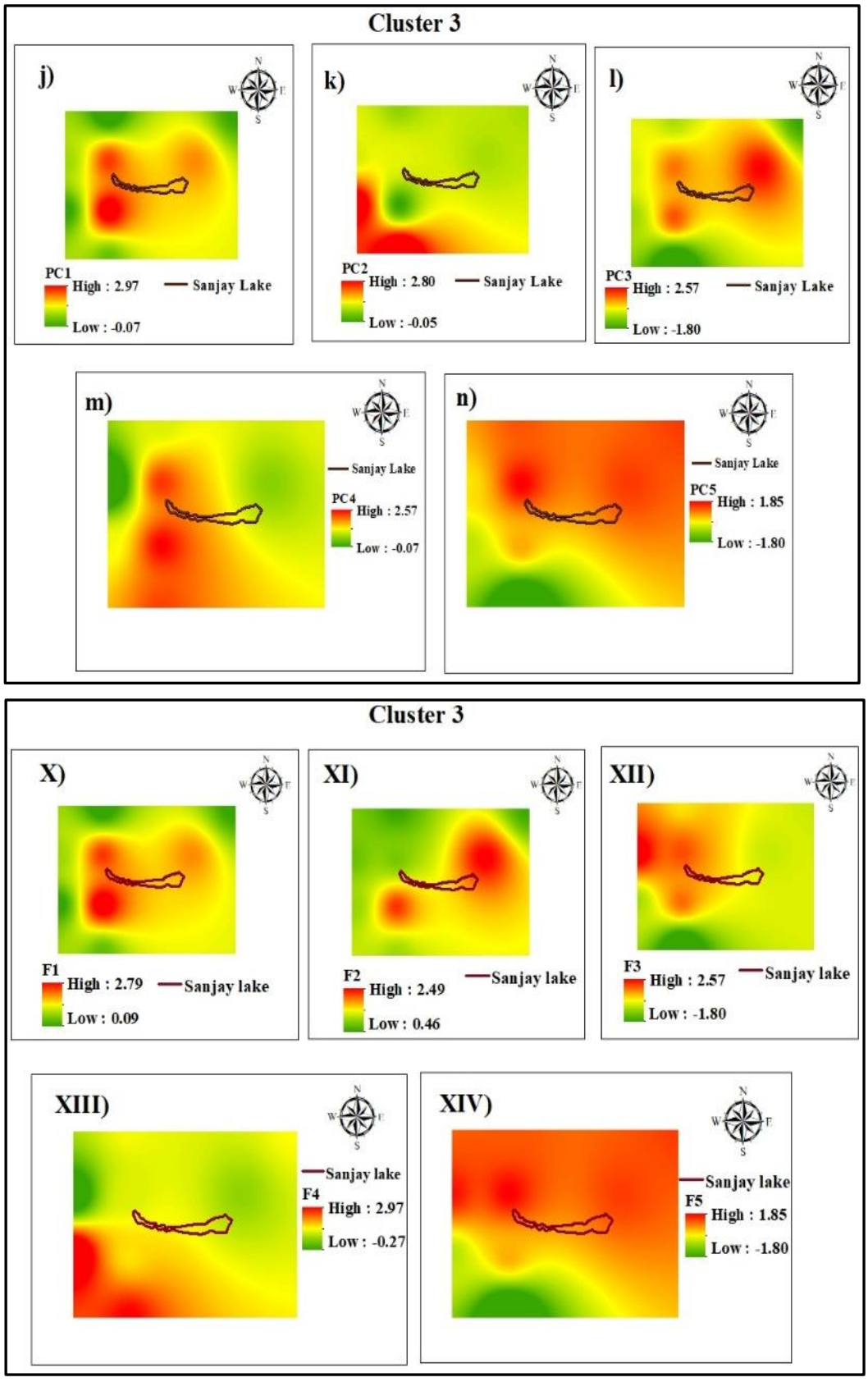

Figure 8.6 f) Spatial distribution of PCA and PMF analysis

8.3.7 Cluster-4

Three principal components were identified (Fig.8.7a). The surface water-groundwater interaction, represented by PC1 and F1, contributes 49.22% variance with eigen value 8.05, showing positive loadings on pH, COD and Co (Fig.8.7b). Higher COD levels in Hindon River (around 1000 mg/l) compared to groundwater (162 mg/l) indicate the introduction of organic pollutants through infiltration or seepage. The presence of clay and kankar in the aquifer can elevate Ca^{+} and HCO_3^{-} levels, raising the pH (Krishan et al., 2023). F1, showing significant contributions to pH (72%) and COD (75%), totalling 29% overall (Fig. 8.7 c & d), highlights surface water-groundwater interaction and possible groundwater pollution effects. High-value areas near the Hindon canal in the eastern part of the study area confirm surface and groundwater interaction as a significant pollution source (Fig.8.7f, o & XV).

Boating lake, represented as Source 2 where PC2 explains 37.05% of variance with Eigen value 6.74, displaying high positive loadings on Cl^{-} and SO_4^{2-} (Fig. 8.7a &b). The strong correlation (0.96) between Cl^{-} and SO_4^{2-} indicates their presence in Cluster 4 is linked to the nearby boating lake. Boating activities introduce Cl^{-} and SO_4^{2-} through fuel spills and cleaning agents, impacting groundwater quality. F3 characterized by high contributions of Cl^{-} (98%) and Na^{+} (80%) amouting 35% overall (Fig.8.7c). Boating-related activities likely increase Na^{+}, Cl^{-}, and SO_4^{2-} concentrations influencing groundwater quality. The spatial distributions of PC2 and F3 show striking similarities, indicating a common pollution source (Fig.8.7f, p & XVII). However, further analysis reveals that the wells near the boating lake exhibit low to moderate loading values, while higher values are observed in the western part of the study area. This suggests that the boating lake is not the point source of this particular analysis (Table 8.6).

Lithology represented as Source 3. PC3 explains 8.10% of variance and exhibits a strong positive loading on Fe and Pb (Fig.8.7a &b). The geological formations in the Indo-Gangetic plain of Gazipur contain iron-rich minerals (Sarkar & Shekhar, 2018). When groundwater interacts with these formations, it can dissolve iron minerals, leading to elevated Fe concentrations in the groundwater. The relationship between Fe,Pb and Zn in PC3 emphasizes the potential influence of "Lithology" factors on groundwater quality. F2, primarily dominated by 100% contribution of Fe and 36% overall (Fig. 8.7c & d), further reinforces the role of iron oxide minerals in geological formations, releasing Fe into the groundwater. The spatial distribution of PC3 and F2 indicates

heavily polluted regions in the western part of the study area and specifically in the southwest part of Cluster 4, while the remaining area exhibits moderate loading (Fig.8.7f, q & XVI). This emphasizes that the surrounding geology plays a crucial role in influencing groundwater quality (Table 8.6).

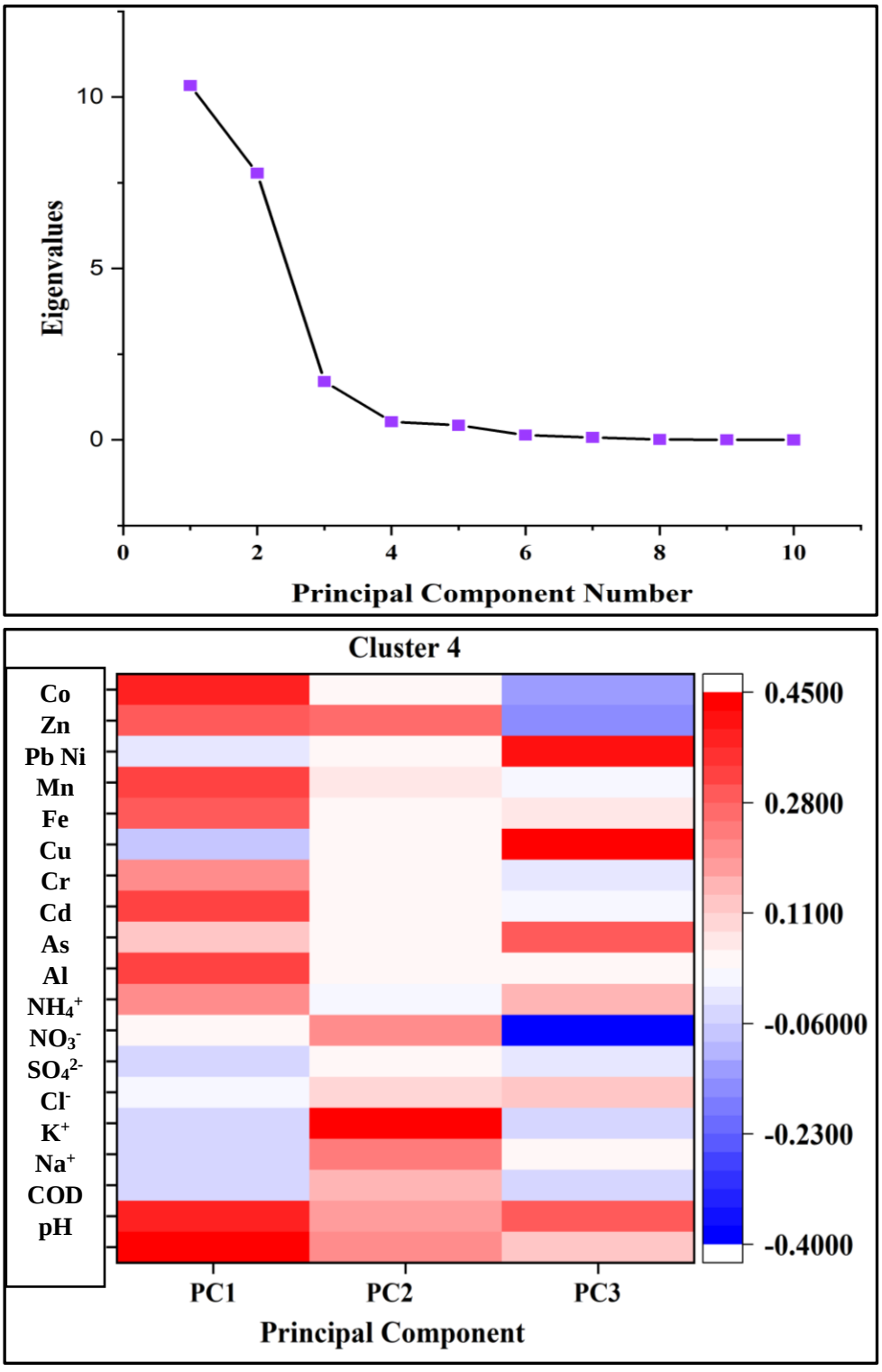

Figure 8.7 for Cluster 4 a) Eigenvalues of principal components are depicted in the Scree plot & b) Principal component profiles obtained using the PCA model

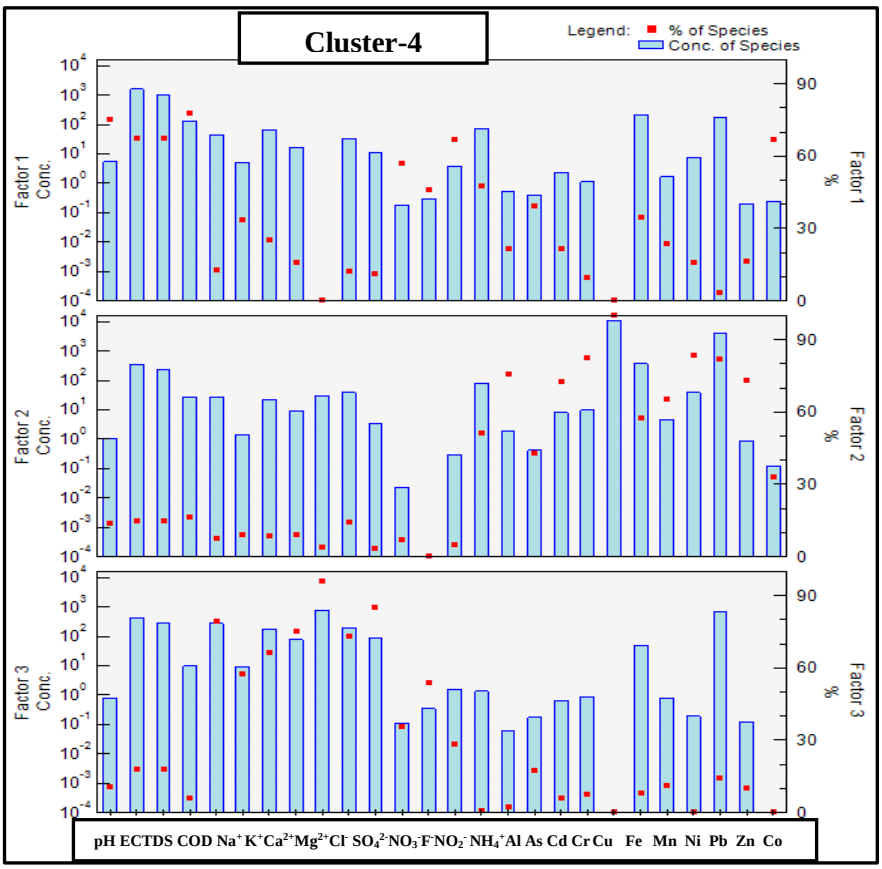

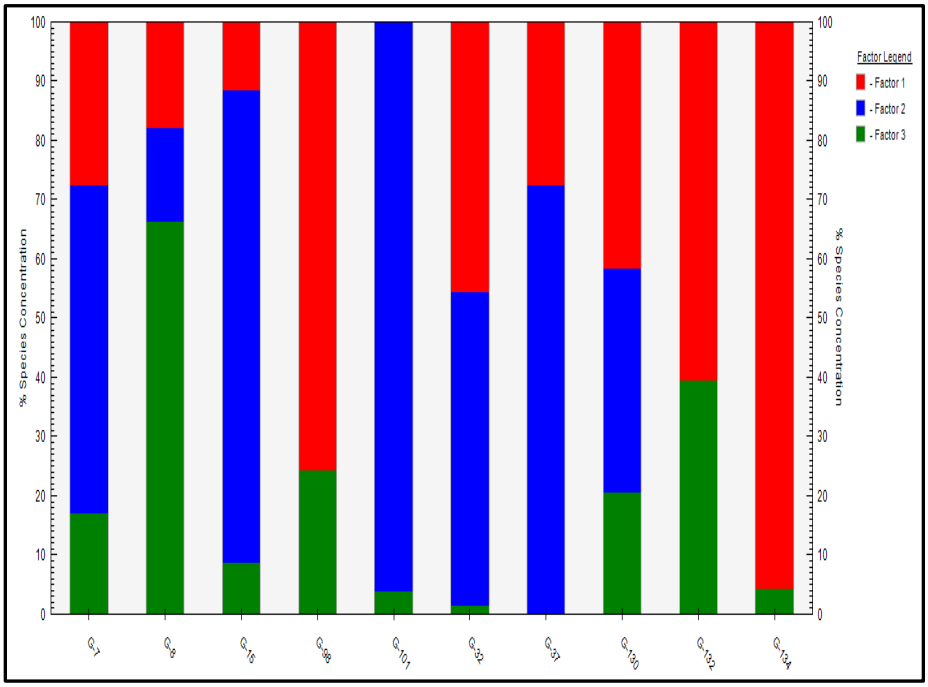

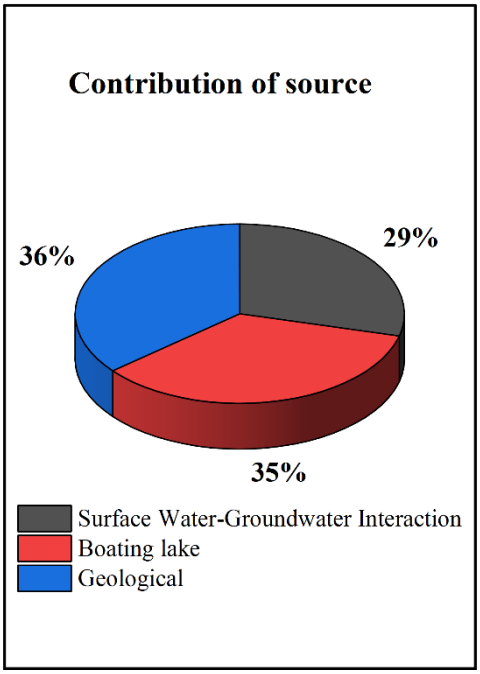

Figure 8.7 c) Factor Contribution profile, d) Factor Contribution profile of each well & e) Overall Contribution

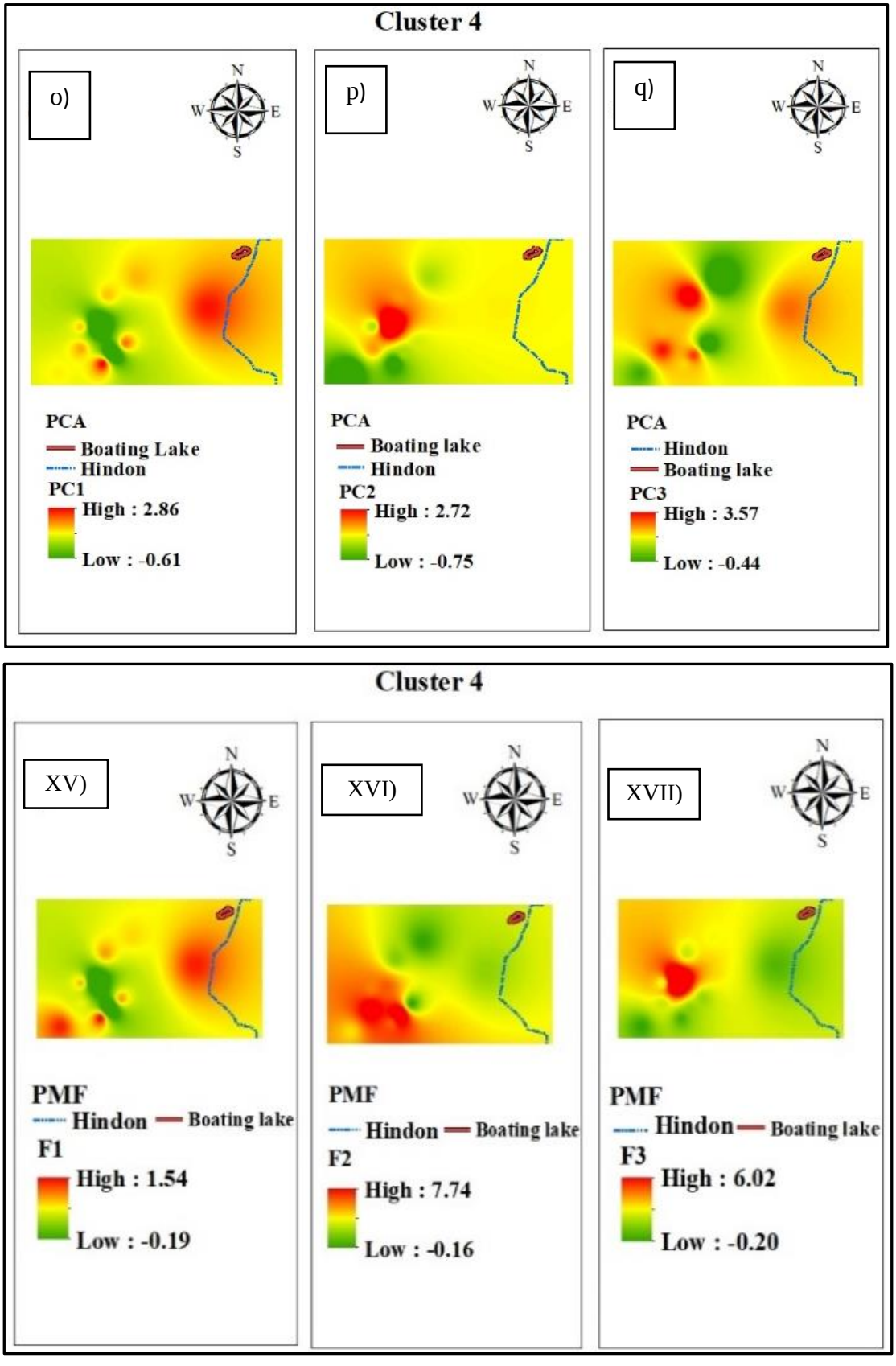

Figure 8.7 f) Spatial distribution of PCA and PMF analysis

8.3.8 Cluster 5

In the Fifth Cluster, three principal components were identified, collectively accounting for 82.93% of the variance, (Fig.8.8 a). Among these components, Source 1, representing anthropogenic activities, exerts a significant impact on groundwater quality, as evidenced by PC1 and F3, explaining 44.74% of the variance with an Eigenvalue of 8.05 (Fig.8.8 a, b & c). Notably, these factors display substantial loadings of Mn, Pb and As, underscoring their role in contaminating groundwater. Industrial processes release Mn, Pb, and As into the environment through emissions and soil disposal, potentially infiltrating groundwater. Aging infrastructure, including old pipes and lead-based paint, contributes to Pb contamination. Runoff from urban road surfaces can transport Mn and Pb into groundwater. Factor 3 contributes significantly to Mn (60%), Fe (60%) and As (69%), suggesting that F3 and PC1 share similar spatial patterns (Fig 8.8 c & d), notably in the Northeast and Southeast (Fig 8.8f, s & XX), collectively contributing 44% to groundwater contamination (Fig 8.8 e).

The Deeper Saline Aquifer exerts a significant influence as Source 2, primarily through PC2 and F2, explaining a noteworthy 28.92% of the variance, with an Eigen value of 5.21 (CGWB, 2017) (Fig 8.8a &b) . PC2 prominently showcases elevated levels of Na^{+}, Cl^{-} and SO_4^{2-} levels through geochemical processes, displaying a strong correlation (r=0.7). This correlation is indicative of the presence of a saline aquifer, particularly prominent in the eastern part of the study area, encompassing Gautam Buddha Nagar and Ghaziabad regions. Factor 2 contributes significantly to Magnesium at 87%, Chlorine at 92% and Sulfate at 95% with overall contribution is 38% (Fig 8.8c). These findings suggest that F2 and PC2 exhibit similar spatial distributions, particularly in the eastern direction (Fig 8.8f, t & XIX). Saline aquifers in the region play a crucial role in shaping the groundwater composition (Table 8.6).

Recharge from Surface representing Source 3, exhibited notable loadings on Cr and Zn within Principal Component 3. PC3 and F3, explaining a significant 9.27% of the variance with an Eigen value of 1.67, (Fig 8.8a,b & c). The highest loading value of Cr (88%) and Zn detected in Cluster 4 groundwater can be attributed to the influence of "Recharge from Surface" (Fig 8.8c). This pose substantial environmental implications, especially in the context of nearby sewage treatment plants and the Hindon River. It is noteworthy that the Hindon canal maintains Cr and Zn levels within prescribed limits. However, emphasizes the role of localized pollution sources, including sewage

treatment facilities introduces the possibility of trace element contamination. Furthermore, both PC2 and F2 share similar spatial distributions (Fig 8.8 f, u & XVIII), particularly evident in the northeastern and southeastern regions of the study area and reflects overall contribution around 18% (Fig 8.8e).

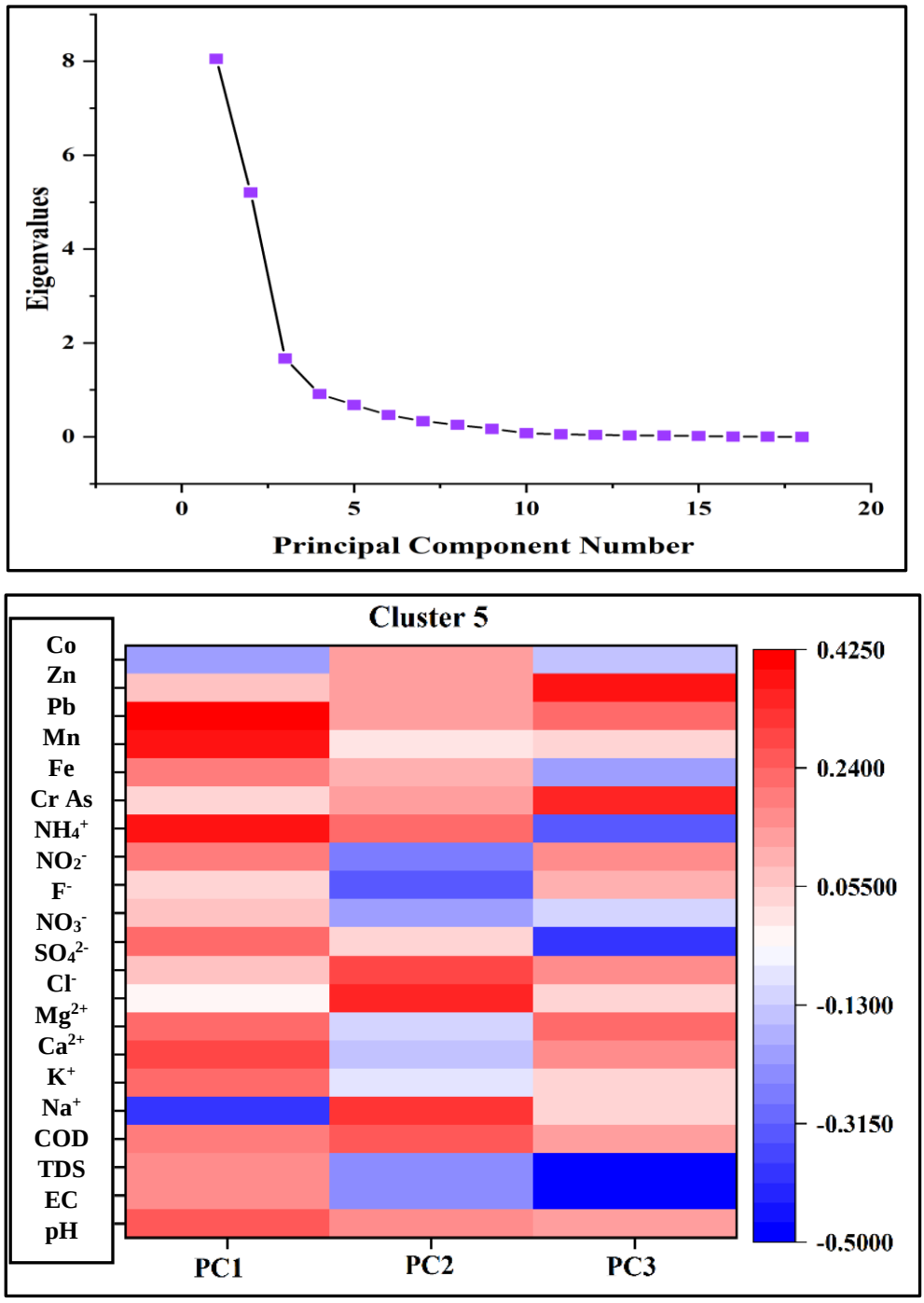

Figure 0 For Cluster 5 a) Eigenvalues of principal components are depicted in the Scree plot & b) Principal component profiles obtained using the PCA model

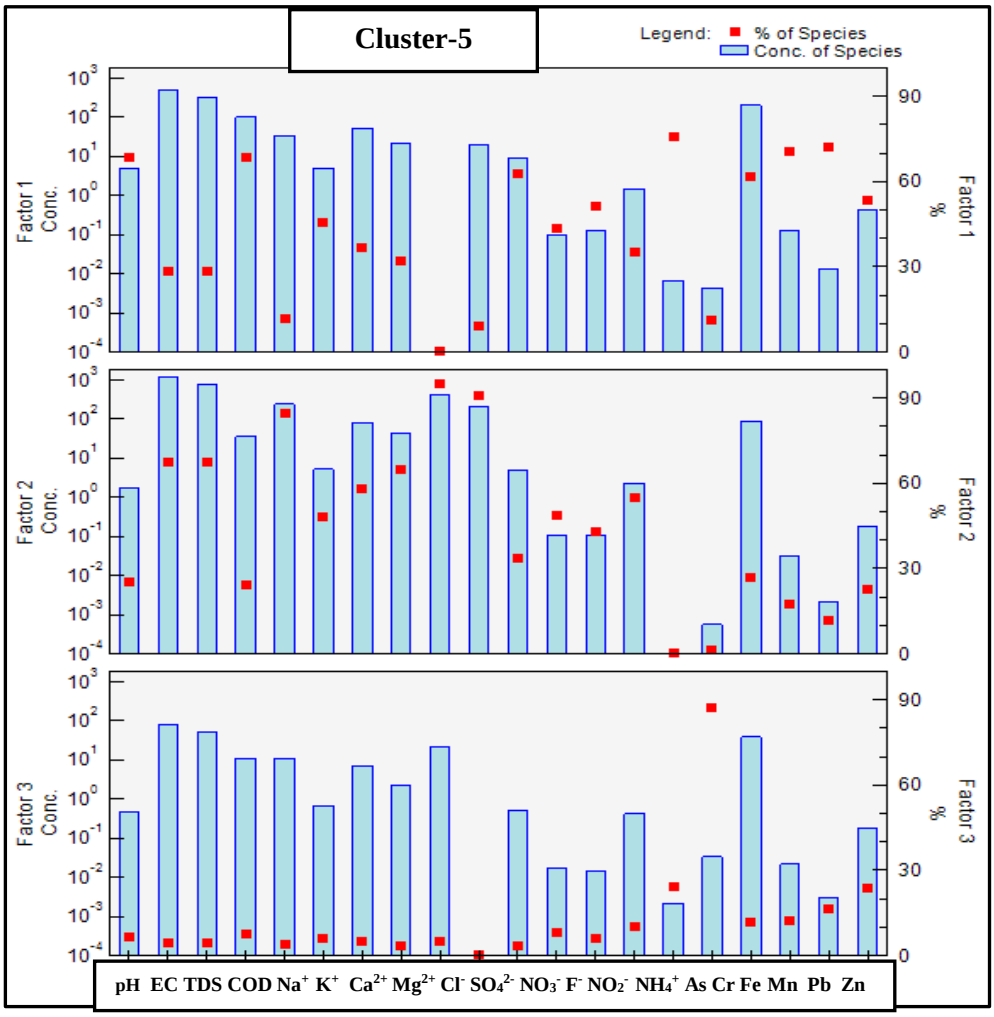

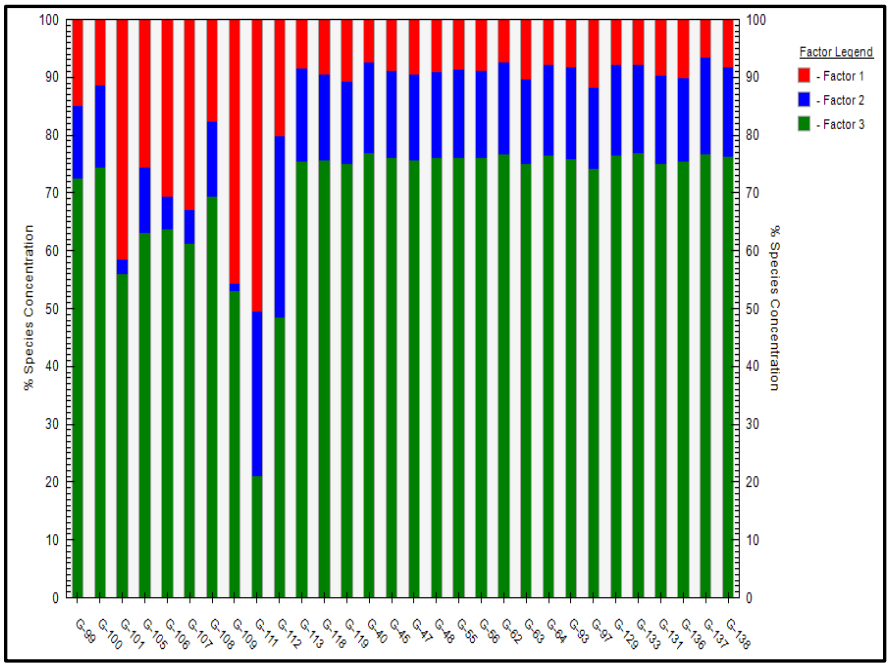

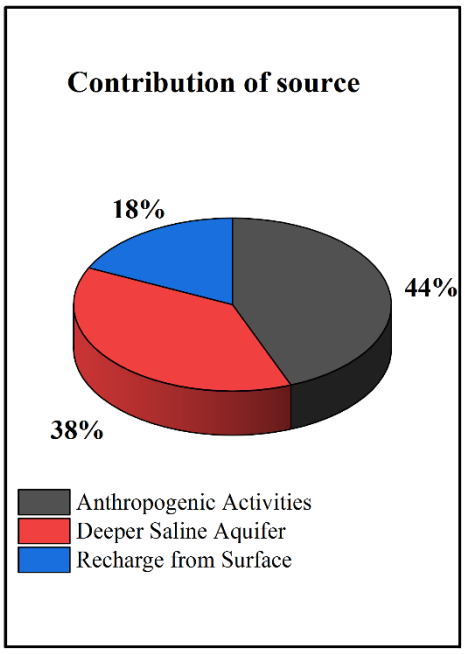

Figure 0 c) Factor Contribution profile, d) Factor Contribution profile of each well & e) Overall Contribution

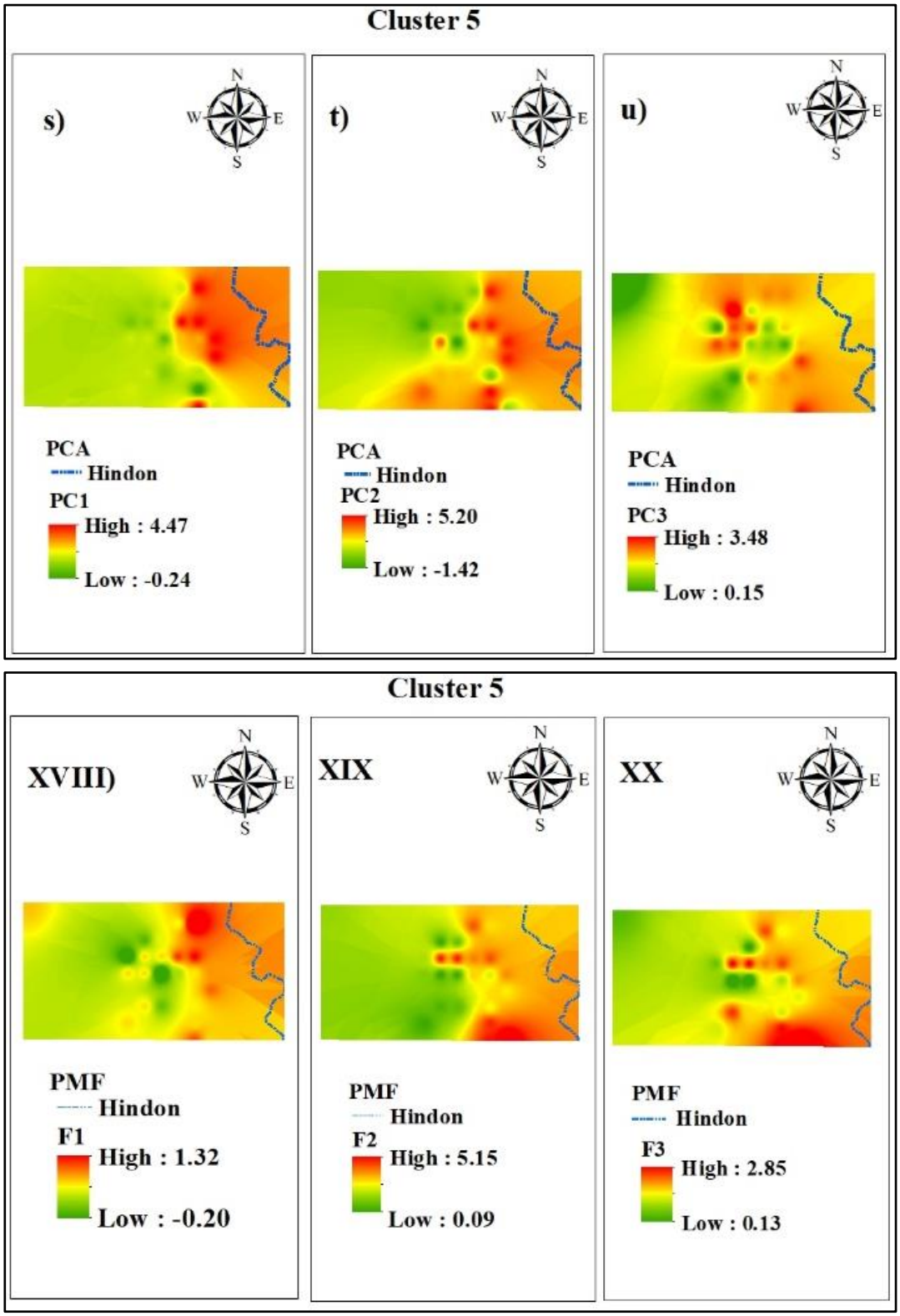

Figure 8.8 f) Spatial distribution of PCA and PMF analysis

Table 8.1 Illustrate the uncertainty value for Cluster-1

Station	pH	COD	Na^+	K^+	Ca^{2+}	Mg^+	Cl^-	SO_4^{2-}	NO_3^-	NH_4^+	As	Cr	Fe	Mn	Pb	Zn	Co
G-124	6.90	206.52	441.92	15.74	274.83	123.88	1109.76	344.41	26.75	9.97	0.01	0.01	1473.97	2.49	0.01	0.89	0.001
G-126	7.10	146.56	462.38	15.97	300.05	139.43	1130.07	353.28	26.77	9.97	0.01	0.01	1496.50	2.49	0.01	0.92	0.001
G-128	7.12	146.56	490.15	21.05	331.96	142.92	1119.90	348.84	27.22	10.03	0.01	0.01	1572.89	2.55	0.01	0.86	0.001
G-65	7.10	186.53	503.96	18.05	349.03	143.50	1130.47	366.34	27.47	5.34	0.01	0.01	1604.32	4.76	0.01	0.87	0.001
G-66	7.14	186.53	507.62	15.07	285.78	135.10	1130.48	394.96	27.57	5.34	0.01	0.01	1439.01	2.46	0.01	0.84	0.001
G-67	7.16	186.53	517.48	18.31	311.42	145.02	1134.60	369.44	28.62	14.32	0.01	0.02	1591.74	2.52	0.01	0.89	0.001
G-68	7.17	186.53	536.64	16.01	307.67	142.58	1138.28	390.69	28.96	9.37	0.01	0.01	2174.45	2.96	0.01	0.93	0.001
G-2	7.20	166.55	555.92	21.67	421.36	152.67	1169.11	377.38	29.61	5.73	0.01	0.01	1673.49	2.89	0.01	1.35	0.001
G-9	7.20	146.56	559.62	24.43	335.58	159.47	1194.13	387.23	29.64	27.38	0.01	0.01	1733.24	2.99	0.01	2.23	0.001
G-3	7.20	186.53	566.93	24.86	355.81	152.67	1235.43	435.89	29.72	9.97	0.01	0.01	1731.11	2.53	0.01	1.34	0.001
G-10	7.40	126.59	576.32	23.65	470.64	159.98	1253.65	518.41	30.09	10.55	0.01	0.01	1575.48	4.25	0.01	0.87	0.001
G-17	7.40	166.55	579.53	20.43	349.55	147.27	1262.81	535.45	31.45	7.64	0.01	0.01	1439.01	2.46	0.01	0.84	0.001
G-18	7.40	186.53	580.44	19.63	314.59	149.95	1275.70	408.88	32.01	11.90	0.01	0.01	1443.88	2.48	0.01	0.85	0.001
G-25	7.40	126.59	583.12	21.88	456.69	173.01	1282.99	500.05	32.15	14.44	0.01	0.01	1446.32	3.10	0.01	1.05	0.001
G-26	7.40	166.55	585.09	17.28	315.00	147.82	1295.03	447.95	32.69	26.80	0.01	0.01	2152.07	4.34	0.01	0.88	0.001
G-20	7.40	166.55	587.72	19.90	351.20	146.32	1303.72	489.34	32.07	8.63	0.01	0.01	3083.76	2.85	0.02	1.34	0.001
G-5	7.50	206.52	600.22	25.39	527.47	170.21	1313.68	381.79	33.48	15.69	0.01	0.01	1894.93	2.75	0.01	0.99	0.001
G-13	7.50	186.53	601.53	20.41	327.26	170.18	1327.71	376.44	33.60	20.71	0.01	0.01	1442.35	2.46	0.01	0.84	0.001
G-15	7.50	206.52	571.62	20.43	342.30	148.89	1327.75	363.43	33.93	12.33	0.01	0.02	2119.34	3.50	0.03	3.02	0.001
G-6	7.50	206.52	606.94	23.27	361.62	195.42	1329.40	481.72	35.32	12.10	0.01	0.01	1444.62	2.46	0.01	0.84	0.001
G-30	7.50	186.53	607.29	22.76	340.13	180.88	1349.95	598.47	35.55	10.34	0.01	0.01	1664.16	3.38	0.01	1.18	0.001
G-35	7.50	186.53	613.46	20.55	335.68	175.55	1362.49	560.76	35.82	7.33	0.01	0.05	1755.00	2.84	0.02	5.31	0.002
G-36	7.60	186.53	621.75	26.55	564.49	171.61	1372.20	492.27	37.24	12.11	0.01	0.01	1453.76	2.48	0.01	0.99	0.001
G-37	7.60	246.51	630.73	29.14	539.76	196.53	1372.27	434.12	37.81	9.76	0.01	0.01	2852.65	2.53	0.01	1.09	0.001
G-44	7.60	166.55	631.41	22.61	395.42	156.51	1376.55	422.84	37.92	10.58	0.01	0.01	4628.26	2.68	0.02	0.88	0.001
G-45	7.60	166.55	631.72	25.24	364.09	161.42	1385.12	576.02	37.92	6.63	0.01	0.01	2337.75	2.58	0.01	0.87	0.001
G-42	7.60	186.53	636.54	24.27	384.41	158.26	1388.78	454.79	38.94	6.31	0.01	0.01	1442.70	2.46	0.01	0.84	0.001
G-50	7.60	166.55	637.39	24.48	386.93	179.72	1392.90	637.50	39.36	16.76	0.01	0.02	6796.47	2.73	0.04	1.12	0.002
G-51	7.70	186.53	666.49	19.80	327.63	159.33	1444.05	703.84	39.85	6.39	0.01	0.01	2086.27	2.71	0.01	1.04	0.002
G-52	7.70	146.56	685.38	19.77	333.57	162.37	1458.06	470.25	41.41	6.67	0.01	0.01	1668.81	2.63	0.01	1.88	0.001
G-53	7.70	226.51	690.88	20.94	345.85	166.45	1508.49	499.12	43.39	6.20	0.01	0.01	2925.32	2.90	0.02	0.94	0.001
G-58	7.80	226.51	692.32	23.36	356.79	176.06	1571.37	563.96	46.73	9.62	0.01	0.01	1442.13	2.46	0.01	0.86	0.001
G-59	7.80	186.53	717.49	20.66	337.53	167.46	1596.01	581.97	52.21	11.77	0.01	0.01	1444.16	2.47	0.01	0.86	0.001
G-60	7.80	186.53	737.94	21.54	336.48	175.31	1598.95	647.10	56.90	10.37	0.01	0.01	5208.62	2.83	0.01	0.93	0.002
G-61	7.80	186.53	741.17	23.87	354.24	200.55	1629.59	542.12	56.95	9.69	0.01	0.01	7131.29	2.49	0.01	0.87	0.001
G-62	7.80	166.55	750.70	22.03	353.63	175.01	1648.66	613.33	58.12	5.34	0.01	0.01	1439.01	2.46	0.01	0.84	0.001

G-78	7.80	166.55	764.46	27.05	524.78	220.52	1838.51	649.00	59.52	13.40	0.02	0.01	1694.07	2.66	0.01	0.89	0.001
G-79	7.90	146.56	764.46	27.05	524.78	220.52	1873.93	981.82	61.04	9.44	0.01	0.03	4494.42	10.32	0.02	3.06	0.003
G-85	7.90	186.53	906.51	22.74	381.30	191.90	1958.68	523.35	74.97	25.16	0.01	0.01	1515.48	2.61	0.01	0.88	0.002
G-87	7.90	206.52	956.65	22.16	406.15	206.44	1958.68	411.07	76.50	6.91	0.02	0.03	3496.81	16.65	0.02	1.01	0.004
G-90	8.00	226.51	999.13	25.98	448.80	320.91	2178.40	845.49	82.24	9.37	0.03	0.01	1751.23	2.64	0.01	0.90	0.002
G-92	8.00	146.56	1130.73	36.12	573.97	329.52	2282.67	321.94	89.84	9.69	0.01	0.01	1439.01	2.46	0.01	0.84	0.001
G-94	8.00	206.52	1470.94	27.03	449.79	220.88	2962.18	1116.86	104.46	9.39	0.04	0.01	1582.68	2.79	0.01	0.91	0.003
G-96	8.00	206.52	1504.29	28.50	496.65	245.37	3078.07	1257.88	120.34	11.77	0.01	0.01	1439.01	2.46	0.01	0.84	0.001
G-97	8.10	166.55	2785.66	92.65	1827.46	792.53	7554.28	2096.58	120.34	12.52	0.01	0.01	1439.01	2.46	0.01	0.84	0.001

Table 8.2 Illustrate the uncertainty value for Cluster-2

Station	**pH**	**COD**	**Na^+**	**K^+**	**Ca^{2+}**	**Mg^+**	**Cl^-**	**SO_4^{2-}**	**NO_3^-**	**NH_4^+**	**Al**	**As**	**Cr**	**Cu**	**Fe**	**Mn**	**Ni**	**Pb**	**Zn**	**Co**
G-119	7.2	132	251	24	235	67	404	139	48	6	0.06	0.006	0.004	0.006	0.68	16.051	0.005	0.004	0.465	0.003
G-120	7.1	172	305	31	273	77	529	161	48	8	0.03	0.006	0.006	0.004	0.269	15.454	0.005	0.002	0.154	0.003
G-121	7.1	152	244	24	226	63	398	132	45	6	0.04	0.005	0.004	0.004	0.333	16.58	0.004	0.002	0.153	0.003
G-122	7.5	172	295	16	221	89	388	114	86	6	0.09	0.018	0.015	0.015	0.964	55.9	0.014	0.006	0.269	0.01
G-123	7.4	152	329	16	229	96	440	255	106	8	0.05	0.006	0.005	0.004	0.323	15.479	0.005	0.002	0.152	0.003
G-125	7.6	172	106	10	115	34	169	92	30	3	0.06	0.006	0.005	0.007	0.653	16.034	0.004	0.003	0.451	0.003
G-127	7.2	232	324	19	86	75	468	154	64	11	0.03	0.006	0.005	0.004	0.303	15.47	0.005	0.002	0.15	0.003

Table 8.3 Illustrate the uncertainty value for Cluster-3

Station	**pH**	**COD**	**Na^+**	**K^+**	**Ca^{2+}**	**Mg^+**	**Cl^-**	**SO_4^{2-}**	**NO_3^-**	**NH_4^+**	**Al**	**As**	**Cr**	**Cu**	**Fe**	**Mn**	**Ni**	**Pb**	**Zn**	**Co**
G-69	7.4	154	483	23	248	168	904	738	38	7	0.82	0.01	0.01	0.01	1.85	4.85	0.01	0.02	0.66	0.002
G-34	7.9	174	467	20	227	150	868	660	36	5	1.17	0.01	0	0.01	3.41	2.19	0.01	0.01	0.2	0.001
G-41	7.1	194	578	15	186	143	991	560	16	7	0.89	0.01	0.01	0.01	1.45	2.15	0.01	0.02	0.47	0.001
G-42	8.2	214	1326	28	363	298	2625	1203	20	13	0.72	0.01	0	0.01	1.3	2.11	0.01	0.01	0.18	0.001

G-71	7.7	134	495	14	194	102	888	350	52	7	0.8	0.01	0.01	0.01	2.47	5.74	0.01	0.01	0.5	0.002
G-72	7.9	154	932	18	232	139	1801	774	20	7	0.82	0.02	0	0.01	2.62	3.65	0.01	0.02	0.39	0.002
G-74	7.2	194	387	16	155	96	718	342	25	4	0.79	0.01	0	0.01	2.09	7.37	0.01	0.01	0.25	0.002
G-75	7.8	174	432	15	161	121	735	394	27	4	2.47	0.01	0.01	0.02	4.87	7.19	0.02	0.03	0.49	0.003
G-77	7	214	493	15	180	119	897	396	37	5	2.54	0.02	0.01	0.02	4.75	5.29	0.01	0.02	0.66	0.003
G-81	8.2	114	389	9	107	78	749	334	20	5	0.85	0.03	0.01	0.03	1.62	2.19	0.03	0.06	0.26	0.001

Table 8.4 Illustrate the uncertainty value for Cluster-4

Station	pH	COD	Na^+	K^+	Ca^{2+}	Mg^+	Cl^-	SO_4^{2-}	NO_3^-	NH_4^+	Al	As	Cr	Cu	Fe	Mn	Ni	Pb	Zn
G-7	8	144	827	27	550	241	2243	552	237	14	0.0003	0.000005	0.000028	0.000026	773.46	0.002	0.00001	0.00011	0.013
G-8	7	164	2184	72	1396	624	6117	1542	667	15	0.0003	0.000005	0.000023	0.000028	669.09	0.001	0.00001	0.00010	0.014
G-15	8	243	744	33	610	231	1869	757	221	10	0.0009	0.000008	0.000034	0.000038	1120.87	0.002	0.00002	0.00011	0.012
G-98	7	183	651	22	463	205	1727	516	271	8	0.0003	0.000004	0.000019	0.000025	478.66	0.001	0.00001	0.00010	0.010
G-101	7	223	828	28	520	239	2043	701	215	8	0.0008	0.000018	0.000080	0.000096	533.85	0.004	0.00005	0.00040	0.041
G-32	8	263	705	25	439	187	1725	411	186	8	0.0003	0.000005	0.000019	0.000024	605.80	0.001	0.00001	0.00010	0.010
G-37	8	263	580	19	370	173	1559	457	189	10	0.0006	0.000006	0.000023	0.000026	1853.45	0.001	0.00001	0.00010	0.010
G-130	8	203	741	27	461	175	1770	452	195	27	0.0003	0.000005	0.000023	0.000028	1049.17	0.001	0.00001	0.00013	0.014
G-132	7	164	689	30	460	191	1706	476	176	17	0.0002	0.000004	0.000019	0.000022	449.68	0.001	0.00001	0.00009	0.010
G-134	8	203	630	25	398	174	1642	461	169	7	0.0002	0.000004	0.000019	0.000023	450.58	0.001	0.00001	0.00009	0.010

Table 8.5 Illustrate the uncertainty value for Cluster-5

Station	pH	COD	Na^+	K^+	Ca^{2+}	Mg^+	Cl^-	SO_4^{2-}	NO_3^-	NH_4^+	Al	As	Cr	Cu	Fe	Mn	Ni	Pb	Zn
G-99	7	208	504	22	207	129	779	475	36	7.04	1.28	0.15	0.08	0.04	1841	3.0	0.0	0.1	25.7
G-100	7	168	605	21	296	170	1041	672	89	6.55	1.44	0.11	0.09	0.05	3741	1.3	0.0	0.1	11.8
G-101	7	208	617	22	306	170	1094	648	85	6.73	1.71	0.11	0.14	0.10	9871	3.8	0.1	0.4	42.3
G-105	8	168	352	13	137	90	593	361	31	5.61	1.97	0.56	0.11	0.06	4648	3.8	0.0	0.2	11.1
G-106	7	208	523	12	203	144	860	535	41	8.08	1.19	0.10	0.08	0.03	1836	3.6	0.0	0.1	16.8
G-107	7	168	1583	57	581	443	2372	1613	140	12.62	2.02	0.11	0.12	0.12	6172	4.1	0.1	0.3	37.0
G-108	8	148	414	18	176	106	678	411	34	6.74	7.66	0.20	0.10	0.05	3731	3.2	0.0	0.1	11.3
G-109	7	168	492	22	202	126	800	442	42	7.82	1.24	0.12	0.13	0.10	2727	4.5	0.1	0.7	57.1
G-111	8	208	408	19	178	105	675	396	34	9.75	1.67	0.37	0.49	0.08	5026	2.1	0.0	0.2	17.6
G-112	7	188	703	21	274	139	1494	391	37	14.32	1.19	0.10	0.08	0.03	1808	1.1	0.0	0.1	11.0

G-113	7	168	991	21	300	184	1601	1139	38	14.95	1.27	0.10	0.10	0.03	1981	1.1	0.0	0.1	11.0
G-118	7	168	562	22	265	151	865	520	98	10.93	1.26	0.12	0.08	0.03	2025	1.5	0.0	0.1	11.0
G-119	7	128	477	26	252	119	823	406	48	8.35	1.22	0.10	0.08	0.03	2222	1.7	0.0	0.1	11.3
G-40	8	168	1301	30	378	300	2507	1225	34	15.09	1.18	0.10	0.08	0.03	1812	1.1	0.0	0.1	11.0
G-45	8	148	752	20	252	137	1319	650	39	6.83	1.22	0.10	0.08	0.03	2707	1.2	0.0	0.1	11.0
G-47	8	148	360	24	185	107	593	402	66	6.27	1.21	0.10	0.08	0.03	3006	1.2	0.0	0.1	11.0
G-48	8	188	1318	29	382	196	2258	1047	47	26.06	1.30	0.10	0.08	0.03	5789	1.3	0.0	0.1	11.2
G-55	8	208	449	19	210	140	669	459	52	6.95	1.27	0.10	0.08	0.03	2015	1.2	0.0	0.1	11.0
G-56	8	148	543	16	206	124	934	453	60	7.55	1.25	0.10	0.08	0.03	1991	1.2	0.0	0.1	11.0
G-62	7	188	504	20	217	160	746	503	35	8.77	1.19	0.10	0.08	0.03	1809	1.1	0.0	0.1	11.0
G-63	8	148	443	15	201	111	745	425	28	6.32	1.25	0.10	0.08	0.03	2033	1.3	0.0	0.1	11.0
G-64	8	208	450	19	193	113	739	437	34	8.34	1.19	0.10	0.08	0.03	1810	1.1	0.0	0.1	11.1
G-93	7	228	401	12	141	99	563	351	27	4.50	1.29	0.10	0.08	0.03	2080	1.1	0.0	0.1	11.0
G-97	7	228	482	14	170	112	585	373	27	4.50	1.30	0.10	0.08	0.03	2054	1.1	0.0	0.2	11.0
G-129	8	208	451	19	187	115	736	348	49	7.70	1.20	0.11	0.08	0.03	1985	1.2	0.0	0.1	11.0
G-133	8	168	578	21	267	159	986	638	86	6.77	1.19	0.10	0.08	0.03	1858	1.1	0.0	0.1	11.0
G-131	8	168	402	19	183	107	652	402	38	8.07	1.24	0.11	0.08	0.03	2178	1.3	0.0	0.1	11.0
G-136	8	208	506	19	210	130	789	458	70	7.64	1.18	0.10	0.08	0.03	1814	1.3	0.0	0.1	11.7
G-137	8	228	447	23	201	132	687	441	54	8.43	1.21	0.10	0.08	0.03	1932	1.1	0.0	0.1	11.0
G-138	7	188	521	23	189	146	853	532	41	9.60	1.21	0.10	0.08	0.03	2102	1.2	0.0	0.1	11.0

Table 8.6: Summarizing the major dominating factors and sources in the results obtained from PCA & EPA- PMF

Cluster	PCA	Eigen value	Percentage of Variance	Dominating Parameter	PMF	Dominating Parameter	Parameter contribution	Source	Overall % Contribution
Cluster-1	**PC1**	8.57	42.83%	Zn & Cr	F3	Zn	89%	Gazipur drain	14
	PC2	4.18	20.92%	NH4 & F	F2	NH4	87%		14
	PC3	1.89	9.47%	Fe & Mn	F4	Fe & Mn	78% & 78%	Leachate absoprtion from Landfill	25
	PC4	1.44	7.21%	Cl, NO3 & SO4	F1	Cl & NO3	78% & 75%		24
	PC5	1.04	5.22%	pH & COD	F5	pH & COD	70% & 75%		23
Cluster-2	**PC1**	10.76	43.03%	K, Ca & Na	F4	K & Ca	60% & 63%	Recharge from Soil	24.4
	PC2	7.64	30.56%	NO2 & NH4	F3	NO2 & NH4	72% & 50%	Farmland	24.2
	PC3	3.61	14.44%	Zn & Fe	F1	Zn	78%	Older Alluvium	15
	PC4	1.44	5.74%	Mn, Pb & Co	F2	Mn & Co	100% & 82%	Yamuna River	36.0
Cluster-3	**PC1**	10.48	52.40%	Mn & Fe	F1	Mn & Fe	52% & 59%	Sanjay Lake	20
	PC2	3.52	17.61%	Cl, SO4 & K	F4	Cl, SO4 & K	75% & 62%	Farmland	25
	PC3	1.94	9.69%	F & K	F2	F & K	40% & 37%	Medical waste	14
	PC4	1.2	6.00%	No2 & NO3	F3	NO2 & NO3	52% & 38%	Effluent discharge from Power plant	16
	PC5	1.09	5.45%	As & Pb	F5	As & Pb	78% & 60%	Urbanization	25
Cluster-4	**PC1**	10.45	49.22%	pH, COD & Co	F1	pH & COD	72% & 75%	Surface Water-Groundwater Interaction	29
	PC2	6.74	37.05%	Cl & SO4	F3	Cl & Na	98% & 80%	Boating lake	35
	PC3	1.2	8.10%	Fe & Zn	F2	Fe & Pb	100% & 85%	Geological	36
Cluster-5	**PC1**	8.05	44.74%	Mn,Pb & As	F3	Mn,Pb & As	79%,73% & 73%	Anthropogenic Activities	44
	PC2	5.21	28.92%	Na, Cl and SO4	F2	Cl and SO4	98% & 95%	Deeper Saline Aquifer	38
	PC3	1.66847	9.27%	Cr & Zn	F1	Cr	89%	Recharge from Surface	18

References

Baluch, M. A., Hashmi, H. N., & Yu, L. (2019). Investigating the Impact of Anthropogenic and Natural Sources of Pollution on Quality of Water in Upper Indus Basin (UIB) by Using Multivariate Statistical Analysis. *Journal of Chemistry*, *2019*. https://doi.org/10.1155/2019/4307251

Banda, T. D., & Kumarasamy, M. (2020). Application of multivariate statistical analysis in the development of a surrogate water quality index (WQI) for South African watersheds. *Water (Switzerland)*, *12*(6). https://doi.org/10.3390/W12061584

CGWB. (2017). *AQUIFER MAPPING AND GROUND WATER MANAGEMENT PLAN, Parts of NCR, Uttar Pradesh*.

Cloutier, V., Lefebvre, R., Therrien, R., & Savard, M. M. (2008). Multivariate statistical analysis of geochemical data as indicative of the hydrogeochemical evolution of groundwater in a sedimentary rock aquifer system. *Journal of Hydrology*, *353*(3-4), 294–313. https://doi.org/10.1016/j.jhydrol.2008.02.015

Dalai, T. K., Rengarajan, R., & Patel, P. P. (2004). Sediment geochemistry of the Yamuna River System in the Himalaya: Implications to weathering and transport. *Geochemical Journal*, *38*(5), 441–453. https://doi.org/10.2343/geochemj.38.441

Herojeet, R., Rishi, M. S., Lata, R., & Sharma, R. (2016). Application of environmetrics statistical models and water quality index for groundwater quality characterization of alluvial aquifer of Nalagarh Valley, Himachal Pradesh, India. *Sustainable Water Resources Management*, *2*(1), 39–53. https://doi.org/10.1007/s40899-015-0039-y

Krishan, G., Bhagwat, A., Sejwal, P., Yadav, B. K., Kansal, M. L., Bradley, A., Singh, S., Kumar, M., Sharma, L. M., & Muste, M. (2023). Assessment of groundwater salinity using principal component analysis (PCA): a case study from Mewat (Nuh), Haryana, India. *Environmental Monitoring and Assessment*, *195*(1), 1–15. https://doi.org/10.1007/s10661-022-10555-1

Mohammad Salim Moyel, N. A. H. (2015). Water quality assessment of the Shatt al-Arab River, Southern Iraq. *Journal of Coastal Life Medicine*, *3*(6), 459–465. https://doi.org/10.12980/jclm.3.2015j5-26

Mohapatra, P. K., Vijay, R., Pujari, P. R., Sundaray, S. K., & Mohanty, B. P. (2011). Determination of processes affecting groundwater quality in the coastal aquifer beneath Puri city India: A multivariate statistical approach. *Water Science and Technology*, *64*(4), 809–817. https://doi.org/10.2166/wst.2011.605

Nathan, N. S., Saravanane, R., & Sundararajan, T. (2018). Statistical evaluation of the effect of secondary municipal wastewater and solid waste leachate on ground water quality at lawspet in puducherry, India. *Environment Protection Engineering*, *44*(1), 85–102. https://doi.org/10.5277/epel80107

Sarkar, A., & Shekhar, S. (2018). Iron contamination in the waters of Upper Yamuna basin. *Groundwater for Sustainable Development*, *7*, 421–429. https://doi.org/10.1016/j.gsd.2017.12.011

Subba Rao, N., Prakasa Rao, J., & Subrahmanyam, A. (2007). Principal component analysis in groundwater quality in a developing urban area of Andra Pradesh. *Journal of the Geological Society of India*, *69*(5), 959–969.

Chapter 9: Workshop and Training Programs

9.1 Day 1

9.1.1 Introduction of Participants:

- Typically includes a brief overview of individuals attending a meeting, seminar, or workshop.
- Names, affiliations, roles, and the diverse backgrounds of participants

9.1.2 Groundwater Contamination - How, Where, and Why:

- How: Contamination occurs through various sources like industrial waste, agriculture (fertilizers, pesticides), landfills, and improper disposal of chemicals.
- Where: Can happen near industrial sites, agricultural areas, urban zones, or due to leaking underground storage tanks.
- Why: Factors include human activities, natural geological conditions, and insufficient regulatory measures.

9.1.3 Groundwater Quality Monitoring:

- Involves regular sampling and analysis of groundwater to assess its chemical, physical, and biological properties.
- Detects pollutants, tracks changes over time, and ensures compliance with quality standards.
- Utilizes various techniques such as field measurements, laboratory analysis, and remote sensing.

9.1.4 Introduction to the Facilities of Water Quality Lab:

- Highlights the available equipment, resources, and capabilities of the water quality laboratory.
- Discusses different instruments used for water analysis (spectrophotometers, chromatographs, etc.).
- Explains procedures for sample processing, analysis, and quality assurance within the lab.

9.2 Day 2

9.2.1 Hydrogeology:

- Studies the movement, distribution, and quality of underground water.
- Focuses on the geological aspects affecting groundwater occurrence and behavior.
- Involves understanding aquifer properties, flow patterns, and interactions with surface water.

9.2.2 Basics of Groundwater Flow:

- Groundwater moves through porous spaces in the subsurface (aquifers).

- Driven by gravity, it flows from areas of high pressure to low pressure.
- Factors influencing flow include hydraulic conductivity, gradient, and aquifer properties.

9.2.3 Estimation of Recharge:

- Recharge refers to the replenishment of groundwater.
- Methods include direct measurements (like lysimeters), water balance calculations, and modeling.
- Factors affecting recharge estimation include precipitation, infiltration rates, and land use changes.

9.2.4 Sample Preparation and Preservation for Water Quality Analysis:

- Involves specific procedures to ensure accurate and reliable water quality data.
- Properly clean and sterilize sampling equipment before use.
- Preserve samples in appropriate containers at suitable temperatures to prevent contamination or degradation.
- Follow standardized protocols for sample collection, handling, and storage to maintain integrity.

9.3 Day 3

9.3.1 Aquifer Parameter Estimation using Pump Tests:

- Pump tests involve pumping water from a well at a constant rate to analyze the aquifer's response.
- Measures drawdown (change in water level) to determine hydraulic properties like transmissivity and storage coefficient.
- Analyzes aquifer characteristics, such as permeability and porosity, crucial for understanding water flow.

9.3.2 Characterization for Groundwater Analysis:

- Includes determining aquifer lithology, porosity, permeability, and hydraulic conductivity.
- Geophysical methods (like seismic surveys) and drilling techniques aid in understanding subsurface properties.
- Helps predict water movement, contamination risks, and suitability for extraction.

9.3.3 Application of Isotopes for Water Quality Monitoring:

- Isotopes are variants of elements with different atomic masses used as natural tracers in water.
- Helps identify water sources, track movement, and understand chemical reactions.
- Useful in studying contamination sources and natural processes affecting water quality.

9.3.4 Elaborating on Aquifer Characterization for Groundwater Analysis:

- Involves geological surveys, well logging, and core sampling to assess subsurface formations.
- Determines hydrogeological properties like hydraulic conductivity, storativity, and transmissivity.
- Models aquifer behavior, aiding in groundwater management and sustainable resource utilization.

9.4 Day 4

9.4.1 Groundwater Quality Data Processing:

- Involves collecting water samples from wells or sources.
- Analyzes parameters like pH, dissolved oxygen, nitrates, heavy metals, etc.
- Utilizes statistical methods and software for data interpretation and trend analysis.
- Helps identify pollutants, assess water quality, and determine potential risks.

9.4.2 Introduction of Contamination Transport Modeling:

- Predicts the movement and behavior of contaminants in groundwater.
- Considers factors like aquifer properties, flow rates, and chemical properties of contaminants.
- Various models (e.g., MODFLOW, MT3DMS) simulate contaminant spread over time and space.
- Assists in understanding potential pollution scenarios and planning remediation strategies.

9.4.3 Linked Simulation Optimization Modeling for Management of Polluted Sites:

- Integrates contaminant transport models with optimization techniques.
- Optimizes remediation strategies considering costs, effectiveness, and site-specific constraints.
- Balances extraction, treatment, or containment methods to minimize contamination.

9.4.4 Aquifer Characterization for Groundwater Analysis:

- Involves assessing geological formations, porosity, permeability, etc.
- Uses methods like well logging, geophysical surveys, and core sampling.
- Helps model water flow, predict contaminant migration, and manage groundwater resources.
- Critical for understanding the behavior of pollutants in the aquifer.

Day 5

9.5.1 Groundwater Flow Modeling using MODFLOW:

- MODFLOW is a widely used groundwater flow simulation software.
- Utilizes mathematical equations to represent groundwater flow in aquifers.
- Considers factors like aquifer geometry, hydraulic conductivity, recharge rates, and boundary conditions.
- Helps predict water levels, flow directions, and interaction between surface water and groundwater.

9.5.2 Nitrate Transport Modeling in Coastal Aquifers:

- Nitrate transport involves the movement of nitrates (from fertilizers, sewage, etc.) in groundwater.
- Coastal aquifers face unique challenges due to saltwater intrusion and sensitivity to pollution.
- Models consider nitrate sources, aquifer properties, and transport mechanisms (advection, dispersion, and reactions).
- Helps in understanding how nitrates move, accumulate, and impact coastal water quality.

9.5.3 Contaminant Transport Modeling:

- Involves simulating the movement of various contaminants in groundwater.
- Accounts for factors such as contaminant properties, aquifer characteristics, and boundary conditions.
- Models predict the spread, concentration, and potential impact of contaminants over time.
- Supports decision-making for remediation strategies and risk assessment.